UNIVERSITY OF CALIFORNIA,
IRVINE

Maternal and fetal immune adaptations with pregravid obesity

DISSERTATION

submitted in partial satisfaction of the requirements
for the degree of

DOCTOR OF PHILOSOPHY

in Biological Sciences

by

Suhas Sureshchandra

Dissertation Committee:
Professor Ilhem Messaoudi, Chair
Professor Andrea J. Tenner
Associate Professor Melissa Lodoen

2020

DEDICATION

To the women who raised me -

My beloved late grandma,

Ammani,

and

my mother

Whose loving spirit and unwavering support sustains me still

"Of all the paths you take in life, make sure a few of them are dirt"

John Muir.

TABLE OF CONTENTS

LIST OF FIGURES

LIST OF TABLES

ACKNOWLEDGEMENTS

Over the past six years I have received support and encouragement from a great number of individuals. Dr. Ilhem Messaoudi has been a great mentor, colleague, and friend. I am deeply indebted to her, for her trust, understanding, encouragement, and enthusiasm for science and for pushing me farther than I thought I could go. Her guidance has made this a thoughtful and rewarding journey. The Messaoudi lab has been a fun team to work with both in lab and outside. Norma and Allen, thank you for all help you have provided me over the years. Andrea, thank you for training me to be a better bench scientist.

None of this work would have been possible without the samples provided by Dr. Nicole Marshall's group at Oregon Health and Science University. I'm deeply appreciative of the work done by the Maternal Fetal Medicine group at OHSU and for an excellent ongoing collaboration. I would also like to thank my current and past committee members for taking the time to critique my work and providing useful feedback. I am ineffably indebted to my high school zoology lecturer Mr. Harikrishna D., who envisioned that a career in research was my best bet in life. I also acknowledge with a deep sense of reverence, my gratitude towards my undergraduate mentors Dr. Sobha V. Nair and Dr. Reshma S.V.

Thanks to all my friends, my road trip companions, for being my sounding board throughout my Ph. D journey. Most of all, I am fully indebted to my parents, my sisters, my brother, and my aunts, who have supported me morally, physically, and economically over the years. Thank you for your unconditional love and faith in me. Any omission in this brief acknowledgement does not mean lack of gratitude.

Curriculum Vitae

Suhas Sureshchandra
Institute for Immunology
Department of Molecular Biology and Biochemistry
University of California, Irvine

EDUCATION

University of California, Irvine 2017-2020
Irvine, CA
Ph.D. Candidate Biological Sciences, emphasis Immunology
Advisor: Dr. Ilhem Messaoudi

University of California, Riverside 2014-2017
Riverside, CA
Ph.D. Genetics, Genomics, and Bioinformatics (transferred)
Advisor: Dr. Ilhem Messaoudi

Indiana University, Bloomington 2009-2011
Bloomington, IN
Master of Science, Bioinformatics

Visveswaraya Technological University, Bangalore, India 2005-2009
Bachelor of Engineering, Biotechnology

RESEARCH / EMPLOYMENT

University of California, Irvine & University of California, Riverside 2015 - 2020
Doctoral Candidate
Investigating the
1) impact of obesity on myeloid cell adaptations during gestation.
2) disruptions in fetal immune programming with maternal obesity.
3) impact of long term ethanol consumption on monocytes and macrophages.

Medical College of Georgia, Augusta GA 2011-2013
Senior Research Associate

Center for Genomics and Bioinformatics, Indiana University 2010-2011
Bioinformatics Analyst

Indiana University School of Informatics and Computing Summer 2010
Research Assistant, Sun Kim Lab

TEACHING EXPERIENCE

University of California, Irvine
Fundamentals of AIDS (Fall ’18 and Winter ’19)
Biochemistry (Winter ’18)
Immunology and Hematology (Winter ’18)

TECHNICAL SKILLS

Immunology: Extensive experience in human and NHP immunology – tissue and blood processing, flow cytometry, cell sorting (MACS and FACS), imaging flow cytometry, cytokine assays (Intracellular, ELISA, Luminex), metabolic profiling of immune cells.

Genomics: RNA profiling (bulk and droplet based single cell RNA sequencing, microRNA), DNA methylation (targeted bisulfite approach), chromatin profiling (ATAC-Seq and ChIP-Seq).

Bioinformatics: Extensive experience in genome assembly, comparative genomics, next-generation sequencing analyses (bulk and single cell transcriptomics, epigenomics), data integration and visualization.

Programming: R, Python, Bash scripting.

MANUSCRIPTS (*In Prep*)

Sureshchandra S. et al. "Functional rewiring of cord blood monocytes with pregravid obesity." *(In preparation)*

Sureshchandra S. et al. "Single cell RNA sequencing reveals immune adaptations to pregravid obesity at the maternal fetal interface." *(In preparation)*

Sureshchandra S, Marshall NE, Mendoza N, Jankeel A, Messaoudi I. "Genomic analyses reveal disruption in pregnancy associated activation of monocytes with obesity". *(Submitted)*

Sureshchandra S, Wilson RM, Mendoza N, Jankeel A, Marshall NE, Messaoudi I. "Phenotypic and epigenetic adaptations of cord blood CD4+ T cells to maternal obesity" *(Under review)*

PUBLICATIONS

Franklin-Murray AL, Mallya S, Jankeel A, Sureshchandra S, Messaoudi I, Lodoen MB. "Toxoplasma gondii dysregulates barrier function and mechanotransduction signaling in human endothelial cells" *mSphere*; 2020. PMID:31996420

Sureshchandra S, Marshall NE, Messaoudi I. "Impact of pregravid obesity on maternal and fetal immunity: Fertile grounds for reprogramming" *J Leukocyte Biology*; 2019. PMID:31483523

Sureshchandra S, Stull C, Ligh BJK, Nguyen SB, Grant KA, Messaoudi I. "Chronic heavy drinking drives distinct transcriptional and epigenetic changes in splenic macrophages" *Ebiomedicine*; 2019. PMID:31005514

Sureshchandra S, Raus A, Jankeel A, Ligh BJK, Walter NAR, Newman N, Grant KA, Messaoudi I. "Dose-dependent effects of chronic alcohol drinking on peripheral immune responses" *Scientific Reports*; 2019. PMID:31127176

Rhoades N, Mendoza N, Jankeel A, Sureshchandra S, Alvarez AD, Doratt B, Heidari O, Hagan R, Brown B, Scheibel S, Marbley T, Taylor J, Messaoudi I. "Altered immunity and

microbial dysbiosis in aged individuals with long-term controlled HIV infection" *Front Immunology*; 2019. PMID:30915086

Barr T, Lewis SA, Sureshchandra S, Doratt B, Grant KA, Messaoudi I. "Chronic ethanol consumption alters lamina propria leukocyte response to stimulation in a region-dependent manner" *FASEB J*; 2019. PMID:30897342

Sureshchandra S, Marshall NE, Wilson RM, Barr T, Rais M, Purnell JQ, Thornburg JL, Messaoudi I. "Inflammatory determinants of pregravid obesity in placenta and peripheral blood" *Front Physiology*; 2018. PMID:30131724

Barr T, Sureshchandra S, Ruegger P, Zhang J, Ma W, Borneman J, Grant KA, Messaoudi I. "Concurrent gut transcriptome and microbiota profiling following chronic ethanol consumption in nonhuman primates" *Gut Microbes*; 2018. PMID:29517944

Sureshchandra S, Wilson RM, Rais M, Marshall NE, Purnell JQ, Thornburg KL, Messaoudi I. "Maternal pregravid obesity remodels the DNA methylation landscape of cord blood monocytes disrupting their inflammatory program" *Journal of Immunology*; 2017. PMID:28887432

Messaoudi I, Handu M, Rais M, Sureshchandra S, Park BS, Fei SS, Wright H, White AE, Jain R, Cameron JL, Winters-Stone JM, Varlamov O. "Long-lasting effect of obesity on skeletal muscle transcriptome" *BMC Genomics*; 2017. PMID:28545403

Menicucci AR, Sureshchandra S, Marzi A, Feldmann H, Messaoudi I. "Transcriptome analysis reveals a previously unknown role for CD8+ T-cells in rVSV-EBOV mediated protection" *Scientific Reports*; 2017. PMID:28428619

Landrith TA, Sureshchandra S, Rivera A, Jang JC, Rais M, Nair MG, Messaoudi I, Wilson EH. "CD103+ CD8 T cells in the toxoplasma-infected brain exhibit a tissue resident memory transcriptional profile" *Frontiers in Immunology*; 2017. PMID:28424687

Arnold N, Girke T, Sureshchandra S, Messaoudi I. "Acute simian varicella virus infection causes robust and sustained changes in gene expression in the sensory ganglia" *Journal of Virology*; 2016. PMID:27681124

Arnold N, Girke T, Sureshchandra S, Nguyen C, Rais M, Messaoudi I. "Genomic and functional analysis of the host response to acute simian varicella infection in the lung" *Scientific Reports*; 2016. PMID:27677639

Sureshchandra S, Rais M, Stull C, Grant KA, Messaoudi I. "Transcriptome profiling reveals disruption of innate immunity in chronic heavy ethanol consuming female rhesus macaques" *PLoS One*; 2016. PMID:27427759

Edwards MR, Liu G, Mire CE, Sureshchandra S, Luthra P, Yen B, Shabman RS, Leung DW, Messaoudi I, Geisbert TW, Amarasinghe GK, Basler CF. "Differential regulation of interferon responses by Ebola and Marburg virus VP35 proteins" *Cell Reports*; 2016. PMID:26876165

Barr T, Girke T, Sureshchandra S, Nguyen C, Grant KA, Messaoudi I. "Alcohol consumption modulates host defense in rhesus macaques by altering gene expression in circulating leukocytes" *Journal of Immunology*; 2016. PMID:26621857

Jin B, Ernst J, Tiedemann R, Xu H, Sureshchandra S, Kellis M, Dalton S, Liu C, Choi JH, Robertson KD. "Linking DNA methyltransferases to epigenetic marks and nucleosome structure genome-wide in human tumor cells" *Cell Reports*; 2012. PMID:23177624

Tae H, Ryu D, Sureshchandra S, Choi JH. "ESTclean: a cleaning tool for next-gen transcriptome shotgun sequencing" *BMC Bioinformatics*; 2012. PMID:23009593

Peterson MP, Whittaker DJ, Ambreth S, Sureshchandra S, Buechlein A, Podicheti R, Choi JH, Lai Z, Mockatis K, Colbourne J, Tang H, Ketterson ED. "De novo transcriptome sequencing in a songbird, the dark-eyed junco (Junco hyemalis): genomic tools for an ecological model system" *BMC Genomics*; 2012. PMID:222776250

FUNDING

UCI – Center for Multiscale Cell Fate Research (CMCF) Interdisciplinary Opportunity Award (IOA) - $8,500. Project Title – "*Mapping in vivo myeloid cell fates following chronic alcohol consumption*"

Otto Shaler International Graduate Student Fellowship – Spring 2019 (Resident tuition and fees for Spring 2019 and $6000 stipend).

HONORS AND AWARDS

The AAI Young Investigator Award, UCI Immunology Fair 2019, Irvine CA

Society for Leukocyte Biology (SLB) Student Presidential Award 2019, Boston MA

Travel Award, Society for Leukocyte Biology 2019 Meeting, Boston MA

NIH-USDA Young Investigator Award, Aspen Snowmass Perinatology Symposium 2019, Snowmass CO

Otto W. Shaler Scholarship, UC Irvine, 2019, Irvine CA

Travel Award, Society for Leukocyte Biology 2018 Meeting, Chandler AZ

Krishna and Sujata Tewari Scholar Award, UCI School of Biological Sciences 2018, Irvine CA

Robert Warner Award for Nucleic Acid Research, UCI School of Biological Sciences 2018, Irvine CA

Flow Cytometry Training Fellowship, SoCalFlow Meeting 2018, Irvine CA

Travel Award, Alcohol and Immunity Research Interest Group (AIRIG) 2018 Meeting, Denver CO

Travel Award, Society for Leukocyte Biology 2017 Meeting, Vancouver BC

William D. Redfield Graduate Fellowship, UCI School of Biological Sciences 2017, Irvine CA

Travel Award, Gordon Research Conference on Alcohol induced end-organ damage 2017, Ventura CA

Travel Award, Alcohol and Immunity Research Interest Group (AIRIG) 2016 Meeting, Chicago IL

Best Poster Award, UCI Immunology Fair 2016, Irvine CA

Travel Award, Society for Leukocyte Biology 2015 Meeting, Raleigh NC

Dean's Distinguished Fellowship, UC Riverside 2014-2015, Riverside CA

University Gold Medalist (Highest CGPA among the graduating class of 650 students), VTU, Belgaum India.

Prof. MRD Scholarship (Top 5% of undergraduate engineering class – '06, '07, '08', '09)

PRESENTATIONS

2019 Immunology Fair, UC Irvine (Dec 2019); Poster (*Awarded Best Poster*)
2019 Society for Leukocyte Biology, Boston MA (Nov 2019); Oral presentation (*Student Presidential Award*)
2019 Aspen Snowmass Perinatology Symposium, Aspen CO (Aug 2019); Poster
2018 Society for Leukocyte Biology, Chandler AZ (Oct 2018); Poster
2018 Alcohol and Immunity Research Interest Group, Denver CO (Jan 2018); Poster
2017 Society for Leukocyte Biology, Vancouver BC (Oct 2017); Oral presentation
2017 Gordon Conference on Alcohol Induced End-Organ Damage, Ventura CA (March 2017); Poster
2017 Immunology LA, Los Angeles CA (July 2017); Poster
2016 Immunology Fair, UC Irvine (Dec 2016); Poster (*Awarded Best Poster*)
2016 Alcohol and Immunity Research Interest Group, Chicago IL (Nov 2016); Oral presentation
2016 Cold Spring Harbor Meeting - Systems Biology: Global Analysis of Gene Expression, Long Island NY (March 2016); Poster
2015 Society for Leukocyte Biology, Raleigh NC (Sept 2015); Poster

MENTORING

Gouri Ajith, (Genetics Undergrad, UCI)	2019 - 2020
Sneha Anand, (Biology Undergrad, UCI)	Fall 2019
Brian Jin Kee Ligh (Biomedical Engg Undergrad, UCI)	2018 - 2019
Selene Bich Nguyen (Biology Undergrad, UCI)	2018 - 2019
Andrew N. Tang (Biology Undergrad, UCI)	2018 - 2019
Vivian Hye-In Chi (Biology Undergrad, UCI) (UROP '17)	2017 – 2018
Christina Nguyen (Biology Undergrad, UCR)	2016 - 2017

WORKSHOPS

Computational Immunology Summer School Boston University, MA	June 2018
Multicolor Flow Cytometry SoCal Flow, UC Irvine	April 2018
Mentoring Excellence Program Graduate Division, UC Irvine	Winter 2018

Becoming an effective mentor — Winter 2018
School of Medicine, UC Irvine

SOCIETIES

American Association for Immunologists (2019 – Present)
Clinical Epigenetics Society (2017 – Present)
Society for Leukocyte Biology (2015 – Present)

ABSTRACT OF THE DISSERTATION

Maternal and fetal immune adaptations with pregravid obesity

by

Suhas Sureshchandra

Doctor of Philosophy in Biological Sciences

University of California, Irvine, 2020

Professor Ilhem Messaoudi, Chair

Maternal obesity is a significant risk factor for obstetric complications such as preterm labor, preeclampsia, and chorioamnionitis. Furthermore, pregnant women with obesity are more prone to infections during pregnancy and following postpartum procedures, suggesting a compromised immune system. We therefore hypothesized that the immune adaptations associated with a healthy gestation are disrupted with obesity. Indeed, our analyses suggest that a healthy pregnancy was associated with systemic changes indicative of innate immune activation. Specifically, monocyte responses to LPS were increaed with gestational age in lean subjects, with concomitant enhancement of chromatin accessibility, which poised cells for a greater response. This trajectory was disrupted in pregnant women with obesity resulting in attenuated monocyte responses to LPS. Furthermore, epigenetic, metabolic, and functional measurements strongly support the induction of immunotolerance with pregravid obesity. These findings may explain the increased susceptibility to infections observed during pregnancy and following cesarean delivery in women with obesity.

Profiling of immune cells at the maternal fetal interface suggests that immunotolerance in peripheral monocytes extends to tissue resident macrophages as well. A combination of flow cytometry and single cell RNA sequencing of placental immune cells suggests increased infiltration of tissue resident macrophages in both the decidual and villous membranes with pregravid obesity. Trajectory analysis and baseline cytokine profiles indicate that macrophages from both placental membranes are less inflammatory with obesity. Specifically, macrophages from both maternal and fetal membranes downregulate signatures of immune activation, but upregulate signatures of lipid metabolism. Furthermore, in the villi, pregravid obesity results in expansion of macrophage subsets involved in apoptotic signaling, and immune-stromal cell crosstalk, but are refractory to LPS stimulation. Collectively these findings suggest that obesity skews placental macrophages towards a regulatory phenotype, providing the basis for a compensatory mechanism to limit inflammatory exposures at the fetal front.

Indeed, this restraining of inflammation on the fetal front is evident when fetal monocytes are exposed to pathogenic insults. Specifically, cord blood monocytes from babies born to obese mothers mount a dampened cytokine response to both TLR agonists and *E. coli*. Monocytes from obese group also exhibit poor transcriptional response to secondary interferon stimulation. Baseline DNA methylation profiles provide evidence of M2-like skewing of cells. Functionally, cells from obese group are more phagocytic but less migratory towards a chemokine gradient, confirming their regulatory phenotype. These findings further our understanding of mechanisms that explain the increased risk of infection in neonates born to mothers with high pre-pregnancy BMI.

CHAPTER 1

Introduction

Incorporates components from the published article:
Sureshchandra S, Marshall NE, Messaoudi I. Impact of pregravid obesity on maternal and fetal immunity: Fertile grounds for reprogramming. J Leukoc Biol. 2019;106(5):1035-50. doi: 10.1002/JLB.3RI0619-181R. PubMed PMID: 31483523

Almost 36% of women of childbearing age in the US are categorized as obese (BMI > 30) (Ogden et al., 2013). Several studies have linked high maternal BMI before/during pregnancy with a higher incidence of several obstetric and post-partum complications, including gestational diabetes (Chu et al., 2007a; Torloni et al., 2009), gestational hypertension, preeclampsia (PE) (Salihu et al., 2012; Wang et al., 2013), higher need for caesarean delivery (Chu et al., 2007c), microbial infections (urinary and genital tract infection, and sepsis) (Basu et al., 2011a; Magann et al., 2013; McLean et al., 2012; Robinson et al., 2005; Stapleton et al., 2005), chorioamnionitis (Hadley et al., 2019; Korkmaz et al., 2016), and post-partum surgical site infections (Anderson et al., 2013; Meenakshi et al., 2012; Paiva et al., 2012; Salim et al., 2012). Pregravid (pre-pregnancy) obesity also poses significant risks to the fetus including early pregnancy loss, preterm delivery (Aune et al., 2014; Cnattingius et al., 2013), stillbirth (Chu et al., 2007b), and delivery of large-for-gestational-age infants (Norman and Reynolds, 2011).

In line with the developmental origins of health and disease (DOHaD) hypothesis, epidemiologic studies have linked pregravid obesity with detrimental cardiometabolic, neurocognitive, and behavioral outcomes in the offspring (Catalano et al., 2009a; Gaillard et al., 2014a; Gaillard et al., 2014b; Gaillard et al., 2015; Godfrey et al., 2017; Tie et al., 2014; Yu et al., 2013). More recent studies have also revealed a significant impact on the fetal immune system indicated by a higher incidence of bacterial and viral infections in neonates born to mothers with obesity that require admission to the neonatal intensive care unit (Rastogi et al., 2015; Suk et al., 2016). Moreover, the higher incidence of pregravid obesity has been implicated in the rising prevalence of allergic diseases (childhood wheeze and

atopy) (Rajappan et al., 2017) and asthma (Guerra et al., 2013; Pike et al., 2013; Watson and McDonald, 2013) during early life (Dumas et al., 2016; Kumar et al., 2010), childhood (Haberg et al., 2009; Lowe et al., 2011; Scholtens et al., 2010), and adolescence (Patel et al., 2012). In this chapter, we aim to provide an overview of our current understanding of the impact of pregravid obesity on 1) maternal and offspring immunity, 2) the maternal-fetal interface, and 3) cellular and molecular mechanisms that mediate these changes.

1.1 Modeling maternal obesity.

Ex vivo studies using human samples provide the ideal system to study the impact of pregravid obesity on fetal immunity (Sureshchandra et al., 2017; Wilson et al., 2015). In clinical studies, obesity is defined as a body mass index (BMI) that exceeds 30kg/m^2. Clinical studies have the advantage of collecting longitudinal data on fat mass, gestational weight gain, and postpartum weight retention/loss as well as identifying the areas of fat deposition that provide a comprehensive picture of the obesogenic perinatal environment (Dulloo et al., 2010). However, studies involving human samples can also be challenging to control and interpret. Firstly, it is not clear if the experimental readouts in human studies are direct consequences of obesity or mediated by comorbidities associated with obesity. Although large epidemiological studies are successful in establishing associations between maternal BMI and adverse offspring outcomes, they do not provide precise mechanisms of action. Finally, it is not feasible to study the impact of maternal obesity on immune cells in maternal/fetal tissue compartments. Nevertheless, the placenta, cord blood, and microbiota provide practical avenues to study fetal reprogramming.

The use of animal models obviates some aforementioned hurdles and allows a more mechanistic approach to identify molecular underpinnings of observed outcomes (Williams

et al., 2014). One major challenge with animal models is establishing the duration of nutritional insult, which is critical in mimicking outcomes observed in human subjects. In this section, we briefly describe frequently used animal models for studying the impact of maternal obesity on both the maternal and fetal immune systems. Extensive details of these models have been reviewed in (Alfaradhi and Ozanne, 2011; Nathanielsz et al., 2007; Williams et al., 2014). Rodent models are often used to study developmental reprogramming, owing to their short gestation, genetic homogeneity, ease of genetic manipulation, and access to multiple tissues (Li et al., 2011). These studies have linked maternal overnutrition using high fat diet (HFD) or western diet (WD) to poor fetal growth, metabolic syndrome, and behavioral outcomes in the offspring (Bouanane et al., 2010; Elahi et al., 2009; Samuelsson et al., 2008).

Rat models using Sprague-Dawley and Wistar strains have also been used to study the effects of nutritional status during pregnancy on short term and long-term offspring health (Dunn and Bale, 2009; Jones et al., 2009; Kirk et al., 2009). In contrast to mouse strains, rats are outbred thereby providing greater genetic heterogeneity and offering the advantage of having larger placentas and fetuses. Finally, rodent models have been developed to study the impact of maternal adiposity on fetal health, independent of dietary fat intake (Shankar et al., 2008). However, several key differences exist between rodent and human immune systems. First, unlike humans, splenic hematopoiesis persists in rodents for several weeks after birth (Holladay and Smialowicz, 2000). Secondly, T and B cell development is not complete at birth and several subsets of T lymphocytes are absent in 10 days old pups (Ladics et al., 2000). These limitations can be in part overcome by the use of larger animal models. For example, sheep are precocial species like humans and have been

used to study fetal growth and metabolic consequences in the context of maternal obesity (George et al., 2010; Long et al., 2015). Furthermore, sheep models of maternal obesity have recapitulated increased offspring predisposition to cardiac (Huang et al., 2010) and hepatic dysfunction (Nicholas et al., 2013). However, sheep have a distinct placentation compared to humans and hence, may not be ideal for studying immune development at the maternal-fetal interface.

Non-human primates (NHPs) are closely related to humans and have been used extensively to study fetal-placental adaptations. NHPs are born with a fully functional immune system that shares significant homology with that of humans, making them a particularly attractive alternative for *in utero* immune reprogramming studies. Although rhesus macaques have a bidiscoid placenta (Grigsby, 2016), baboons have very similar placental structure as humans (Comuzzie et al., 2003). Research groups have leveraged baboons (Farley et al., 2009), rhesus macaques (McCurdy et al., 2009; Sullivan et al., 2010), and Japanese macaques (Frias et al., 2011) to model adiposity and inflammation both on the maternal and fetal fronts.

1.2 Evidence of fetal immune reprogramming by pregravid obesity.

Recent studies have documented that the adverse impact of maternal pregravid obesity on fetal cellular developmental processes extend beyond the cardiovascular and central nervous system and have a significant impact on phenotypic and functional aspects of offspring immunity (Figure 1.1). The profile of the immune system and the magnitude of its responses vary significantly with gestational and post birth age. Greater details about the cellular ontogeny and developmental timing of immune cells in utero can be obtained from these reviews (Dowling and Levy, 2014; Kollmann et al., 2017; Kollmann et al., 2012).

Fetal hematopoiesis occurs in distinct spatial and temporal sites: the extraembryonic yolk sac, the fetal liver, and the bone marrow (Figure 1.2). Development of fetal innate immune cells in these sites occur in waves starting as early as day 18 (Fukuda, 1973). Neutrophils (De Kleer et al., 2014) and monocytes (De Kleer et al., 2014; Mikkola and Orkin, 2006) appear in the fetal liver at gestational weeks 5 and 6 respectively. Monocyte progenitors then colonize various organs and compartmentalize into specialized life-long tissue-resident macrophages (De Kleer et al., 2014). Mature B-lymphocytes appear first in the fetal liver at 8 weeks of gestation, then in circulation at gestational week 12 (Thilaganathan et al., 1993). By contrast, T cell progenitors appear in the thymus at week 8-9 and in circulation at 14 weeks of gestation. Therefore, *in utero* development of both branches of the immune system in humans provides a unique window of opportunity for maternal nutritional status to influence fetal developmental reprogramming. In this section, we summarize our current understanding of the influence of maternal obesity on fetal immune profile and response.

1.2.1 Impact of maternal obesity on phenotypic and functional changes in cord blood cells.

Clinical studies are limited to the profiling of cord blood, which serves as an excellent surrogate for a snapshot of the fetal immune system at birth (Levy, 2005). These studies link pregravid maternal BMI and changes in immune cell frequency and phenotype in cord blood (Gonzalez-Espinosa et al., 2016; Ibrahim et al., 2017; Wilson et al., 2015). Our recent study reported a drop in eosinophils and CD4+ T cells in the cord blood (Wilson et al., 2015) with pregravid obesity after controlling for several maternal factors (race, maternal infection, gestational diabetes, gestational hypertension, and preeclampsia). A

second retrospective study reported that pregravid maternal BMI positively correlated with frequencies of NK T cells and regulatory CD8+ T cells and negatively correlated with that of CD34+ stem cells in cord blood samples (Gonzalez-Espinosa et al., 2016). More recent work reported higher numbers of immunosuppressive nucleated RBCs (Ibrahim et al., 2017) in cord blood of babies born to mothers with obesity.

From a functional standpoint, maternal BMI is negatively correlated with cord blood CD4+ T cell IL-4 production (Wilson et al., 2015). Additionally, cord blood monocytes are hyporesponsive to *ex vivo* stimulation with TLR agonists in the absence of any differences in the relative frequencies of classical and non-classical monocytes (Wilson et al., 2015) or differences in surface expression of CD14, CD16 or TLR4 (Sureshchandra et al., 2017). This phenotype was consistent when purified monocytes were used, suggesting a cell-intrinsic defect (Sureshchandra et al., 2017). A more recent study reported that cord blood monocyte-derived macrophages (MoDM) from babies born to mothers with obesity showed a basal anti-inflammatory phenotype and exhibited unbalanced responses to M1 and M2 polarization stimuli (Cifuentes-Zuniga et al., 2017). These *in vitro* findings are line with recent clinical data indicating increased incidences of severe bacterial infections (Kleweis et al., 2015) and sepsis (Polnaszek et al., 2018) necessitating NICU admission in neonates born to mothers with BMI >30 (Rastogi et al., 2015; Scott-Pillai et al., 2013) and highlight the importance of cord blood monocytes as critical early pathogen sensors and phagocytes in the neonate. Surprisingly, pregravid maternal BMI did not impact resting gene expression in cord blood monocytes, suggesting a significant role for epigenetic poising. Indeed, dampened monocyte responses to LPS were mirrored at the transcriptional level and was partially explained by loss of DNA cytosine methylation at

promoters of inflammatory genes such as *PPARG*, *FOLR2*, and *ITGAX* (Sureshchandra et al., 2017).

Poor *ex vivo* monocyte responses in the offspring with pregravid obesity could potentially be tied to an altered inflammatory intrauterine environment. Very high maternal BMI (>35) has been associated with elevated systemic levels of inflammatory mediators, notably TNFα and CRP in the cord plasma (Dosch et al., 2016; McCloskey et al., 2018). In addition to these canonical inflammatory markers, maternal BMI is also a strong indicator of cord blood levels of malondialdehyde (MDA) and nitric oxide (NO), contributing to increased oxidative stress in the newborn (Gallardo et al., 2015). In agreement with this hypothesis, transcriptional studies in cord blood from mothers with high BMI have demonstrated elevated expression of genes involved in cellular response to oxidative stress and inflammatory signaling, independent of offspring adiposity (Edlow et al., 2016). Gene expression studies in NHP models have extended these findings and reported altered expression of several markers of vascular inflammation and altered endothelial cell function in offspring of dams with high pregravid BMI (Fan et al., 2013). Additionally, PBMC isolated from offspring of obese and lean baboons (based on pre-pregnancy BMI) revealed widespread transcriptional changes in genes inherent to antigen presentation pathways, complement and coagulation pathways, leukocyte trans-endothelial migration, signaling pathways (BCR signaling, MAPK, and VEGF signaling) (Farley et al., 2009). These observations provide evidence of fetal reprogramming events that persist during early childhood.

1.2.2 Maternal obesity and alterations in offspring lymphoid tissue resident cells.

Studies using a variety of animal models have assessed the impact of pregravid maternal obesity on tissue-resident immune cells in the offspring (Figure 1.1). Some of the earliest studies using mice demonstrated that the pups born to dams fed a HFD during gestation had an altered immune system regardless of postnatal diet (Myles et al., 2013; Odaka et al., 2010). One key study concluded that gestational HFD exposure results in fewer splenic lymphocytes and thinner thymic cortex (Myles et al., 2013). More importantly, pups born to dams fed a HFD diet during gestation exhibit impaired antigen-specific immune responses as evidenced by: (a) higher mortality rates in an *E. coli* sepsis model; (b) increased bacterial burden; (c) larger abscesses following Methicillin-resistant Staphylococcus aureus (MRSA) infection (Myles et al., 2013); and exacerbated respiratory disease following infection with respiratory syncytial virus (RSV) (Ferolla et al., 2013; Griffiths et al., 2016). Furthermore, *in utero* HFD exposure resulted in reduced production of IL-6 and TNFα by fetal splenocytes following ex vivo LPS stimulation. In contrast, IL-17, IL-6, and TNFα production by colonic lamina propria lymphocytes (LPLs) was significantly higher in pups born to HFD-fed dams following stimulation (Myles et al., 2013). Additionally, pups born to obese dams were also more likely to develop signs of experimental autoimmune encephalitis (EAE) (Myles et al., 2013). This heightened susceptibility correlated with reduced frequencies of regulatory T cells both in the spleen and the colon (Myles et al., 2013). Finally, offspring with HFD exposure both during gestation and post weaning produced higher antigen-specific (ovalbumin) IgE and lower IgG following *in vivo* immunization, potentially linking maternal pregravid obesity to increased risk of allergic responses and autoimmunity in the offspring (Odaka et al., 2010).

Taken together, data from both rodent models and human studies suggest that pregravid maternal obesity dysregulates offspring immunity, where antimicrobial defenses are dampened while aberrant inflammatory responses such as autoimmune responses are enhanced.

1.2.3 Maternal obesity and immune homeostasis in non-lymphoid tissues in the offspring.

Several lines of evidence suggest that maternal obesity significantly reprograms the liver of the offspring, contributing to metabolic disease. Exposure to an obesogenic diet both during gestation and post weaning contributes to higher frequencies of Kupffer cells in the offspring liver. Furthermore, Kupffer cells in the offspring of HFD-fed dams were less phagocytic and produced higher levels of ROS (Mouralidarane et al., 2013). Gene expression studies in infant rhesus macaques exposed to HFD during gestation provide substantial evidence of oxidative stress in fetal livers during the third trimester as evidenced by elevated expression of metabolic enzymes and lipotoxicity (McCurdy et al., 2009). Furthermore, cellular changes in fetal livers are observed as early as 8-12 weeks of gestation, with increased recruitment of proinflammatory macrophages in fetuses of dams exposed to WSD (Friedman et al., 2018). Surprisingly, bone marrow derived macrophages isolated 8 weeks postnatal from pups exposed to WSD *in utero* were hyper-responsive to LPS, as evidenced by elevated *Il1b*, *Tnf*, *Il6*, and *Il10* transcript levels (Friedman et al., 2018). This phenotype is in contradiction to the dampened response to LPS generated by cord blood monocytes in humans and splenocytes in mice and could potentially be explained by the extended culturing required to derive macrophages from bone marrow cells. Taken together, these observations indicate that the impact of pregravid maternal

obesity is highly dependent on the tissue examined, the stimulus used, and the age of the offspring.

More recent work has mechanistically linked liver inflammation in the offspring of mothers with obesity to alterations in the gut microbiome. Specifically, mice that received a fecal transplant from two-week old human babies born to mothers with obesity exhibit histological evidence of periportal inflammation, impaired macrophage phagocytosis, and dampened cytokine production, all hallmarks of non-alcoholic fatty liver disease (NAFLD) (Soderborg et al., 2018). Furthermore, hepatic gene expression signatures in recipient mice suggest ER stress and reprogramming of innate immune cells (Soderborg et al., 2018). Similar phenotypes have also been reported in adipose tissues, where offspring of obese dams had higher *CD68*, *CCR2*, and *TNFA* transcript levels, indicative of a shift towards a more inflammatory phenotype potentially due to increased infiltration of macrophages (Murabayashi et al., 2013). Whether these macrophages respond differently to stimulation is still untested. Finally, reduced expression of *Glut4* gene in the subcutaneous fat of these offspring suggests potential metabolic reprogramming (Murabayashi et al., 2013).

In addition to the liver and spleen, exposure to HFD during gestation alters inflammatory responses in the fetal gut. Specifically, rodent studies have reported enhanced susceptibility to DSS induced colitis in the offspring that was accompanied by up regulation of NF-κB signaling and expression of *Il1b*, *Il6*, and *Il17* genes (Bibi et al., 2017). This phenotype was associated with increased neutrophil infiltration in the gut, paralleled with higher *Ccl2* transcripts (Bibi et al., 2017). A sheep model of maternal obesity reported similar changes in the fetal gut as early as the second trimester, with increased expression of monocyte/macrophage genes *TNF*, *IL1B*, *IL6*, *IL8*, *CCL2*, *CD68*, *ITGAM* (encoding CD11b),

and *CD14* in fetal large intestine (Yan et al., 2011). Furthermore, both mRNA and protein levels of TGF-β were elevated in gut tissue obtained from offspring of obese ewes. TGF-β plays a critical role in maintaining immune homeostasis and regulating interactions between the microbiota and lymphocytes in the gut (Bauche and Marie, 2017). Increased levels of TGF-β could potentially predispose the offspring to inflammatory conditions such as IBD (Yan et al., 2011). In line with these observations, mice exposed to gut microbes from two-week-old infants born to mothers with obesity had impaired gut barrier indicated by reduced gene expression of tight junction proteins *Tjp1* and *Ocln* and increased intestinal permeability (Soderborg et al., 2018). In addition, infants born to mothers with obesity show dysbiosis in their gut microbiome (Collado et al., 2010; Mueller et al., 2016) for up to 2 years (Galley et al., 2014). Mechanisms by which changes in microbial abundance or composition modulate gut immune responses still remains to be investigated.

Finally, mouse models have recently revealed that the impact of maternal obesity extends to microglia in the offspring brain. Specifically, CD11b+ cells from offspring born to obese dams exhibit exaggerated TNFα responses to LPS (Edlow et al., 2018). This observation is in line with an increased incidence of autism, and Attention Deficit/Hyperactivity Disorder (ADHD) in offspring of mothers with obesity (Gardner et al., 2015; Jo et al., 2015; Li et al., 2016; Rodriguez, 2010).

1.2.4. Pregravid obesity and changes in offspring stem cells.

Data from several studies indicate that hematopoietic stem cell (HSC) populations are exquisitely sensitive to an obesogenic environment. Using a combination of colony formation assays, flow cytometry, and gene expression experiments, studies showed that

maternal HFD restricts physiological expansion of fetal HSCs, compromises repopulation of precursor cells in fetal liver, and biases cellular differentiation towards the myeloid branch (Kamimae-Lanning et al., 2015). This bias towards myeloid lineage and dysregulated hematopoiesis was shown to be dependent on toll-like receptor 4 (TLR4) signaling (Liu et al., 2018). Moreover, metabolic rewiring and increased energy demand of stem cells have been recently reported in mesenchymal stem cells isolated from human cord blood samples obtained from babies born to mothers with obesity (Iaffaldano et al., 2018). These findings suggest that maternal obesity dysregulates bone marrow niche thereby potentially impacting maturation and development of various immune subsets pre- and postnatally.

1.3. Pregravid obesity and inflammation at the maternal-fetal interface

Structurally, the interface between the uterine mucosa and extraembryonic tissue comprise the "maternal-fetal interface" or the placenta. At term, this interface includes the maternal portion called the decidua (or decidua basalis), which is primarily the uterine mucosal layer after it has undergone the implantation-associated differentiation process called decidualization. The fetal portion of the placenta is called the villous chorion, which allows for the transfer of nutrients from maternal blood to fetal circulation. A successful pregnancy involves complex interactions between the immune cells residing at the maternal-fetal interface (Maltepe and Fisher, 2015) and circulating maternal factors that could culminate into secretion of immune mediators into fetal circulation (Altmae et al., 2017; Bronson and Bale, 2014). During the first trimester, the placenta enables the establishment of pregnancy, providing physical support and immunologic tolerance to the developing embryo (Suryawanshi et al., 2018). As gestation progresses, the placenta takes over the roles of facilitating gas exchange as well as the transfer of nutrients, waste

products, hormones, and other immune mediator that support fetal growth and impact development and maturation of the offspring immune system (Zaretsky et al., 2004). Finally, closer to parturition, the cells in the placenta promote contraction of the uterus, the expulsion of the baby and rejection of the placenta (Romero et al., 2006). In the following section, we briefly summarize the impact of pregravid obesity on placental structure and function as well as the role of these changes in reprogramming the fetal immune system (Figure 1.3).

1.3.1 Pregravid obesity and placental structure.

Data from animal model studies show that consumption of HFD increased placental glucose, amino acid, and fatty acid nutrient transport in dams (Acosta et al., 2015; Jansson et al., 2013; Jones et al., 2009; Lager et al., 2016; Rosario et al., 2015) (Figure 3). Evidence for altered trophoblastic invasion and vessel remodeling have been reported in a rat model of HFD induced obesity (Hayes et al., 2014; Lenartowicz et al., 2015). Furthermore, placentas of rhesus macaque dams fed a HFD exhibited reduced blood flow, increased calcification and risk for infarction (Frias et al., 2011). A reduction in placental microvessel density has been observed as early as mid-gestation in a mouse model of diet-induced obesity (Stuart et al., 2018). In obese human subjects, significant structural changes in the placenta have been observed, ranging from alterations in placental maturity, vessel density, muscularity in blood vessels (Roberts et al., 2011) and non-branching angiogenesis in term placentas (Dubova et al., 2011).

Inflammation in the placenta has a bidirectional effect on both the maternal and fetal immune systems (Mor and Cardenas, 2010). Transcriptional studies using human term placenta have reported changes in genes regulating inflammation, lipid storage and

transport (Hirschmugl et al., 2017), insulin resistance, as well as angiogenesis in both the decidua (Altmae et al., 2017) and villi (Saben et al., 2014; Sureshchandra et al., 2018) with pregravid obesity. Similarly, RNA-Seq analysis of villous tissue revealed downregulation of several genes involved in inflammation (*IL1R2, IL2RB, C3, TNFSF10*), immune tolerance (*HLAG*), cell matrix communication, nutrient transport, and retinoic acid metabolism with pregravid obesity (Sureshchandra et al., 2018). While the source of placental inflammation is not clear, it has been linked to the high levels of oxidative stress and lipotoxicity in the decidua of obese mothers (Saben et al., 2014). In the next section, we describe the consequences of pregravid obesity on the immune landscape at the maternal-fetal interface.

1.3.2 Pregravid obesity and immune adaptations in the placenta.

Technical advances in single cell RNA sequencing has allowed for high throughput profiling of immune cells in the early placental bed in an unbiased manner (Suryawanshi et al., 2018; Vento-Tormo et al., 2018). These studies indicate the presence of NK cells, macrophages, and T-cells as well as differences in origin, phenotype, and function of immune cells within the decidua and villous compartments. For example, the decidual immune cells, which are of maternal origin, are primarily composed of NK cells, macrophages, and T cells. Immune cells in the villi, which are of fetal origin, are primarily composed of macrophages (Suryawanshi et al., 2018). The composition of placenta-resident immune cells shifts considerably over the course of gestation (Ander et al., 2019; Lewis et al., 2018; Mor et al., 2017). For instance, studies have reported decreased IL-35 and IL-9 levels and concurrent drop in CD11c+ myeloid cells and regulatory T cell populations over the course of gestation (Lewis et al., 2018).

Local changes in frequencies, phenotype, and functions of immune cells in the decidua and villi have been attributed in the pathogenesis of several obstetric complications such as preterm labor (Cappelletti et al., 2016), preeclampsia (Boucas et al., 2017; Faas and De Vos, 2018; Geldenhuys et al., 2018) and chorioamnionitis (Ben Amara et al., 2013). Indeed, first trimester placentas from women with obesity show reduced uterine NK cell numbers, which normally comprise ~70% of the leukocyte population in early human decidua and play a central role in uterine artery remodeling and altered expression of genes associated with matrix remodeling and growth factor signaling (Perdu et al., 2016) (Figure 1.3). Furthermore, first trimester uNK cells from women with obesity exhibited an imbalance in the expression of NK cell receptors KIR2DL1 (inhibitory receptor) and KIR2DS1 (activating receptor), ultimately favoring HLA-C2 directed activation (Castellana et al., 2018). Finally, leptin levels have been linked to altered expression of CD56 and CD16 on circulating NK cells during pregnancy (Orlova and Shirshev, 2009). Therefore, it is possible that obesity-associated increase in leptin levels could also modulate phenotype and function of uterine NKs, however, this hypothesis has yet to be tested.

Macrophages comprise 20% of the decidual leukocyte population. These cells are distinct in their origin but are functionally similar to their fetal counterpart called the "Hofbauer cells". Decidual macrophages play important roles in maintaining immune tolerance (Gustafsson et al., 2008), protecting the fetus against infectious agents (Singh et al., 2005), spinal artery remodeling (Nagamatsu and Schust, 2010), and clearance of apoptotic bodies from the placental vasculature (Abrahams et al., 2004). Although these cells are extremely heterogeneous, the phenotypic and functional changes in the decidual macrophage populations over the course of gestation remain ill-defined (Houser, 2012). In

humans, pregravid obesity results in an increased accumulation of macrophages (CD68+) in the placenta (Challier et al., 2008; Roberts et al., 2011). In line with these observations, higher transcript levels of pro-inflammatory genes *IL6*, *CCL2*, *IL8*, and *TLR4* are detected in a baboon model of HFD-induced obesity (Frias et al., 2011; Yang et al., 2016). Similarly, chorionic villi macrophages obtained from placentas of diet-induced obese dams generate exacerbated responses to LPS (higher TNFα, IL-6, and IL-1β) both at the gene and protein levels, suggesting functional reprogramming of fetal macrophages as well (Edlow et al., 2018). A more recent study demonstrated reduced frequency of M1-like macrophages (HLA-DR+ CD163-) in the decidua with pregravid obesity (Laskewitz et al., 2019), potentially a compensatory mechanism against obesity-associated inflammation.

In addition to immune cells, the placenta harbors a low abundance but metabolically rich microbiome (Aagaard et al., 2014) that varies from the decidua to basal plates to the fetal membranes (Parnell et al., 2017). This microbial community is disrupted with preterm labor (Prince et al., 2016), preeclampsia (Amarasekara et al., 2015) and gestational weight gain (Antony et al., 2015), and pregravid obesity (Sureshchandra et al., 2018). Some of these studies were carried out using placenta samples of preterm births; therefore, our understanding of the impact of pregravid obesity on microbial communities within the term placental decidua remains limited.

1.4 Pregravid-obesity induced changes in systemic maternal immunity.

1.4.1 Immunological adaptations with pregnancy and obesity.

Immune cells within the decidual membranes are derived primarily from maternal circulation. Therefore, inflammatory changes in the placenta could be linked to pregravid obesity-induced changes in systemic immunity. Recent proteomic and immunological

studies in peripheral blood have suggested the existence of an "immunological clock of pregnancy" characterized by enhanced immune activation with gestation (Aghaeepour et al., 2017; Aghaeepour et al., 2018) (Figure 1.4). Changes in the maternal adaptive immune include decreased Th1/Th17 and increased Th2/Treg responses (Aghaeepour et al., 2017; Luppi et al., 2002b; Polese et al., 2014). Changes in maternal innate immune responses include increased surface expression of CD11a, CD11b, CD49d, CD14, CD64, and CD54 on monocytes during third trimester (Faas et al., 2000; Naccasha et al., 2001; Sacks et al., 1998). Moreover, production of pro-inflammatory cytokines IL-1β, IL-12, IL-6 and oxygen free radicals following stimulation with LPS or bacteria (Aghaeepour et al., 2017; Luppi et al., 2002b; Sacks et al., 2003) as well as responses to viral particles by NK cells (Kay et al., 2014), monocytes (Aghaeepour et al., 2017) and plasmacytoid dendritic (pDC) cells (Le Gars et al., 2016) were enhanced with gestation. While the mechanisms regulating these changes are still unknown, several studies have hypothesized a role for placental microparticles (Redman et al., 2012), fetal DNA (Bianchi et al., 1996), and maternal metabolic and cytokine changes (Aghaeepour et al., 2018; Sacks et al., 2001). However, it should be noted that these studies were largely carried out using total peripheral blood mononuclear cells (PBMC) and therefore intrinsic changes within specific immune cell subsets remain largely ill defined.

The impact of pregravid obesity on the maternal immune system and the immune clock of pregnancy are still unclear. One study reported reduced CD8+ and NK T cells, impaired Th1 and Th2 cytokine responses and proliferation following polyclonal activation (Sen et al., 2013). A second study showed fewer circulating plasmacytoid DCs (pDCs), increased differentiation of CD4 T cells, reduced Th17 response, and dysregulated cytokine

responses following TLR stimulation (Sureshchandra et al., 2018). Therefore, there is an urgent need for longitudinal studies that better capture disruption of the pregnancy immunological clock with pregravid obesity. Dysregulation of innate immune responses is in line with poor infection outcomes during pregnancy and delayed wound healing following C-section in pregnant women with obesity.

1.4.2 Maternal obesity and circulating cytokine environment

Obesity exacerbates inflammatory changes normally associated with pregnancy (Pendeloski et al., 2017) (Figure 1.3). While most studies have consistently reported increased IL-6 levels with higher pregravid BMI in pregnant women (Basu et al., 2011a; Catalano et al., 2009a; Christian and Porter, 2014; Curry et al., 2008; Friis et al., 2013; Holtan et al., 2015; Ramsay et al., 2002; Roberts et al., 2011; Sen et al., 2014; Stewart et al., 2007), others have reported no associations at all (Aye et al., 2014; Farah et al., 2012; Kac et al., 2011). These inconsistencies arise due to sample size limitations, variability in exclusion criteria, racial differences in cohorts, and the precise time of sample collection (first, second, third trimester, at term, during labor or post-partum). On the other hand, all studies report a significant increase in CRP, a canonical marker of inflammation produced by the liver, during various stages of pregnancy with pregravid BMI (Basu et al., 2011a; Catalano et al., 2009a; Challier et al., 2008; Christian and Porter, 2014; Gavrila et al., 2003; Kac et al., 2011; Sen et al., 2013; Sen et al., 2014; Stewart et al., 2007; Sureshchandra et al., 2018). Pregravid obesity also impacts circulating levels of GM-CSF and FGF-2 (Sureshchandra et al., 2018). In contrast, several studies found no association between high pregravid BMI and circulating TNFα (Aye et al., 2014; Challier et al., 2008; Farah et al., 2012; Founds et al., 2008; Sen et al., 2013; Walsh et al., 2013), IL-1β (Christian and Porter,

2014; Farah et al., 2012; Ferraro et al., 2012; Roberts et al., 2011; Sureshchandra et al., 2018), or anti-inflammatory IL-10 (Friis et al., 2013; Sen et al., 2014; Stewart et al., 2007; Sureshchandra et al., 2018) during pregnancy.

Profiles of circulating chemokines have also been shown to vary with pregnancy (Du et al., 2014; Segerer et al., 2009). Significant shifts in chemokine profiles, notably CCL2 (MCP-1) at the maternal-fetal interface, have been shown to trigger labor (Bardou et al., 2014) and in some cases even initiate obstetric complications (Du et al., 2014). Pregravid obesity has been shown to elevate circulating innate immune cell recruiting factors CCL2 at various stages of pregnancy (Aye et al., 2014; Friis et al., 2013; Madan et al., 2009; Sureshchandra et al., 2018) and CXCL8 at term (Sureshchandra et al., 2018). There is emerging evidence of some cytokines such as IL-6 bidirectionally crossing placental barriers (Zaretsky et al., 2004), however, whether similar patterns exist for other hormone/cytokines is still unclear.

Glucose tolerance and insulin resistance, often observed during pregnancy, are exacerbated with high pregravid BMI. Women with obesity exhibit significantly high levels of insulin at term, which vary linearly with BMI (Sureshchandra et al., 2018). Similarly, other mediators associated with insulin resistance are also impacted by pregravid obesity. For example, leptin, a pro-inflammatory mediator that modulates appetite, implantation, and immune responses during pregnancy increases with gestation (Briana and Malamitsi-Puchner, 2009) and drops immediately after delivery (Schubring et al., 1998; van der Wijden et al., 2013). During pregnancy (Franco-Sena et al., 2016), serum leptin levels positively correlate with BMI and fat mass and remain significantly higher in obese mothers at term (Franco-Sena et al., 2016; Ozias et al., 2015; Sureshchandra et al., 2018). In

contrast, while some studies report a positive association between pregravid BMI and circulating resistin levels (Kusminski et al., 2005; Palik et al., 2007), others report no relationship (Rea and Donnelly, 2004; Shetty et al., 2004). Taken together, these studies highlight the systemic impact of high BMI on chronic inflammation, immune activation, glucose tolerance, and insulin resistance.

1.5 Mechanisms linking maternal obesity and fetal immune dysfunction – role of epigenetic reprogramming.

The mechanisms that link the maternal obesogenic environment with immune dysregulation observed in the offspring are not completely understood (Figure 1.5). It is well accepted that the fetus is exposed to a heightened inflammatory milieu. Direct and indirect exposure to this inflammation, via nutrients or cytokines occurs through the placenta. The placenta itself harbors cells (immune and non-immune) that respond to conditions of oxidative stress and nutrient deficits by secreting various immune mediators, hormones, and growth factors into the fetal circulation. Indeed, newborns of mothers with obesity have higher levels of leptin, and IL-6 in cord blood compared to newborns of lean mothers (Catalano et al., 2009a). However, no studies to date have systematically measured maternal and cord blood cytokine levels in matched mother-baby pairs to assess potential transplacental transfer of inflammatory factors with the exception of IL-6 (Aaltonen et al., 2005; Zaretsky et al., 2004).

Maternal lipids are also known to cross the placenta and contribute to fetal cholesterol synthesis, particularly during early gestation (Herrera et al., 2006). Fetal exposure to excess lipids, particularly saturated fatty acids, can activate proinflammatory pathways impacting nutrient metabolism, mitochondrial function, hematopoietic stem cell

fate, and immune cell plasticity. Excess nutrients such as lipids can rewire cellular metabolism through epigenetic mechanisms, triggering transcriptional adaptations that ultimately alter immune cell function. For example, maternal obesity has also been shown to alter expression of mitochondrial and lipid metabolism genes in human infant umbilical vein endothelial cells (Costa et al., 2016). Evidence of transcriptional reprogramming has been reported as early as the blastocyst stage in rats, with up-regulation of NF-κB regulated *Ccl4* and *Ccl5* in embryos of obese dams (Borengasser et al., 2011). These observations could explain the heightened inflammatory response of bone marrow derived macrophages and tissue-resident macrophages in pups born to obese dams following LPS stimulation (Edlow et al., 2018; Friedman et al., 2018; Soderborg et al., 2018). Interestingly, animal studies have demonstrated that parental diet influences lipid content, mitochondrial activity, and epigenomes of oocytes and sperm, predisposing the offspring to metabolic conditions such as obesity and insulin resistance (Lane et al., 2014; Lane et al., 2015; Wu et al., 2015). These findings suggest that in addition to exposure to inflammation during gestation, a significant contribution to fetal reprogramming is promoted within gametes.

Several studies have reported significant changes in gene expression patterns in various fetal compartments as a consequence of pregravid obesity. These transcriptional alterations can be regulated via epigenetic mechanisms such as DNA methylation, chromatin remodeling, and post-transcriptional regulation via microRNAs, which have been hypothesized as central to the fetal origins of adult health and disease (Calkins et al., 2015). DNA methylation patterns are established mainly during embryogenesis or early postnatal life. Within the immune system, DNA methylation play critical roles in

hematopoiesis and can vary within cells of a particular lineage depending on their source (fetal liver, cord blood, bone marrow vs. peripheral blood) (Farlik et al., 2016). Additionally, methylation patterns overlapping enhancers and promoters of lineage-determining factors define differentiation trajectories of immune cells during development (Farlik et al., 2016). Maternal hyperglycemia has been shown to decrease methylation of the leptin gene (*LEP*) in the offspring, contributing to high leptin levels in cord blood of babies born to obese mothers (Gallardo et al., 2015). Similarly, maternal BMI has been linked to methylation levels of several loci in the cord blood, the majority of which persist into adolescence independent of paternal BMI and gestational weight gain; (Sharp et al., 2015; Sharp et al., 2017). Studies focusing on immune cells have demonstrated that high maternal BMI is inversely correlated with methylation levels within the promoter of inflammatory genes in cord blood mononuclear cells (Liu et al., 2014) that persisted for up to three years of age (Herbstman et al., 2013). Recent studies carried out using targeted bisulfite sequencing in purified cord blood monocytes demonstrated that pregravid maternal obesity is associated with DNA hypomethylation, particularly at promoters of transcription factors such as *PPARG* that are associated with dampened transcriptional responses to LPS (Sureshchandra et al., 2017).

Maternal pregravid obesity is also associated with reduced abundance of the repressive histone mark H3K27me3 and increased expression of Zfp423, a key regulator committing cells to adipogenic lineage (Yang et al., 2013) within fetal adipose tissue in rodent models. Furthermore, altered expression of *Wnt* genes in livers of offspring born to dams on HFD show hyperacetylation of Histone H4 and H3K9 (Yang et al., 2012). Additionally, studies in Japanese macaques have demonstrated elevated acetylation of the

histone marks H3K9, H3K14, and H3K18 in fetal hepatic tissue exposed to HFD *in utero* (Aagaard-Tillery et al., 2008). Elevated histone acetylation, particularly in fetal livers has been linked to reduced SIRT1 (histone deacetylase) activity. Interestingly, these epigenetic changes alter expression of metabolic regulators PPARs and fatty acid synthases (Suter et al., 2012) and mitochondrial *SIRT3* transcripts (Borengasser et al., 2011). On the other hand, repressive marks such as H3K9Me3 have been shown to be amplified on *TLR4* and *LBP* gene promoters in splenocytes of HFD-fed dams offspring contributing to poor responses to LPS stimulation (Myles et al., 2013). Collectively, these data indicate the cell specific nature of epigenetic burden and the need for more studies linking these changes with functional outcomes in the offspring.

Finally, the expression of metabolic hormones at the maternal fetal interface can also be regulated via epigenetic mechanisms. For example, studies have reported elevated leptin levels in cord blood with higher maternal BMI (Catalano et al., 2009a; Wilson et al., 2015) where it is negatively associated with leptin promoter methylation (Kadakia et al., 2017). A more recent study has demonstrated hypermethylation of *LEPR* (leptin receptor) promoter in the villi with high maternal BMI (Nogues et al., 2019). The biological consequences of these changes are an exciting future research avenue, given the poignant role for leptin in both nutrient sensing and regulating immune responses.

The precise series of events by which maternal environment/inflammation alter fetal epigenome are still unclear. However, it has been hypothesized that excess lipid exposure *in utero* (Heerwagen et al., 2010) or maternal cytokines and hormones exposes the fetus to inflammation, potentially impacting cellular metabolism in immune precursor cells (Kamimae-Lanning et al., 2015) thereby rewiring the epigenomes of mature fetal

immune cells. To that extent, efforts to decrease excess maternal lipid availability via dietary interventions has been proposed to be an efficient strategy to limit fetal reprogramming. Furthermore, molecular targets (such as TBK1) for limiting inflammation in the adipose tissue have been recently identified, providing new therapeutic avenues (Zhao et al., 2018). Recent studies using murine models have demonstrated that short-term maternal treatment with the antioxidant pyrroloquinoline quinone (PQQ) can mitigate fetal immune developmental reprogramming (Friedman et al., 2018).

In addition to limiting in utero exposure of maternal inflammation, defining the contribution of epigenetic defects towards fetal immune reprogramming could pave the way for future therapeutic interventions. Whether these changes contribute to adverse outcomes seen in offspring of obese mothers or of they represent cellular adaptations to sustained in utero exposure to inflammation is still up for debate. Future work in animal models will have to test if epigenetic changes in fetal cells can be linked to specific changes in offspring immune function. Nevertheless, these studies will demonstrate the importance of epigenetic mechanisms in intergenerational health and identify prospective therapeutic targets to limit reprogramming.

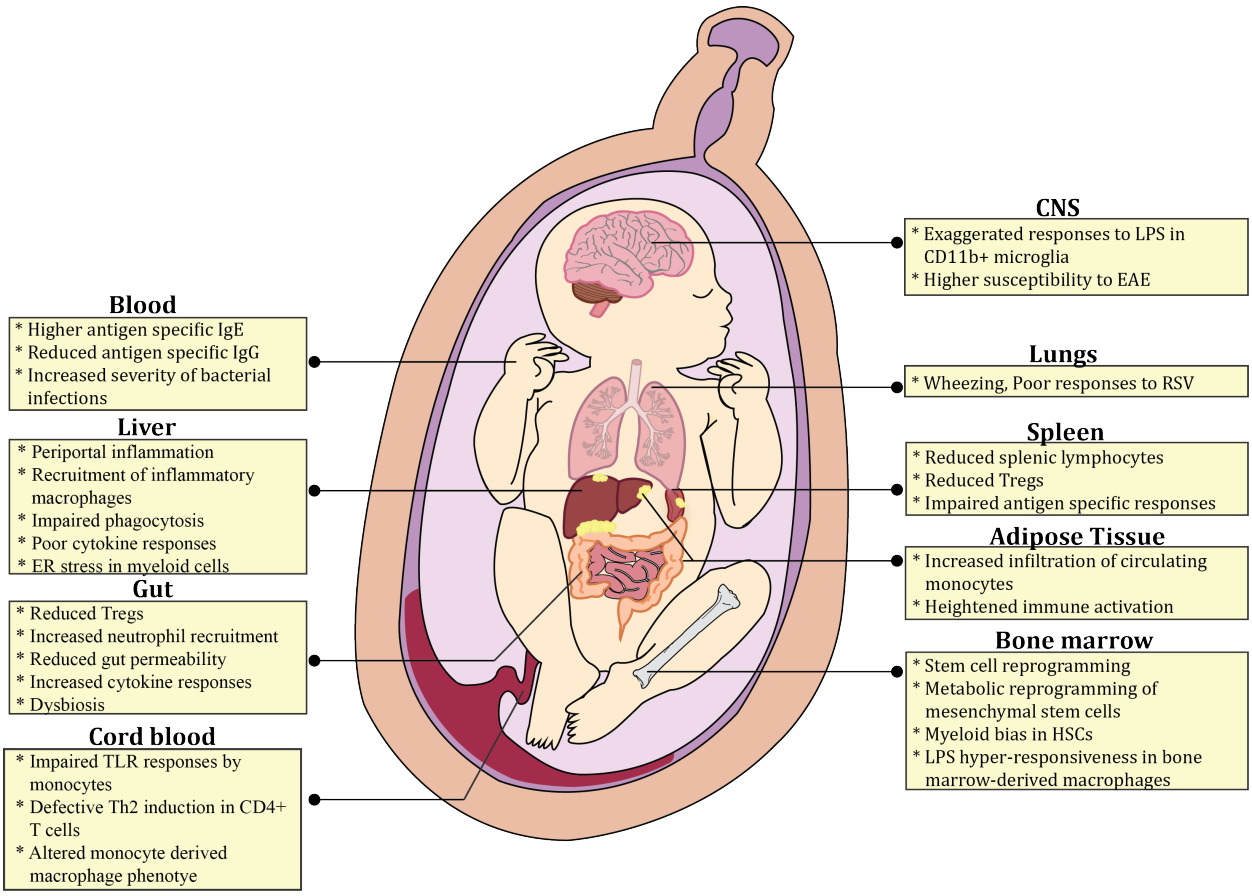

Figure 1.1 Pleiotropic impact of high pregravid BMI on circulating and tissue resident immune cells.

Studies using animal models and humans have demonstrated a significant tissue specific burden of maternal pre-gestational HFD/WSD and pregravid obesity on fetal immunity. Offspring of dams fed a HFD/WSD during gestation exhibit reduced frequencies of Tregs in spleen and gut, poor TLR responses, as well as impaired phagocytosis and antigen presentation in the liver and spleen. Heighted inflammation in the liver and adipose tissue is evidenced by increased infiltration of macrophages and high basal activation. Immune cells in the gut and microglia from the CNS exhibit hyper inflammatory responses to ex vivo stimulation, which correlated with increased incidence of autoimmune disease. Immune responses to microbial infection are dampened and monocytes respond poorly to stimulation with TLR agonists. Immune defects can be traced back to progenitors in the bone marrow suggesting long term and potentially irreversible effect of maternal pregravid obesity on offspring immunity.

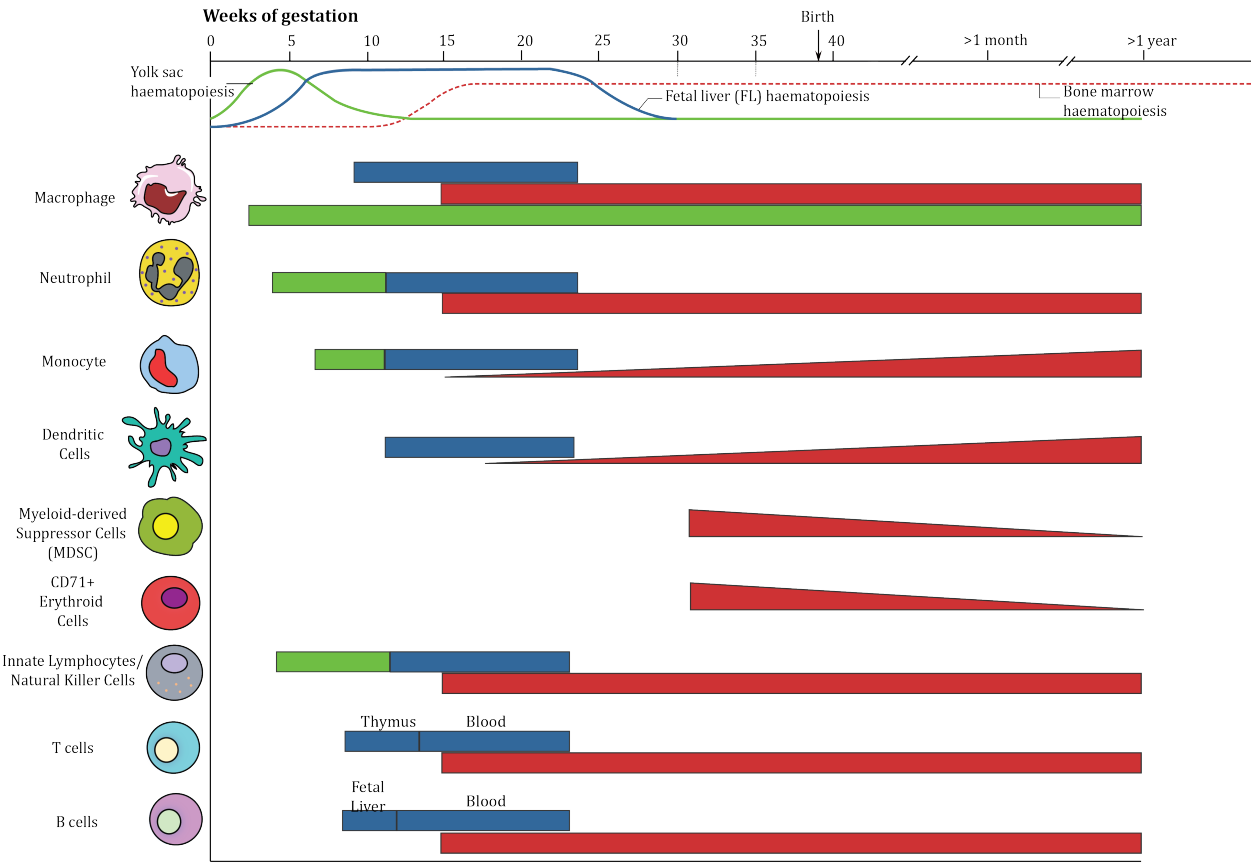

Figure 1.2 Overview of the ontogeny of the human immune system and composition of circulating immune cells at birth.

Hematopoiesis in a developing fetus occurs in three waves demonstrated on a gestational timeline – in the yolk sac (green lines and bars), fetal liver (blue lines and bars), and bone marrow (red lines and bars). Innate immune cells such as monocytes, neutrophils, macrophages, and innate lymphocytes begin their origins in the yolk sac, followed by fetal liver for a brief period. After week 15, granulocyte monocyte precursors originate from the bone marrow. Adaptive immune cells such as T cells and B cells emerge in the fetal liver at week 10, and in blood shortly after. Fetal blood prior to birth is also rich in myeloid derived suppressive cells (MDSCs) and CD71+ erythroid cells. The timing of each cell type is shown on the gestational time scale colored by their place of origin. Gradient bars demonstrate changes in frequencies of cells over the course of gestation.

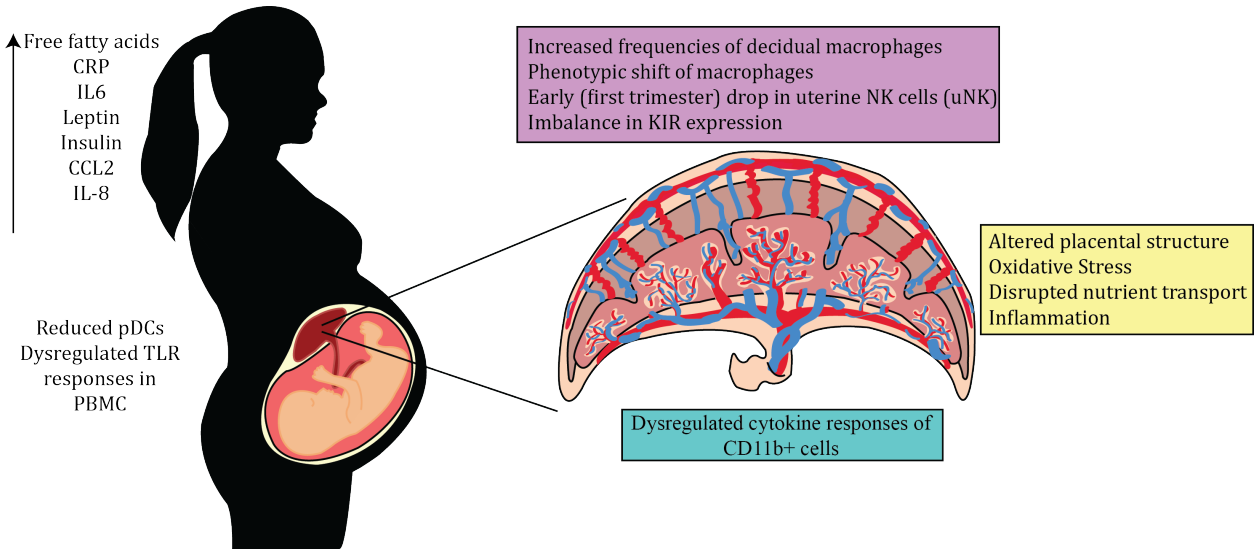

Figure 1.3 Impact of pregravid obesity on maternal systemic immunity and adaptations at the maternal-fetal interface.

The superimposition of pregravid obesity and pregnancy is associated with altered plasma levels of free fatty acids, inflammatory factors and hormones. These changes mirror disruptions in the placenta that include altered structure, microbiome, and potentially the balance of immune cells in both the decidua and villi.

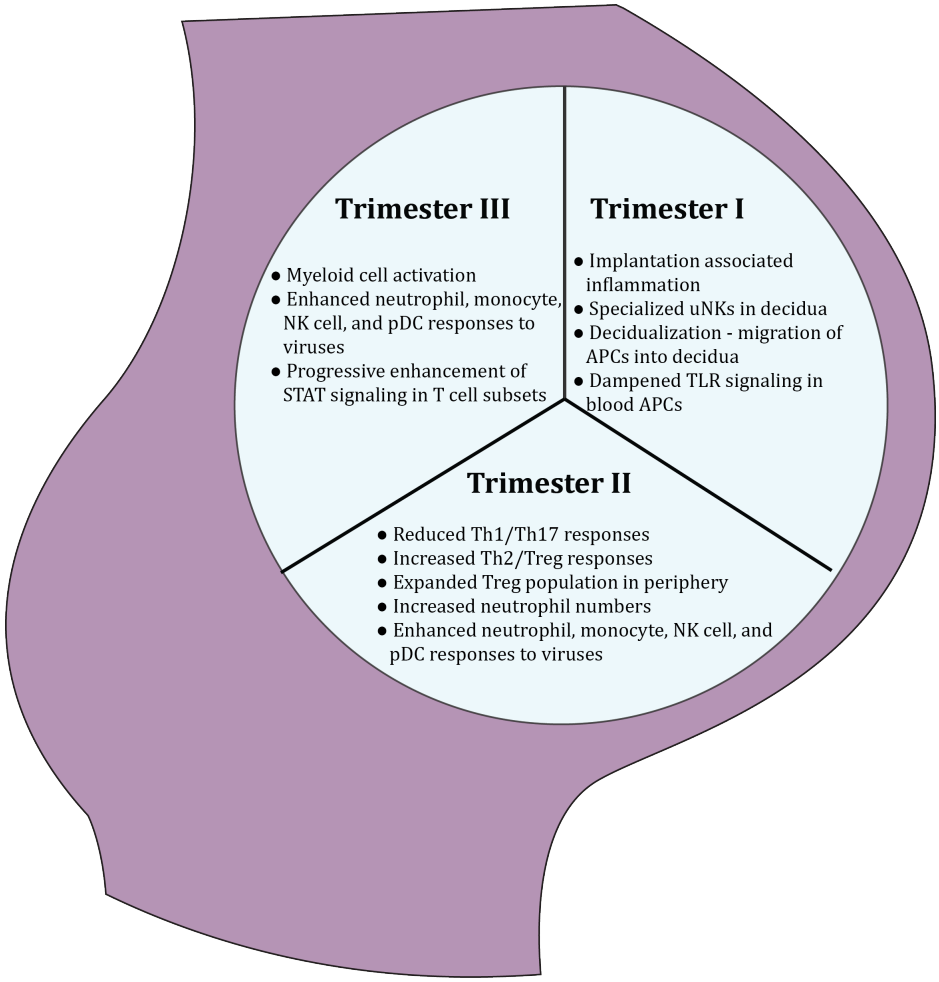

Figure 1.4 Immunological clock of human pregnancy.
Healthy gestation is associated with chronological changes in peripheral immunity and adaptations at the maternal fetal interface. Early gestation is associated with seeding of blood derived NK cells, dendritic cells, and monocytes into the placenta. During the first trimester, TLR signaling in circulating innate cells is suppressed. Second and third trimesters are associated with myeloid cell activation; progressive enhancement of viral responses in innate immune cells, and augmented STAT signaling in T cells. Inflammation at the maternal fetal interface contributes to dysregulated activation of labor.

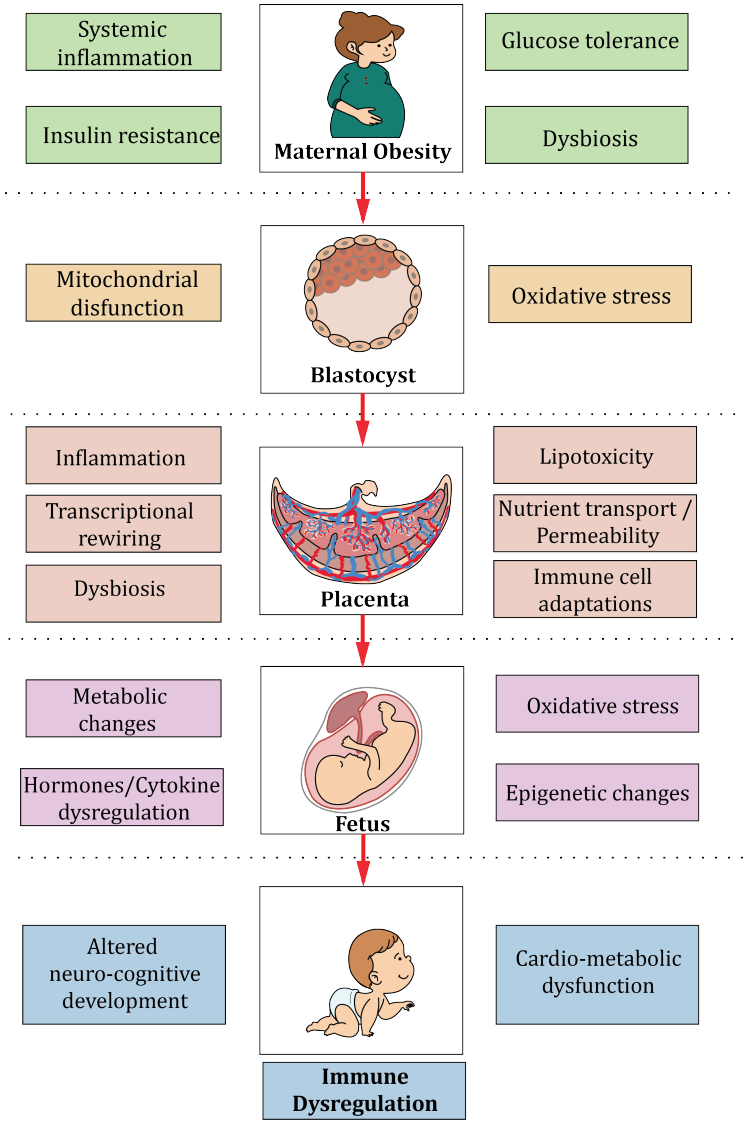

Figure 1.5 Mechanisms linking obesity associated changes on the maternal front and adverse immunological outcomes in the fetus and offspring.
Inflammatory exposures associated with pregravid obesity results in cellular reprogramming of gametes, metabolic dysfunction of the blastocyst, and significant structural and compositional changes in the placenta. A combination of early cellular epigenomic reprogramming and gestational exposure to maternal inflammation via direct or indirect placenta derived transfer of circulating maternal factors (immune mediators, hormones, lipids, exosomes) shift the immune cells on the fetal side to a refractory state. These cellular adaptations predispose the newborn to a wide array of disorders with significant immunological burden.

CHAPTER 2

Impact of pregravid obesity on the functional and molecular adaptations of circulating monocytes during pregnancy.

Suhas Sureshchandra[1, 2], Norma E. Mendoza[1], Allen Jankeel[1], Randall M. Wilson[4], Maham Rais[4], Samantha Castaneda[1], Andrew N. Tang[1], Selene B. Nguyen[1], Brian Jin Kee Ligh[1], Jonathan Q. Purnell[6], Kent L. Thornburg[6], Nicole E. Marshall[5], Ilhem Messaoudi[1, 2]

[1]Department of Molecular Biology and Biochemistry, University of California- Irvine, Irvine CA, USA
[2]Institute for Immunology, University of California-Irvine, Irvine CA, USA
[3]School of Medicine, University of California-Irvine, Irvine CA, USA
[4]Division of Biomedical Sciences, University of California-Riverside, Riverside, CA, USA.
[5]Maternal Fetal Medicine, Oregon Health and Science University, Portland OR, USA.
[6]The Knight Cardiovascular Institute, Oregon Health and Science University, Portland OR, USA

Incorporates components from the published article:
Sureshchandra S, Marshall NE, Wilson RM, Barr T, Rais M, Purnell JQ, et al. Inflammatory Determinants of Pregravid Obesity in Placenta and Peripheral Blood. Front Physiol. 2018;9:1089. doi: 10.3389/fphys.2018.01089. PubMed PMID: 30131724; PubMed Central PMCID: PMCPMC6090296

ABSTRACT

A healthy pregnancy is associated with progressive changes in the maternal immune system that facilitates placentation, fetal growth, fetal tolerance, and labor. Disturbances of this pregnancy "immune clock" by obesity contribute to poor infection outcomes, and adverse pregnancy outcomes such as preeclampsia and preterm birth. However, the mechanisms by which pregravid obesity disrupts maternal immunity are still unknown. To address this question, we collected blood samples from 117 women during the first and third trimesters of pregnancy to determine the impact of both pregnancy and high pregravid BMI on circulating immune mediators, immune cell subset frequencies, and peripheral immune responses. Our analysis revealed significant alterations in the circulating inflammatory environment with pregnancy and obesity. Moreover, monocyte responses to LPS were enhanced during normal BMI pregnancy and were associated with transcriptional changes and increased chromatin accessibility. This trajectory was disrupted in pregnant women with BMI>30 and was accompanied by lack of epigenetic changes strongly suggesting that pregravid obesity disrupts pregnancy-associated monocyte activation, skewing them towards immunotolerance. These findings may explain the increased susceptibility to infections observed during pregnancy and following cesarean delivery in women with obesity.

INTRODUCTION

The maternal immune system undergoes several fine-tuned adaptations over the course of pregnancy (Mor and Cardenas, 2010). These changes are believed to facilitate implantation, fetal tolerance, fetal growth and development, and finally labor and parturition without compromising protection against microbial infections (Mor et al., 2011). A recently described "immunological clock" of pregnancy suggests that peripheral immune adaptations do not necessarily follow waves of pro- and anti-inflammatory phases (Mor and Cardenas, 2010), but rather a progressive activation of signaling molecules (Aghaeepour et al., 2017) and alterations in the circulating proteome (Aghaeepour et al., 2018). Specifically, while the peripheral adaptive immune system is skewed towards Th2/Treg responses and away from Th1/Th17 responses (Luppi et al., 2002b; Polese et al., 2014; Sacks et al., 2003), circulating innate immune cells are progressively activated over the course of a healthy pregnancy. This activation is manifested through higher production of pro-inflammatory cytokines IL-6, IL-1β, and IL-12 following *ex vivo* stimulation with LPS and bacteria (Aghaeepour et al., 2017; Faas et al., 2014; Luppi et al., 2002a; Naccasha et al., 2001; Sacks et al., 2003; Sacks et al., 1998) or viral particles (Kay et al., 2014; Le Gars et al., 2016). However, the precise mechanisms underlying this progressive activation of the innate immune branch are poorly defined.

A third of women of reproductive age in the US meet the definition of obese (body mass index (BMI)>30) (Flegal et al., 2016), making pregravid obesity one of the most critical and common health challenges during pregnancy. High pregravid BMI increases the risk for gestational diabetes (Chu et al., 2007a; Torloni et al., 2009), gestational

hypertension, preeclampsia (Huda et al., 2014; Wang et al., 2013), early pregnancy loss, placental abruption, abnormal fetal growth, premature labor, and stillbirth (Aune et al., 2014; Kim et al., 2016). High pregravid BMI is also an independent risk for infection during pregnancy (urinary and genital tract infections, sepsis) (Robinson et al., 2005; Sebire et al., 2001; Stapleton et al., 2005), labor (chorioamnionitis) (Cnattingius et al., 2013; Hadley et al., 2019), and post-partum (surgical site infections following cesarean) (Acosta et al., 2012; Conner et al., 2014; McLean et al., 2012; Salim et al., 2012).

Mechanisms underlying these adverse events are poorly understood, but it is believed to be mediated in part by the heightened inflammatory state associated with obesity (Leddy et al., 2008). Pregravid obesity is marked by elevated circulating levels of inflammatory mediators C reactive protein (CRP) and IL-6 (Aye et al., 2014; Basu et al., 2011a; Schmatz et al., 2010; Sureshchandra et al., 2018), subclinical endotoxemia, and signs of heightened inflammation in the adipose tissue compartment (Basu et al., 2011a). Increased exposure to subclinical levels of LPS with obesity could potentially alter both phenotype and fitness of innate immune cells. Indeed, we recently reported dysregulation in secretion of immune mediators, especially those expressed by monocytes and dendritic cells (DCs), following *ex vivo* stimulation with TLR agonists of peripheral blood mononuclear cells (PBMC) collected at gestational week 37 from subjects with obesity (Sureshchandra et al., 2018).

Amongst innate immune cells, monocytes and macrophages play critical roles at various stages of pregnancy. Circulating monocytes play seminal roles in implantation, placentation, and labor, while decidual monocyte-derived macrophages play critical roles in angiogenesis, tissue development, and wound healing at the maternal fetal interface

(Basu et al., 2011b; Mor and Abrahams, 2003; Mor et al., 2011). Monocytes/macrophages have also been implicated in several obesity-associated complications during pregnancy such as preeclampsia (Faas et al., 2014; Przybyl et al., 2016), preterm labor (Gomez-Lopez et al., 2014), poor placental development (Faas and de Vos, 2017), and chorioamnionitis (Ben Amara et al., 2013). However, several questions still remain unaddressed: (1) how does pregravid obesity alter innate immune responses and function throughout pregnancy; (2) what are the cellular and molecular mechanisms of underlying those changes?

To answer these questions, in this study, we defined longitudinal changes in circulating immune mediators, peripheral innate immune cell subsets and responses of monocytes and DCs to *ex vivo* stimulation during early and late stages of gestation in both lean and obese women to elucidate the impact of pregravid obesity on the pregnancy immunological clock using a combination of immunological, transcriptional and epigenetic analyses. Our analysis revealed a gestation-associated trajectory of monocyte activation that is accompanied by an enhanced response to LPS and poising of the epigenome towards a state of heightened activation, and parallel changes in systemic metabolic and cytokine milieu. Our findings suggest that pregravid obesity dysregulates immunological pregnancy clock by skewing monocytes towards an immunoregulatory phenotype. This phenotype parallels attenuated transcriptional responses to LPS and lack of epigenetic plasticity observed with pregnancy. At T3, we observed fewer non-classical monocytes, and down-regulation of type-I interferon signaling and antigen presenting molecules with obesity. Tolerance at T3 is also evidenced from lack of metabolic plasticity and poor response to M1 macrophage inducing signals. Interestingly, while cytokine responses to LPS were dampened, protective functions such as phagocytosis were enhanced. Finally, systemic

changes in cytokine and chemokine environment with obesity at T3 instruct a regulatory environment that manifests as tolerance in monocytes. Collectively, these findings provide novel insight into mechanisms by which pregnancy associated adaptations can modify the severity of inflammatory conditions, protecting the developing fetus from its effects, but potentially compromising maternal host defense.

MATERIALS AND METHODS

Human subjects and experimental design

This study was approved by the Institutional Ethics Review Board of Oregon Health and Science University, University of California, Riverside and the University of California, Irvine. Written consent was obtained from all subjects. The study comprised of four independent cohorts of mothers with uncomplicated pregnancies. For cohort I (Table 2.1), a total of 25 non-smoking women (11 lean and 14 obese) without diabetes who had an uncomplicated, singleton pregnancy were enrolled at 37 weeks of gestation and initially grouped according to pregravid body mass index. The racial distribution was as follows: 19 Caucasian, 2 Asian-American/Pacific Islander, 1 American-Indian/Alaskan native, 1 African-American, and 2 unknown.

For cohort II (Table 2.2), a total of 117 non-smoking women (69 lean and 48 obese) who had an uncomplicated, singleton pregnancy were enrolled for this study. A total of 65 women classified as lean (37) or obese (28) were enrolled during first trimester (~week 12, designated as T1). A large subset of these women (29 lean and 27 obese) also provided a blood sample during the third trimester (~Week 37, designated as T3). Additionally, 32 women classified as lean and 20 women classified as obese were recruited only at T3. The racial distribution of the entire cohort was as follows: 101 Caucasian, 7 Asian American, 2 Pacific Islander, 6 American Indian/Alaskan native, 6 African American, and 3 declined to report. Exclusion criteria for cohorts I, II, and III include active maternal infection, documented fetal congenital anomalies, substance abuse, chronic illness requiring regular medication use, preeclampsia, gestational diabetes, chorioamnionitis, significant medical

conditions (active cancers, cardiac, renal, hepatic, or pulmonary diseases), or an abnormal glucose tolerance test. For single cell studies in maternal blood at delivery time point, we used samples from cohort III (Table 2.3). For this cohort, maternal blood was collected at delivery time point. For all cohorts, women underwent a fasting blood draw and body composition via air displacement plethysmography using a BodPod (Life Measurement Inc). Due to strong positive correlation between pre-pregnancy BMI and total body fat determined using the BodPod approach (Supplemental Figure 2.1A for cohort I, Supplemental Figure 2.2A for cohorts II and III), participants were stratified as lean or obese based on pre-pregnancy BMI (Tables 2.1, 2.2, and 2.3)

Plasma and Peripheral Blood Mononuclear Cell (PBMC) isolation

Complete blood counts were obtained by Beckman Coulter Hematology analyzer (Brea, CA). Peripheral blood mononuclear cells (PBMC) and plasma were obtained by standard density gradient centrifugation over Ficoll (GE Healthcare). PBMC were frozen in 10% DMSO/FBS and stored in liquid nitrogen until analysis. Plasma was stored at -80°C until analysis.

Luminex assay

Immune mediators in plasma were measured using a customized multiplex human factor panel (R & D Systems, Minneapolis MN) measuring cytokines (IFNβ, IFNγ, IL-1β, IL-10, IL-12p70, IL-13, IL-15, IL-17A, IL-18, IL-1RA, IL-2, IL-21, IL-4, IL-5, IL-7, TNFα, IL-23, IL-31, IL-22, IL-27), chemokines (CCL2/MCP-1, CCL3/MIP-1α, CCL4/MIP-1β, CCL5/RANTES, CCL11/Eotaxin, CXCL1/GROα, CXCL8/IL-8, CXCL9/MIG CXCL10/IP-10, CXCL11/I-TAC, CXCL12/SDF-1α, CXCL13/BCA-1, growth factors (BDNF, GM-CSF, HGF, EGF, VEGF, PDGF-BB) and additional molecules (PD-L1, S100). Metabolic hormones were measured using a

3-plex kit measuring insulin, leptin, and PYY (Millipore, Burlington MA). Adipokines were assayed using a 5-plex kit measuring adiponectin, adpisin, lipocalin-2, total PAI-1, and resistin (Millipore, Burlington MA). Samples were diluted per manufacturer's instructions and run in duplicates on the MAGPIX Instrument (Luminex, Austin, TX). Data were fit using a 5P-logistic regression on xPONENT software.

ELISA

C-Reactive Protein (CRP) and IL-6 were measured using a high sensitivity ELISA (Life Technologies, Carlsbad CA). Plasma soluble CD14 (sCD14) was measured using ELISA per manufacturer's instruction (Hycult Biotech, Uden, Netherlands)

PBMC and monocyte phenotyping

1 X 10^6 PBMC were stained using the following cocktail of antibodies to characterize innate immune cells and their subsets: PE-CD3, PE-CD19, PB-CD16, PE-Cy7-CD11c, AF700-CD14, PCP-Cy5.5-CD123, BV711-CD56, and APC-Cy7-HLA-DR to delineate innate immune cell populations. An additional 10^6 PBMC from a subset of samples were stained using the following panel 1: AF700-CD14, APC-Cy7-HLA-DR, FITC-CD62L, PB-CD16, BV711-CD64, PE-Dazzle594-PD-L1, and panel 2: AF700-CD14, APC-Cy7-HLA-DR, PB-CCR5, AF488-TLR2, PCP-Cy5.5-CD163, BV605-CCR2, PE-eF610-CD11c, PE-Cy7-CD11b. After surface staining, cell pellets were washed twice in PBS and resuspended in cold FACS buffer (PBS with 2% FBS and 1mM EDTA). All samples were acquired with the Attune NxT Flow Cytometer (ThermoFisher Scientific, Waltham MA) and analyzed using FlowJo 10.5.0 (Ashland OR). Multi-dimensional analysis using tSNE was performed in FlowJo using default settings after concatenation of samples with each group and down sampling to 50,000 cells in the final desired gate.

Intracellular cytokine assay and monocyte activation

To measure cytokine responses of monocytes and dendritic cells, 10^6 PBMC were stimulated for 16h at 37°C in RPMI supplemented with 10% FBS in the presence or absence of 1 ug/mL LPS (TLR4 ligand, *E.coli* 055:B5; Invivogen, San Diego CA); Brefeldin A (Sigma, St. Louis MO) was added after 1 hour incubation. Cells were stained for APC-Cy7-CD14 and PCP-Cy5.5-HLA-DR, fixed, permeabilized, and stained intracellularly for APC-TNFα and PE-IL-6. To measure immune activation, a subset of PBMC samples were stimulated with LPS for 16h without Brefeldin A, washed twice with PBS and surface stained using a cocktail of following antibodies for 20 minutes: AF700-CD14, HLA-DR-APC-Cy7, PB-CD16, BV510-CD40, PE-Cy7-CD80, PCP-Cy5.5-CD83, BV605-CD86. Cell pellets were washed twice in PBS and resuspended in cold FACS buffer (PBS with 2% FBS and 1mM EDTA). All samples were acquired with the Attune NxT Flow Cytometer (ThermoFisher Scientific, Waltham MA) and analyzed using FlowJo 10.5 (Ashland OR).

Isolation of monocytes

Monocytes were purified from freshly thawed PBMC using CD14 antibodies conjugated to magnetic microbeads per the manufacturer's recommendations (Miltenyi Biotec, San Diego CA). Magnetically bound monocytes were washed and eluted for collection. Positive selection was chosen to ensure high purity of the population, which was assessed using flow cytometry and was on average ≥95%.

Monocyte stimulation

10^5 purified monocytes were cultured in RPMI supplemented with 10% FBS with or without 1 ug/mL LPS (TLR4 ligand, *E.coli* 055:B5; Invivogen, San Diego CA) in 96-well tissue culture plates at 37C in a 5% CO_2 environment for 8 hours. Plates were spun down:

supernatants were used to measure production of immune mediators; and cell pellets were resuspended in Qiazol (Qiagen) for RNA extraction. Both cells and supernatants were stored in -80C until they could be processed as a batch.

Bulk RNA-Seq

Total RNA was isolated from monocytes using mRNeasy kit (Qiagen, Valencia CA). Quality and concentrations were measured using Agilent 2100 Bioanalyzer. Libraries were generated using TruSeq Stranded Total RNA-Seq kit (Illumina, San Diego CA). Briefly, following rRNA depletion, mRNA was fragmented for 8 min, converted to double stranded cDNA and adapter ligated. Fragments were then enriched by PCR amplification and purified. Size and quality of the library was verified using Qubit and Bioanalyzer. Libraries were multiplexed and sequenced on the HiSeq4000 platform (Illumina, San Diego CA) to yield an average of 20 million 100 bp single end reads per sample.

RNA-Seq analysis

Quality control of raw reads was performed retaining bases with quality scores of ≥20 and reads ≥35 base pair long. Reads were aligned to human genome (hg38) using splice aware aligner TopHat using annotations available from ENSEMBL (GRCh38.85) database. Quantification of read counts was performed using GenomicRanges package in R and normalized to derive transcripts per million (TPM) counts. To detect the effect of pregravid obesity in resting monocytes at T1 and T3 respectively, differential expression analysis was performed using quasi-likelihood linear modeling in edgeR. To test pair wise longitudinal changes with lean and obese groups, data was fit into negative binomial GLMs with a design matrix that preserved sample ID information. Lowly expressed genes were filtered at the count stage, eliminating ones with 0 counts in at least 3 samples regardless of the group.

Due to the relatively low number of genes passing the standard FDR cutoff (FDR <0.05), genes with expression difference (relaxed statistical p-value <0.01) were included in subsequent analyses.

Responses to LPS were modeled pairwise at each time point using negative binomial GLMs following low read count filtering. Genes with expression difference (FDR <0.05) were considered differentially expressed genes (DEG). Functional enrichment of DEG was performed using Metascape and InnateDB. Transcription factors that regulate expression of DEG were predicted using ChEA3 tool using ENSEMBL ChIP database. Heatmaps of fold change or TPMs were generated and bubble plots for enrichment of Transcription Factor (TF) regulation or Gene Ontology (GO) terms was generated using ggplot in R. Gene expression data have been deposited in NCBI's Sequence Read Archive (SRA accession number pending).

Cell Sorting and single cell RNA-Seq

PBMC from delivery time point were thawed and live cells were sorted into RPMI (supplemented with 30% FBS) using the BD FACS Aria Fusion and SYTOX Blue (1:1000, ThermoFisher). Sorted cells were counted in triplicates and resuspended in PBS with 0.04% BSA in a final concentration of 1200 cells/uL. Cells were immediately loaded in the 10X Genomics Chromium with a loading target of 17,600 cells. Libraries were generated using the V3 chemistry per the manufacturer's instructions (10X Genomics, Pleasanton CA). Libraries were sequenced on Illumina NovaSeq with a sequencing target of 50,000 reads per cell.

Single cell RNA-Seq data analysis

Raw reads were aligned and quantified using the Cell Ranger Single-Cell Software Suite (version 3.0.1, 10X Genomics) against the GRCh38 human reference genome using the STAR aligner. Downstream processing of aligned reads was performed using Seurat (version 3.1.1) (Satija et al., 2015). Droplets with ambient RNA (cells fewer than 400 detected genes), potential doublets (cells with more than 4000 detected genes, and dying cells (cells with more than 20% total mitochondrial gene expression) were excluded during initial QC. Data objects from lean and obese group were integrated using Seurat (Stuart et al., 2019). Data normalization and variance stabilization was performed using *SCTransform* function (Hafemeister and Satija, 2019) using a regularized negative binomial regression, correcting for differential effects of mitochondrial and ribosomal gene expression levels and cell cycle. Dimension reduction was performed using *RunPCA* function to obtain the first 30 principal components followed by clustering using the *FindClusters* function in Seurat. Visualization of clusters was performed using UMAP algorithm as implemented by Seurat's *runUMAP* function. Cell types were assigned to individual cluster using *FindMarkers* function with a fold change cutoff of at least 0.5 and using a known catalog of well-characterized scRNA markers for PBMC (Zheng et al., 2017).

Single cell analysis of monocytes

Three monocyte clusters expressing high levels of *CD14* were extracted from dimension reduced Seurat object using the *subset* function based on relative expression of *CD14*, *FCGR3A*, and *HLA-DR*. Cells were re-clustered and visualized using UMAP. Doublet clusters were identified by iterative clustering removing clusters with high expression of genes associated with T cells, B cells, and NK cells. Three monocyte subsets were identified based on expression levels of *CD14*, *HLA-DRA*, and *FCGR3A*. Differential expression analysis was

tested using Wilcoxon rank sum test followed by bonferroni correction using all genes in the dataset. For gene scoring analysis, we compared gene signatures and pathways from KEGG (https://www.genome.jp/kegg/pathway.html) in subpopulations using Seurat's *AddModuleScore* function. Two-way functional enrichment of differential signatures was performed on Metascape (Zhou et al., 2019). Differential hierarchies within the monocyte compartment were reconstructed using Monocle (version 2.8.0). Briefly, clustering was performed using t-SNE and differential genes identified using Monocle's *differentialGeneTest*. These genes (q-value < 1e-10) were used for ordering cells on a pseudotime.

Neutral Lipid Staining

Neutral lipids in monocytes were quantified in monocytes using flow cytometry. Briefly, 500,000 PBMC were surface stained (CD14-AF700, HLA-DR-APC-Cy7) for 20 minutes at 4C, washed twice, and resuspended in 500 uL warm 1X PBS containing 1 ug/mL BODIPY™ 493/503 (ThermoFisher Scientific, Waltham MA). Cells were incubated at 37C for 10 minutes and samples were acquired with the Attune NxT Flow Cytometer (ThermoFisher Scientific, Waltham MA) and analyzed using FlowJo 10.5 (Ashland OR).

Metabolic Assays

Basal Oxygen Consumption Rate (OCR) and Extracellular Acidification Rate (ECAR) were measured using Seahorse XF Glycolysis Rate Assay on Seahorse XFp Flux Analyzer (Agilent Technologies) following manufacturer's instructions. Briefly 200,000 purified monocytes were seeded on Cell-Tak (Corning) coated 8-well culture plates in phenol free RPMI media containing 2 mM L-glutamine, 10 mM L-glucose, 1mM sodium pyruvate, and 5mM HEPES. Seeded plates were placed in 37C incubator without CO_2 and run on the XFp with extended

basal measurements, followed by serial injections of Rotenone/Actinomycin (final well concentration 0.5 uM) to block oxidative phosphorylation followed by 2-Deoxy-D-Glucose (2-DG, 500 mM) to block glycolysis. Cellular responses to stress under activated conditions were measured using Seahorse XF Glycolysis Stress Assay. Purified monocytes were seeded in the in glucose free media and cultured in the presence/absence of 1 ug/mL LPS for 1 hour in 37C incubator without CO_2. Plates were run on the XFp for 8 cycles of basal measurements, followed by an acute injection of L-glucose (100 mM), oligomycin (50 uM), and 2-DG (500 mM). Analysis and interpretation of data was done on Seahorse Wave desktop software (Agilent Technologies).

Phagocytosis Assay

Cellular phagocytosis was measured using pH-sensitive pHrodo® E. coli BioParticles® conjugates (ThermoFisher Scientific, Waltham MA). 500,000 PBMC were activated with 100 ng/mL LPS for 4h, washed twice and incubated for an additional 2 hours in media containing pHrodo conjugates at 1 mg/mL conjugates. Pellets were washed twice, surface stained (CD14-AF700, HLA-DR-APC-Cy7), and resuspended in ice-cold FACS buffer. All samples were acquired with the Attune NxT Flow Cytometer (ThermoFisher Scientific, Waltham MA) and analyzed using FlowJo 10.5 (Ashland OR).

Cytosolic ROS assay

For intracellular ROS measurements, 500,000 PBMC were stimulated with 1 ug/mL LPS for 4 hours. For negative control, cells were incubated in serum-free media containing 200 uM anti-oxidant N-acetylcysteine (NAC) for 1.5 hours. Both negative and positive controls were incubated with tert-butyl hydroperoxide (TBHP) for 30 minutes to induce oxidative stress. All samples were then incubated with 2.5 uM CellROX Deep Red (Life Technologies) at 37C

for 30 minutes, washed twice, surface stained (CD14-FITC, HLA-DR-PCP-Cy5.5) and samples were acquired with the Attune NxT Flow Cytometer (ThermoFisher Scientific, Waltham MA) and analyzed using FlowJo 10.5 (Ashland OR).

***In vitro* Macrophage Differentiation**

100,000 purified monocytes were cultured in 24-well tissue culture plates treated for increased attachment (VWR) in RPMI supplemented with 1% Human AB Serum (Omega Scientific) for 7 days with media supplemented on day 3. On day 7, cells were polarized to M1-like macrophages using 1 ug/mL LPS and 100 ng/mL IFNγ (Peprotech) or M2-like macrophages using 100 ng/mL IL-4 (Peprotech) and cultured for an additional 24 hours (day 8). Cell pellets from day 7 and day 8 were surface stained (CD16-PB; CD64-BV711; HLA-DR-APC-Cy7; CD86-BV605; CD163-PCP-Cy5.5; CD209-R-PE) and analyzed using flow cytometry. Supernatants were collected and quantified for secreted cytokines and chemokines using a 29-plex luminex assay (R & D Systems).

ATAC-Seq

ATAC-Seq libraries were generated using a recently described modified protocol (OMNI-ATAC) to reduce mitochondrial reads (Corces et al., 2017). Briefly, 50,000 purified monocytes were lysed in lysis buffer (10mM Tris-HCl (pH 7.4), 10 mM NaCl, 3 mM $MgCl_2$), for 3 min on ice to prepare the nuclei. Immediately after lysis, nuclei were spun at 500g for 10 min to remove the supernatant. Nuclei were then incubated with transposition mixture (100 nM Tn5 transposase, 0.1% Tween-20, 0.01% Digitonin and TD Buffer) at 37C for 30 min. Transposed DNA was then purified with AMPure XP beads (Beckman Coulter) and partially amplified for 5 cycles using the following PCR conditions - 72C for 3 min; 98C for 30s and thermocycling at 98C for 10s, 63C for 30s and 72C for 1 min. To avoid

overamplification, qPCR was performed on 5 uL of partially amplified library. Additional cycles of amplification for the remainder of the sample were calculated from the saturation curves (cycles corresponding to a third of the saturation value). Fully amplified samples were purified with AMPure beads and quantified on the Bioanalyzer (Agilent Technologies, Santa Clara CA).

ATAC-Seq – Read Preprocessing and alignment

Paired reads from sequencing were quality checked using FASTQC and trimmed to retain reads with quality scores of ≥20 and minimum read lengths of 50 bp. Trimmed paired reads were aligned to the human genome (hg38) using Bowtie2 (–X 2000 –k 1 –very-sensitive –no-discordant –no-mixed). Reads aligning to mitochondrial genome and allosomes were removed using samtools. PCR duplicate artifacts were then removed using Picard. Finally, poor quality alignments and improperly mapped reads were filtered using samtools (samtools view –q 10 –F 3844). To reflect the accurate read start site due to Tn5 insertion, BAM files were repositioned using ATACseqQC package in R (Ou et al., 2018). The positive and negative strands were offset by +4bp and -5bp respectively. Samples within a group were merged and sorted using samtools.

ATAC-Seq – Peak Calling and downstream analyses.

Sample QC and statistics for merged BAM files were generated using HOMER makeTagDirectory function. Accessible chromatin peaks were called for mapped paired reads using HOMER findpeak function (-minDist 150 –region –fdr 0.05). PCA and sample clustering were performed on accessible peaks using DiffBind. Differentially accessible regions (DAR) in either direction were captured using HOMER getDiffererentialPeaks function (-q 0.05). DAR were annotated using the human GTF annotation file (GRCh38.85)

and ChIPSeeker with a promoter definition of -1000 bp and +100 bp around the transcriptional start site (TSS). Peaks overlapping 5'UTRs, promoters, first exons and first introns were pooled for functional enrichment of genes. For intergenic changes, the genes closest to the intergenic DAR were considered. Functional enrichment of this pooled list of genes was performed using DAVID (Fisher p-value <0.05). BAM files were converted to bigWig files using bedtools and visualized on the new WashU EpiGenome browser.

Statistics

All statistical analyses were conducted in Prism 8 (GraphPad). All definitive outliers in two-way and four-way comparisons were identified using ROUT analysis (Q=0.1%). Data was then tested for normality using Shapiro-Wilk test (alpha=0.05). If data were normally distributed across all groups, differences with obesity and pregnancy were tested using ordinary one-way ANOVA with unmatched samples. Multiple comparisons were corrected using Holm-Sidak test adjusting the family-wise significance and confidence level at 0.05. If gaussian assumption was not satisfied, differences were tested using Kruskall-Wallis test (alpha=0.05) followed by Dunn's multiple hypothesis correction test. Differences in normally distributed datasets were tested using an unpaired t-test with Welch's correction (assuming different standard deviations). Two group comparisons that failed normality tests were carried out using Mann-Whitney test.

RESULTS

Pregravid obesity is associated with a state of chronic low-grade inflammation.

We first asked if obesity alters the circulating inflammatory environment at term. Using blood samples collected from pregnant mothers at week 37 of gestation (third trimester, T3) (Cohort I, Table 2.1), we measured plasma metabolic hormones, IL-6, and CRP (Figure 2.1A). Obesity was associated with chronic low-grade inflammation, characterized by higher levels of IL-6 (Figure 2.1B) and CRP (Figure 2.1C). Insulin levels had an increasing trend (Figure 2.1D), whereas leptin was significantly elevated with obesity. However, both leptin and insulin increased linearly with maternal BMI (Supplemental Figures 2.1B and 2.1C)

Both pregnancy and pregravid obesity alter the circulating metabolic and inflammatory environment.

To study the impact of maternal obesity over the course of gestation, we leverage a new cohort of mothers (Cohort II, Table 2.2) – for a subset of subjects, blood was collected at both week 12 (T1) and week 37 (T3) and for another set of subjects, blood was collected at T3 alone. Pre-pregnancy BMI and fat mass were recorded to stratify subjects as lean (BMI < 25) and obese (BMI >30). Human subject demographics are summarized in Table 2.2. Pregravid BMI correlated strongly with fat mass percentages, both at T1 and T3 (Supplemental Figure 2.2A). Gestational weight gain was significantly lower in the obese group (Supplemental Figure 2.2B). We measured plasma levels of circulating metabolic hormones, adipokines, cytokines, chemokines, and growth factors were at T1 and T3 (Figure 2.2A). At both T1 and T3, high pregravid BMI was associated with elevated circulating CRP (Figure 2.2B) and IL-6 (Figure 2.2C) levels. While systemic levels of insulin

(Figure 2.2D) and leptin (Figure 2.2E) increased with gestation in the lean group, their plasma levels were significantly higher in the obese group at both time points (Figures 2.2D and 2.2E). Plasma levels of resistin were also higher in the obese group at both time points (Supplemental Figure 2.2C). Finally, plasma levels of the adipokines, adipsin (Supplemental Figure 2.2D) and adiponectin (Supplemental Figure 2.2E) increased with pregnancy in both groups and no differences between the groups were noted. No differences were detected in plasma levels of gut hormone peptide YY (PYY) with either time or pregravid obesity (Supplemental Figure 2.2F).

Luminex analysis of plasma revealed significant changes in levels of immune mediators from T1 to T3 in both groups (Figure 2.2F). Levels of both pro-inflammatory (TNFα, IL-2, IFNβ, IL-7, IL-17A, IL-18, IL-23) and regulatory (IL-4, IL-10, and IL-13) cytokines, as well as chemokines (CCL3, CXCL9, and CXCL11) significantly increased during pregnancy, independent of pregravid BMI (Figure 2.2F). Furthermore, while both IL-18 and IL-10 significantly increased in both groups, the magnitude of their change positively correlated with BMI (Figure 2.2G). Interestingly, plasma levels of regulatory factors IL-1RA, CCL22 were higher in the obese group at T3 (Figure 2.2H, Supplemental Figure 2.3). Levels of growth factor EGF decreased with gestation in the lean group only (Figure 2.2I). Finally, while IL-27, a known monocyte activator was elevated with gestation; its plasma concentrations were significantly lower in the obese group at T3 (Figure 2.2J).

Pregravid obesity alters the frequencies of monocyte subsets and disrupts pregnancy-associated activation trajectory of circulating monocytes.

Incidentally, in Cohort II, the most interesting differences in cytokines and chemokines with maternal obesity were myeloid associated mediators (Supplemental

Figure 2.3). Given these differences, we next investigated if pregravid obesity is associated with changes in this subset. Complete blood cell (CBC) counts revealed increased numbers of white blood cells (WBC) with pregnancy in both groups and with pregravid obesity (Supplemental Figure 2.4A). These differences were primarily mediated by increased numbers of granulocytes with pregravid obesity (Supplemental Figure 2.4B), with no major differences in total lymphocyte (Supplemental Figure 2.4C) or monocyte numbers (Supplemental Figure 2.4D). Multi-parameter flow cytometry analysis of innate immune cells in PBMC from lean pregnant women (Supplemental Figure 2.5A) revealed no changes in major cell populations (Supplemental Figures 2.5B-2.5F) with pregnancy, except in a subset of NK cells ($CD56^{bright}CD16^{+}$) (Supplemental Figure 2.5G). Pregravid obesity was however associated with a significantly lower frequency of non-classical (CD16+) monocytes (Figure 2.3A) and a modest drop in plasmacytoid DC (pDC) numbers at T3 (Figure 2.3B). Myeloid DC (mDC) numbers remained unchanged with obesity (Supplemental Figure 2.5H).

We next investigated monocytes responses to *ex vivo* LPS stimulation (Figure 2.2A). PBMC were stimulated with LPS for 16 hours and cytokine responses measured using intracellular staining followed by flow cytometry (Cohort II, Supplemental Figure 2.6A). Pregnancy in lean women, but not those with obesity, was associated with increased frequency of $IL6^{+}TNF^{+}$ producing monocytes (Figure 2.3C), but not dendritic cells (Supplemental Figure 2.6B), in response to LPS stimulation. Indeed, frequency of $IL6^{+}TNF^{+}$ monocytes at T3 negatively correlated with maternal pregravid BMI (Figure 2.3D). Additionally, at T3, monocytes from pregnant women with obesity exhibited dampened induction of early activation markers CD40 (Figure 2.3E) and CD86 (Figure 2.3F) but not

CD80 (Supplemental Figure 2.6C) and CD83 (Supplemental Figure 2.6D). In line with the increased monocyte responses to LPS with pregnancy in lean pregnant women, levels of circulating soluble CD14 (sCD14), a surrogate for *in vivo* monocyte activation were also increased (Figure 2.3G) between T1 and T3 in lean but not women with obesity. sCD14 levels were higher in the obese group at T1 (Figure 2.3G), potentially indicating myeloid activation due to obesity.

Single cell RNA-Seq reveals significant shifts in monocyte phenotypes at T3.

Pair wise longitudinal comparison of the transcriptome of resting monocytes (Cohort II) from the lean group (n=3/time point) showed modest changes, with increased expression of MHC molecules (*B2M*, *HLA-DRA*) and proinflammatory genes (e.g. *VCAN*, *LYZ*) (P-value <0.001) at T3 relative to T1 (Supplemental Figure 2.7A). On the other hand, pregravid obesity (n=3/time point) was associated with a modest suppression of genes involved in of interferon signaling (*STAT1*, *GBP5*, *PSMB8*) and response to reactive oxygen species (*STRBP*, *HEBP2*, *TRAP1, TRPA1*) (P-value <0.001) at T3 (Supplemental Figure 2.7B).

To better capture the impact of pregravid obesity on circulating monocytes at T3, we performed single cell RNA-sequencing of total PBMC (n=2/group) obtained at delivery time point (Cohort III, Table 2.3) and computationally extracted the monocyte clusters (~600 cells/group) using expression of CD14 transcripts (clusters 7, 11, and 16 in the initial UMAP of PBMC; Supplemental Figure 2.8A). Following subsequent iterations of doublet removal and UMAP clustering, we observed 6 major clusters of monocytes (Figure 2.4A) representing the three subsets traditionally identified by flow cytometry: classical monocytes – clusters I, III, IV; non-classical monocytes - clusters II and IV; intermediate-cluster VI based on expression of *CD14*, *FCGRA* (CD16), and *HLA-DRA* (Figure 2.4B and

Supplemental Figure 2.8B). Trajectory analysis using Monocle confirmed these observations placing non-classical monocytes at the end of the pseudotime with intermediate monocytes transitioning from classical to non-classical subsets (Figure 2.4C and Supplemental Figure 2.8C). Pregravid obesity was associated with a dramatic drop in the number of non-classical monocytes (cluster IV) (Figures 2.4D and 2.4E), a significant increase in classical monocytes (cluster III) (Figures 2.4D and 2.4E) expressing markers of insulin resistance (*CD44*, *LMNA*, *THBD*) (Figure2.4B), and a reduction of cluster V (Figures 2.4B, 2.4D and 2.4E) expressing proinflammatory genes (*VCAN*, *S100A9*, *LYZ*) (Figure 2.4B).

Differential gene expression analysis between lean and obese groups showed transcriptional changes associated with immune activation, signaling, differentiation, and apoptosis in both classical and non-classical clusters (Figure 2.4F). Specifically, we detected reduced expression of *STAT1*, *TNFSF10*, *HLA-DRA*, and *FCGR3A* (Figure 2.4G) in all monocyte subsets with pregravid obesity. Reduced expression of surface HLA-DR and CD16 (encoded by *FCGR3A*) with pregravid obesity was confirmed using flow cytometry (Figure 2.4H). As observed with bulk RNA sequencing (Supplemental Figure 2.7B), we observed downregulation of genes within the interferon-signaling pathway with pregravid obesity (Figure 2.4F), across all clusters (Supplemental Figure 2.8D) including interferon-stimulated genes (*IFIT3*, *ISG15*, *OAS1*) (Supplemental Figure 2.8E). Finally, pregravid obesity was associated with up-regulation of genes encoding immunoregulatory molecules (*AHR*, *CD52*, and *CD163*) (Figure 2.4I)

Defects in monocyte responses with maternal obesity at T3 are cell intrinsic.

We next investigated whether pregravid obesity-associated reduction in cytokine production by circulating monocytes in response to LPS is cell intrinsic. Monocytes were

isolated from PBMC obtained from lean subjects and those with obesity at T1 and T3 and stimulated with LPS for 8 hours (Cohort II, Table 2.2) (Figure 2.5A and Supplemental Figure 2.9A). Significant differences in the monocyte response to LPS with pregravid obesity were detected at both T1 (Supplemental Figure 2.9B) and T3 (Supplemental Figure 2.9C). Although gene expression changes were more robust at the T3 time point for both the lean (Figure 2.5B) and obese groups (Figure 2.5C), a large number of DEG detected at T3 in the obese group were predominantly down regulated (Figure 2.5C), supporting the notion of immunotolerance. Moreover, functional enrichment revealed a higher proportion of genes that play a role in myeloid activation, leukocyte adhesion, cytokine signaling and response to LPS in lean group in T3 compared to T1 (Figure 2.5D).

In contrast, at T3, in the obese group, we observed few transcriptional changes associated with the response to LPS, myeloid cell activation, and cytokine signaling (Figure 2.5D and Figure 2.5E). Additionally, we detected lower induction of key inflammatory cytokine *IL6*, *IL1B* (Figure 2.5E), *IL1A*, and *TNF* (Figure 2.5F) and chemokines *CCL3* (Figure 2.5E), *CCL4* (Figure 2.5F) transcripts in the obese group. Interestingly, transcript levels of transcription factors/activators *NFKB1*, *FOSB*, *CIITA* (Figure 2.5F) and *RXRA*, *CEBPZ* (Supplemental Figures 2.9D and 2.9E) were dramatically reduced with obesity at T3 but not at T1. These findings were supported by transcription factor analysis of DEG using ChEA3, which revealed reduced number of genes regulated by RELA, IRF, and STAT with obesity, particularly at T3 (Figure 2.5G). Not surprisingly, in the lean group, we observed enhanced numbers of IRF1, STAT1, and STAT3- regulated DEGs with LPS at T3 compared to T1 (Figure 2.5G). Finally, we report poor induction of key regulators of chromatin

reorganization (*KDM2B*, *SIRT1*, *SIRT2*, *EP300*, *KDM4C*) with LPS in obese group at T3 (Figures 2.5D and 2.5H), suggestive of epigenetic constraints to immune activation.

Pregravid obesity disrupts pregnancy-associated epigenetic trajectory of circulating monocytes.

We next asked if there exists a pregnancy-associated epigenetic clock that explains the enhanced monocyte responses at T3 relative to T1 during a lean pregnancy. We therefore profiled chromatin accessibility within purified resting monocytes from lean and obese group (Cohort II) at both time points under resting conditions using ATAC-Seq (Figure 2.2A). Principal Component Analysis (PCA) revealed significant shift in ATAC profiles of monocytes from T1 to T3 in lean subjects (Figure 2.6A), with 7132 regions open at T3 (Figure 2.6B), most of which overlapping promoter regions (Figure 2.6C). Genes regulated by open promoter regions were involved in leukocyte activation, myeloid differentiation, and regulation of oxidative stress (Supplemental Figure 2.10A). Furthermore, genes regulated by intergenic regions with enhanced chromatin accessibility play roles in the inflammatory response to lipids and LPS (Supplemental Figure 2.10B).

In contrast, limited changes in chromatin accessibility were noted between T1 and T3 in the obese group (Figures 2.6A and 2.6B). Moreover, a comparison between leans vs. obese monocytes revealed more dramatic differences in chromatin accessibility at T3 (Figures 2.6B and 2.6D) than at T1 (Figures 2.6B and Supplemental Figure 2.10C). Roughly 40% of loci closed in obese group (but open in lean group) (Figure 2.6D) overlapped promoter regions of genes involved in cytokine production, Fc receptor mediated signaling, and wound healing (Figure 2.6E), as illustrated by pileups of inflammatory genes *HLA-DRA* (Figure 2.6F), *TNF* (Figure 2.6G), *IL6ST* (Supplemental Figure 2.10D), and activation

marker *CD80* (Supplemental Figure 2.10E). An unbiased motif-based approach showed that promoter regions closed with pregravid obesity harbor binding sites for transcription factors PU.1 and AP-1 and interferon regulators IRF1, IRF3, and IRF8 (Figure 2.6H).

Additionally, GREAT enrichment of closed intergenic loci (Figure 2.6I) revealed a number of associations with immune effector process, phagocytosis, cytokine responses, and immune activation (Figure 2.6I). The limited number of promoter-associated regions that were more open in obese group (Figure 2.6D) regulated genes primarily involved in histone methylation, and metabolic processes (Supplemental Figures 2.10F and 2.10G). Interestingly, while the large number of intergenic regions open in obese group, failed to enrich to any GO terms by GREAT, motif analysis suggests enhanced binding sites for factors that regulate regulatory M2-like macrophages (STAT6 and LXR) (Figure 2.6J).

Pregravid obesity is associated with metabolic and functional rewiring of circulating monocytes at term

The initiation of pro-inflammatory effector mechanisms requires a shift of cellular metabolism towards aerobic glycolysis. Given the immunotolerant phenotype of monocytes observed in pregnant women with obesity at T3, we asked if the reduced response to LPS is associated with a lack of metabolic plasticity. Baseline extracellular acidification rate (ECAR) measurements suggested reduced cellular preference for glycolysis with pregravid obesity (Figure 2.7A). We also observed attenuated induction of ECAR following LPS stimulation and glucose injection (Figure 2.7B). Furthermore, monocytes from subjects with obesity accumulated higher levels of neutral lipids (Figure 2.7C).

In addition to lack of metabolic flexibility, we detected changes in effector functions in monocytes with obesity at T3 (Cohort II). Fewer cells from the obese group

phagocytosed *E. coli* (Figure 2.7D), albeit the number of pathogen particles/cell was significantly higher (Figure 2.7E). Furthermore, pregravid obesity resulted in higher levels of cytosolic ROS following LPS stimulation (Figures 2.7F and Supplemental Figure 2.11A).

Maternal obesity alters the differentiation trajectory of circulating monocytes at T3.

Monocytes exhibiting signs of immune tolerance (reduced responsiveness to LPS challenge) demonstrate defects in differentiation and polarization trajectory. Therefore, we next investigated the impact of pregravid obesity on macrophage polarization potential using *in vitro* differentiation of monocytes collected at T3 using IFNγ (M1 like) and IL-4 (M2 like) conditioning (Figure 2.8A). Monocytes from subjects with obesity showed dampened induction of surface CD64 (Figure 2.8B) and CD86 (Figure 2.8C) following IFNγ stimulation with no differences in HLA-DR induction (Supplemental Figure 2.11B). In line with dysregulated M1 polarization, secretion of pro-inflammatory cytokines TNFα and IL-12 (Figure 2.8D) and chemokines CXCL9 (Supplemental Figure 2.11C) and CXCL11 (Supplemental Figure 2.11D) was reduced following IFNγ stimulation. Although we observed no differences in the expression of M2-like macrophage surface markers CD163 (Supplemental Figure 2.11E) and CD209 (Supplemental Figure 2.11F) following IL-4 conditioning, we observed lower production of M2-like macrophage immune molecules IL-10 (Figure 2.8E), CCL11 (Supplemental Figure 2.11G) and PDGF-BB (Supplemental Figure 2.11H).

DISCUSSION

Maternal obesity poses significant risks to maternal health, including increased susceptibility to infections during pregnancy (Robinson et al., 2005; Sebire et al., 2001; Stapleton et al., 2005), labor (Acosta et al., 2012; McLean et al., 2012; Salim et al., 2012) and post-partum (Acosta et al., 2012; McLean et al., 2012; Salim et al., 2012), suggesting disruptions in the pregnancy "immune clock". This phenomenon refers to precisely timed adaptations in the maternal immune system, notably increased neutrophil numbers, enhanced innate immune responses (Le Gars et al., 2016), augmented STAT signaling in CD4+ T cells and NK cells (Aghaeepour et al., 2017), and significant changes in the circulating proteome (Aghaeepour et al., 2018). Previous studies profiling the impact of pregravid obesity on maternal peripheral immune have fallen short by focusing on one particular type of measurement at one stage of pregnancy (Acosta et al., 2012; McLean et al., 2012; Salim et al., 2012; Sureshchandra et al., 2018). Therefore, in this study, we used a systems approach to characterize the impact of pregravid obesity on pregnancy associated "immune clock", using a combination of proteomic, functional, and genomic assays.

We began by profiling longitudinal differences in plasma inflammatory factors between the first (T1) and third (T3) trimesters in lean subjects and those with pregravid obesity (BMI > 30). Transition from T1 to T3 in lean subjects was associated with increased levels of several pro-inflammatory (TNFα, S100B, IL-2, IFNβ, IL-17A, IL-18, IL-23) and regulatory (IL-4, IL-10, and IL-13) factors. These observations are consistent with previous reports of systemic immune activation and counter-regulation over the course of pregnancy (Aghaeepour et al., 2017; Denney et al., 2011; Holtan et al., 2015; Melczer et al., 2002). In addition to these analytes and as previously reported (Basu et al., 2011a;

Catalano et al., 2009b; Challier et al., 2008; Christian and Porter, 2014; Friis et al., 2013; Gavrila et al., 2003; Kac et al., 2011; Ramsay et al., 2002; Roberts et al., 2011; Sen et al., 2013; Sen et al., 2014; Stewart et al., 2007), significantly higher levels of IL-6 and CRP were observed both at T1 and T3 in subjects with obesity, highlighting a state of chronic low-grade inflammation. Higher levels of IL-6 and CRP have been linked to obstetric complications (Christian and Porter, 2014; Stewart et al., 2007).

Interestingly, regulatory factors (IL-1RA, PDGF, CCL22) were significantly elevated whereas monocyte activator IL-27 was lower in plasma of mothers with obesity at T3. In contrast, circulating levels of pro-inflammatory IL-1β increased with gestation in lean mothers but remained unchanged in mothers with obesity. Moreover, levels of CCL2 and CRP while initially higher at T1 in mothers with obesity, decreased at T3. These observations strongly suggest that systemic inflammation associated with obesity at T1 is distinct from that at T3. At T3, most factors impacted by obesity were myeloid cell regulating and suggest a shift towards immune regulation in pregnant women with obesity to potentially protect the developing fetus.

Levels of insulin, leptin, and adiponectin also increased with gestational age in the leans, likely a consequence of metabolic adaptations to the nutritional demands of a growing fetus. In contrast, in subjects with obesity, systemic levels of insulin, leptin, and resistin were significantly higher relative to lean counterparts both at T1 and T3. Moreover, T1 to T3 transition was not associated with an increase in the levels of these metabolic hormones. Aberrant levels of insulin and leptin have been associated with both miscarriage (Baban et al., 2010; Laird et al., 2001) and preeclampsia (Laivuori et al., 2000), both of which are increased with pregravid obesity.

Profiling circulating immune cell subsets at T1 and T3 revealed modest cellular adaptations. Pregnancy was associated with increased total WBC counts, as previously reported (Chandra et al., 2012). The most significant change with pregnancy was an increase in CD56++CD16+ subset of NK cells. This subset of regulatory NK cells has been shown to increase with gestational age (Airas et al., 2008), and is the dominant NK cell subset (>95%) in the placental decidua (Le Bouteiller, 2013). As reported in previous studies (Aghaeepour et al., 2017), no significant differences were seen in other innate immune cell subsets.

Pregravid obesity was associated with higher granulocyte counts, as previously described for non-gravid obese individuals (Rosales, 2018), a reduction in non-classical (CD16+) monocytes, lower overall expression of HLA-DR on monocytes, and as we recently reported (Sureshchandra et al., 2018), a lower frequency of pDC at T3. Comparison of monocyte transcriptomes at T3 from lean mothers and those with obesity using high resolution single cell RNA sequencing confirmed a significant reduction of non-classical monocytes, and expression of both *CD16* and *HLA-DR*. Additionally, RNA-Seq analysis showed increased expression of inflammatory molecules *LYZ*, *VCAN* and *HLA-DR* in monocytes from lean subjects. In contrast, longitudinal changes in monocytes from mothers with obesity suggest suppression of antiviral responses coupled with up-regulation of regulatory molecules such as *CD163*, *AHR*, and *CD52*.

The most striking functional change detected in lean subjects between T1 and T3 was activation of circulating monocytes indicated by enhanced cytokine responses to LPS, elevated levels of plasma sCD14, a surrogate for *in vivo* myeloid activation, and increased levels of IL-27, which activates monocytes via STAT1 signaling pathway (Kalliolias and

Ivashkiv, 2008). Our observations are in line with earlier studies that have demonstrated that monocyte responses to influenza are enhanced with gestational age (Le Gars et al., 2016). Furthermore, pregnancy has been shown functionally rewire circulating monocytes, enhancing its intracellular ROS levels (Sacks et al., 1998) but reducing its phagocytic function (Lampe et al., 2015). Several factors have been proposed to be responsible for monocyte activation with pregnancy including elevated levels of leptin, cytokines (Sacks et al., 2001), exposure to placental microparticles released into circulation by syncytial trophoblasts (Redman et al., 2012), fetal DNA (Bianchi et al., 1996), or circulation of peripheral monocytes through the placenta (Mellembakken et al., 2002). Our analyses in purified monocytes suggest that these cells are primed for heightened responses with gestation. Indeed, RNA-Seq comparisons of LPS responses strongly suggest enhanced expression of pro-inflammatory molecules (*IL6*, *IL1B*, *TNF*) and induction of transcription factors (RELA, IRF1, STAT3) at T3 relative to T1. Interestingly, pregnancy is associated with enhanced endogenous STAT5ab signaling in T cells, development of regulatory T cells (Aghaeepour et al., 2017), which facilitate fetal tolerance during pregnancy. Thus, enhancement of innate immune responses over the course of pregnancy might be a mechanism to counter dampened T cell responses to avoid putting the mother at risk for infections.

Pregravid obesity disrupted pregnancy-associated monocyte activation, with a significantly reduced number of and TNFα/IL-6 producing monocytes in response to LPS stimulation. Similarly, RNA Seq analysis revealed dampened induction of cytokine and chemokine genes as well as failure to upregulated expression of key transcription factors NFKB1 and FOSB following LPS stimulation. The dampened monocyte response is further

evident from reduced surface expression of activation markers CD40 and CD86. Collectively, these differences in the innate immune system provide a potential explanation for the increased incidence of viral infections in obese pregnant women (Karlsson et al., 2012). It is possible that the state of chronic low-grade inflammation associated with obesity in combination with pregnancy-induced increase in circulating immune mediators result in a state of immune tolerance in circulating monocytes.

Additionally, pregravid obesity, led to a failure in the induction of transcripts associated with chromatin organization following LPS treatment at T3, suggesting potential epigenetic constraints. Indeed, we report a significant increase in chromatin accessibility within promoter and intergenic loci that regulate inflammatory responses between T1 and T3 in monocytes from lean subjects. Epigenetic changes with healthy pregnancy have been shown in human uterine NK cells (Gamliel et al., 2018) and mouse mammary glands (Dos Santos et al., 2015). Our study is the first to highlight chromatin remodeling in circulating immune cells, providing first clues of an epigenetic clock of human pregnancy. While the precise mechanisms regulating this epigenetic clock are not clear, studies have demonstrated that both type I interferons and TNF can cooperatively reprogram the epigenome of myeloid cells resulting in increased chromatin accessibility at inflammatory loci (Park et al., 2017) and establishment of transcriptional memory at the chromatin level (Kamada et al., 2018). However, our analysis of circulating immune mediators shows dramatic increase in plasma levels of both TNF and type-I interferons in both lean and obese groups, making this mechanism less likely to regulate chromatin defects in obese group at T3.

Pregravid obesity altered this epigenetic clock, resulting in monocytes undergoing minimal chromatin changes with gestation. A direct comparison of profiles at T3 shows a lack of remodeling within of promoter and enhancer regions that regulate cytokine-signaling (*TNF*), myeloid cell activation (*CD80*), and immune effector process (*HLA-DRA*) in monocytes from subjects with obesity. Moreover, regions that were accessible in monocytes from lean subjects (but remained closed in obese subjects) contained putative binding sites for transcription factors that orchestrate pro-inflammatory responses (AP-1, IRF1, IRF3, and IRF8). In contrast, regions that were accessible in monocytes from subjects with obesity harbored binding sites for regulatory factors such as STAT6 and SMAD2. Epigenetic priming mechanisms play critical roles in tolerance and training of innate immune memory, and our findings support the hypothesis that pregravid obesity results in tolerance in circulating monocytes. This hypothesis is supported by the reduction in *HLA-DR* expression in monocytes at T3, at protein, transcript, and epigenetic level. Lower MHC class II molecule expression has been described in models of endotoxin tolerance and in sepsis patients during late stages of immunoparalysis (Wolk et al., 2003).

An immunotolerant state has been shown to affect functional plasticity in monocytes. Functional assessment of purified monocytes at T3 showed a reduction in the number of monocytes that can phagocytose bacteria but an increased aggregate pathogen engulfment per cell. Furthermore, with obesity at T3, monocytes had an enhanced oxidative burst following LPS exposure. This is in contrast to studies describing reduced *ex vivo* E. coli and S. aureus induced ROS production in tolerant monocytes (Grondman et al., 2019). These differences in outcomes could possibly be explained by different triggers of oxidative stress (LPS vs. pathogen). Immune tolerance can also impact the ability of

monocytes to differentiate towards M1- or M2-like state under different polarization conditions (O'Carroll et al., 2014). In agreement with transcriptional and cytokine responses, monocyte-derived macrophages (MoDM) from mothers with obesity polarized poorly to M1 but not to M2 skewing conditions. Cytokine secretion, however, were dampened under both conditions, suggesting overall reduced plasticity compared to the lean counterparts.

Another manifestation of immune tolerance is the lack of metabolic plasticity (Cane et al., 2019). Indeed, monocytes obtained from humans injected with low dose LPS show a lack of metabolic plasticity, failing to upregulate glycolysis, pentose phosphate pathway (PPP), and downregulate lipid metabolic pathways when re-challenged *ex vivo* with LPS (Grondman et al., 2019). Our analysis of maternal monocytes at T3 showed reduced basal extracellular acidification rate (ECAR) with obesity indicative of dampened preference for glycolysis. Additionally, we observed poor induction of glycolysis following LPS injection. This coupled with the accumulation of higher levels of neutral lipids further supporting metabolic reprogramming with maternal obesity.

In summary, this study revealed that long-term exposure to obesity disrupts the monocyte activation trajectory associated with pregnancy, thereby providing a potential explanation for increased susceptibility in pregnant subjects with obesity to viral infections during gestation and postpartum. The study also provides a conceptual framework of an epigenetic clock that supports the immune clock of pregnancy. We were able to demonstrate that pregravid obesity disrupts the pregnancy immune clock, altering the metabolic, molecular and functional phenotype of peripheral monocytes towards a regulatory phenotype. Future studies will focus on generating a comprehensive model of

monocyte activation with additional gestational time points as well as assessing the impact of pregravid obesity on the monocyte response to pathogens. Peripheral blood monocytes are recruited to become decidual macrophages; hence future experiments will also interrogate the impact of pregravid obesity at the maternal fetal interface.

	Lean (n=11)	**Obese (n=14)**	**p-value**
Gestational age at delivery	40.2 ± 1.1	40.1 ± 1.1	0.71
Mode of delivery			0.97
a) Vaginal	72.7	71.4	
b) Primary cesarean	18.2	21.4	
c) Repeat cesarean	9.1	7.1	
Fetal birth weight (kg)	3.45 ± 0.49	3.58 ± 0.53	0.54
Fetal sex (female %)	45.5	42.9	0.90
Ponderal index (g/cm^3)	24.4 ± 1.2	26.7 ± 3.6	0.05
Placental weight	456 ± 86	482 ± 117	0.54
Pregravid BMI	22.27 ± 1.95	37.5 ± 5.0	<0.0001

Table 2.1 Characteristics of subjects recruited in Cohort I. Maternal blood was collected during week 37 visit. Cord blood samples were collected during delivery.

	Lean (n=69)	Obese (n=48)	p-value
Maternal Age	32.8 ± 4.7	29.4 ± 9	n.s.
Pregravid BMI	21.9 ± 1.7	35.2 ± 5.2	<0.0001
Fat mass at 12 weeks (kg)	17.3 ± 4.1	42.6 ± 11.4	<0.0001
Fat mass at 37 weeks (kg)	22 ± 5.5	44.2 ± 11.1	<0.0001
Gestational Weight Gain (kg)	15 ± 4.5	10.4 ± 7.6	<0.001
Fetal birth weight (kg)	3.45 ± 0.49	3.58 ± 0.53	0.54
Fetal sex (female %)	45.5	42.9	0.90
Ponderal index (g/cm^3)	24.4 ± 1.2	26.7 ± 3.6	0.05
Placental weight	456 ± 86	482 ± 117	0.54

Table 2.2 Combined characteristics of subjects recruited in Cohorts II and III. Blood was collected at gestational weeks 12 (T1) and 37 (T3) for Cohort II. For Cohort III, only T3 samples were collected. Cord blood was collected at delivery time point.

	Lean (n=36)	Obese (n=32)	p-value
Maternal Age	33.4 ± 5.47	32.63 ± 4.55	n.s.
Pregravid BMI (kg/m^2)	21.9 1 ± 1.88	38.41 ± 8.27	<0.0001
Gestational Age at delivery	38.51 ± 1.65	38.01 ± 1.04	n.s.
Fetal sex (% female)	48.38	35.71	
History of Cesarean (%)	33.3	40.6	
Mode of delivery (% Cesarean)	100	100	

Table 2.3 Characteristics of subjects recruited in Cohort IV. Samples were collected during scheduled term cesarean deliveries. Maternal blood, cord blood, placental decidua, and chorionic villi membranes were collected as part of the study.

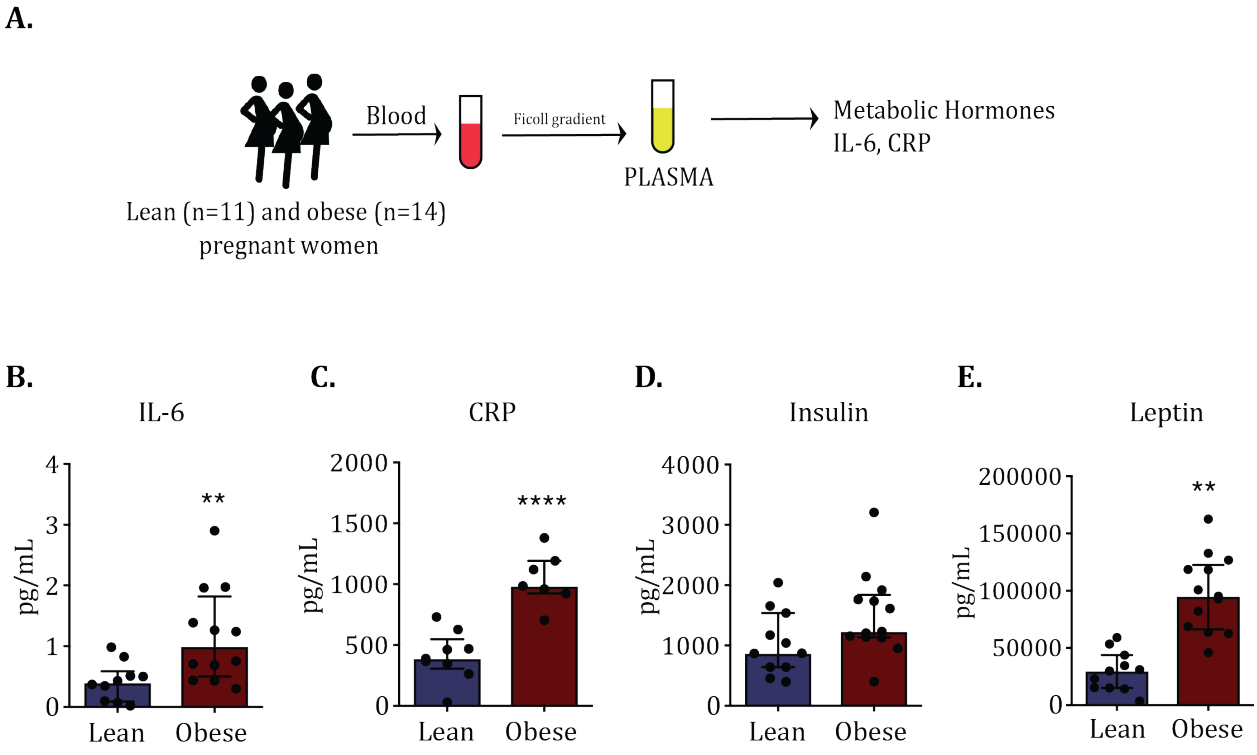

Figure 2.1 Maternal obesity is associated with a state of chronic low-grade inflammation at term.
(A) Experimental design - Maternal blood was collected during week 37 visit. Plasma levels of CRP and IL-6 were measured using ELISA. Levels of metabolic hormones were measured using luminex. (B-E) Plasma levels of (B) IL-6, (C) C-reactive protein (CRP), (D) insulin, and (E) leptin. (P-values: * - $p<0.05$; **- $p<0.01$; **** - $p<0.001$)

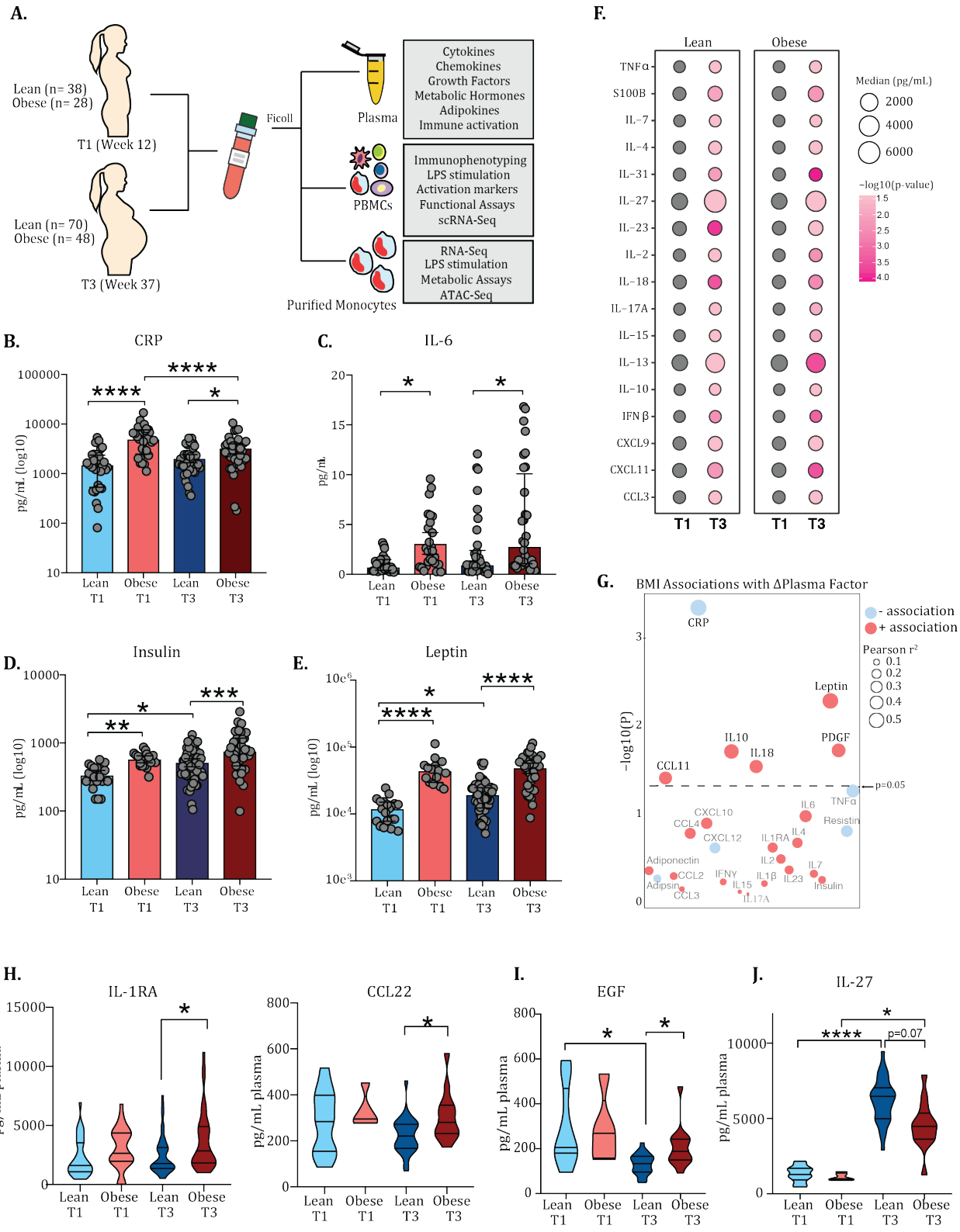
A.
Lean (n= 38)
Obese (n= 28)
T1 (Week 12)
Lean (n= 70)
Obese (n= 48)
T3 (Week 37)
Ficoll
Plasma
PBMCs
Purified Monocytes
Cytokines
Chemokines
Growth Factors
Metabolic Hormones
Adipokines
Immune activation
Immunophenotyping
LPS stimulation
Activation markers
Functional Assays
scRNA-Seq
RNA-Seq
LPS stimulation
Metabolic Assays
ATAC-Seq
B.
CRP
pg/mL (log10)
C.
IL-6
pg/mL
D.
Insulin
E.
Leptin
Lean T1
Obese T1
Lean T3
Obese T3
F.
Lean
Obese
TNFα
S100B
IL-7
IL-4
IL-31
IL-27
IL-23
IL-2
IL-18
IL-17A
IL-15
IL-13
IL-10
IFN β
CXCL9
CXCL11
CCL3
T1
T3
Median (pg/mL)
2000
4000
6000
−log10(p-value)
G.
BMI Associations with ΔPlasma Factor
- association
+ association
Pearson r²
−log10(P)
p=0.05
CRP
Leptin
IL10
IL18
PDGF
CCL11
TNFα
IL6
Resistin
CXCL10
CCL4
CXCL12
IL1RA
IL4
IL2
IL7
Adiponectin
IL23
IFNγ
IL1β
IL15
Adipsin
CCL2
CCL3
IL17A
Insulin
H.
IL-1RA
CCL22
pg/mL plasma
I.
EGF
J.
IL-27
p=0.07

(previous page) **Figure 2.2 Experimental Design and longitudinal changes in maternal inflammatory environment with gestation and obesity.**
(A) Blood samples obtained from a total of 117 women (69 lean and 48 obese) during early (week 12 – T1) and late (week 37 – T3) pregnancy. For a subset of subjects recruited at T1 (37 lean and 28 obese) blood was also collected at T3 (29 lean and 27 obese). For the remaining subjects, blood was collected only at T3 (32 lean and 20 obese). Circulating levels of inflammatory mediators, metabolic hormones, and adipokines were measured using luminex and ELISA. PBMC were isolated from blood, and monocyte subsets were profiled single cell RNA sequencing. Further assessment of monocyte phenotype, their cytokine and functional responses was done using flow cytometry. Purified monocytes were profiled using RNA-Seq and ATAC-Seq. (B, C) Dot plots depicting changes in plasma levels of inflammatory mediators (B) CRP and (C) IL-6 measured using high sensitivity ELISA. (D, E) Circulating levels of metabolic hormones (D) insulin, (E) leptin were measured using multiplex ELISA. Levels of significance: * - $p<0.05$, ** - $p<0.01$, *** $p<0.001$, **** - $p< 0.0001$. Bars denote median with interquartile ranges. (F) Bubble plot representing immune mediator levels in plasma that increase with gestation independent of BMI. Size of the bubble represents median values of analytes in pg/mL (log2 transformed). The colors at T3 represent the levels of significance relative to T1. (G) Association between changes in plasma analyte level with gestation (T3-T1) and BMI. Size of the bubble reflects the strength of Pearson's correlation, and color indicates direction of association (red-positive; blue-negative). (H-J) Four-way violin plots comparing plasma levels of (H) anti-inflammatory IL-1RA and M2-associated chemokine CCL22, (I) growth factor EGF, and (J) pro-inflammatory IL-27. Levels of significance: *- $p<0.05$, ****- $p<0.0001$.

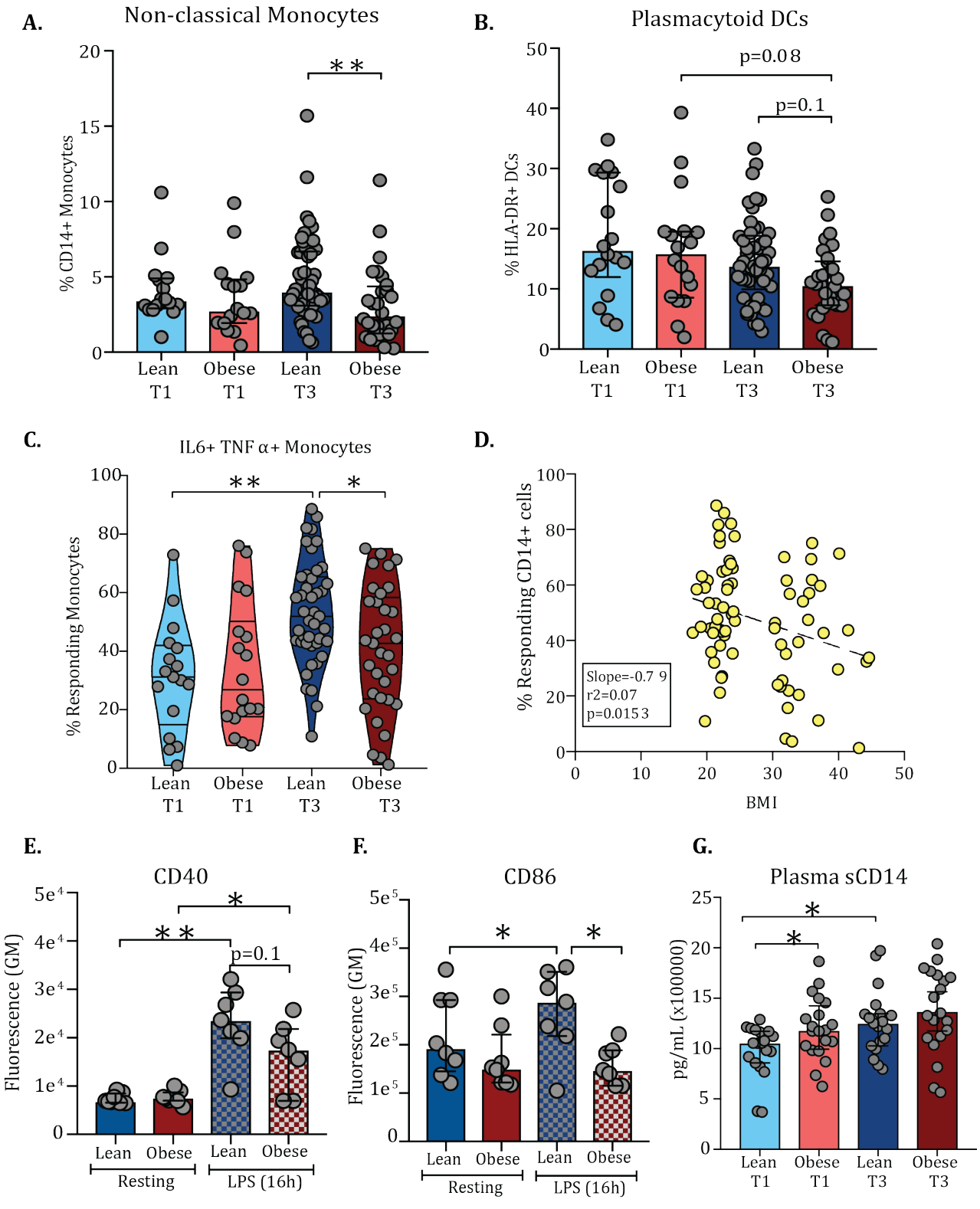
A.
Non-classical Monocytes
% CD14+ Monocytes
20
15
10
5
0
**
Lean T1
Obese T1
Lean T3
Obese T3
B.
Plasmacytoid DCs
% HLA-DR+ DCs
50
40
30
20
10
0
p=0.08
p=0.1
Lean T1
Obese T1
Lean T3
Obese T3
C.
IL6+ TNF α+ Monocytes
% Responding Monocytes
100
80
60
40
20
0
**
*
Lean T1
Obese T1
Lean T3
Obese T3
D.
% Responding CD14+ cells
100
80
60
40
20
0
Slope=-0.7 9
r2=0.07
p=0.015 3
0
10
20
30
40
50
BMI
E.
CD40
Fluorescence (GM)
5e⁴
4e⁴
3e⁴
2e⁴
1e⁴
0
*
**
p=0.1
Lean
Obese
Lean
Obese
Resting
LPS (16h)
F.
CD86
Fluorescence (GM)
5e⁵
4e⁵
3e⁵
2e⁵
1e⁵
0
*
*
Lean
Obese
Lean
Obese
Resting
LPS (16h)
G.
Plasma sCD14
pg/mL (x100000)
25
20
15
10
5
0
*
*
Lean T1
Obese T1
Lean T3
Obese T3

(previous page) **Figure 2.3 Pregnancy and obesity associated changes in innate immune phenotype and ex vivo response.**
(A) Frequencies of non-classical monocytes ($CD14^{+}CD16^{++}$) and (B) plasmacytoid cells ($HLA\text{-}DR^{+}CD123^{high}CD11c^{-}$) (C) Violin plot showing percentage of IL6 and TNF producing monocytes following 16h LPS stimulation (D) Linear associations between BMI and monocyte responses to LPS at T3. Deviations in slope of regression line were tested using F-test. Surface expression of (E) CD40 and (F) CD86 on monocytes ($CD14^{+}HLA\text{-}DR^{+}$) following 16h LPS stimulation at T3. (G) Plasma levels of soluble CD14 measured at both time points using ELISA. Levels of significance: * - $p<0.05$, ** - $p<0.01$. Bars denote median and interquartile ranges.

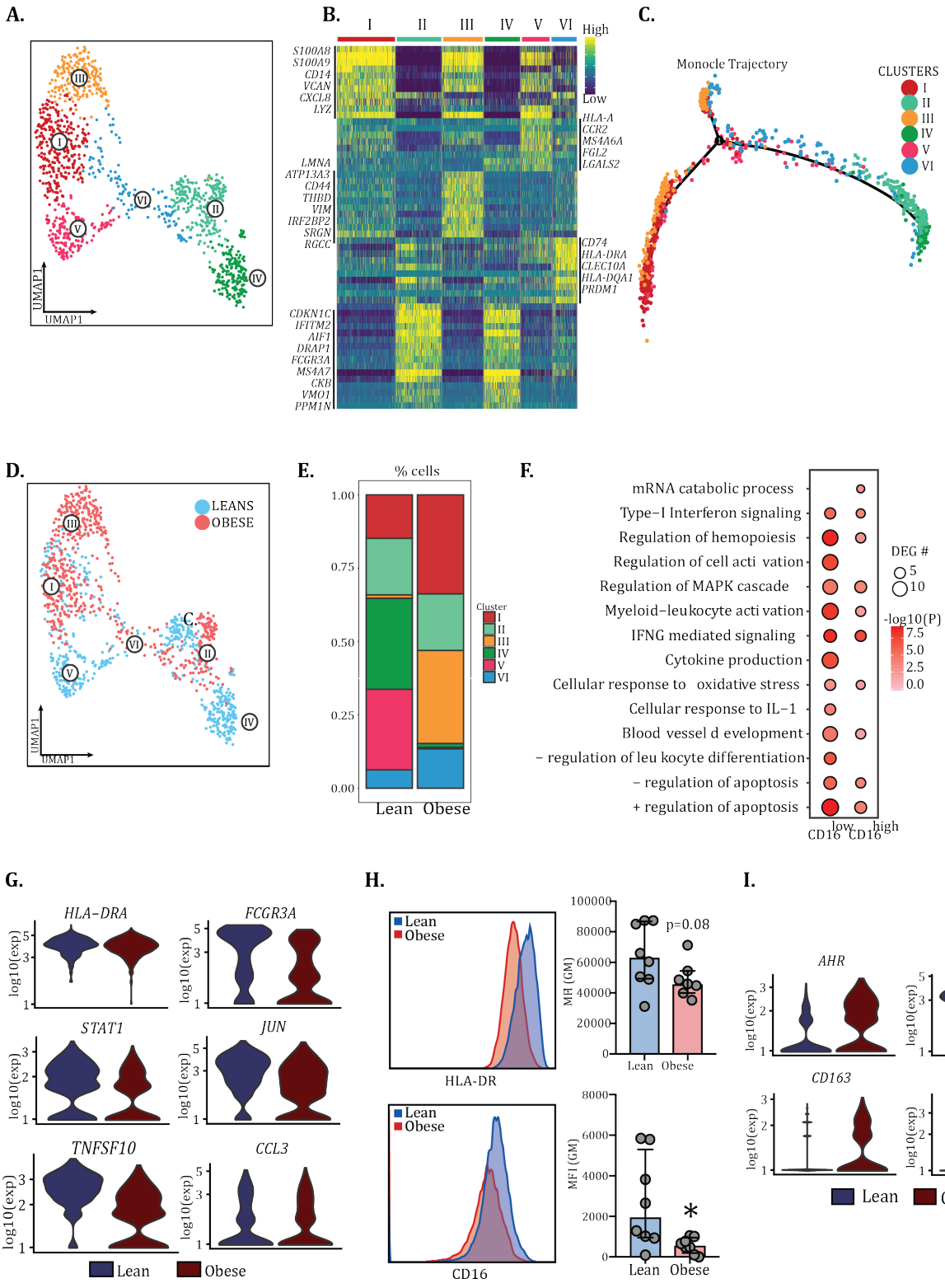
A.
B.
C.
D.
E.
F.
G.
H.
I.
UMAP1
UMAP2
I
II
III
IV
V
VI
High
Low
S100A8
S100A9
CD14
VCAN
CXCL8
LYZ
HLA-A
CCR2
MS4A6A
FGL2
LGALS2
LMNA
ATP13A3
CD44
THBD
VIM
IRF2BP2
SRGN
RGCC
CD74
HLA-DRA
CLEC10A
HLA-DQA1
PRDM1
CDKN1C
IFITM2
AIF1
DRAP1
FCGR3A
MS4A7
CKB
VMO1
PPM1N
Monocle Trajectory
CLUSTERS
LEANS
OBESE
% cells
Cluster
Lean
Obese
mRNA catabolic process
Type−I Interferon signaling
Regulation of hemopoiesis
Regulation of cell acti vation
Regulation of MAPK cascade
Myeloid−leukocyte acti vation
IFNG mediated signaling
Cytokine production
Cellular response to oxidative stress
Cellular response to IL−1
Blood vessel d evelopment
− regulation of leu kocyte differentiation
− regulation of apoptosis
+ regulation of apoptosis
DEG #
-log10(P)
CD16
low
high
HLA−DRA
FCGR3A
STAT1
JUN
TNFSF10
CCL3
log10(exp)
HLA-DR
CD16
MFI (GM)
p=0.08
AHR
CD52
CD163
THBS1

(previous page) **Figure 2.4 Single cell RNA sequencing of monocytes from lean mothers and mothers with obesity at term.**
(A) UMAP visualization of monocytes following segregation of $CD14^{high}$ clusters in UMAP projection of PBMC from lean (n=2) and obese (n=2) subjects, colored by cell state (clusters) and (B) Heatmap showing expression pattern of top 10 distinguishing markers per cell state with selected markers indicated (yellow = high expression; green = intermediate expression; blue = low expression) phenotype. (C) Trajectory analysis of monocyte expression places them in the order of phenotype with cells are colored by their original clusters. (D) UMAP visualization of monocytes, colored by phenotype. (E) Relative frequencies of UMAP clusters in either group. (F) Pairwise functional enrichment of gene signatures differentially expressed with obesity in classical and non-classical monocyte subsets. Bubble size and color are indicative of number of genes within each ontology term and the significance of its enrichment. (G) Violin plots showing log-transformed, normalized expression levels for select genes downregulated with pregravid obesity (H) Surface expression of HLA-DR and CD16 using flow cytometry. Error bars represent medians with interquartile range. (I) Violin plots showing log-transformed normalized expression levels for select genes up regulated with pregravid obesity.

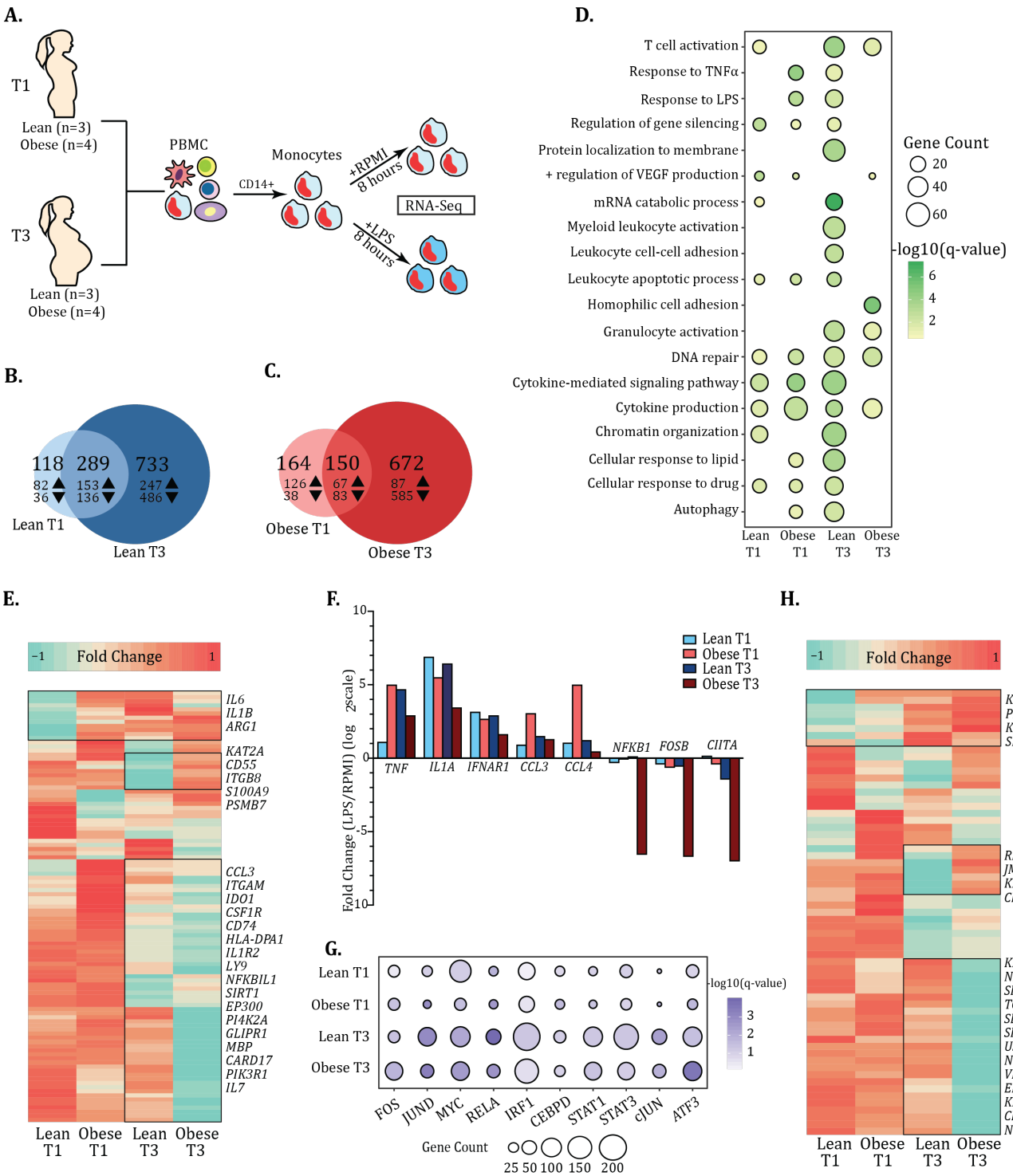
A.
T1
Lean (n=3)
Obese (n=4)
T3
Lean (n=3)
Obese (n=4)
PBMC
CD14+
Monocytes
+RPMI 8 hours
+LPS 8 hours
RNA-Seq
B.
118 289 733
82 153 247
36 136 486
Lean T1
Lean T3
C.
164 150 672
126 67 87
38 83 585
Obese T1
Obese T3
D.
T cell activation
Response to TNFα
Response to LPS
Regulation of gene silencing
Protein localization to membrane
+ regulation of VEGF production
mRNA catabolic process
Myeloid leukocyte activation
Leukocyte cell-cell adhesion
Leukocyte apoptotic process
Homophilic cell adhesion
Granulocyte activation
DNA repair
Cytokine-mediated signaling pathway
Cytokine production
Chromatin organization
Cellular response to lipid
Cellular response to drug
Autophagy
Lean T1
Obese T1
Lean T3
Obese T3
Gene Count
20
40
60
-log10(q-value)
6
4
2
E.
−1
Fold Change
1
IL6
IL1B
ARG1
KAT2A
CD55
ITGB8
S100A9
PSMB7
CCL3
ITGAM
IDO1
CSF1R
CD74
HLA-DPA1
IL1R2
LY9
NFKBIL1
SIRT1
EP300
PI4K2A
GLIPR1
MBP
CARD17
PIK3R1
IL7
Lean T1
Obese T1
Lean T3
Obese T3
F.
Fold Change (LPS/RPMI) (log 2scale)
10
5
0
-5
-10
Lean T1
Obese T1
Lean T3
Obese T3
TNF
IL1A
IFNAR1
CCL3
CCL4
NFKB1
FOSB
CIITA
G.
Lean T1
Obese T1
Lean T3
Obese T3
-log10(q-value)
3
2
1
FOS
JUND
MYC
RELA
IRF1
CEBPD
STAT1
STAT3
cJUN
ATF3
Gene Count
25 50 100 150 200
H.
−1
Fold Change
1
KAT2A
PRMT1
KMT2E
SETD6
REST
JMJD1C
KDM7A
CHD1
KDM2B
NR3C1
SIRT1
TGFB1
SETDB1
SIRT2
USP3
NCOA3
VEGFA
EP300
KDM4C
CHD6
NCOR1
Lean T1
Obese T1
Lean T3
Obese T3

(previous page) **Figure 2.5 Cell intrinsic defects in monocyte responses to LPS with maternal obesity.** (A) Experimental design for RNA-seq. (B-C) Venn diagrams comparing LPS induced DEG between T1 and T3 in purified monocytes from (B) lean and (C) obese groups following 8h LPS exposure. Numbers of Up- and down-regulated DEG (FDR≤0.05) are annotated with corresponding arrows (D) Bubble plot representing gene ontology terms enriched following LPS stimulation in all four groups following LPS stimulation. Both up- and down-regulated genes are included. Size of the bubble represents numbers of genes mapping to the term while color indicates level of significance. (E) Heatmap comparing fold changes of DEG (both up- and down-regulated) that mapped to GO terms "cytokine production" and "Myeloid leukocyte activation". Green indicates down-regulation while orange indicates up-regulation. (F) Fold change of key inflammatory genes in response to LPS. (G) Bubble plots representing number of DEG regulated by specific LPS inducible transcription factors predicted by ChEA3. Size of the bubble represents the numbers of DEG regulated by each transcription factor. Color of the bubble represents the level of significance for each prediction. (H) Heatmap comparing fold changes of DEG (both up- and down-regulated) that mapped to GO terms "Chromatin organization". Green indicates down-regulation while orange indicates up-regulation.

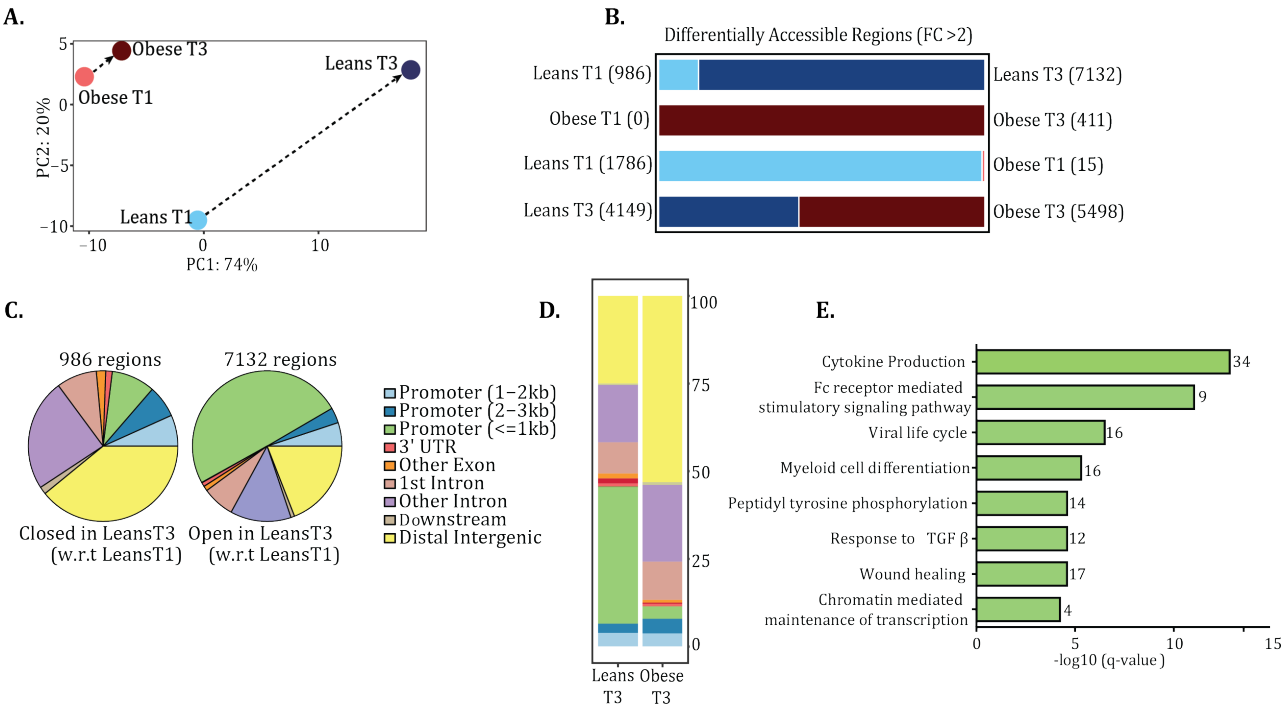

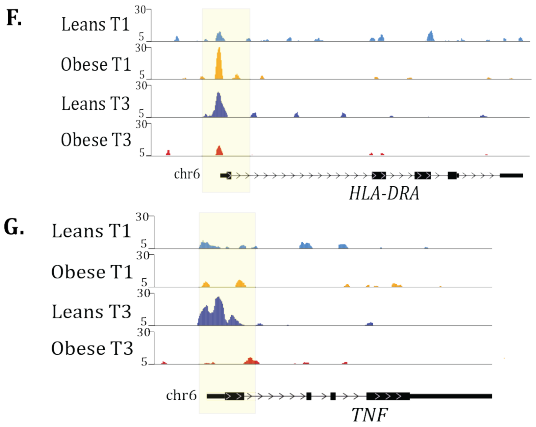

H.

TF	Motif	Enrichment/ Background	-log10(P)	q-value
PU.1		12..08% / 4.14%	1.146e+2	0.00
AP-1		10.26% / 3.62%	9.245e+1	0.00
NFY		13.33% / 6.23%	7.12e+1	0.00
IRF8		7.7% / 2.9%	3.8e+1	0.00
IRF3		4.12% / 1.59%	3.232e+1	0.00
IRF1		2.06% / 0.72%	1.98e+1	0.00

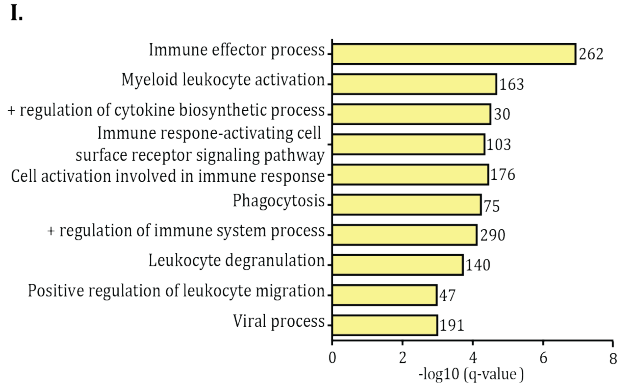

J.

TF	Motif	Enrichment/ Background	-log10(P)	q-value
STAT6		33.03% / 6.22%	9.26e+2	0.00
SMAD2		36.2% / 12.01%	5.56e+2	0.00
LXR		5.23% / 1.54%	8.89e+1	0.00

(previous page) **Figure 2.6 Epigenetic adaptations with pregnancy and maternal obesity.**
(A) PCA of chromatin accessibility profiles in monocytes isolated at T1 and T3 from lean and obese subjects. Arrows represent trajectory from T1 to T3. (B) Bar graphs with numbers of differentially accessible regions (DAR) identified in each comparison. Numbers in parenthesis denote open regions identified in a particular group in relative to the comparison group. (C) Pie charts showing genomic contexts of loci identified as DAR with gestation in the lean group. (D) Genomic annotations of 4149 and 5,498 DAR identified as open in lean and obese group respectively at T3. (E) Functional enrichment of genes regulated by promoter associated DAR open in lean group relative to obese group (FC>2). Genes associated with these regions are quantified next to each term (F-G) WashU Epigenome tracks for (F) *HLA-DRA* and (G) *TNF* locus with promoter vicinity highlighted in yellow. (H) Enrichment of motifs in promoter associated open DAR in lean group. Only motifs identified in myeloid cells are included in the table. (I) Gene ontologies of intergenic associations identified by GREAT as significantly open in lean group at T3. (J) Enrichment of motifs in open intergenic DAR in obese group. Only motifs identified in myeloid cells are included in the table.

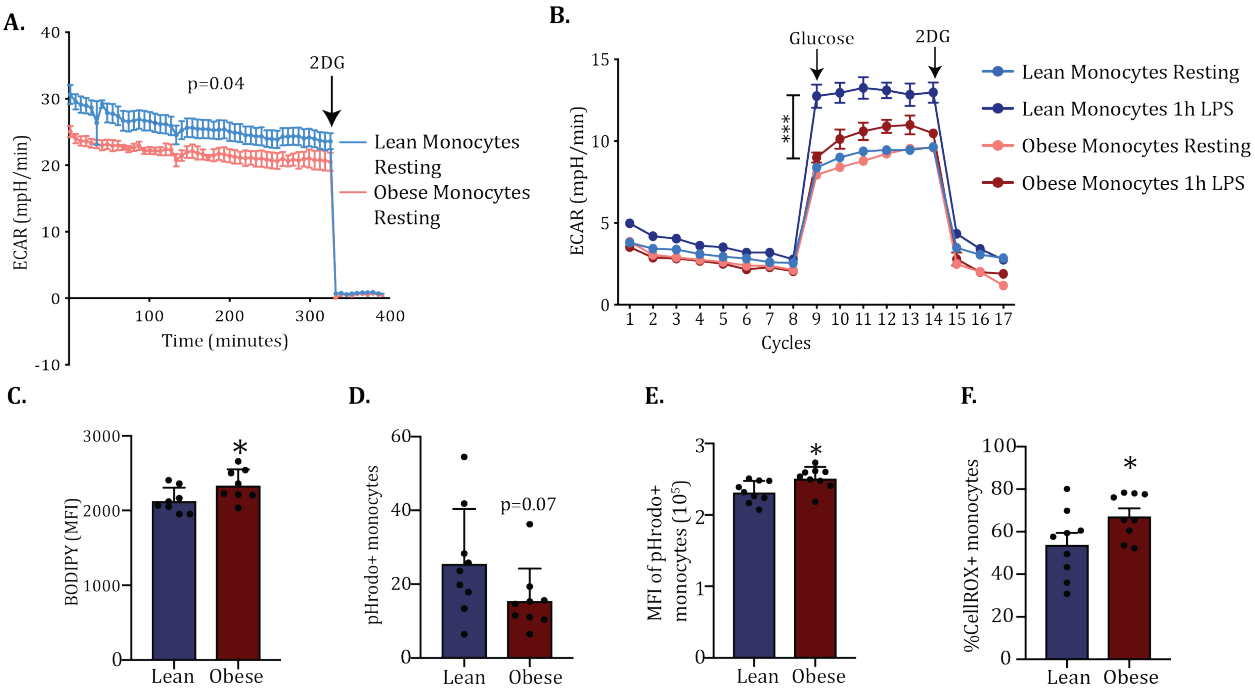

Figure 2.7 Metabolic and functional reprogramming of monocytes with maternal obesity at term.

(A) Mean ECAR of purified monocytes from lean (blue) and obese (red) group (n=3/group) under basal conditions using glycolytic rate assay. (B) Mean ECAR of LPS activated monocytes (acute injection) from lean (blue) and obese (red) under glucose-free conditions, and post glucose injection using glycolytic stress assay. (C) Bar graphs comparing MFIs of BODIPY within CD14+ gate in PBMC (D) Bar graphs comparing pHrodo+ CD14+ cells following incubation of PBMC with pHrodo conjugated *E. coli* for 4 hours and (E) pHrodo signal within the pHrodo+ monocytes. Y-axis represents median fluorescence intensity. (F) Cytosolic ROS readouts in LPS activated monocytes using FACS analysis of CellROX treated PBMC. P-values: * - $p<0.05$; *** - $p<0.001$.

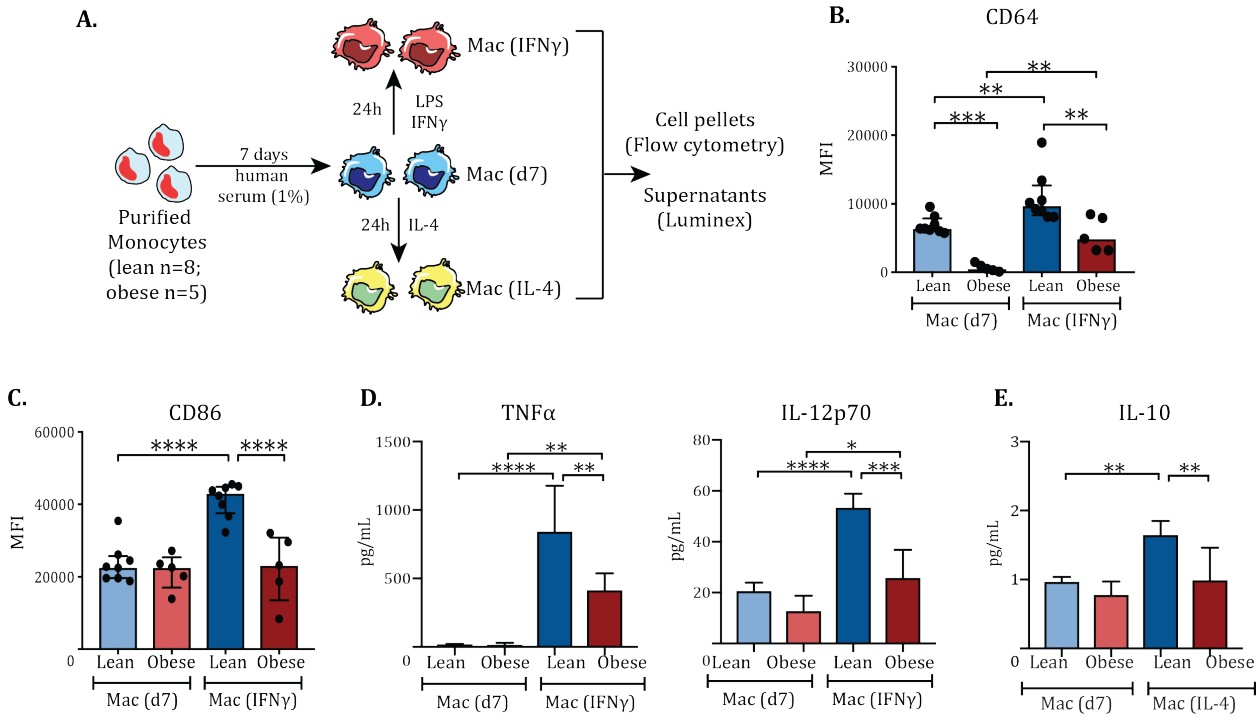

Figure 2.8 Macrophage fate and phenotype with maternal obesity.
(A) Experimental design for monocyte differentiation and polarization assay. (B) Bar graphs comparing surface CD64 and (C) CD86 expression following LPS and IFNγ stimulation on day 7. (D) Secreted TNFα and IL-12 levels following LPS and IFNγ stimulation on day 7 using luminex. (E) Secreted IL-10 levels following IL-4 stimulation on day 7. P-values: * - p<0.05; ** - p<0.01; *** - p<0.001; **** - p<0.0001. (F) Evolving model describing the trajectory of monocyte activation with gestation and pregravid obesity.

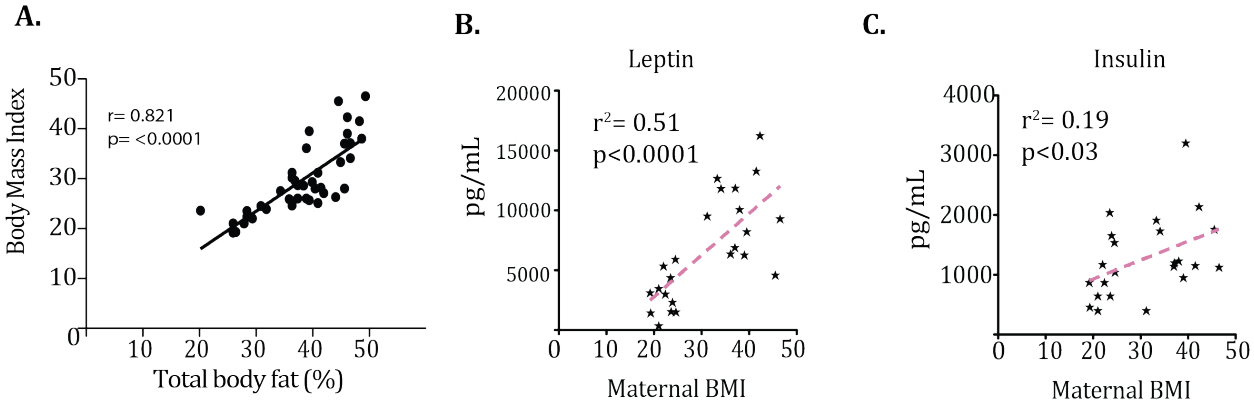

Supplemental Figure 2.1 Body Mass Index in relation to fat mass.
(A) Body fat composition correlated significantly with body mass index (BMI). Human subjects were therefore stratified by BMI and defined as lean and obese. (B-C) BMI associated linear increases in circulating (B) leptin and (C) insulin levels.

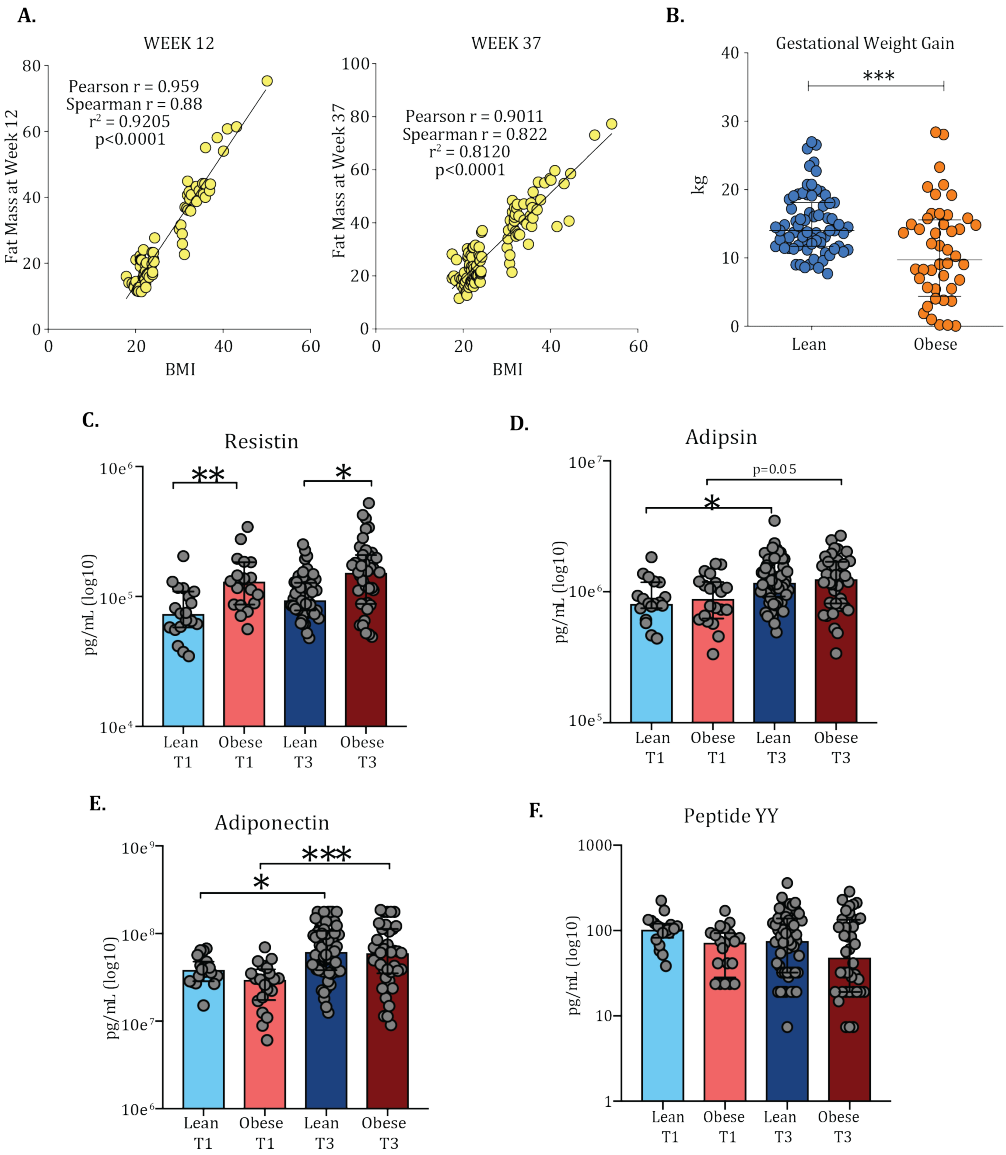

Supplemental Figure 2.2 Longitudinal changes in weight and hormones.
(A, B) Linear regression of fat mass and pregravid BMI at (A) T1 and (B) T3. (C) Dot plots demonstrating gestational weight gain (GWG) in lean and obese subjects. (C, D, E, F) Dot plots of circulating levels of (C) resistin, (D) adipsin, (E) adiponectin, and (F) peptide YY (PYY) at T1 and T3.

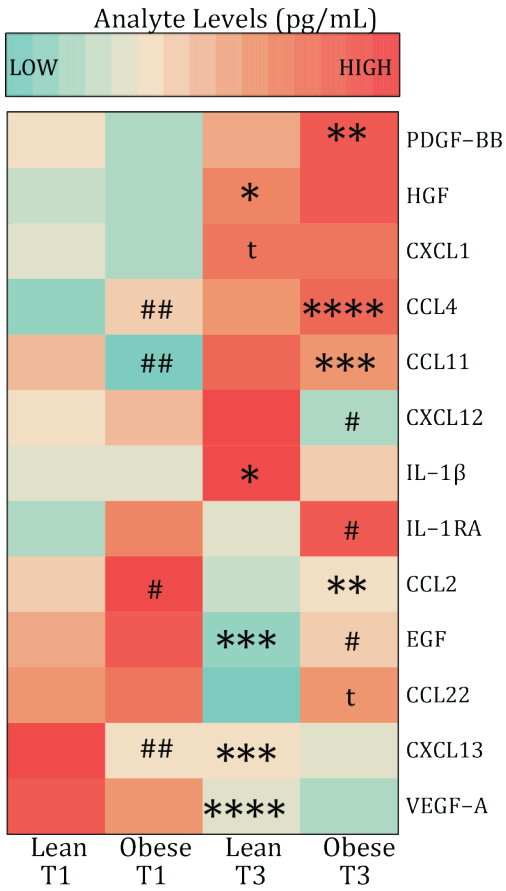

Supplemental Figure 2.3 Plasma cytokine/chemokine/growth factor profiling. Heatmap representing median values of plasma immune mediators significantly impacted by pregravid obesity. Significant changes with gestational age are indicated in * and significant changes with pregravid obesity are indicated in #. Levels of significance: t – p<0.1, */# - p<0.05, **/## - p<0.01, *** p<0.01, **** - p< 0.0001.

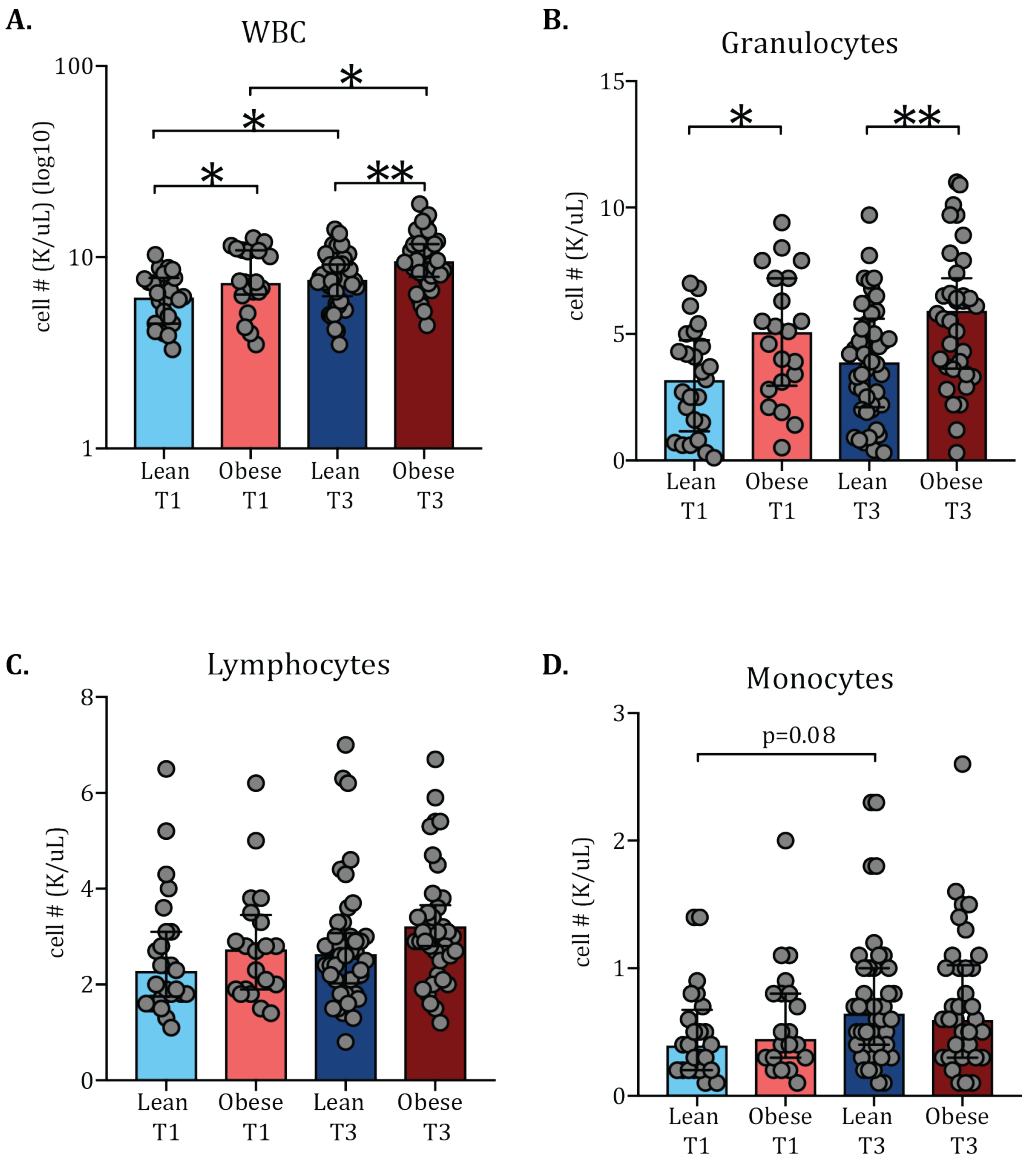

Supplemental Figure 2.4 Complete Blood Counts (CBC).
(A) Numbers of white blood cells (WBC), (B) granulocytes, (C) lymphocytes, and (D) monocytes measured in whole blood.

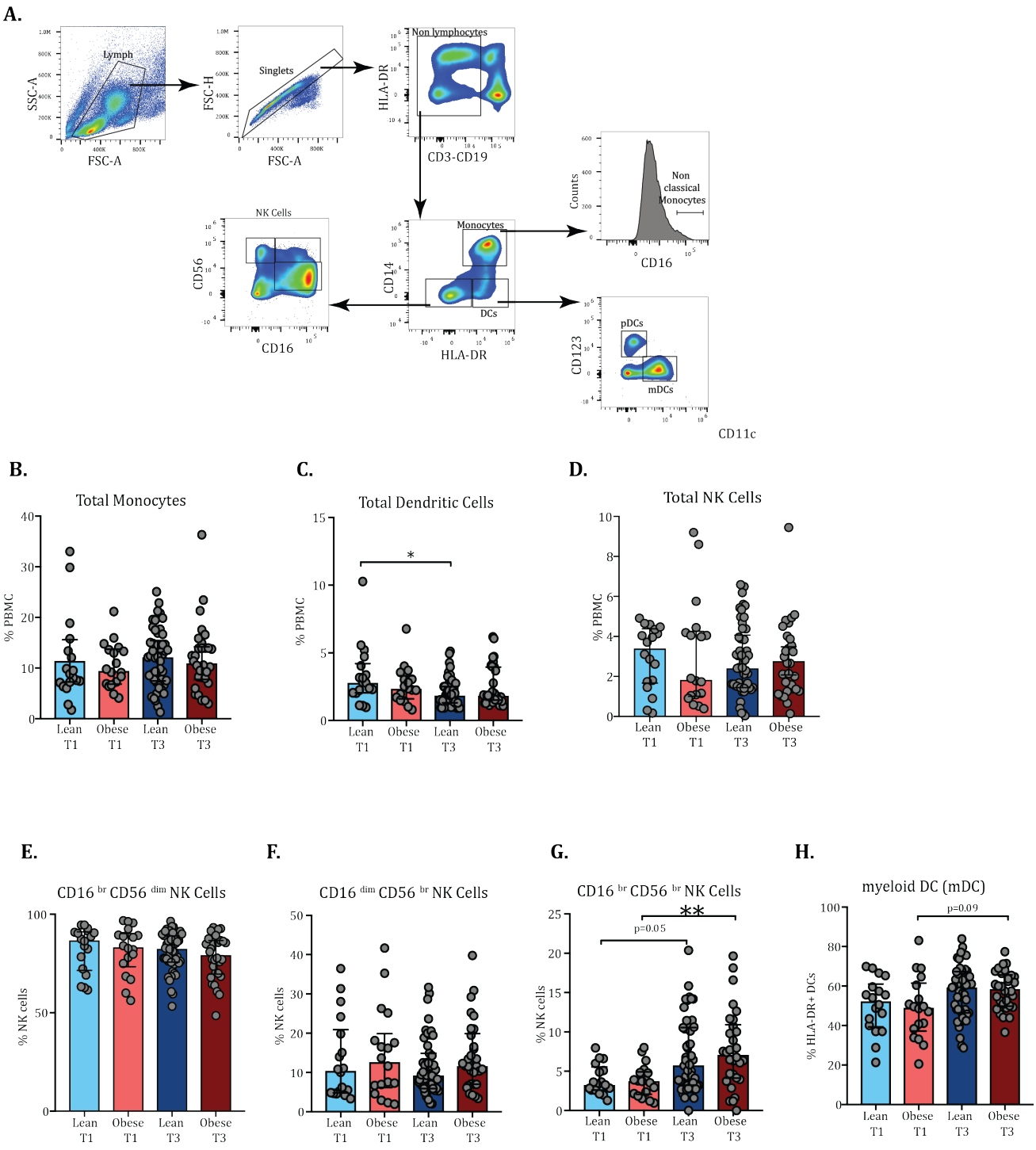

Supplemental Figure 2.5 Phenotyping of innate immune cells using flow cytometry. (A) Gating strategy for characterization of innate immune cell populations from PBMC. (B) Percentages of total monocytes, (C) DC, and (D) NK cells in PBMC. (E-G) Percentages of Natural Killer (NK) cell subsets (H) Percentages of mDCs ($CD11c^{high}$) within DC population.

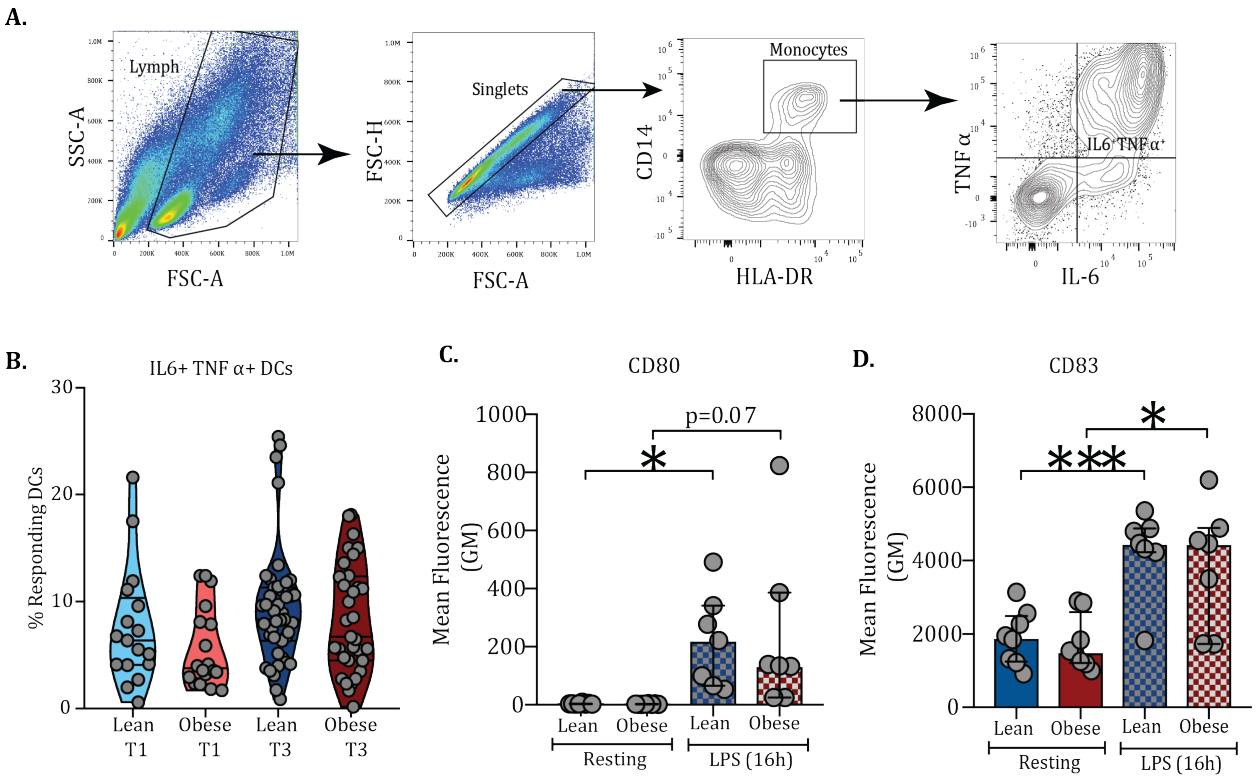

Supplemental Figure 2.6 Cytokine responses to *ex vivo* stimulation.
(A) Gating strategy for measuring frequency of responding monocytes following *ex vivo* stimulation with LPS using intracellular cytokine staining. (B) Violin plot showing percentage of IL6 and TNF producing dendritic cells following 16h LPS stimulation. Surface expression of (C) CD80 and (D) CD83 on monocytes ($CD14^{+}HLA\text{-}DR^{+}$) following 16h LPS stimulation at T3 time point.

A.

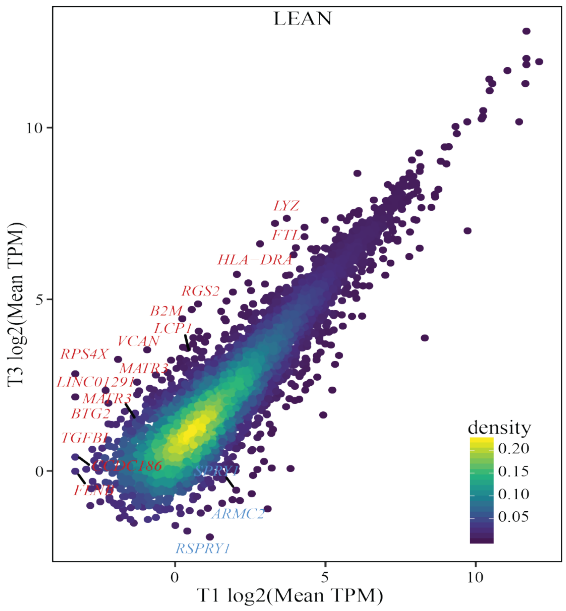

B.

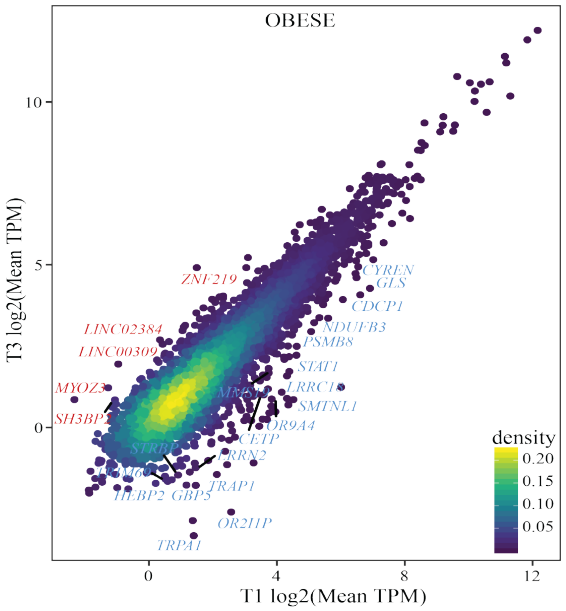

Supplemental Figure 2.7 Baseline transcriptional differences with pregnancy.
Scatter plot depiction of normalized transcript counts (TPM) on a log2 scale from resting monocyte at T1 and T3 (projected on X and Y axes respectively) obtained from (A) lean and (B) obese groups. Only genes with significant expression differences ($p<0.001$) are annotated.

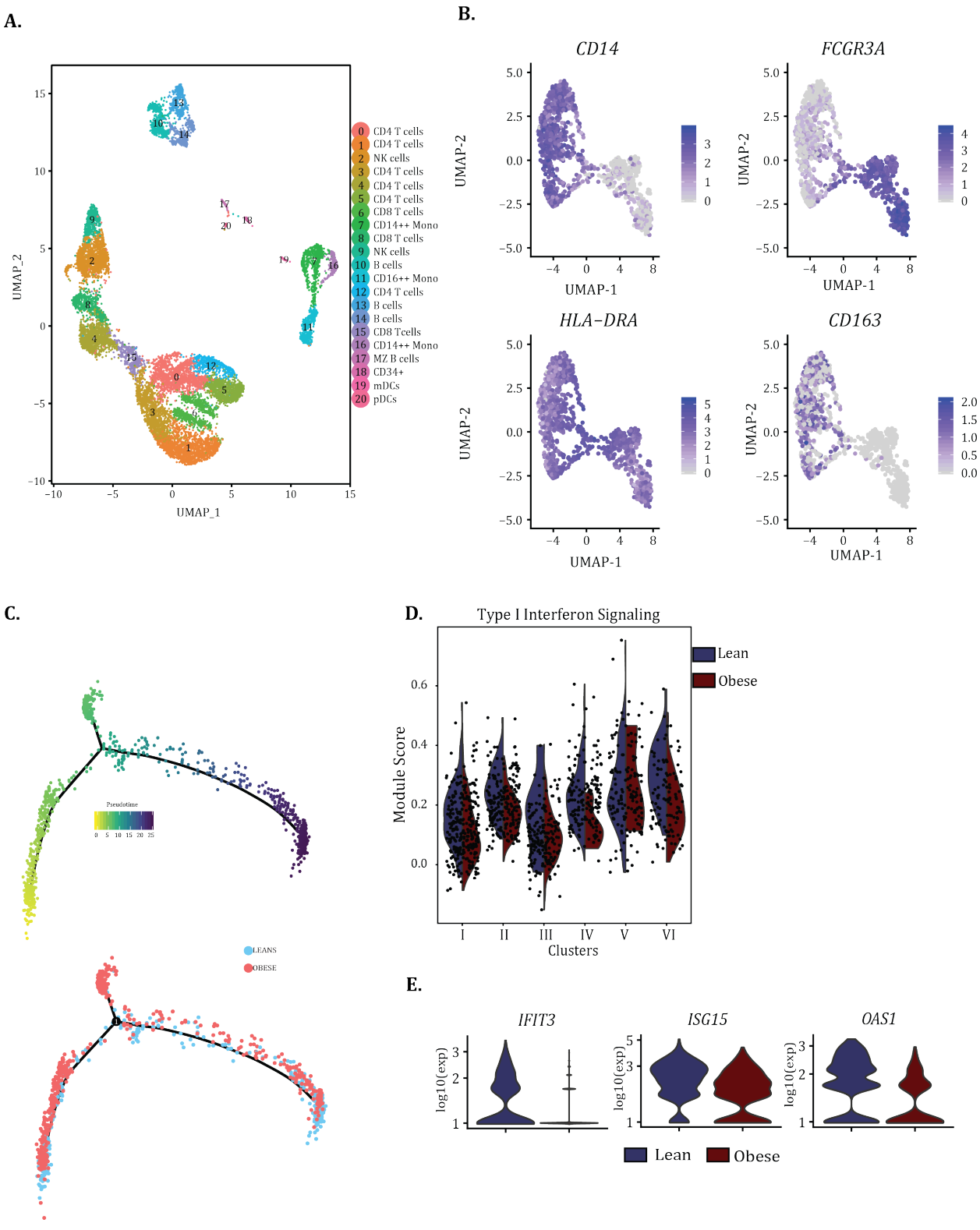
A.
B.
C.
D.
E.
UMAP_1
UMAP_2
0 CD4 T cells
1 CD4 T cells
2 NK cells
3 CD4 T cells
4 CD4 T cells
5 CD4 T cells
6 CD8 T cells
7 CD14++ Mono
8 CD8 T cells
9 NK cells
10 B cells
11 CD16++ Mono
12 CD4 T cells
13 B cells
14 B cells
15 CD8 Tcells
16 CD14++ Mono
17 MZ B cells
18 CD34+
19 mDCs
20 pDCs
CD14
FCGR3A
HLA-DRA
CD163
UMAP-1
UMAP-2
Pseudotime
LEANS
OBESE
Type I Interferon Signaling
Module Score
Clusters
I
II
III
IV
V
VI
Lean
Obese
IFIT3
ISG15
OAS1
log10(exp)

(previous page) **Supplemental Figure 2.8 Baseline transcriptional differences with pregnancy. Single cell RNA profiling of monocytes at term.**
(A) UMAP visualization of PBMC isolated from lean mothers (n=2) and mothers with obesity (n=2) mothers at delivery time point. Live cells were enriched using FACS and profiled using droplet based single cell RNA sequencing. (B) Feature plots of characteristic markers to delineate subtypes of monocytes based on their levels of expression as gradient of purple. (C) Pseudotime ordering of monocytes revealing progressive shifts in cellular states with pregravid obesity. (D-E) Violin plots showing log-transformed, normalized expression levels for select genes (D) down-regulated and (E) up-regulated with pregravid obesity.

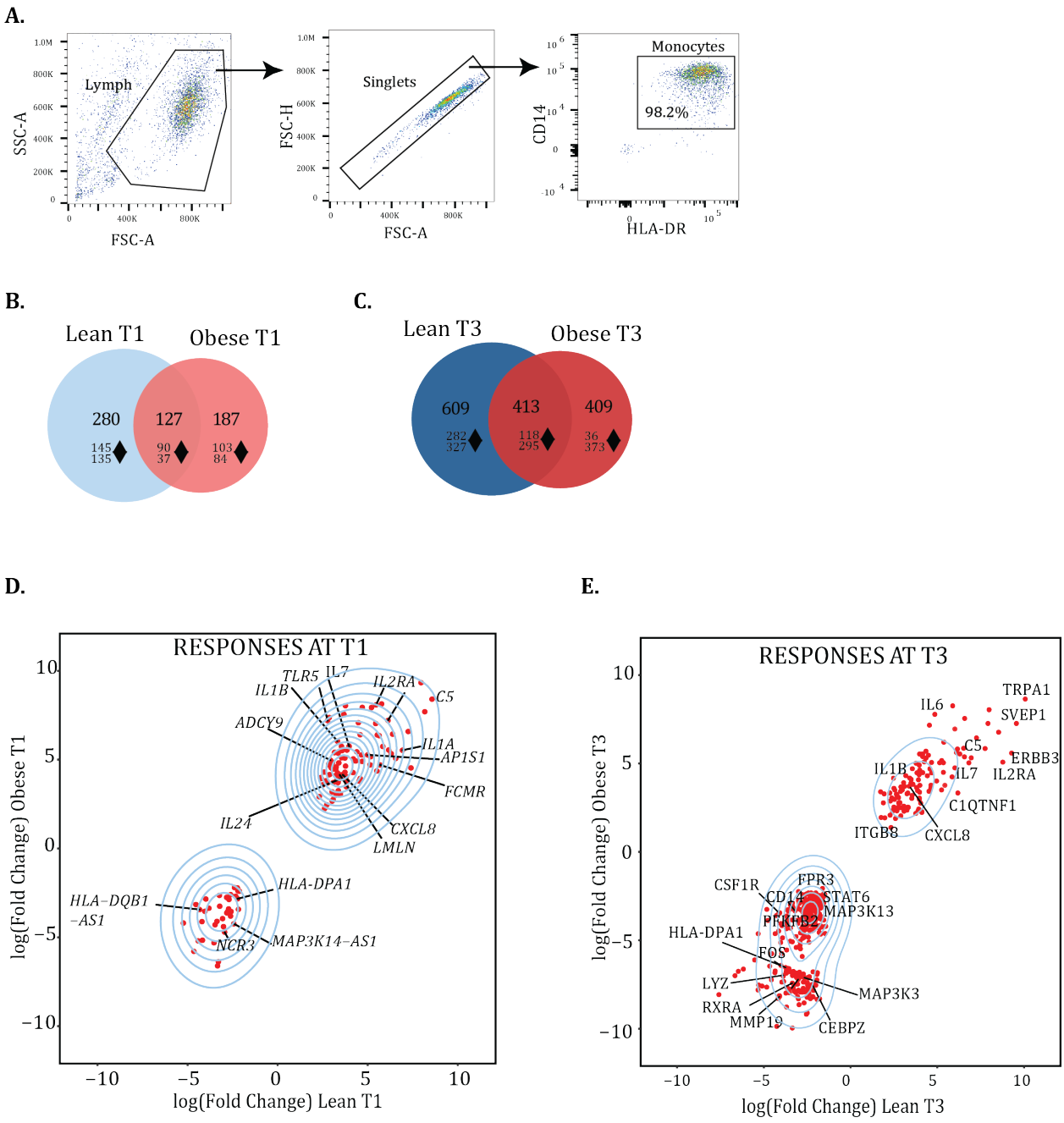

Supplemental Figure 2.9 Profiling transcriptional responses to LPS.
(A) Gating strategy for assessment of purity of monocytes following magnetic bead separation. (B) Comparing LPS responsive DEG in lean and obese group at T1 and (C) T3 (D-E) Density scatterplot comparing fold changes of DEG responsive to LPS in both groups at (D) T1 – 127 common genes and (E) T3 – 413 common genes.

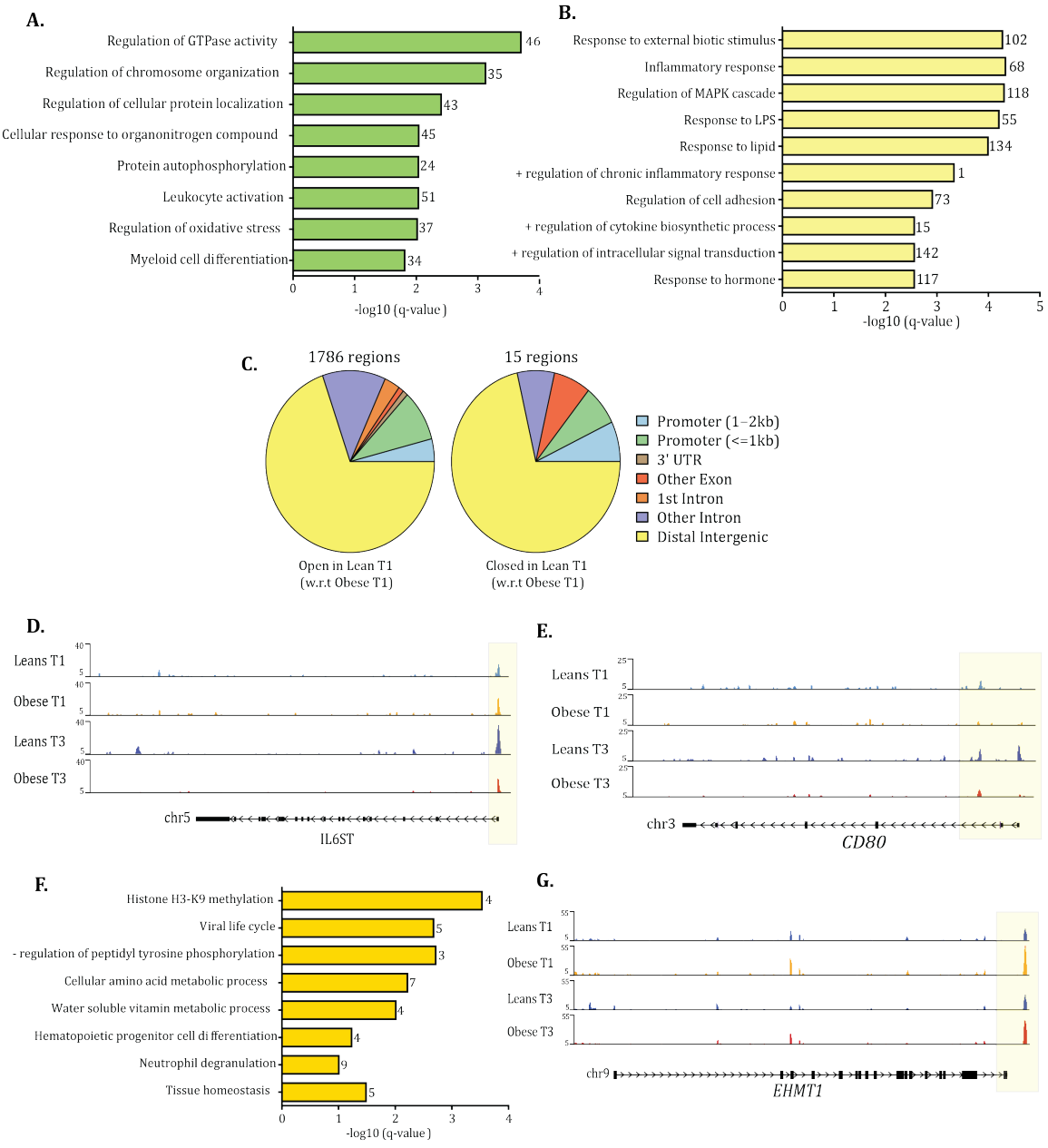

Supplemental Figure 2.10 Epigenetic adaptations with pregnancy and obesity.
(A) Functional enrichment of genes regulated by promoter associated and (B) intergenic DAR open in lean group at T3 relative to T1 (FC>2). Genes associated with these regions are quantified next to each GO term. (C) Genomic contexts of DAR comparing monocyte ATAC peaks from leans and obese group at T1. (D-E) WashU Epigenome tracks for (D) *IL6ST* and (E) *CD80* locus with promoter vicinity highlighted in yellow. (F) Gene ontologies of intergenic associations identified by GREAT as significantly open in obese group at T3. (G) WashU Epigenome tracks for *EHMT1* significantly more open with obesity.

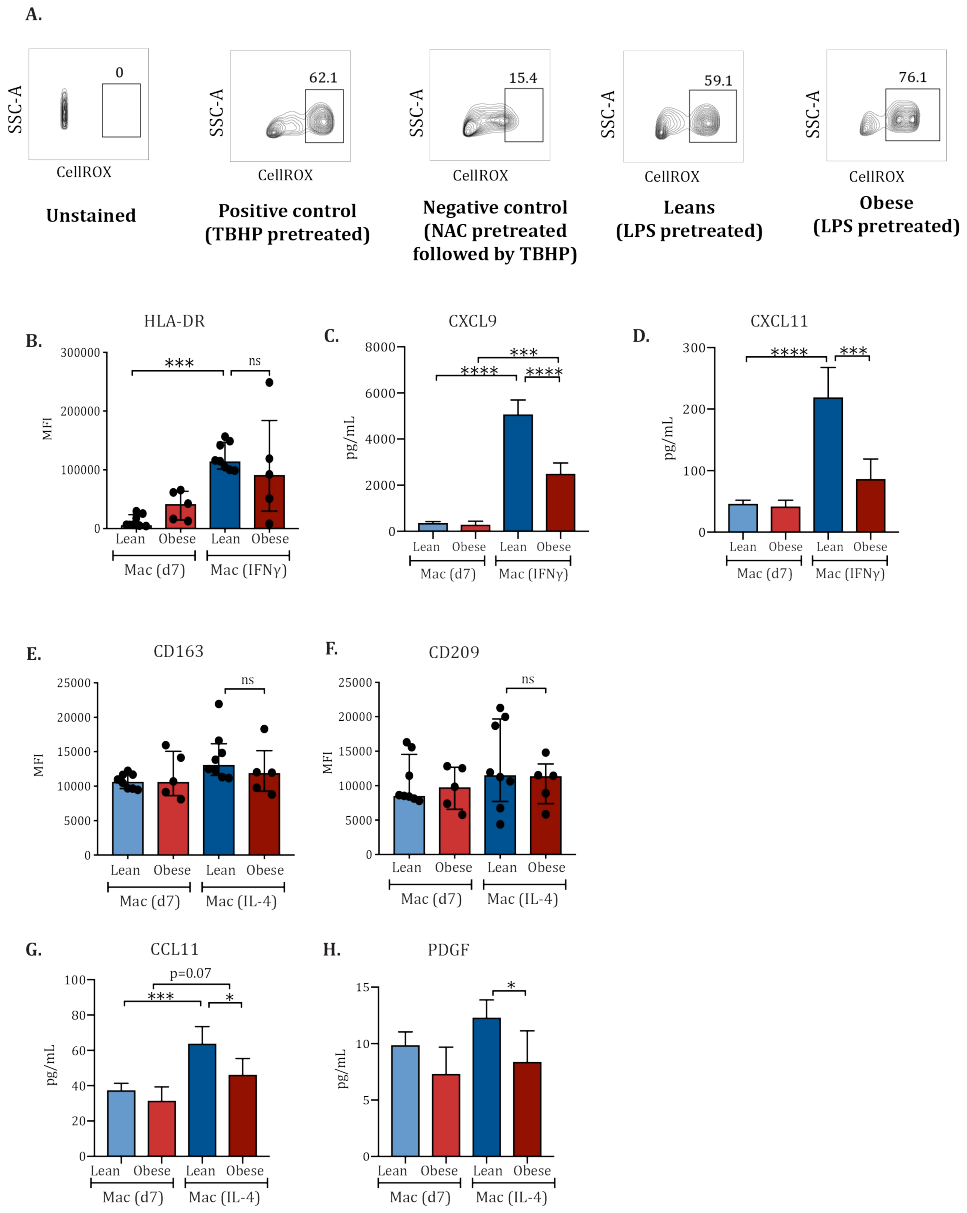

Supplemental Figure 2.11 Functional rewiring of monocytes with maternal obesity at term.

(A) Contour plots of CellROX signal from monocytes gated in lean and obese samples. NAC and TBHP treated monocytes serve as negative and positive controls respectively. (B) Bar graphs comparing surface expression of HLA-DR and secreted levels of M1 associated chemokines (C) CXCL9 and (D) CXCL11 following LPS and IFNγ stimulation on day 7. (E) Bar graphs comparing surface expression of M2 associated markers CD163 and (F) CD209, and M2-associated chemokine (G) CCL11 (eotaxin) and growth factor (H) PDGF. Levels of significance: * - $p<0.05$; *** - $p<0.001$; ****-$p<0.0001$. Bars represent medians and IQR.

CHAPTER 3

Immunological adaptations in placenta with gestation and maternal obesity

Suhas Sureshchandra[1, 2], Norma E. Mendoza[1], Michael Z. Zulu[1, 2], Allen Jankeel[1], Gouri Ajith[1], Nicole E. Marshall[4], Ilhem Messaoudi[1, 2]

[1]Department of Molecular Biology and Biochemistry, University of California- Irvine, Irvine CA, USA
[2]Institute for Immunology, University of California-Irvine, Irvine CA, USA
[3]Division of Biomedical Sciences, University of California-Riverside, Riverside, CA, USA.
[4]Maternal Fetal Medicine, Oregon Health and Science University, Portland OR, USA.
[5]The Knight Cardiovascular Institute, Oregon Health and Science University, Portland OR, USA

Manuscript in preparation

ABSTRACT

A healthy pregnancy is associated with immune adaptations at the maternal fetal interface. These adaptations have the potential to be dysregulated with pregravid obesity, altering the intrauterine environment and increasing the risk for several obstetric complications. Here, we profile the transcriptome of roughly 36,000 immune cells from placentas and matched blood samples isolated >37 weeks of gestation following cesarean section. Our analyses revealed that the proportion of lymphoid cells and overall immune activation state are augmented in the decidua with gestation. At term, there are two major subsets of decidual and villous macrophages with distinctive inflammatory and functional profiles that can be distinguished by HLA-DR expression. Pregravid obesity results in an expansion of the tissue resident DR^{hi} macrophage subset both in decidua and chorionic villous. However, in the decidua, these cells exhibit a state of dampened activation with obesity. Moreover, in the villi, obesity is associated with expansion of regulatory macrophages that that are refractory to LPS stimulation. Collectively these findings suggest that obesity skews placental macrophages towards a regulatory phenotype, possibly as a compensatory mechanism to limit inflammatory insults to the fetus.

INTRODUCTION

The maternal fetal interface is composed of maternal derived membranes – the decidua, and the placental membranes of fetal origin (Maltepe and Fisher, 2015). Over the course of pregnancy, the placenta facilitates gas, nutrient, and waste exchanges between the fetus and the mother. The placental membranes harbor immune cells, which facilitate trophoblast invasion, maternal tolerance, clearance of debris, and fetal protection from maternal infections (Ander et al., 2019). First trimester decidua (10-12 weeks) is comprised of decidual NK cells (dNKs, ~70% of immune cells), decidual macrophages (20-25%) and T cells (3-10%) (Manaster and Mandelboim, 2010) (Liu et al., 2017). On the other hand, fetal membranes are particularly enriched in macrophages called Hofbauer cells (Suryawanshi et al., 2018; Vento-Tormo et al., 2018). Immune cells within the decidua undergo dynamic changes in both phenotype and frequencies over the course of gestation. This includes a reduction in NK cell and macrophage numbers in the third trimester (Williams et al., 2009), but no significant differences in T cell numbers, at least in decidua basalis (Williams et al., 2009). T cells have been shown to increase with gestation age under conditions of spontaneous labor (Gomez-Lopez et al., 2013). However, independent of labor, T cells are the primary immune cells of the decidua in the third trimester, mainly due to a reduction of dNK cells. Recent surveys of early maternal fetal interface have demonstrated that these immune cells exist in complex states and phenotypes (Suryawanshi et al., 2018; Vento-Tormo et al., 2018) and abnormal immune adaptations in the placenta contributes significantly to pathogenesis of pre-term labor, preeclampsia, and fetal growth restriction (Aplin et al., 2020).

Pregravid obesity is a risk factor for several obstetric complications including gestational diabetes and gestational hypertension (Gaillard et al., 2013), preeclampsia (Bartsch et al., 2016), placental abruption (Doi et al., 2020), preterm delivery (Marchi et al., 2015), and need for cesarean (Poobalan et al., 2009), (Sureshchandra et al., 2019). Furthermore, high pregravid BMI is associated with adverse fetal outcomes such as fetal overgrowth, altered body composition, and neural tube defects (Catalano and Ehrenberg, 2006). The long-term consequences of pregravid obesity are well-documented - increasing risks for cardiovascular disease (Reynolds et al., 2013), diabetes, infectious morbidity (Gutvirtz et al., 2019), and cancer in the offspring (Parsons et al., 2001). This predisposition has been argued to stem from placental adaptations (Thornburg and Marshall, 2015), mediated by increased levels of oxidative stress (Malti et al., 2014), hypoxia (Wallace et al., 2019), impaired placental transport efficiency (Aye et al., 2015; Jones et al., 2009), altered lipid turnover (Hirschmugl et al., 2017), and altered placental structure (Roberts et al., 2011) (Myatt and Maloyan, 2016). Furthermore, recent work has demonstrated the role of placental inflammation as a potential contributor to fetal reprogramming. This includes aberrant expression of inflammatory factors (Aye et al., 2014), dysregulated cell turnover, and immune cell rewiring. For example, first trimester uNK cells in mothers with obesity demonstrated an imbalance of inhibitory and activating receptors resulting in aberrant activation (Castellana et al., 2018). Furthermore, the number of resident CD68+ cells (macrophages) was 2-3 fold higher in the placental villi of obese as compared to lean women at term (Challier et al., 2008). These observations suggest potential immune cell adaptations with obesity at the maternal fetal interface.

To assess the impact of pregravid obesity on immune cell adaptations, both in the decidua and villous chorion, we carried out a multi-pronged study to profile immune cells in term placentas obtained from lean and obese subjects undergoing scheduled cesarean section. From these samples collected, we used single cell RNA-sequencing to profile the immune compartment (CD45+) from matched placental decidua and chorionic villi obtained at term and compare it to that detected in first trimester maternal fetal interface (Vento-Tormo et al., 2018). We used flow cytometry and functional assays to define the macrophage subsets at term, identify differences between macrophage populations from two membranes, and identified key adaptations with maternal obesity.

Integration of single cell RNA sequencing data highlights an expansion of T cell fraction with gestational age and concomitant reduction in macrophages and NK cells. We see a shift in the predominant NK cell subset from dNK1 subset at 12 weeks to dNK3 subset at term. At term, all cells express markers associated with activation, most likely due to labor. Compared to the decidua, the immune compartment of chorionic villous is composed mostly of macrophages. Both decidual macrophages and Hofbauer cells are largely divided into two clusters, distinguished by expression of HLA-DR. These two subsets have distinct functional attributes and basal cytokine profiles but do not comply with traditional M1/M2 macrophage paradigm.

With pregravid obesity, we report a reduction in T cells in the decidua and expansion of HLA-DR^{high} macrophages in both maternal and fetal membranes. However, contrary to previous observations of heightened immune activation with maternal obesity, these cells express a regulatory phenotype, secrete lower levels of inflammatory cytokines, down-regulated signatures of cytokine signaling, and in the case of villi, respond poorly to

LPS stimulation. In the chorionic villi, this skewing of macrophages towards a regulatory state is accompanied by an enrichment of a unique population of M2-like tissue remodeling macrophages and elevated levels of IL-1RA protein. These adaptations in the placenta could potentially impact host defense at the maternal fetal interface and contribute to macrophage mediated obstetric complications such as chorioamnionitis and preeclampsia.

MATERIALS AND METHODS

Human subjects

This study was approved by the Institutional Ethics Review Board of Oregon Health and Science University and the University of California, Irvine. A total of 78 non-smoking women (36 lean, 10 overweight, and 32 obese) who had an uncomplicated pregnancy were enrolled for this study. Written informed consent was obtained from all participants. Due to strong positive correlation between pre-pregnancy BMI and total body fat in our previous studies (Sureshchandra et al., 2018), we used pre-pregnancy BMI as a surrogate for maternal pregravid obesity and stratified participants into lean or obese based on pre-pregnancy BMI (Table 2.3). The study includes 36 lean women with a mean age of 33.4 years and pre-pregnancy BMI of 21.91 ± 1.88 kg/m^2; and 32 women with obesity with a mean age of 32.6 years and pre-pregnancy BMI of 38.41 ± 8.27 kg/m^2 (Table 2.3). Only samples from scheduled term C-section deliveries were included in the analysis.

Sample collection and processing

Placental decidua and villous chorion membranes were separated immediately, placed in individual conical immersed in RPMI supplemented with 10% FBS and antibiotics. Samples were collected by the Maternal Fetal Medicine unit at Oregon Health and Science University, Portland OR, and then shipped overnight to University of California, Irvine for further processing. Decidual and villous tissues were washed in HBSS to remove contaminating blood and any visible blood vessels macroscopically separated and then washed for 10 minutes in HBSS before processing. Tissues were minced into approximately 0.2-0.3 mm^3 cubes and enzymatically digested in 0.5mg/mL collagenase V (Sigma, C-9722)

solution in 50 mL R3 media (RPMI 1640 with 3% FBS, 1% Penicillin-Streptomycin, 1% L-glutamine, and 1M HEPES) at 37C for 1 hour. The disaggregated cell suspension was passed through tea strainers to eliminate visible chunks of fat/tissue. Cells were pelleted from the filtrate, passed through 70-um cell sieve, centrifuged and resuspended in R3 media. Red blood cells were lysed using RBS lysis buffer (155 mM NH_4Cl, 12 mM $NaHCO_3$, 0.1 mM EDTA in double-distilled water) and resuspended in 5 mL R3. The cell suspension was then layered on a discontinuous 60% and 40% percoll gradient and centrifuged for 30 minutes with brakes off. Immune cells at the interface of 40% and 60% gradients were collected, washed in HBSS, counted, and cryopreserved for future analysis.

Blood processing

Blood samples from delivery time point were carefully layered on a Ficoll-Paque (GE Healthcare) gradient and centrifuged at 2000 rpm for 30 minutes without brakes. Plasma was collected from top layer and stored at -80C for future analysis. Peripheral Blood Mononuclear cells (PBMC) from the interphase between plasma and the Ficoll-Paque gradient were collected, washed in HBSS, followed by centrifugation at 2000 rpm for 5 minutes. Pellets were resuspended in FetalPlex (Gemini BioProducts) with 10% DMSO (Sigma) and stored in liquid nitrogen for future analysis.

Immunophenotyping

1-2 X 10^6 fresh decidual and villous cells were washed with PBS and stained using the following cocktail of antibodies: CD45 (BV605), CD20 (BV510), CD4 (R-PE), CD8b (PE-Texas Red), CD14 (AF700), HLA-DR (APC-Cy7), CD16 (PB), CD11c (PE-Cy7), CD123 (PerCP-Cy5.5), for 20 minutes in dark at 4C. Samples were washed twice in FACS buffer and resuspended in 400 uL. All samples were acquired with the Attune NxT Flow Cytometer

(ThermoFisher Scientific, Waltham MA), immediately after addition of SYTOX Red Dead Cell Stain (1:1000) (ThermoFisher CA). Data were analyzed using FlowJO (Ashland OR).

For a more comprehensive analysis of macrophage phenotypes, 1-2 X 10^6 freshly thawed decidual and villous cells were stained using the following cocktail of antibodies: CD3 (PE-Cy7), CD20 (PE-Cy7), CD14 (AF700), HLA-DR (APC-Cy7), CD11c (PE-eFluor610), CD16 (PB), CD68 (APC), CD86 (BV605), TLR4 (BV711), CD163 (PCP-Cy5.5), CD206 (BV510), CD209 (R-PE), and live dead stain (SYTOX Green). Cell pellets were washed twice in DPBS and resuspended in cold FACS buffer (DPBS with 2% FBS and 1mM EDTA). All samples were acquired with the Attune NxT Flow Cytometer (ThermoFisher Scientific, Waltham MA) and analyzed using FlowJo 10.5 (Ashland OR).

Intracellular Cytokine Staining

To measure cytokine responses of decidua/villous macrophages, 10^6 thawed cells were stimulated for 8h at 37°C in RPMI supplemented with 10% FBS in the presence or absence of 1 ug/mL LPS (TLR4 ligand, *E.coli* 055:B5; Invivogen, San Diego CA); Brefeldin A (Sigma, St. Louis MO) was added after 1 hour incubation. Cells were surface stained using the following antibodies: APC-Cy7-CD14, PCP-Cy5.5-HLA-DR for 20 min in the dark at 4C, fixed and permeabilized using Fixation buffer (Biolegend) at 4C for 20 min, and stained intracellularly for APC-TNFα and PE-IL-6 overnight in 1X Permeabilization Wash buffer (Biolegend). Cell pellets were washed once in Permeabilization Wash buffer and twice in ice-cold FACS buffer (DPBS with 2% FBS and 1mM EDTA). Cell pellets were resuspended in 400 uL FACS buffer and analyzed with the Attune NxT Flow Cytometer (ThermoFisher Scientific, Waltham MA) and analyzed using FlowJo 10.5 (Ashland OR).

Macrophage subsets and baseline cytokine measurements.

Live decidua macrophage subsets (CD14+ HLA-DR^{high} and HLA-DR^{low}, and SYTOX Blue negative) were sorted using BD FACS Aria Fusion. Peripheral blood monocytes were sorted from PBMC obtained at delivery for comparison. 50,000-sorted cells were placed in a 96-well plate overnight to measure cytokine production. Supernatants were collected and stored in -80C until further analysis using Luminex.

Imaging flow cytometry

Briefly, 500,000 decidua leukocytes were surface stained (CD14-APC, CD11c-PE-Cy7; HLA-DR-APC-Cy7). Cells were fixed with 1X fixation buffer (Millipore) for 10 minutes at room temperature (RT), stained using a Fixable Yellow LIVE/DEAD dye (ThermoFisher Scientific), washed, and resuspended in 0.25X fixation buffer. All washes were performed using 1X Assay buffer. Samples were run on Amnis ImageStream XMark II Imaging flow cytometer (Luminex Corporation) and data analyzed on Ideas Analysis Software (Luminex Corporation).

FACS and Single Cell RNA library preparation

Freshly thawed immune cells from decidua and villi were stained with CD45-FITC at 4C in 1% FBS in DPBS without calcium and magnesium. Cells were washed twice and sorted on BD FACS Aria Fusion into RPMI (supplemented with 30% FBS) following addition of SYTOX Blue stain for live versus dead discrimination. Cells were then counted in triplicates on a TC20 Automated Cell Counter (BioRad), washed and resuspended in PBS with 0.04% BSA in a final concentration of 1200 cells/uL. Single cell suspensions were then immediately loaded on the 10X Genomics Chromium Controller with a loading target of 17,600 cells. Libraries were generated using the V3 chemistry per manufacturer's instructions (10X

Genomics, Pleasanton CA). Libraries were sequenced on Illumina HiSeq with a sequencing target of 20,000 reads per cell.

Single cell RNA-Seq data analysis

Raw reads were aligned and quantified using the Cell Ranger Single-Cell Software Suite (version 3.0.1, 10X Genomics) against the GRCh38 human reference genome using the STAR aligner. Downstream processing of aligned reads was performed using Seurat (version 3.1.1)(Satija et al., 2015). Droplets with ambient RNA (cells fewer than 400 detected genes), potential doublets (cells with more than 4000 detected genes, and dying cells (cells with more than 20% total mitochondrial gene expression) were excluded during initial QC. Data objects from lean and obese group were integrated using Seurat (Stuart et al., 2019). Data normalization and variance stabilization were performed using *SCTransform* function (Hafemeister and Satija, 2019) using a regularized negative binomial regression, correcting for confounding effects of mitochondrial and ribosomal gene expression levels and cell cycle.

To remove potential contaminating blood cells, we integrated placental leukocytes scRNA-Seq datasets with those from matched maternal PBMC (Chapter 2) using Seurat's *IntegrateData* function. Placenta cells clustering with PBMC were removed from downstream analyses. B cell clusters from placenta and blood, which demonstrated strong overlap, were excluded from our analysis.

Dimension reduction was performed using *RunPCA* function to obtain the first 30 principal components followed by clustering using the *FindClusters* function in Seurat. Clusters were visualized using UMAP algorithm as implemented by Seurat's *runUMAP* function. Cell types were assigned to individual clusters using *FindMarkers* function with a fold change cutoff of

at least 0.4 and using a known catalog of well-characterized scRNA markers for human PBMC (Zheng et al., 2017), tissue resident lymphoid cells (Szabo et al., 2019), and leukocytes in first-trimester human placentas (Vento-Tormo et al., 2018).

To study the evolution of immune landscape of placental decidua with gestational age, we used recently described atlas of CD45+ cells in decidua from five expectant mothers undergoing elective pregnancy termination (Vento-Tormo et al., 2018). Raw data were downloaded for 6 individuals (D6-10, D12) and analyzed as described above resulting in 24,849 cells. Cells were downsampled (6,116) to match number of cells from term decidua and integrated using Seurat's *IntegrateData* function and markers compared using *FindMarkers* function.

Single cell analysis of placental macrophages

Macrophage clusters expressing high levels of *CD14* were extracted from the Seurat object using the *subset* function. Markers distinguishing each of these macrophage clusters were identified using *FindAllMarkers* function. For gene scoring analysis, we compared gene signatures and pathways from KEGG (https://www.genome.jp/kegg/pathway.html) in subpopulations using Seurat's *AddModuleScore* function. Differential expression analysis was tested using *FindMarkers* function with DESeq2 option. Genes expressed in at least 40% of cells within the cluster and with an adjusted p-value <0.05 were considered significant. One-way and multi group functional enrichment of differential signatures was performed on Metascape.

Pseudo-temporal analysis

Pseudotime trajectory of macrophages was reconstructed using Monocle (version 2.8.0). Briefly, clustering was performed using t-SNE and differential genes identified using

Monocle's *differentialGeneTest*. Top 1000 genes with q-value < 1e-10 were used for ordering cells on a pseudotime and visualized using the DDRTree method. Genes that change as a function of the pseudotime were identified using *differentialGeneTest* and a select number of significant genes were visualized as a heatmap.

Immune mediator measurements

200 mg of flash frozen decidua/villous tissue was placed in a tube with silica carbide beads and 400 uL RPMI and rapidly agitated in a bead beater for 5 cycles (30 seconds each). Vials were centrifuged for 10 minutes at 1,000 X g and roughly 300 uL of tissue lysate collected, further centrifuged for 10 minutes at 10,000 X g to remove any residual particles. Supernatants were collected and frozen at -80C until future analysis using Luminex.

Proteins in cell supernatants and placental tissue homogenate were measured using Human Custom 29-plex Multi-Analyte Kit (R&D Systems) measuring the following analytes: CCL2 (MCP-1), CCL4 (MIP-1β), CXCL9 (MIG), CXCL11 (I-TAC), GM-CSF, IFNγ, IL-1RA, IL-4, IL-7, IL-12p70, IL-18, PD-L1, S100B, VEGF, IL-15, CCL3, CCL11, CXCL10, CXCL13, IFNβ, IL-1b, IL-2, IL-6, CXCL8 (IL-8), IL-17A, IL-23, PDGF-BB, TNFα, and IL-10. Samples were processed per manufacturer's instructions, recorded and analyzed on the Magpix xPONENT system version 4.2 (Luminex Corporation).

BODIPY Staining

Neutral lipids in macrophages were quantified using flow cytometry. Briefly, 500,000 decidual/villous leukocytes were surface stained (CD14-AF700, HLA-DR-APC-Cy7) for 20 minutes at 4C, washed twice, and resuspended in 500 uL warm 1X PBS containing 1 ug/mL BODIPY™ 493/503 (ThermoFisher Scientific). Cells were incubated at 37C for 10 minutes and analyzed using flow cytometry.

Phagocytosis Assay

Phagocytosis was measured using pH-sensitive pHrodo® E. coli BioParticles® conjugates (ThermoFisher Scientific). 500,000 decidual/villous leukocytes were incubated for 2 hours in media containing pHrodo conjugated with *E. coli* (1 mg/mL concentration). Pellets were washed twice, surface stained (CD14-AF700, HLA-DR-APC-Cy7), and resuspended in ice-cold FACS buffer. Samples were analyzed using flow cytometry.

Cytosolic ROS assay

For cellular ROS measurements, 500,000 decidual/villous leukocytes were incubated with 2.5 uM CellROX Deep Red (Life Technology) at 37C for 30 minutes. For negative control, cells were incubated in serum-free media containing 200 uM anti-oxidant N-acetylcysteine (NAC) for 1.5 hours. Both negative and positive controls were incubated with tert-butyl hydroperoxide (TBHP) for 30 minutes to induce oxidative stress. All samples were then surface stained (CD14-FITC, HLA-DR-PCP-Cy5.5) and subjected to FACS analysis.

Glucose Uptake Assay

To measure glucose uptake, 500,000 decidual/villous leukocytes were resuspended in glucose free media and incubated with 60 mM 2-NBDG, a fluorescent glucose analog for 30 minutes at 37C. Samples were washed in DPBS, surface stained (CD14-AF700, HLA-DR-APC-Cy7) and subjected to FACS analysis.

Statistical analyses

All statistical analyses were conducted in Prism 8 (GraphPad). All definitive outliers in two-way and four-way comparisons were identified using ROUT analysis (Q=0.1%). Data were then tested for normality using Shapiro-Wilk test (alpha=0.05). If data were normally

distributed across all groups, differences with were tested using ordinary one-way ANOVA with unmatched samples. Multiple comparisons were corrected using Holm-Sidak test adjusting the family-wise significance and confidence level at 0.05. If gaussian assumption was not satisfied, differences were tested using Kruskall-Wallis test (alpha=0.05) followed by Dunn's multiple hypothesis correction test. Differences in normally distributed two groups were tested using an unpaired t-test with Welch's correction (assuming different standard deviations). Two group comparisons that failed normality tests were tested for differences using Mann-Whitney test. For subsets of cells within a sample, differences were tested using paired t-tests.

RESULTS

Gestational adaptations of immune cells in decidua.

To define the immune landscape of placental decidua at term, we combined droplet-based single-cell transcriptome profiles of sorted CD45+ decidual cells and matched peripheral blood mononuclear cells (PBMC) from 4 gravid women undergoing cesarean (Figure 3.1A and Supplemental Figure 3.1A). Clusters were generated after quality control and integration of data from decidual leukocytes and PBMC (Supplemental Figure 3.1B and Figure 3.1B). PBMC profiles were used to eliminate cells that could be blood contaminants, but also provided a useful control for studying the process of decidualization (Supplemental Figures 3.2A and 3.2B). Indeed, structural markers defining tissue resident T cells (*ANXA1*, *EZR*, *TUBA1A*) and macrophages (*VIM*) were highly expressed in decidual leukocytes compared to PBMC (Supplemental Figure 3.2C), confirming their tissue resident identity. Clusters were annotated (Figure 3.1C) based on a combination of known immune cell markers and previously defined markers of immune cells in early human placenta (Vento-Tormo et al., 2018). Specifically, the lymphoid cell clusters at T3 were composed of naïve and memory subsets of CD4 T cells (*IL7R*, *CCR7*) and CD8 T cells (*IL7R*, *CD8A*, *CCR7*, *CTLA4*), and a distinct cluster of regulatory T cells expressing low *IL7R* but high *FOXP3* and *CTLA4* (Figures 3.1B and 3.1C). As described in early placental decidua (Vento-Tormo et al., 2018), we observed three clusters of Natural Killer (NK) cells expressing *NKG7* and variable levels of *XCL1*, *CD160*, and *NCAM1*. Myeloid fractions were comprised of dendritic cells (*FCERIA*), and two clusters of macrophages, both expressing high levels of *CD14* and *CD68* (Figures 3.1B and 3.1C).

However, direct comparison of this dataset to that reported for first trimester placenta (Vento-Tormo et al., 2018) revealed a reduction in percentages of natural killer cells (NK cells) and macrophages that is accompanied by an expansion of T cells (both CD4 and CD8), notably regulatory T cells (Supplemental Figure 3.3A and Figure 3.1D). Within the NK cell clusters, we observed a reduction in the larger dNK1 population expressing *B4GALNT1*, *CYP26A1*, and *EPAS1* at term (Supplemental Figure 3.3B) and an increase in dNK3 subset, expressing high *CD160* (Supplemental Figure 3.3C).

Finally, compared to first trimester both T cells and NK cells at term expressed high levels of *IFNG* (Supplemental Figure 3.4A) and *NFKB1* (Supplemental Figure 3.4B). Furthermore, decidual macrophages expressed higher levels of *NFKB1* (Supplemental Figure 3.4B), *NLRP3* (Supplemental Figure 3.4C), chemokine *CXCL8* (Supplemental Figure 3.4D), pro-inflammatory cytokine *IL1B* (Supplemental Figure 3.4E), and activation marker *CD83* (Supplemental Figure 3.4E). Interestingly, decidual macrophages had higher module scores for hypoxia signaling, IL-6, and TLR signaling (Supplemental Figures 3.4G-I) compared to blood monocytes as well, suggesting a general state of heightened activation.

Diverse functional states of macrophage subsets in maternal decidua.

UMAP visualization of CD45+ cells in maternal decidua revealed two major subsets of macrophages (Figures 3.1B and 3.1C), with a distinct transcriptional profile compared to subsets of peripheral monocytes (Figure 3.2A). More specifically, one subset, denoted as dMac-1, expressed high levels of antigen presenting molecules *HLA-DRA* (Figures 3.2A and 3.2B) and canonical M2-like macrophage markers (*TREM2, MSR1*) (Figures 3.2A and 3.2B) and tetraspanins (*CD9*, *CD81*) (Supplemental Figure 3.5A). The second subset of decidual macrophages, which we refer to as dMac-2, expressed lower transcript number of *HLA-DRA*

and *CD16* compared to dMac-1, higher levels of pro-inflammatory genes *S100A9*, *S100A10*, *ITGAX*, *IL1B*, and *CXCL8,* and higher levels of M1-associated molecule *TREM1* (Figures 3.2A, 3.2C, Supplemental Figure 3.5B).

Two-way gene ontology (GO) analysis using Metascape revealed that gene highly expressed by dMac-1 enriched to pathways associated with apoptosis, antigen presentation, and response to stress (Figure 3.2D). We also observed a more significant enrichment of genes to cytokine signaling and MAPK cascade in dMac-1 (Figure 3.2D). On the other hand, genes highly expressed in dMac-2 enriched to antiviral response (Figure 3.2D).

The presence of these two decidual macrophage subsets was confirmed by flow cytometry (Figures 3.2E, 3.2F, Supplemental Figure 3.5C). Interestingly, dMac-1 population had higher surface expression of both canonical M1-like (CD86, HLA-DR, TLR4) (Figure 3.2F and Supplemental Figure 3.5D) and M2-like (CD206, CD163) markers (Figure 3.2F, Supplemental Figures 3.5D and 3.5E), suggesting that these cells do not fit the traditional paradigms of M1/M2 polarized states. Both populations of macrophages expressed higher levels of CD68 compared to monocytes in PBMC, confirming their tissue resident identity (Supplemental Figure 3.5D). Interestingly, while gene expression of *ITGAX* was higher in dMac-2 compared to dMac-1 at the RNA level (Figures 3.2A, 3.2C, Supplemental Figure 3.5D), flow cytometry revealed that dMac-1 cells expressed higher surface protein levels of CD11c (encoded by *ITGAX*) compared to dMac-2 cells (Figures 3.2E and 3.2F). Finally, analysis of cells using imaging flow cytometry revealed that the two-macrophage populations with differing diameters, suggesting diversity in cellular morphology as well (Figure 3.2G).

Comparisons of spontaneous secretion of immune mediators showed that FACS sorted dMac-1 and dMac-2 (Supplemental Figure 3.5F) secreted higher levels of inflammatory cytokines (IL-12, IL-23, and TNFα), regulatory cytokines (IL-10) (Figure 3.2H) and monocyte/macrophage-derived chemokines (CXCL9, CXCL11) (Supplemental Figure 3.5G) compared to blood monocytes. Compared to dMac-2, dMac-1 secreted higher levels of TNFα and IL-10 (Figure 3.2H). Distinct functional states is also supported by metabolic readouts, with higher glucose uptake rate (Figure 3.2I) and neutral lipid accumulation (Figure 3.2J) in dMac-1 compared to dMac-2 and blood monocytes. Finally, dMac-1 cells were also more phagocytic (Figure 3.2K) and generated higher baseline ROS (Figure 3.2L), relative to dMac-2 cells.

Decidual immune adaptations to maternal obesity

Within the samples from decidua, we compared the cells from lean (n=2) and obese (n=2) subjects (Supplemental Figure 3.1B and Figure 3.3A). Pregravid obesity was associated with diminished CD4 and CD8 T cell numbers and an expansion of decidual macrophages with obesity (Figure 3.3B). Flow cytometry analysis (Supplemental Figure 3.6A) confirmed the significantly lower CD4 and CD8 T cell frequencies (Figure 3.3C) and an increase in dMac-1 subset only (Figure 3.3D). Moreover, frequency of T cell subsets negatively correlated with BMI (Supplemental Figure 3.6B), while that of dMac-1 positively correlated with BMI (Supplemental Figure 3.6C). NK cell subsets, on the other hand, remained unchanged with pregravid obesity (Supplemental Figures 3.6D and 3.6E).

Given the increased frequencies of dMac-1 subset with obesity, we next assessed heterogeneity within this subset. UMAP visualization identified 3 dMac-1 clusters (Figure 3.1B). Pseudotime analysis defined a differentiation program that begins from pro-

inflammatory dMac-2 expressing high levels of monocyte like signatures (*LYZ*, *VCAN*, *S100A6*, *S100A10*) to dMac-1 (Figure 3.3E and Supplemental Figure 3.7A). The trajectory is defined by decrease in *TREM1* expression (Supplemental Figure 3.7B) and increase in *TREM2* (Supplemental Figure 3.7C) and *CD163* expression (Supplemental Figure 3.7C), a population that expanded with obesity. Genes highly expressed in dMac-1, cluster 1 enrich to growth factor response and wound healing processes, while genes highly expressed within cluster 2 map to cellular activation and chemokine signaling GO terms (Figure 3.3F). Finally, genes highly expressed in cluster 3 play a role in antigen presentation and stromal cell crosstalk (Figure 3.3F). Based on these observations, we argue that dMac-1 population likely represents the maternal derived tissue resident population of macrophages in the decidua, whereas dMac-2 is blood monocyte derived recruited macrophages.

Differential gene expression analysis revealed up-regulation of lipid metabolism associated molecules *APOE* and *FABP5* (Figure 3.3G) and down-regulation of cytokine (*TNF*, *IL6*, *IL1B, IL1RN*), chemokine genes (*CCL3*, *CCL4*) (Figures 3.3H and Supplemental Figure 3.7E) with maternal obesity. Furthermore, dMac-1 cells from decidua of mothers with obesity secreted lower levels of both TNFα and IL-1β relative to those from the lean group (Figure 3.3I). Additionally, protein measurements in decidua tissue lysates suggest significant reduction in proinflammatory cytokines (TNFα, IL-6, GM-CSF) and T cell factors (IL-2, CXCL10, CXCL11) (Supplemental Figure 3.7F) with maternal obesity. Interestingly, obesity was associated with higher surface HLA-DRA and TLR4 expression on dMac-1 cells (Figure 3.3J).

Immune landscape of term villous chorion

The fetal membranes of the placenta (villous chorion) had a very distinct immune cell composition compared to the maternal membranes (decidua). The CD45+ cells in the villous were skewed towards myeloid cells, with significantly lower percentages of CD4, CD8, and NK cells compared to the decidua (Figure 3.4A). Furthermore, within the NK cells, we observed redistribution of CD56 and CD16 expressing cells, with villous NK cells resembling the major blood NK cell subset (CD56+CD16++) (Supplemental Figure 3.8A). As observed in the decidua, we report two macrophage populations in the villi, distinguished by their surface HLA-DR expression, that refer to as vMac-1 (HLA-DR^{high}) and vMac-2 (HLA-DR^{low}) consistent with our annotation in the decidua (Figure 3.4B). Furthermore, the villous macrophage subsets appeared in larger frequencies compared to the macrophage subsets observed in the decidua (Figures 3.4C and Supplemental Figure 3.8C). At the protein level, vMac-1 cells expressed significantly higher levels of surface CD68 and lower levels of TLR4 compared to dMac-1 (Figure 3.4D), while vMac-2 and dMac-2 have comparable expression of all markers that were tested including CD68, TLR4, HLA-DR, CD16, CD11c, and CD86 (Figures 3.4D and 3.4E). We therefore argue that vMac-1 represents a population of bonafide fetal tissue resident macrophages. As previously described (Vento-Tormo et al., 2018), and based on evidence supported by flow cytometry, vMac-2 subset represents a population of maternal monocyte-derived macrophages in fetal membranes. Finally, as observed within decidual macrophage subsets, vMac-1 cells had higher glucose uptake (Figure 3.4F), neutral lipid content (Figure 3.4G), phagocytosis (Figure 3.4H), and baseline cytosolic ROS (Figure 3.4I) compared to vMac-2 cells.

Maternal obesity results in macrophage accumulation in chorionic villi

We next evaluated the impact of maternal pregravid obesity on the immunological landscape of the villous chorion. No differences were detected in the numbers of CD4 T cells, CD8 T cells, or NK cells (Supplemental Figure 3.8C). Although no differences were observed in total numbers of macrophages or vMac-2 cells (Supplemental Figures 3.8D and 3.8E), pregravid obesity was associated with increased numbers of vMac-1 (Figure 3.5A). Therefore, we leveraged single cell RNA-seq data of CD45+ cells in villous chorion to profile macrophages at high resolution. UMAP visualization identified a total of 14 immune cell clusters, with 9 macrophage clusters organizing as vMac-1 (clusters 3-8), vMac-2 (clusters 1, 2) and a distinct cluster 9 (Figure 3.5B).

As described in the decidua, vMac-1 and vMac-2 macrophages were clearly distinguished by *HLA-DR*, *TREM1*, and *TREM2* (Supplemental Figure 3.9A). In line with the flow cytometry data, relative frequency of vMac-1 cells increased with pregravid obesity (Figure 3.5C and Supplemental Figure 3.9B). Functional enrichment of the most highly expressed markers of individual clusters within vMac-1 and vMac-2 cells suggests diverse functions: antiviral responses (vMac-1 cluster5 – *STAT1, ISG20*); antigen presentation (vMac-1 cluster8 – *HLA-DRA*, *CD74*); epithelial cell differentiation and tissue repair (vMac-1 cluster3 - *VEGFA*); metal ion homeostasis (vMac-1 cluster7 – *MARCO*, *FABP5*, *CD9*), response to lipids (vMac-1 cluster6); and fat cell differentiation (vMac-1 cluster4) (Figures 3.5D and 3.5E). Comparison of individual cluster frequencies suggests an expansion of vMac-1 clusters 3, 4 and 6 (Supplemental Figure 3.9C) with maternal obesity.

Interestingly, genes that define cluster9, which was significantly enriched with obesity but did not segregate with vMac-1 or -2, expressed high levels of Hofbauer cell marker *LYVE1* (Figure 3.5E). Genes that delineate cluster9 enriched to apoptotic signaling,

cellular response to IL-4, and stromal crosstalk (fat cell and epithelial cell differentiation) (Figure 3.5D). Additionally, cells in cluster9 expressed high levels of canonical M2-like macrophage markers *CD163*, *CD209*, *FOLR2*, and *IGF1* (Figure 3.5E). As described above for decidual macrophages, pseudotime analysis shows a differentiation trajectory starting with vMac-2 cells, progressing through vMac-1 cells (clusters 3, 4, 5, 6), cluster 7, 8 (expressing *HLA-DR*, *CD9*, *CD81*) and ending at cluster 9 (expressing *LYVE1*, *SELENOP*, *EGR1*) (Figures 3.5F and 3.5G).

Differential expression analysis revealed that maternal obesity down-regulated gene signatures involved in immune response, IFNγ signaling, and wound healing process (*MARCO*, *FN1*, *CXCL3*) (Figures 3.5H and 3.5I) in vMac-1 cells and down-regulation of genes responsive to peptide hormones (*EREG*, *AREG*, *TIMP1*) in both macrophage subsets (Figure 3.5J and Supplemental Figure 3.9D).

Maternal obesity skews villous macrophages (vMac-1) towards a regulatory phenotype.

Finally, we stimulated leukocytes from villous and decidua with LPS (TLR4 agonist) and measured the frequencies of responding macrophages (IL6+TNFα+) (Figure 3.6A). In the decidua, we observed no differences in macrophage responses between lean and obese group in either dMac-1 (HLA-DR^{high}) or dMac-2 (HLA-DR^{low}) (Figure 3.6B). However, in the villous, vMac-1 macrophages from obese group responded poorly relative to those from the lean group (Figure 3.6C). Moreover, obesity attenuated cytosolic ROS levels in both vMac-1 and vMac-2 macrophages (Figure 3.6D). Incidentally, tissue lysates of frozen villous samples from obese group had significantly higher levels of IL-1RA (Figure 3.6E).

DISCUSSION

The immune cell compartment at the maternal fetal interface goes through dynamic changes over the course of gestation (Ander et al., 2019). Surveys of placental immune landscapes have described diverse subsets of dNK cells and T cells in the decidua (Vento-Tormo et al., 2018). A more recent study has described the cellular composition of different placental membranes (basal plate, chorioamniotic membranes, and placental villi) in women undergoing C-section with or without the induction of labor (Pique-Regi et al., 2019). While these studies provide an atlas of cells that make up the placenta, no studies to date have compared the phenotypes of immune cells between matched decidua (maternal) and villous (fetal) compartments or identified immune adaptations with gestation. To facilitate a high-resolution understanding of the placental immune landscape at term, we enriched the CD45+ compartment within placental decidua and chorionic villi at term from mothers undergoing scheduled cesarean and profiled cells using single cell RNA sequencing.

Comparison of early and term decidua immune cell profiles confirms that T cell are the major population of leukocytes in the decidua by the end of pregnancy. Studies have reported a lack of difference in T cell numbers with gestational age, but rather a reduction in dNK cells that results in a relative increase in the relative proportion of T cells (Williams et al., 2009). Decidual T cells at term have been described to be more differentiated than those found in blood, and our data indicates that they express high levels of *IFNG*, suggesting enhanced activation (Aghaeepour et al., 2017).

Decidual NK cells (dNKs) are perhaps the most well studied leukocytes at the maternal fetal interface, owing to their roles in decidualization and implantation during

early weeks of pregnancy. Our data suggests that unlike peripheral NK cells, dNKs are mostly $CD56^{high}$ and express lower levels of CD16. Compared to their peripheral counterparts, these cells secrete a vast array of growth factors, angiogenic factors and cytokines (Hanna et al., 2006). Single cell studies in first-trimester decidua have identified 3 subsets of dNKs – a more abundant dNK1 (expressing high *CYP26A1*, *B4GALNT1*, *ENTPD1*) likely involved in recognition and response to extravillous trophoblasts (EVT), dNK3 (expressing high *CD160*) likely involved in regulating EVT invasion, and dNK2 (expressing *ANXA1* and *ITGB2*) with shared features of dNK1 and dNK2 (Vento-Tormo et al., 2018). Single cell comparisons of early and late decidua profiles revealed an expansion of dNK3 and reduction in dNK1 subsets with gestational age, highlighting NK cell adaptations to facilitate EVT regulation. The frequency of *IFNG* expressing dNK cells, however, increased with gestation, suggesting immune activation with approaching labor.

Finally, macrophages in the decidua, function as primary antigen-presenting cells (APCs), and are phenotypically regulatory cells of an M2-like phenotype (Liu et al., 2017). Under *in vitro* conditions first trimester decidual macrophages secrete high levels of VEGF and MMP9, suggesting their roles in angiogenesis and tissue remodeling (Gustafsson et al., 2008). Moreover, these cells have been shown to phagocytose apoptotic trophoblasts (Abrahams et al., 2004) and protect the fetus against infections (Tang et al., 2015). Our comparisons suggest that decidual macrophages at term express high levels of *CXCL8*, *NLRP3*, *IL1B*, and *NFKB1*, highlighting a shift in their phenotype at term. Furthermore, decidual macrophages at term spontaneously secrete high levels of both proinflammatory cytokines TNFα, IL-1β, IL-23 and regulatory IL-10, reflective of enhanced activation. Indeed, *NFKB1* expression in decidual macrophages has been shown to be higher in

mothers in labor compared to non-labor controls (Pique-Regi et al., 2019), confirming their macrophage activation with gestation and their role in labor (Yan et al., 2002).

Macrophages in early decidua have been described to exist as two distinct subsets, distinguished by surface expression of CD11c (Houser et al., 2011). Gene expression studies in these subsets suggests that CD11c high population (expressing low CD206 and CD209) expresses genes associated with lipid metabolism and inflammation whereas $CD11c^{low}$ population expresses signatures associated with extracellular matrix formation, muscle regulation, and tissue growth (Houser et al., 2011). Both populations are equally phagocytic and secrete both pro- and anti-inflammatory cytokines. However, $CD11c^{high}$ population accumulates neutral lipid droplets and is more efficient at antigen presentation than $CD11c^{low}$ subsets (Houser et al., 2011). Interestingly, both populations did not fit the traditional definition of macrophages using the M1/M2 polarization system. More recent studies have used CCR2, CD11c and HLA-DRA to define three macrophage subsets in the decidua, with $CCR2^{+}$ $CD11c^{high}$ subset being more M1-like macrophages, while $CCR2^{-}$ $CD11c^{high}$ and $CCR2^{-}CD11c^{low}$ subsets skewing towards M2 phenotype (Jiang and Wang, 2020). However, the authors argue that use of subjective markers to define complex in vivo states is rather limiting, and should be interrogated with unbiased approaches such as single cell RNA sequencing.

Our single cell data classified term decidual macrophages by markers that distinguished cells with monocyte-like features (expressing low *HLA-DRA*, but high *TREM1*, *S100A9*, *VCAN*, *LYZ*), which we term dMac-2, and mature tissue resident cells (expressing high *HLA-DRA*, *TREM2*, *APOE*), which we term dMac-1. Surface expression of HLA-DRA was able to distinguish the two subsets, with $HLA\text{-}DR^{high}$ subset being $CD11c^{high}$ and $HLA\text{-}DR^{low}$

subset being CD11c^{low}. At the transcriptional level, dMac-1 expressed signatures of myeloid cell differentiation, apoptosis, antigen presentation, and cytokine signaling, whereas dMac-2 expressed signatures associated with antiviral signaling. Furthermore, dMac-1 accumulated more neutral lipids, was metabolically more active, and more phagocytic compared to dMac-2. Finally, both subsets secreted higher levels of inflammatory cytokines compared to blood monocytes, but dMac-1 cells secreted higher levels of both TNFα and IL-10 and expressed significantly higher levels of CD163+ cells, suggesting that they do not represent M1 or M2 macrophages. However, trajectory analysis of these cells places them along a pseudotime defined by their inflammatory state, starting from dMac-2 and ending in dMac-1. These two subsets have been described in early decidua distinguished by *ITGAX* (gene encoding CD11c) expression (Vento-Tormo et al., 2018). Interestingly, while gene and protein expression of HLA-DRA and TLR4, and CD16 between the two subsets had high agreement, CD11c^{high} (dMac-1) had lower expression of *ITGAX* compared to dMac-2. Nevertheless, as described in early decidua, the *ITGAX* low population (dMac-1 in our case) is a self-renewing population of tissue remodeling macrophages (Vento-Tormo et al., 2018). We therefore conclude that dMac-1 cells represent a population of tissue resident macrophages, whereas dMac-2 cells are blood-derived macrophages in the decidua.

In comparison to the decidua, the chorionic villi are predominantly comprised of macrophages, which we confirmed using both flow cytometry and single cell RNA-Seq. However, as described for the decidua, villous macrophages also appear as two distinct populations with variable HLA-DR expression. Interestingly, vMac-1 cells express high levels of surface CD68 and low levels of TLR4 compared to dMac-1, whereas vMac-2 and dMac-2 appear similar, at least with respect to the markers we tested. It could therefore be

argued that vMac-2 represents a subset of maternal monocyte derived macrophages in the fetal membranes of the placenta, expressing high levels of *S100A9*, as described before (Vento-Tormo et al., 2018). These maternal derived cells mostly populate the chorioamniotic membranes of the placenta (Pique-Regi et al., 2019). Interestingly, vMac-1 cells appear more diverse than their decidual counterparts, with a wide array of functions ranging from host defense to antigen presentation, and tissue repair.

The superimposition of chronic low-grade inflammation associated with obesity and pregnancy associated immune activation has been hypothesized to impart risks for both the mother and the offspring (Sureshchandra et al., 2019). Indeed, high maternal BMI is an independent risk factor for postpartum infections (Cnattingius et al., 2013), premature delivery (Young et al., 2016), and preeclampsia (Gaillard et al., 2013). Mothers with obesity also are at increased risk of post-cesarean wound complications (Conner et al., 2014). Inflammation and a suboptimal immune system at the maternal fetal interface have been proposed to contribute to these risks (Sureshchandra et al., 2019). Hence, we used single cell profiles of CD45+ cells to determine the impact of pregravid obesity on the decidua and villous.

In the decidua, obesity resulted in a reduction in both CD4 and CD8 T cells. T cell cytokine IL-2 and chemokines IP-10 and ITAC were detected at significantly lower levels in the decidual extracts, suggesting poor recruitment of T cells from periphery. On the other hand, both in the decidua and villous, obesity was associated with an enrichment of HLA-DR^{high} subset of macrophages. Phenotypically, these cells expressed both M1 (CD86, HLA-DR) and M2 markers (CD206) and secreted high levels of both regulatory and inflammatory cytokines. With obesity, we observe downregulation of cytokine (*TNF*, *IL6*,

IL1B) and chemokine (*CCL3*, *CCL4*) transcripts and dampened secretion of IL-1β and TNFα. Trajectory analysis also revealed that the macrophages enriched in mothers with obesity, were more regulatory in nature and expressed high levels of lipid regulating genes *APOE* and *FABP5*. Interestingly, dMac-1 cells expressed higher levels of surface TLR4 and HLA-DR with obesity. Given that these molecules are down regulated with activation, this observation would suggest a possible mechanism to limit placental inflammation by controlling immune activation. Indeed, obesity was associated with lower levels of TNF, IL-6, and GM-CSF in decidual extracts. Collectively, these findings suggest obesity-associated infiltration of macrophages in the decidua maintain a regulatory phenotype, potentially to limit inflammation in the placenta. These findings are in contrast to recent studies in high fat diet (HFD) induced maternal obesity in Japanese macaques, where placenta from obese dams up regulated several pro-inflammatory cytokines close to term (Frias et al., 2011). However, authors acknowledge that the phenotype was independent of obesity and more dependent on HFD. Finally, our observations are in line with phenotypic comparisons of macrophages in decidua parietalis, where obesity was associated with lower levels of M1 like macrophages (HLA-DR+ CD163-) (Laskewitz et al., 2019). We argue that these mechanisms are at place to compensate for early gestational pro-inflammatory environment in obese women. A major limitation of human studies is lack of access to tissues during first and second trimester. Future research will have to leverage animal models to test such a hypothesis.

Interestingly, a similar burden of obesity on macrophages was observed in the fetal compartment. Both flow cytometry and single cell RNA profiles support the notion of significantly higher numbers of HLA-DR^{high} macrophages in the villous. These cells are

however, functionally more diverse. More specifically, with obesity we observed enrichment of subsets associated with tissue repair, response to lipid, and fat differentiation. Additionally, a unique cluster of M2-like macrophages, expressing *IGF1*, *CD209*, *FOLR2*, *CD163* was observed in obese group. Furthermore, with obesity, we observed down-regulation of pro-inflammatory molecules *TREM1* and *CXCL3*. More importantly, vMac-1 cells from mothers with obesity were refractory to *ex vivo* challenge, with few IL6+TNF+ cells detected in response to LPS. Taken together, these observations suggest that maternal obesity skews macrophages towards a regulatory phenotype, potentially compromising their critical function at the maternal fetal interface vis-à-vis apoptotic signaling, immune cell-stromal cell crosstalk, and possibly host pathogen response. Finally, elevated levels of regulatory IL-1RA in villous tissue extracts suggest the potential role of tissue microenvironment in influencing local macrophage phenotype. This finding warrants future investigation of obesity associated adaptations in stromal cells and trophoblasts and their potentially dysregulated crosstalk with macrophages to ultimately limit inflammation associated with obesity. Collectively, our findings suggest a regulatory placental environment, with reduced macrophage inflammatory responses, potentially beneficial to limit inflammation under conditions of obesity. However, reduced responses would also suggest compromised host defense resulting in delayed response to infections in the placenta.

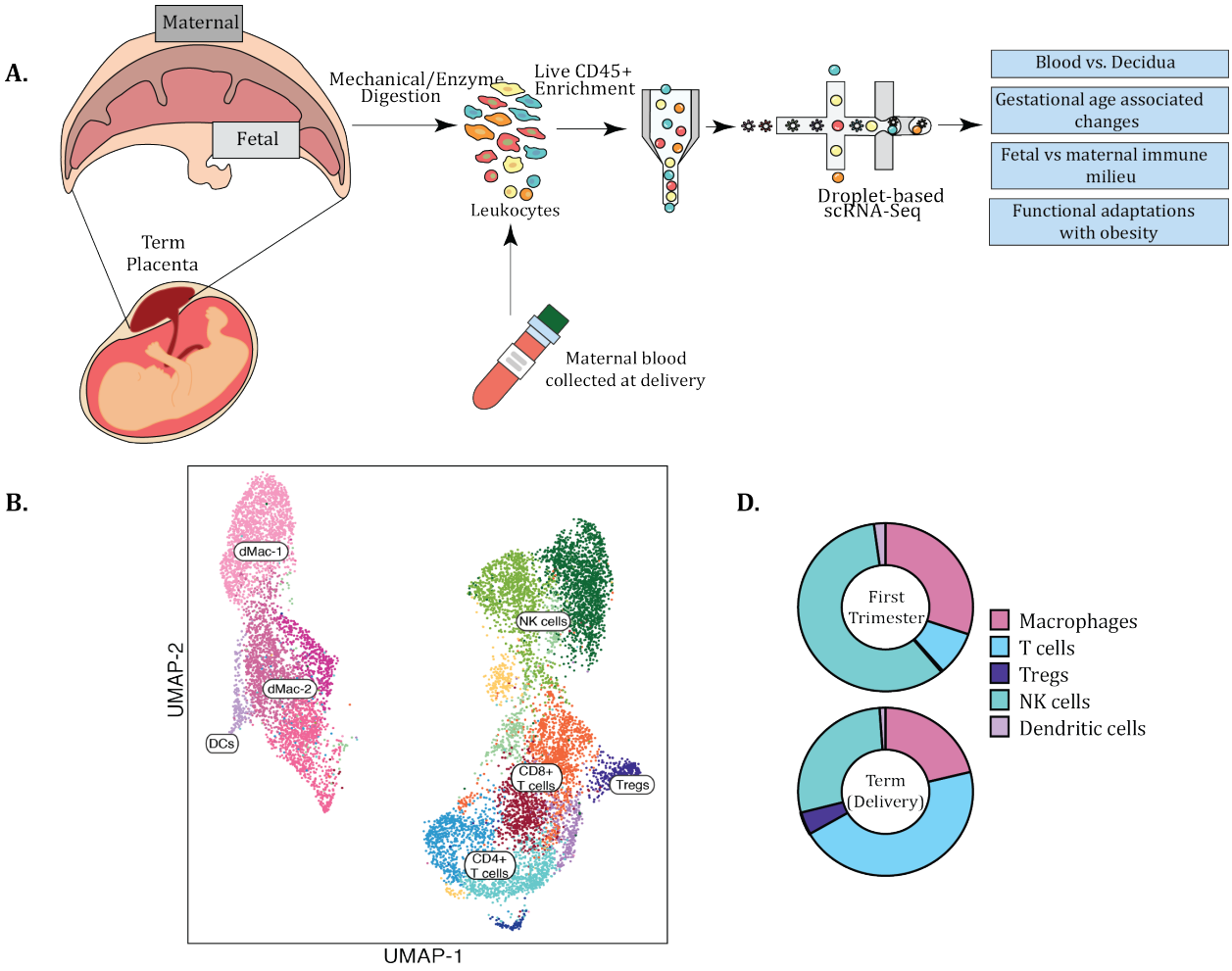
A.
Maternal
Fetal
Term Placenta
Mechanical/Enzyme Digestion
Live CD45+ Enrichment
Leukocytes
Maternal blood collected at delivery
Droplet-based scRNA-Seq
Blood vs. Decidua
Gestational age associated changes
Fetal vs maternal immune milieu
Functional adaptations with obesity
B.
dMac-1
dMac-2
DCs
NK cells
CD8+ T cells
Tregs
CD4+ T cells
UMAP-2
UMAP-1
D.
First Trimester
Term (Delivery)
Macrophages
T cells
Tregs
NK cells
Dendritic cells
C.
IL7R
CCR7
CTLA4
FOXP3
CD8B
NKG7
NCAM1
XCL1
CD160
CD14
CD68
FCER1A
CD4+ T cells
Regulatory T cells
CD8+ T cells
Decidual NK cells
Decidual Macrophages
DCs

(previous page) **Figure 3.1 Defining the term immune landscape of placental decidua.** (A) Experimental Design – CD45+ leukocytes were isolated from matched chorionic villi (n=4) and decidual membranes (n=4) of placentas isolated during term cesarean deliveries. Single cell suspensions were then subjected to single cell RNA sequencing on the 10X platform. Matched blood profiles (n=4) were profiled in parallel to eliminate potential blood contaminating cells. (B) Term decidual cell clusters from scRNA-Seq analysis visualized by UMAP. (C) Violin plots showing log-transformed normalized expression levels of major cell-type determining markers. (D) Changes in frequencies of major immune cell subsets in placental decidua with pregnancy.

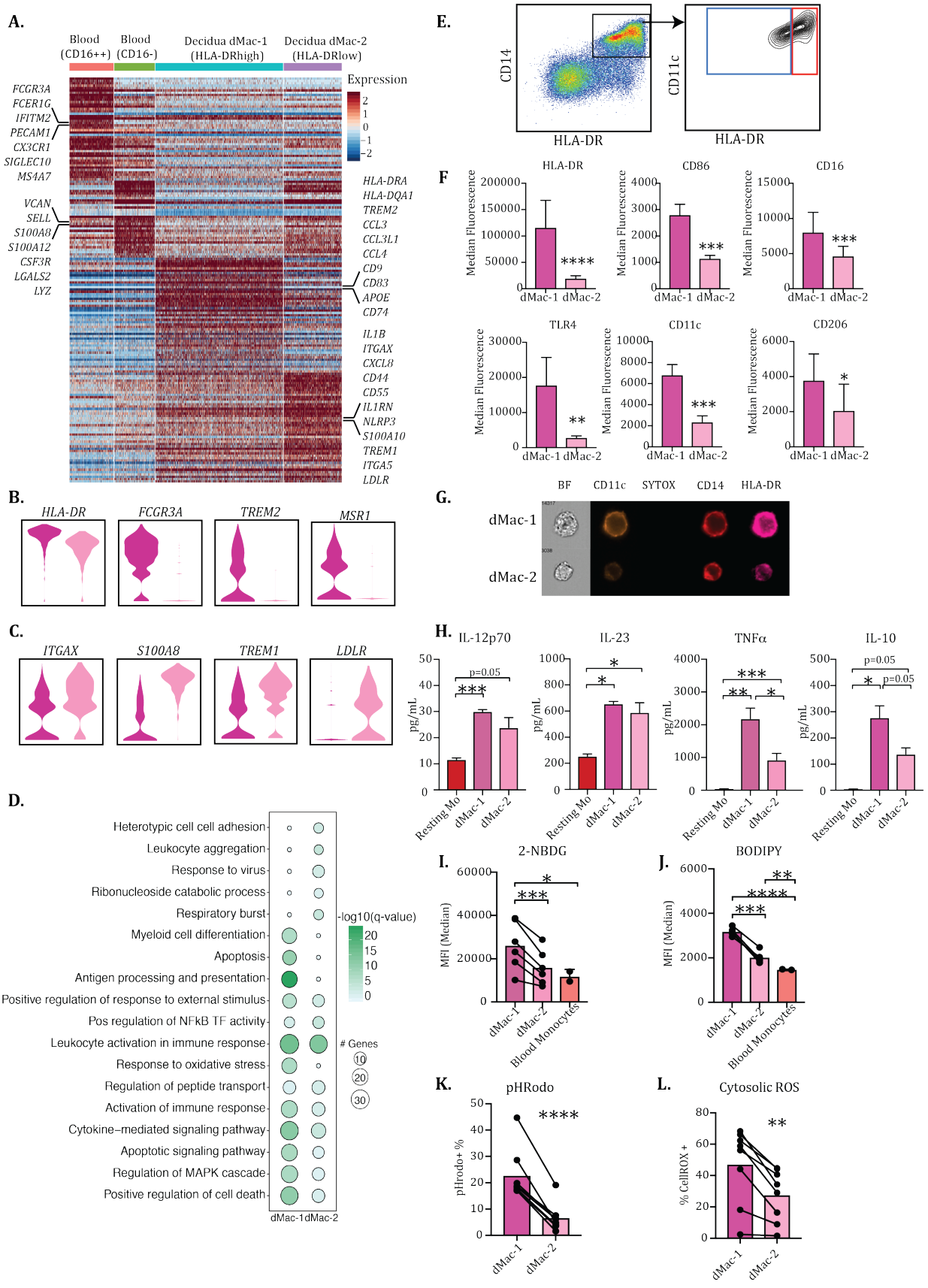
A.
Blood (CD16++)
Blood (CD16-)
Decidua dMac-1 (HLA-DRhigh)
Decidua dMac-2 (HLA-DRlow)
Expression
FCGR3A
FCER1G
IFITM2
PECAM1
CX3CR1
SIGLEC10
MS4A7
VCAN
SELL
S100A8
S100A12
CSF3R
LGALS2
LYZ
HLA-DRA
HLA-DQA1
TREM2
CCL3
CCL3L1
CCL4
CD9
CD83
APOE
CD74
IL1B
ITGAX
CXCL8
CD44
CD55
IL1RN
NLRP3
S100A10
TREM1
ITGA5
LDLR
B.
HLA-DR
FCGR3A
TREM2
MSR1
C.
ITGAX
S100A8
TREM1
LDLR
D.
Heterotypic cell cell adhesion
Leukocyte aggregation
Response to virus
Ribonucleoside catabolic process
Respiratory burst
Myeloid cell differentiation
Apoptosis
Antigen processing and presentation
Positive regulation of response to external stimulus
Pos regulation of NFkB TF activity
Leukocyte activation in immune response
Response to oxidative stress
Regulation of peptide transport
Activation of immune response
Cytokine−mediated signaling pathway
Apoptotic signaling pathway
Regulation of MAPK cascade
Positive regulation of cell death
dMac-1 dMac-2
-log10(q-value)
Genes
E.
CD14
HLA-DR
CD11c
HLA-DR
F
HLA-DR
CD86
CD16
TLR4
CD11c
CD206
Median Fluorescence
dMac-1 dMac-2
G.
BF
CD11c
SYTOX
CD14
HLA-DR
dMac-1
dMac-2
H.
IL-12p70
IL-23
TNFα
IL-10
pg/mL
p=0.05
Resting Mo
dMac-1
dMac-2
I.
2-NBDG
MFI (Median)
dMac-1
dMac-2
Blood Monocytes
J.
BODIPY
MFI (Median)
dMac-1
dMac-2
Blood Monocytes
K.
pHRodo
pHrodo+ %
dMac-1
dMac-2
L.
Cytosolic ROS
% CellROX +
dMac-1
dMac-2

(previous page) **Figure 3.2 Two distinct subsets of macrophages exist in term decidua.** (A) Heatmap of top distinguishing genes between the two-macrophage subsets in the decidua (dMac-1, dMac-2), classical, and non-classical blood monocytes. Each column is a bin of fixed number of cells and each column representing a gene. A subset of genes within each cluster is annotated for reference. High and low expression are represented as red and blue colors respectively. Violin plots comparing the most distinguishing markers of decidua macrophage subsets (B) dMac-1 and (C) dMac-2 (D) Pair-wise GO enrichment of top dMac-1 (130) genes and dMac-2 (117) genes using Metascape. Size of the bubble represents number of genes while color represents the level of statistical significance (E) Surface expression of HLA-DR measured by flow cytometry distinguishes the two subsets of decidual macrophages. (F) Median Fluorescence Intensities (MFI) of macrophage surface markers on dMac-1 and dMac2. (G) Bright field and fluorescence profiles of dMac-1 and dMac-2 captured using imaging flow cytometry. (H) Comparison of baseline secreted cytokine profiles of decidual macrophage subsets and blood monocytes. Bar graphs comparing differences in (I) glucose uptake rate and (J) neutral lipid accumulation within the two macrophage subsets. Bar graphs comparing differences in (K) phagocytosis and (L) resting cytosolic ROS levels between dMac-1 and dMac-2. Error bars represent median with inter-quartile ranges (IQR). (p-values: * - $p<0.05$; ** - $p<0.01$; ** - $p<0.001$; *** - $p<0.0001$).

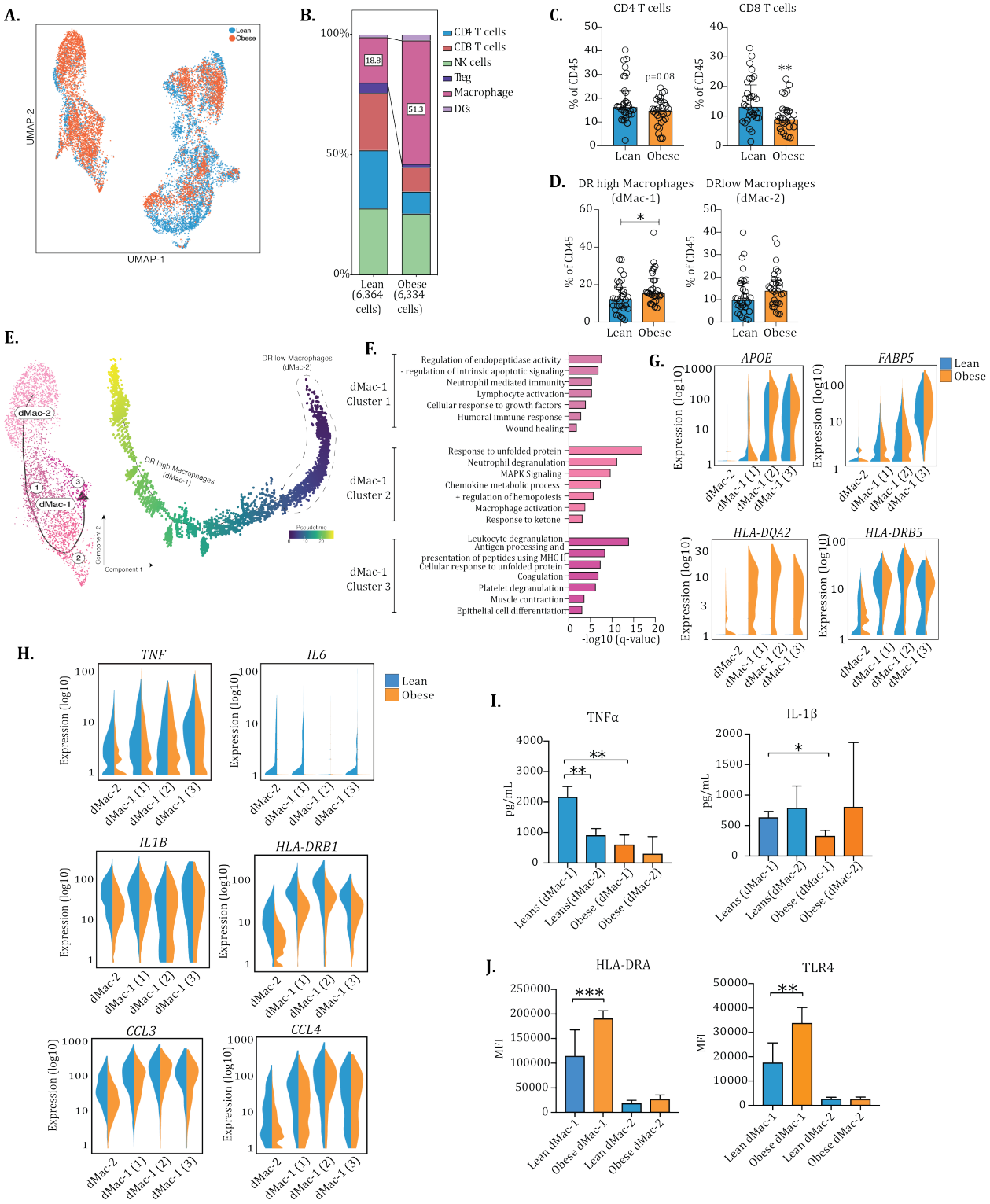
A.
Lean
Obese
UMAP-2
UMAP-1
B.
100%
50%
0%
18.8
51.3
CD4 T cells
CD8 T cells
NK cells
Treg
Macrophages
DCs
Lean (6,364 cells)
Obese (6,334 cells)
C.
CD4 T cells
CD8 T cells
% of CD45
p=0.08
**
Lean
Obese
D.
DR high Macrophages (dMac-1)
DRlow Macrophages (dMac-2)
*
E.
DR low Macrophages (dMac-2)
dMac-2
dMac-1
DR high Macrophages (dMac-1)
Pseudotime
Component 1
Component 2
F.
dMac-1 Cluster 1
Regulation of endopeptidase activity
- regulation of intrinsic apoptotic signaling
Neutrophil mediated immunity
Lymphocyte activation
Cellular response to growth factors
Humoral immune response
Wound healing
dMac-1 Cluster 2
Response to unfolded protein
Neutrophil degranulation
MAPK Signaling
Chemokine metabolic process
+ regulation of hemopoiesis
Macrophage activation
Response to ketone
dMac-1 Cluster 3
Leukocyte degranulation
Antigen processing and presentation of peptides using MHC II
Cellular response to unfolded protein
Coagulation
Platelet degranulation
Muscle contraction
Epithelial cell differentiation
-log10 (q-value)
G.
APOE
FABP5
HLA-DQA2
HLA-DRB5
Expression (log10)
Lean
Obese
dMac-2
dMac-1 (1)
dMac-1 (2)
dMac-1 (3)
H.
TNF
IL6
IL1B
HLA-DRB1
CCL3
CCL4
I.
TNFα
IL-1β
pg/mL
Leans (dMac-1)
Leans(dMac-2)
Obese (dMac-1)
Obese (dMac-2)
J.
HLA-DRA
TLR4
MFI
Lean dMac-1
Obese dMac-1
Lean dMac-2
Obese dMac-2

(previous page) **Figure 3.3 Maternal obesity alters the frequency and phenotype of decidual macrophages** (A) UMAP representation of decidual leukocyte populations highlighting differences with maternal obesity. (B) Stacked bar graphs comparing major immune cell subsets quantified from single cell clusters. Percentages of macrophages within each group are highlighted. Quantification of (C) CD4 and CD8 T cells, and (D) macrophage subtypes with maternal obesity using flow cytometry. (E) Pseudotime ordering of macrophages reveals a trajectory of differentiation/development pathways. Cells are ordered from blue (dMac-2) to yellow (dMac-1) (right). Subsets of dMac-1 are highlighted per the direction of pseudotime (left). (F) Functional enrichment of top genes expressed by dMac-1 subsets highlighting functional diversity identified using Metascape. (G) Violin plots of a subset of genes up regulated with obesity. (H) Violin plots of select inflammatory genes down regulated across several macrophage clusters with maternal obesity. Differentially expressed genes were identified by DESeq2. Y-axis represents log transformed normalized read counts. (I) Bar graphs comparing surface expression of HLA-DR and TLR4 and (J) secreted cytokines TNFα and IL-1β between macrophage subsets with maternal obesity. (K) Differences in phagocytosis of *E.coli* conjugated pHrodo particles, measured using flow cytometry. Bars represent medians with IQR. (p-values: * - $p<0.05$; ** - $p<0.01$; *** - $p<0.001$).

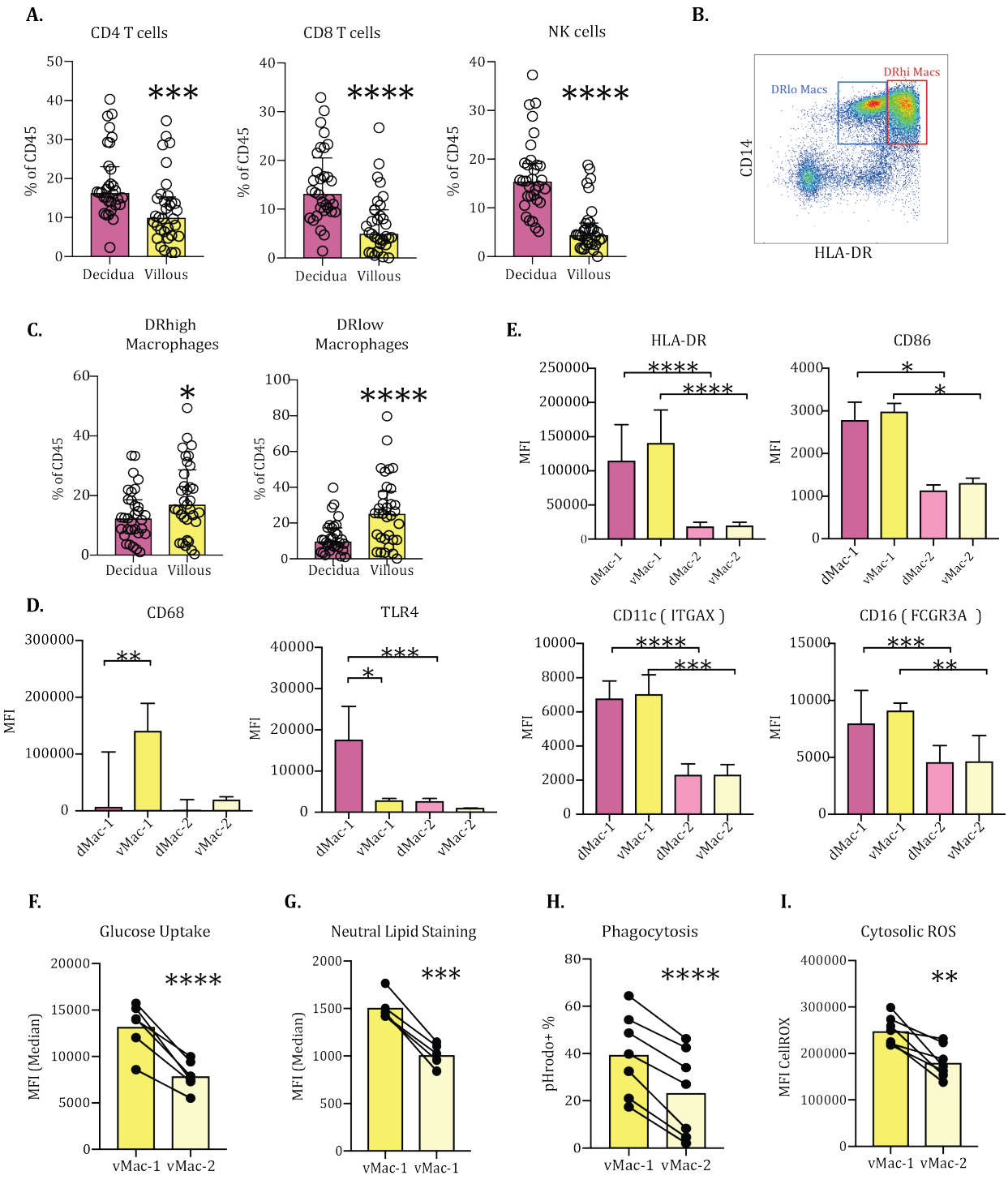
A.
CD4 T cells
CD8 T cells
NK cells
% of CD45
Decidua
Villous
***
****
****
B.
DRhi Macs
DRlo Macs
CD14
HLA-DR
C.
DRhigh Macrophages
DRlow Macrophages
*
****
D.
CD68
TLR4
MFI
**
***
*
E.
HLA-DR
CD86
CD11c (ITGAX)
CD16 (FCGR3A)
****
*
***
dMac-1
vMac-1
dMac-2
vMac-2
F.
Glucose Uptake
MFI (Median)
G.
Neutral Lipid Staining
H.
Phagocytosis
pHrodo+ %
I.
Cytosolic ROS
MFI CellROX

(previous page) **Figure 3.4 Term decidua and villous chorion harbor distinct immune milieu.**
(A) Bar graphs representing shifts in CD4+ T cells, CD8+ T cells, and NK cells across the two membranes of placenta. Only frequencies from placentas of lean mothers are included in this analysis. (B) Flow cytometry discrimination of two macrophage subsets in the villi based on HLA-DR expression. Plot shown is a gate out of live CD45+CD20-CD4-CD8- cells in the villous. (C) Comparison of frequencies of villous and decidua macrophage subsets – DRhigh (vMac-1) and DRlow (vMac-2) (D) Bar graphs of markers distinguishing (CD68 and TLR4) DRhigh macrophages from decidua and villous chorion. (E) Bar graphs highlighting markers identical between macrophage subsets in decidua and villous chorion. Functional differences in villous macrophage subsets characterized by (F) glucose uptake measured by 2-NBDG uptake, (G) neutral lipid accumulation measured by BODIPY fluorescence, (H) phagocytosis measured by *E. col*i uptake, and (I) baseline cytosolic ROS measured by CellROX fluorescence. (p-values: * - $p<0.05$; ** - $p<0.01$; *** - $p<0.001$; **** - $p<0.0001$).

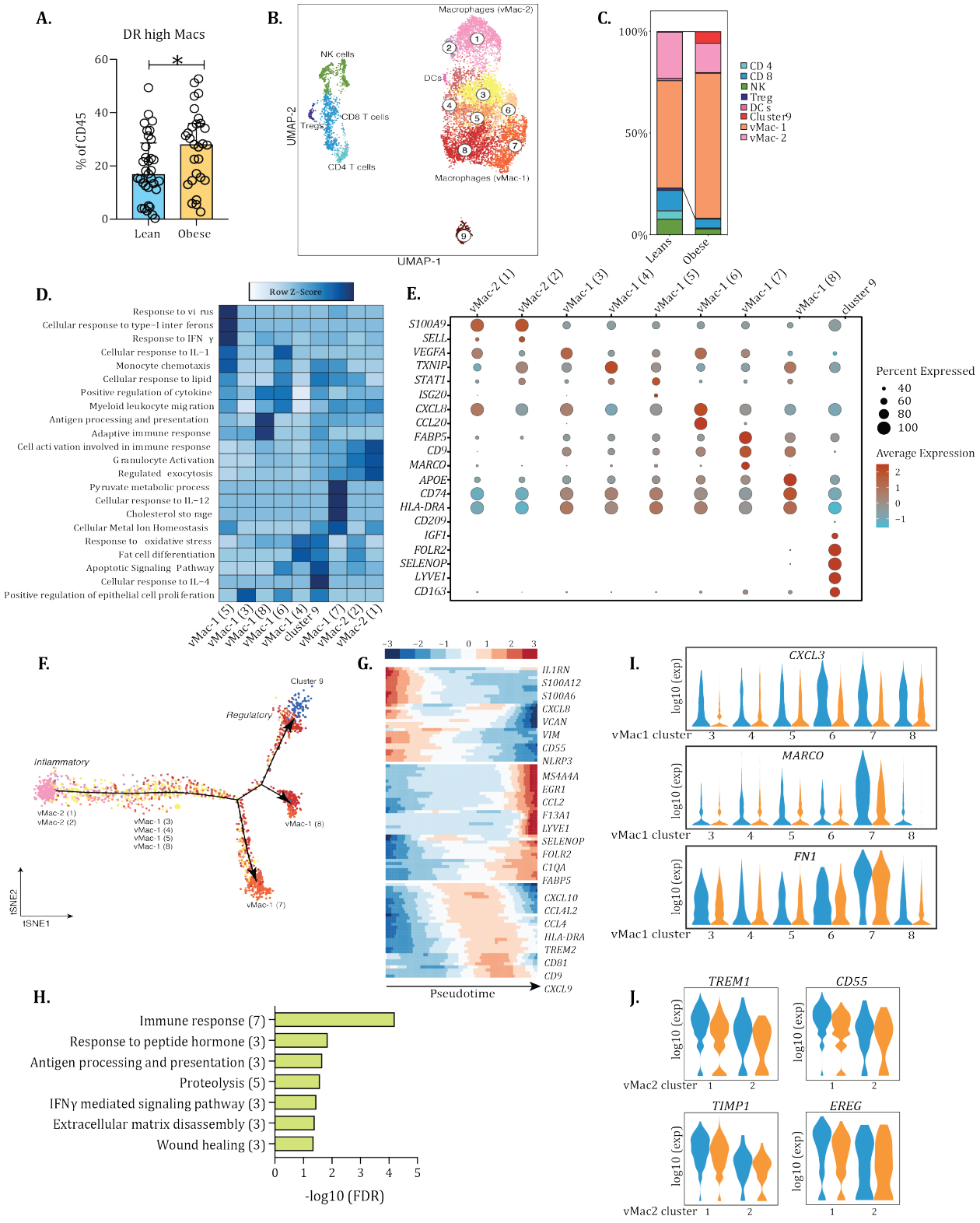
A.
DR high Macs
% of CD45
Lean
Obese
B.
Macrophages (vMac-2)
NK cells
DCs
Tregs
CD8 T cells
CD4 T cells
Macrophages (vMac-1)
UMAP-1
UMAP-2
C.
100%
50%
0%
Leans
Obese
CD 4
CD 8
NK
Treg
DC s
Cluster9
vMac-1
vMac-2
D.
Row Z-Score
Response to vi rus
Cellular response to type−I inter ferons
Response to IFN γ
Cellular response to IL−1
Monocyte chemotaxis
Cellular response to lipid
Positive regulation of cytokine
Myeloid leukocyte mig ration
Antigen processing and presentation
Adaptive immune response
Cell acti vation involved in immune response
G ranulocyte Activation
Regulated exocytosis
Pyruvate metabolic process
Cellular response to IL−12
Cholesterol sto rage
Cellular Metal Ion Homeostasis
Response to oxidative stress
Fat cell differentiation
Apoptotic Signaling Pathway
Cellular response to IL−4
Positive regulation of epithelial cell proli feration
vMac-1 (5)
vMac-1 (3)
vMac-1 (8)
vMac-1 (6)
vMac-1 (4)
cluster-9
vMac-1 (7)
vMac-2 (2)
vMac-2 (1)
E.
vMac-2 (1)
vMac-2 (2)
vMac-1 (3)
vMac-1 (4)
vMac-1 (5)
vMac-1 (6)
vMac-1 (7)
vMac-1 (8)
cluster-9
S100A9
SELL
VEGFA
TXNIP
STAT1
ISG20
CXCL8
CCL20
FABP5
CD9
MARCO
APOE
CD74
HLA-DRA
CD209
IGF1
FOLR2
SELENOP
LYVE1
CD163
Percent Expressed
40
60
80
100
Average Expression
2
1
0
−1
F.
Cluster 9
Regulatory
Inflammatory
vMac-2 (1)
vMac-2 (2)
vMac-1 (3)
vMac-1 (4)
vMac-1 (5)
vMac-1 (8)
vMac-1 (8)
vMac-1 (7)
tSNE2
tSNE1
G.
−3
−2
−1
0
1
2
3
IL1RN
S100A12
S100A6
CXCL8
VCAN
VIM
CD55
NLRP3
MS4A4A
EGR1
CCL2
F13A1
LYVE1
SELENOP
FOLR2
C1QA
FABP5
CXCL10
CCL4L2
CCL4
HLA-DRA
TREM2
CD81
CD9
CXCL9
Pseudotime
I.
CXCL3
MARCO
FN1
log10 (exp)
vMac1 cluster
3
4
5
6
7
8
H.
Immune response (7)
Response to peptide hormone (3)
Antigen processing and presentation (3)
Proteolysis (5)
IFNγ mediated signaling pathway (3)
Extracellular matrix disassembly (3)
Wound healing (3)
0
1
2
3
4
5
-log10 (FDR)
J.
TREM1
CD55
TIMP1
EREG
log10 (exp)
vMac2 cluster
1
2

(previous page) **Figure 3.5 Immunological adaptations to maternal obesity in fetal chorionic villi.**
(A) Bar graphs comparing differences in frequencies of HLA-DR^{high} macrophages in villous chorion with maternal obesity. (B) UMAP representation of CD45+ leukocytes in the villous chorion (n=4). Two subsets of macrophages are annotated as vMac-1 and vMac-2, with their subtypes further annotated as numbers in circles. Gating shown is representative of live CD45. (C) Stacked bar graphs comparing percentages of major immune cell subtypes identified by single cell RNA-Seq between lean and obese subjects. (D) Functional enrichment of diverse subtypes of macrophage clusters based on highly expressing genes within each cluster using Metascape. Colors signify statistical significance of the prediction, ranging from low (light blue) to high (dark blue). (E) Bubble plots depicting expression levels of select top markers distinguishing each cluster from the other. Size of the bubble is representative of the proportion of cells within each cluster expressing the genes. Color represents the level of expression, ranging from blue (low) to red (high). (F) Pseudotemporal ordering places cells in an inflammatory trajectory defining the transition from blood derived to tissue resident macrophages. Arrows depict direction of trajectory. Subsets are annotated based on their position on the trajectory. (G) Clustered heatmap of top 100 genes that determine the pseudotemporal ordering of villous macrophages. Genes are clustered by their relative expression over a progressing trajectory. (H) Functional enrichment of differentially expressed genes (DEG) down-regulated in vMac-1, comparing transcripts between lean and obese group. (I) Violin plots of select inflammatory genes down regulated across several vMac-1 clusters with maternal obesity. (J) Violin plots of select inflammatory genes down regulated across several vMac-2 clusters with maternal obesity. Y-axis represents normalized log-transformed transcript counts. (p-values: * - $p<0.05$).

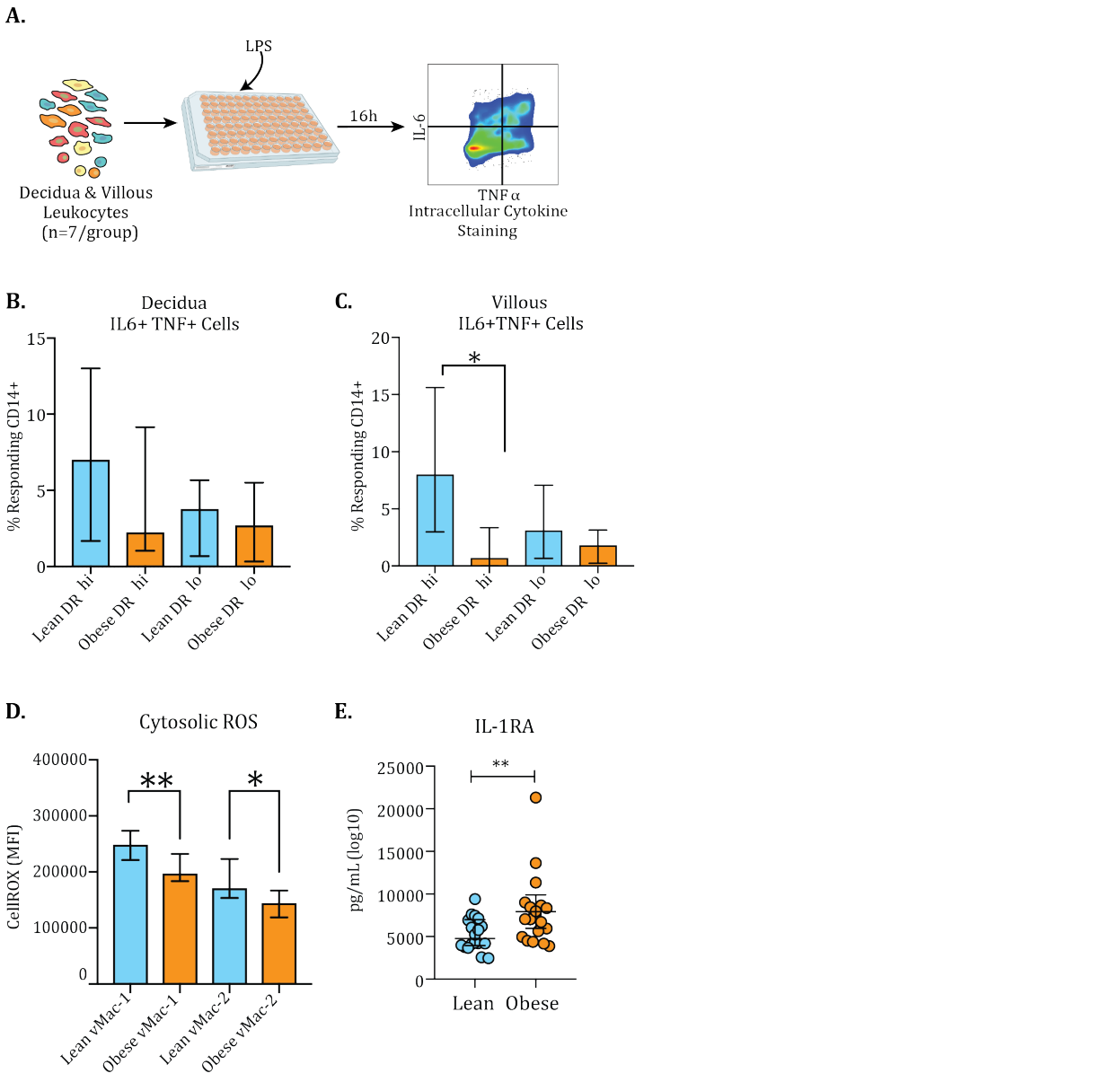

Figure 3.6 Maternal obesity limits inflammatory responses of villous macrophages. (A) Experimental design for measuring cytokine responses in decidual/villous macrophages. Bar graphs comparing IL6+TNFα+ macrophages in following 16h LPS stimulation in (B) decidua and (C) chorionic villi. Percentages on Y-axis are post-stimulation values corrected for baseline cytokine readouts. (D) Bar graph comparing cytosolic ROS using flow cytometry (E) Bar graph comparing IL1RA levels in villous tissue lysate measured using luminex. Bars represent medians and IQR. (p-values: * - $p<0.05$; ** - $p<0.01$).

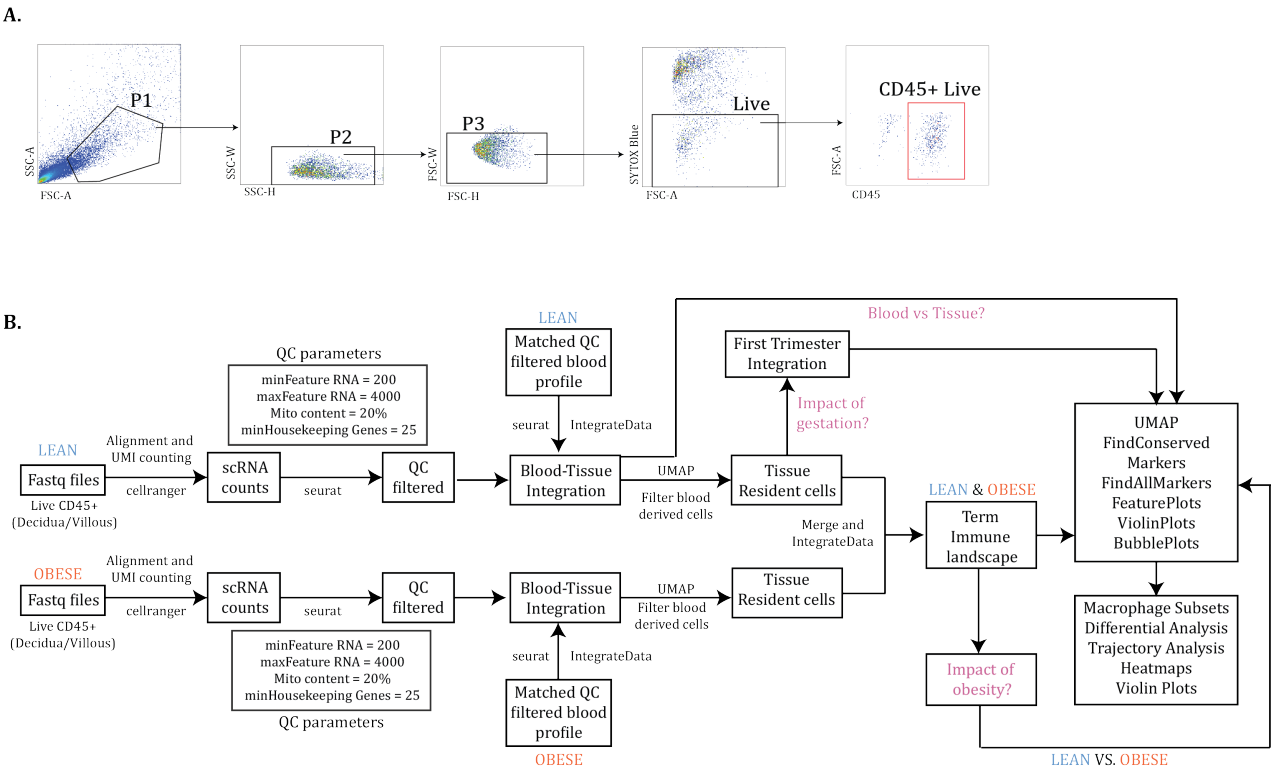

Supplemental Figure 3.1 Workflow for single cell RNA sequencing.
(A) Gating strategy for sorting CD45+ cells from frozen leukocytes from placental decidua and chorionic villi. (B) Analysis strategy for single cell RNA sequencing data. Tissue resident profiles were integrated with matched blood samples to eliminate any contaminant cells from blood and identify unique features defining tissue residence. Term decidua profile was integrated with recently published first-trimester decidua immune landscape to characterize gestational immunological changes at the maternal-fetal interface. Finally, the impact of obesity was assessed by stratifying the samples by matched decidua/villous profiles from lean mothers (n=2) and mothers with obesity (n=2).

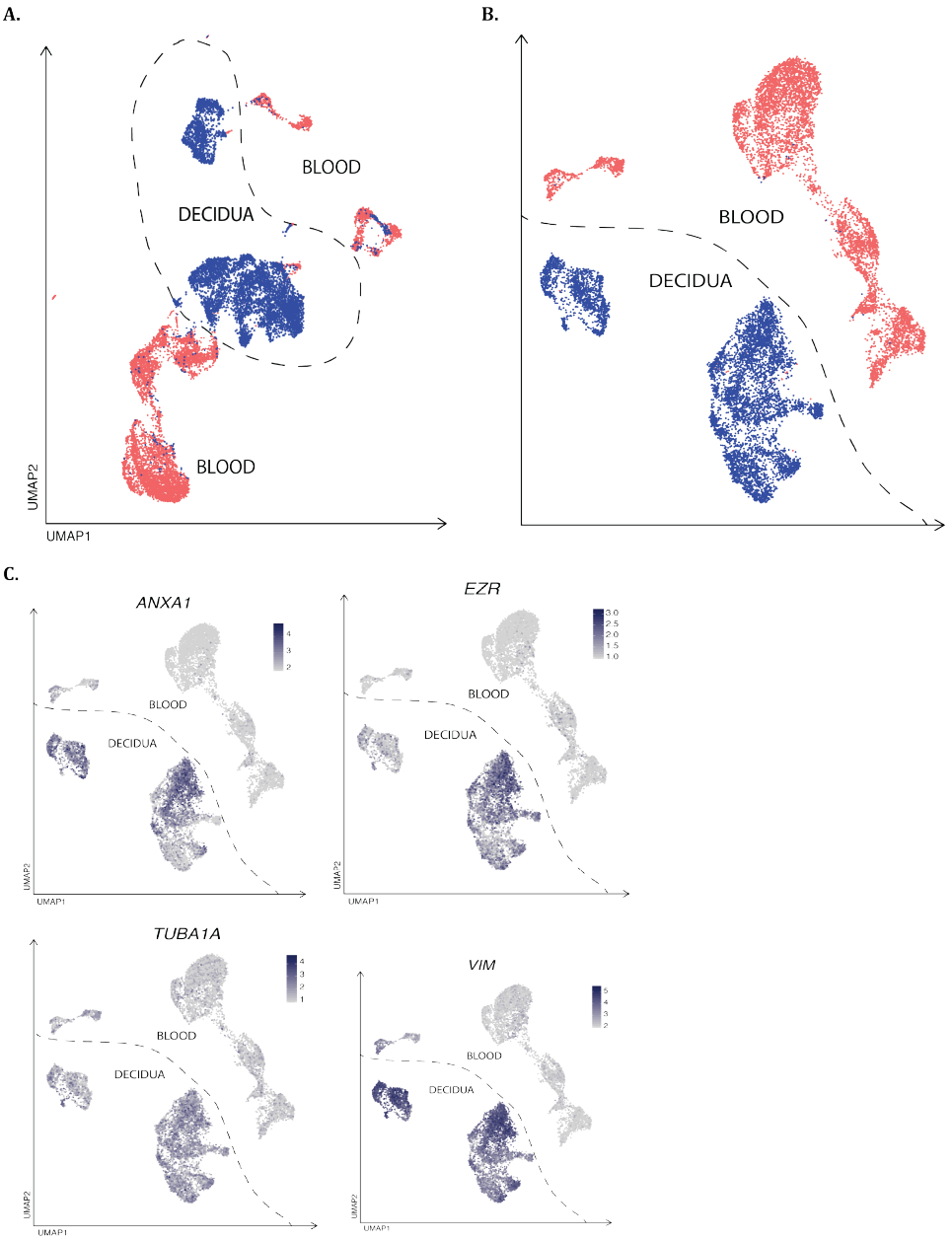

Supplemental Figure 3.2 Comparison of peripheral and decidual leukocytes.
UMAP representation of integrated blood and decidua profiles (A) before and (B) after filtering tissue contaminating blood cells. (C) Feature plots confirming tissue resident identity of isolated decidua cells supported by markers defining tissue resident lymphocytes.

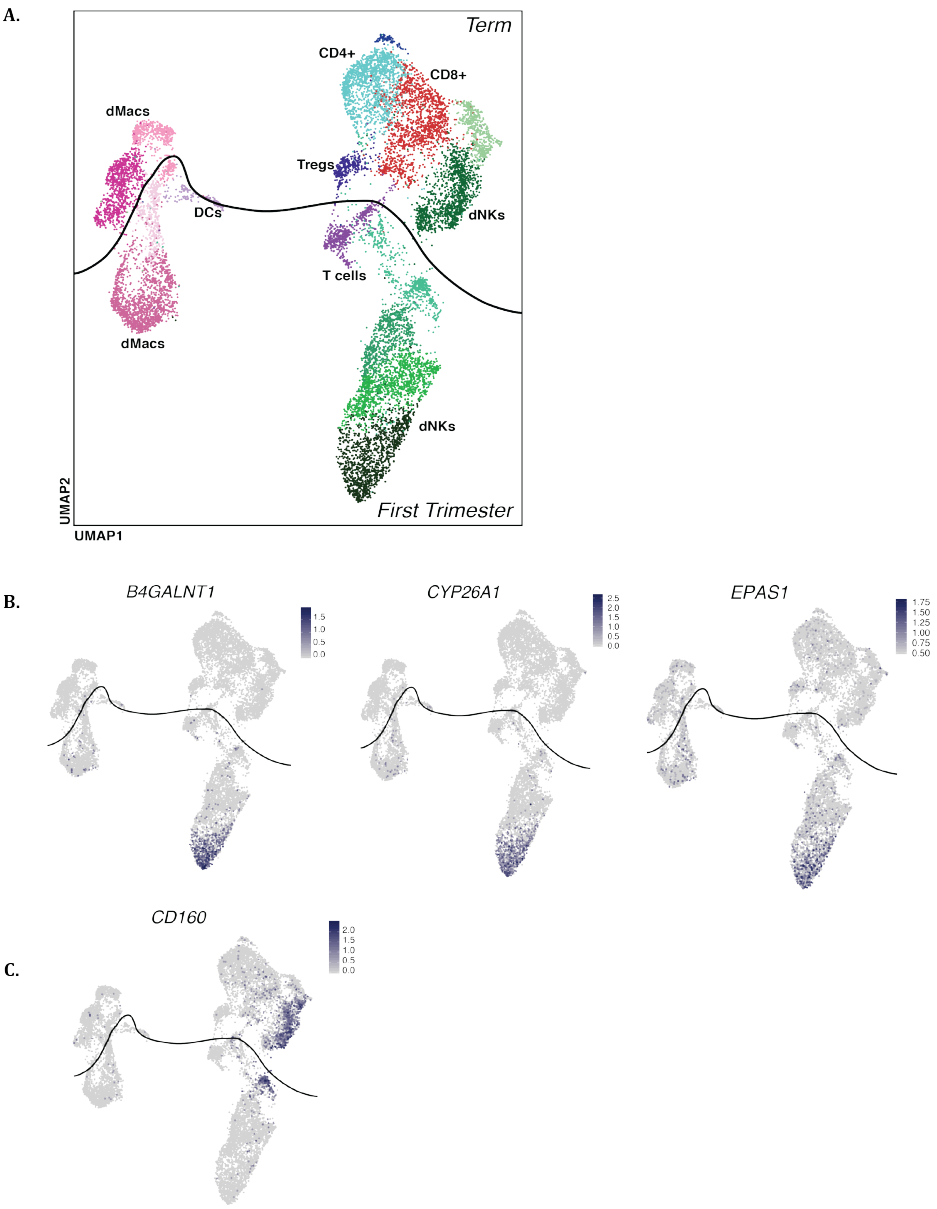

Supplemental Figure 3.3 Comparison of decidual leukocytes from early and late gestation.

(A) UMAP representation of integrated decidua profiles from first and third trimesters. Decidua profiles from first trimester from a recently published study was analyzed and down-sampled for comparison with cells profiled in this study. Feature plots comparing T1 and T3 expression of markers expressed by decidua NK (dNK) subsets - (B) dNK1 and (C) dNK3.

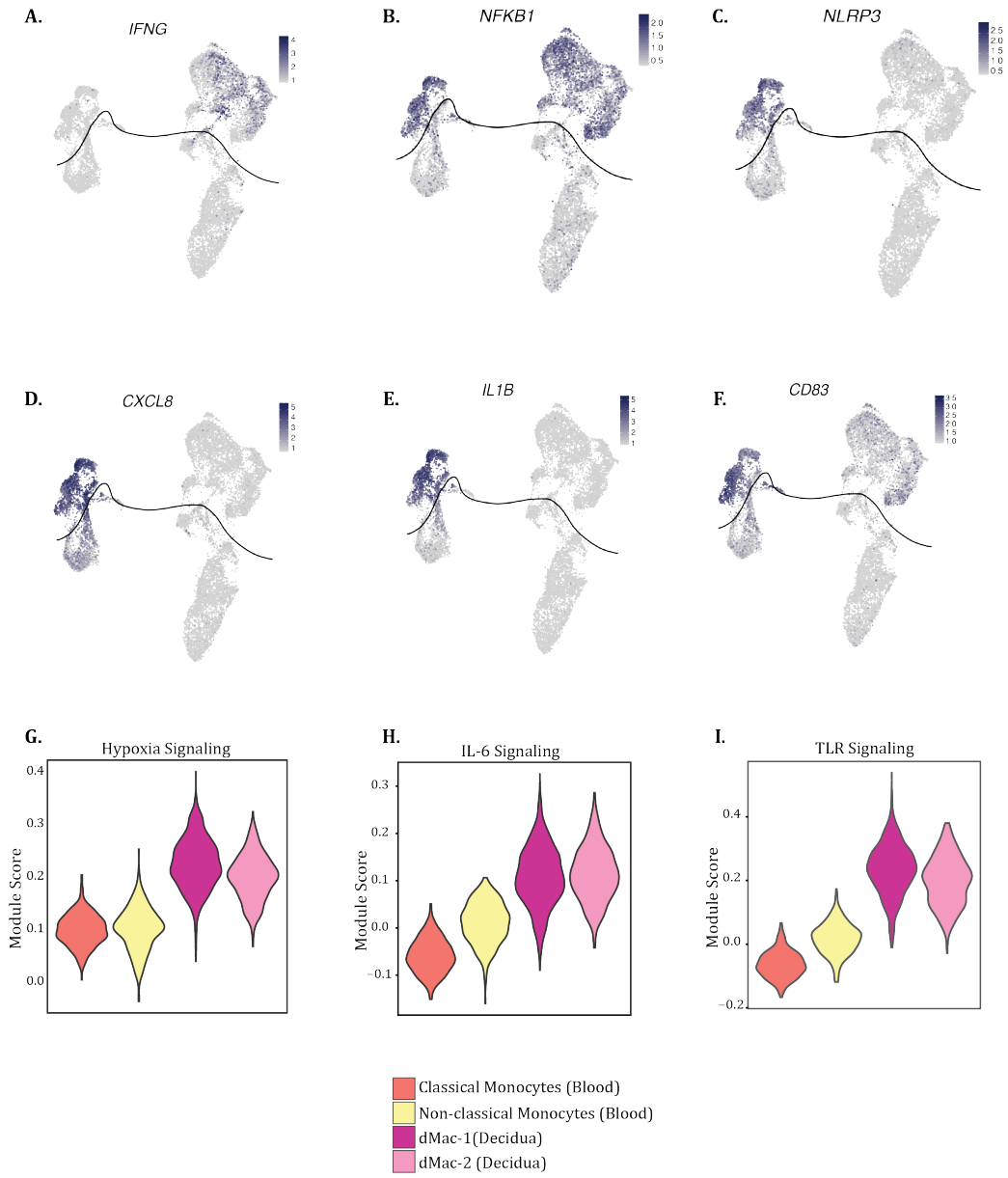

Supplemental Figure 3.4 Decidual immune cell activation at delivery.
Feature plots comparing expression of (A) *IFNG*, (B) *NFKB1*, and (C-F) markers of myeloid cell activation. Violin plots comparing module scores for (G) hypoxia, (H) IL-6, and (I) TLR signaling between two macrophage subsets in decidua and monocyte subsets.

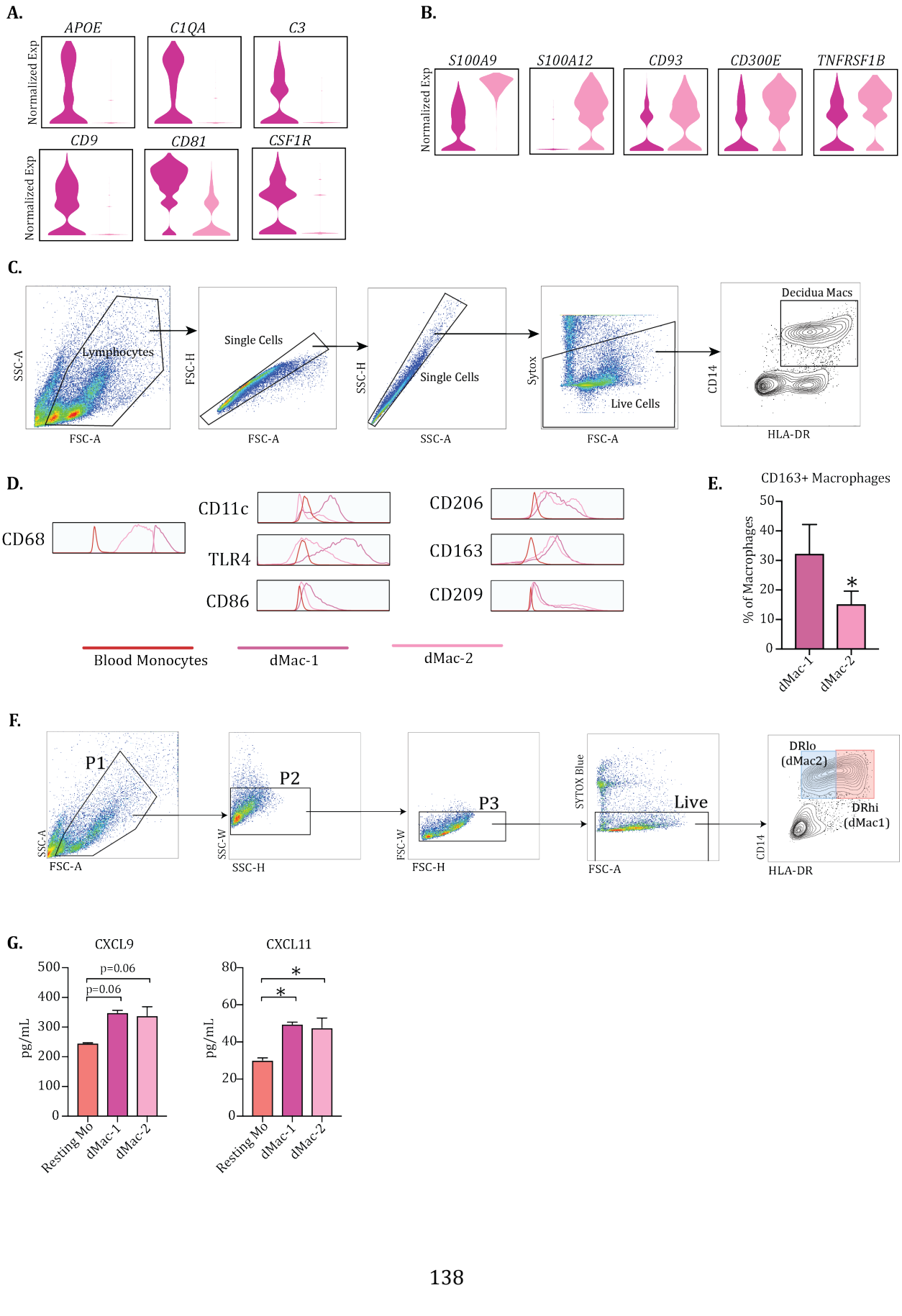
A.
APOE
C1QA
C3
CD9
CD81
CSF1R
Normalized Exp
B.
S100A9
S100A12
CD93
CD300E
TNFRSF1B
C.
Lymphocytes
SSC-A
FSC-A
Single Cells
FSC-H
FSC-A
Single Cells
SSC-H
SSC-A
Live Cells
Sytox
FSC-A
Decidua Macs
CD14
HLA-DR
D.
CD68
CD11c
TLR4
CD86
CD206
CD163
CD209
Blood Monocytes
dMac-1
dMac-2
E.
CD163+ Macrophages
% of Macrophages
dMac-1
dMac-2
F.
P1
SSC-A
FSC-A
P2
SSC-W
SSC-H
P3
FSC-W
FSC-H
Live
SYTOX Blue
FSC-A
DRlo
(dMac2)
DRhi
(dMac1)
CD14
HLA-DR
G.
CXCL9
CXCL11
pg/mL
p=0.06
p=0.06
Resting Mo
dMac-1
dMac-2

(previous page) **Supplemental Figure 3.5 Two subsets of macrophages in maternal decidua at delivery.** Violin plots of (A) dMac-1 and (B) dMac-2 markers identified using single cell RNA-sequencing. (C) Gating strategy for identification of two distinct macrophage subsets in decidua. (D) Histograms of representative markers on HLA-DR^{high} (dMac-1), HLA-DR^{low} (dMac-2) subsets and blood monocytes measured using flow cytometry. (E) Bar graph comparing CD163+ macrophages within HLA-DR^{high} and HLA-DR^{low} subsets in the decidua. (F) Gating strategy for sorting dMac-1 and dMac-2 subsets using FACS. (G) Bar graphs comparing chemokines differentially secreted between decidual macrophage subsets and blood monocytes. Error bars represent median and IQR (p-values: * - $p<0.05$).

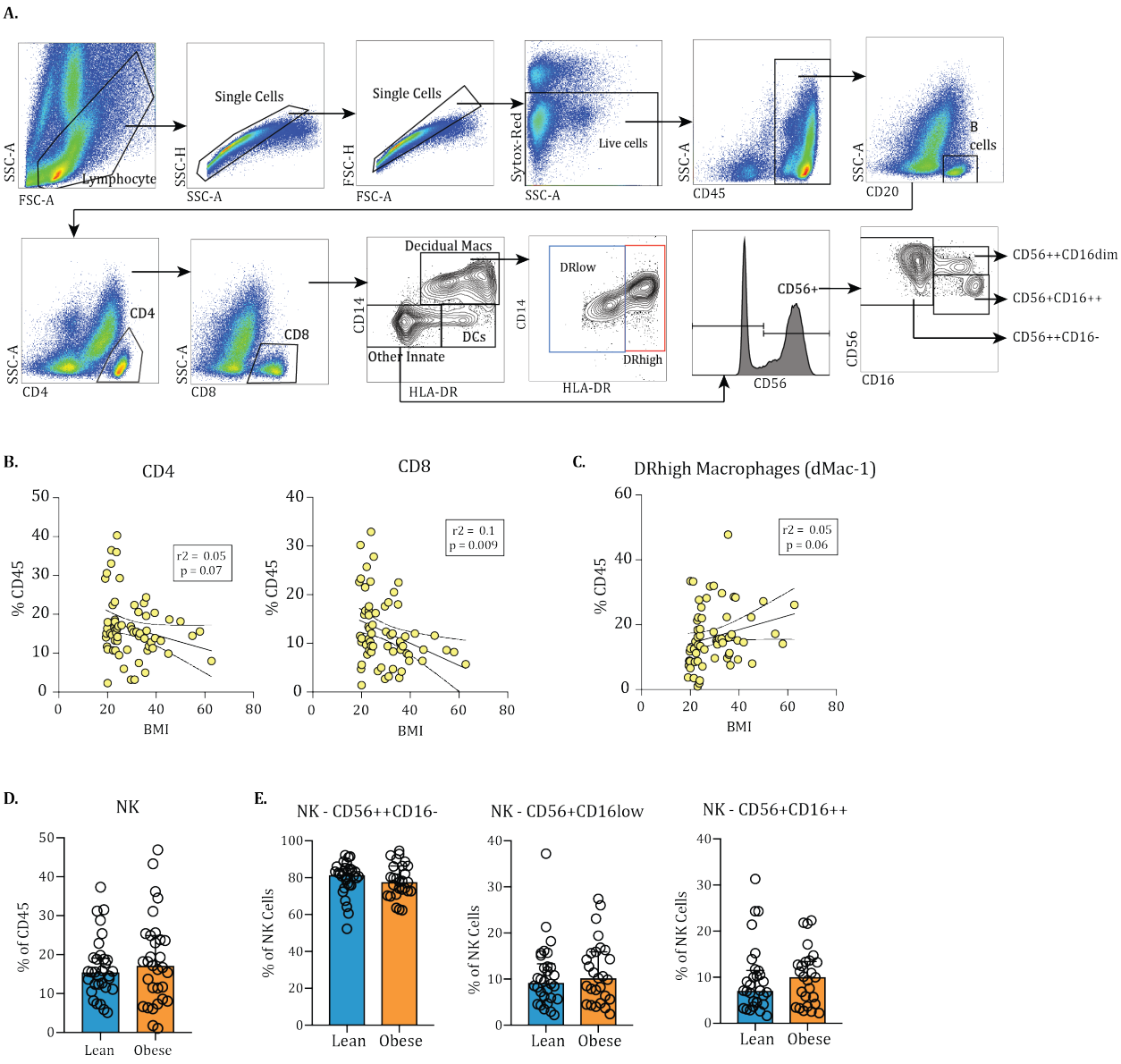

Supplemental Figure 3.6 Phenotyping of immune cell populations in term decidua. (A) Gating strategy for characterization of innate and adaptive immune cell subsets in term decidua. BMI dependent changes in (B) T cell percentages and (C) dMac-1 percentages (within CD45+) (D) Comparison of total Natural Killer (NK) cells and (E) NK cell subsets with obesity.

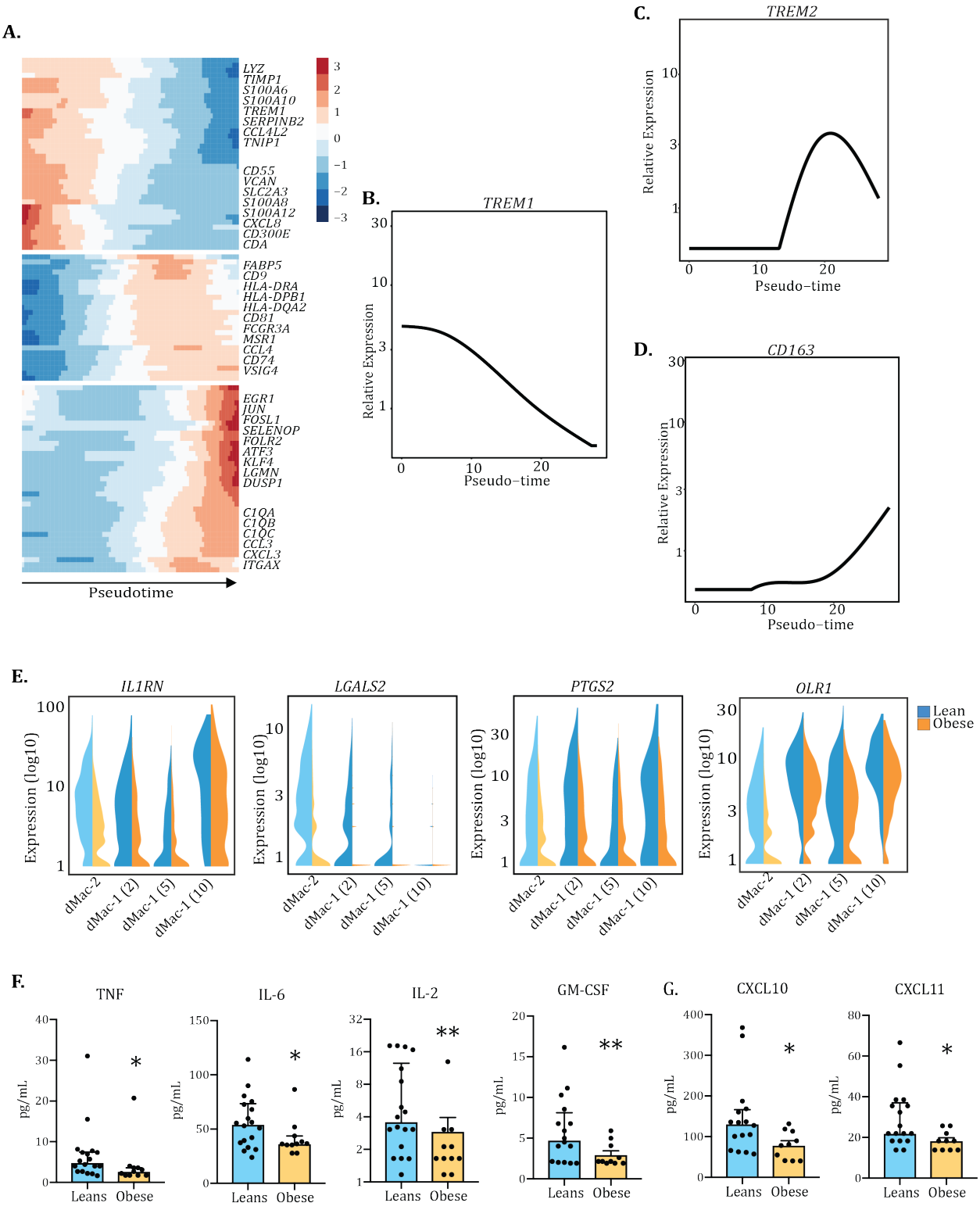
A.
LYZ
TIMP1
S100A6
S100A10
TREM1
SERPINB2
CCL4L2
TNIP1
CD55
VCAN
SLC2A3
S100A8
S100A12
CXCL8
CD300E
CDA
FABP5
CD9
HLA-DRA
HLA-DPB1
HLA-DQA2
CD81
FCGR3A
MSR1
CCL4
CD74
VSIG4
EGR1
JUN
FOSL1
SELENOP
FOLR2
ATF3
KLF4
LGMN
DUSP1
C1QA
C1QB
C1QC
CCL3
CXCL3
ITGAX
Pseudotime
B.
TREM1
Relative Expression
Pseudo−time
C.
TREM2
Relative Expression
Pseudo−time
D.
CD163
Relative Expression
Pseudo−time
E.
IL1RN
LGALS2
PTGS2
OLR1
Expression (log10)
dMac-2
dMac-1 (2)
dMac-1 (5)
dMac-1 (10)
Lean
Obese
F.
TNF
IL-6
IL-2
GM-CSF
pg/mL
Leans
Obese
G.
CXCL10
CXCL11

(previous page) **Supplemental Figure 3.7 Decidual macrophage adaptations with maternal obesity.**
(A) Heatmap of top 100 genes determining the pseudotemporal ordering of decidual macrophages. Genes are clustered by their relative expression over a progressing trajectory. Pseudotemporal changes in gene expression of inflammatory marker (B) *TREM1* and regulatory markers (C) *TREM2*, and (D) *CD163* in decidual macrophages. (E) Violin plots of select inflammatory genes down regulated across several macrophage clusters with maternal obesity. Differentially expressed genes were identified by DESeq2. Y-axis represents log transformed normalized read counts. (F) Bar graphs comparing cytokines TNFα, IL-6, IL-2, and growth factor GM-CSF and (G) T cell chemokines CXCL10 and CXCL11 in decidua tissue lysates measured using luminex. Bars represent medians with IQR. (p-values: * - $p<0.05$; ** - $p<0.01$).

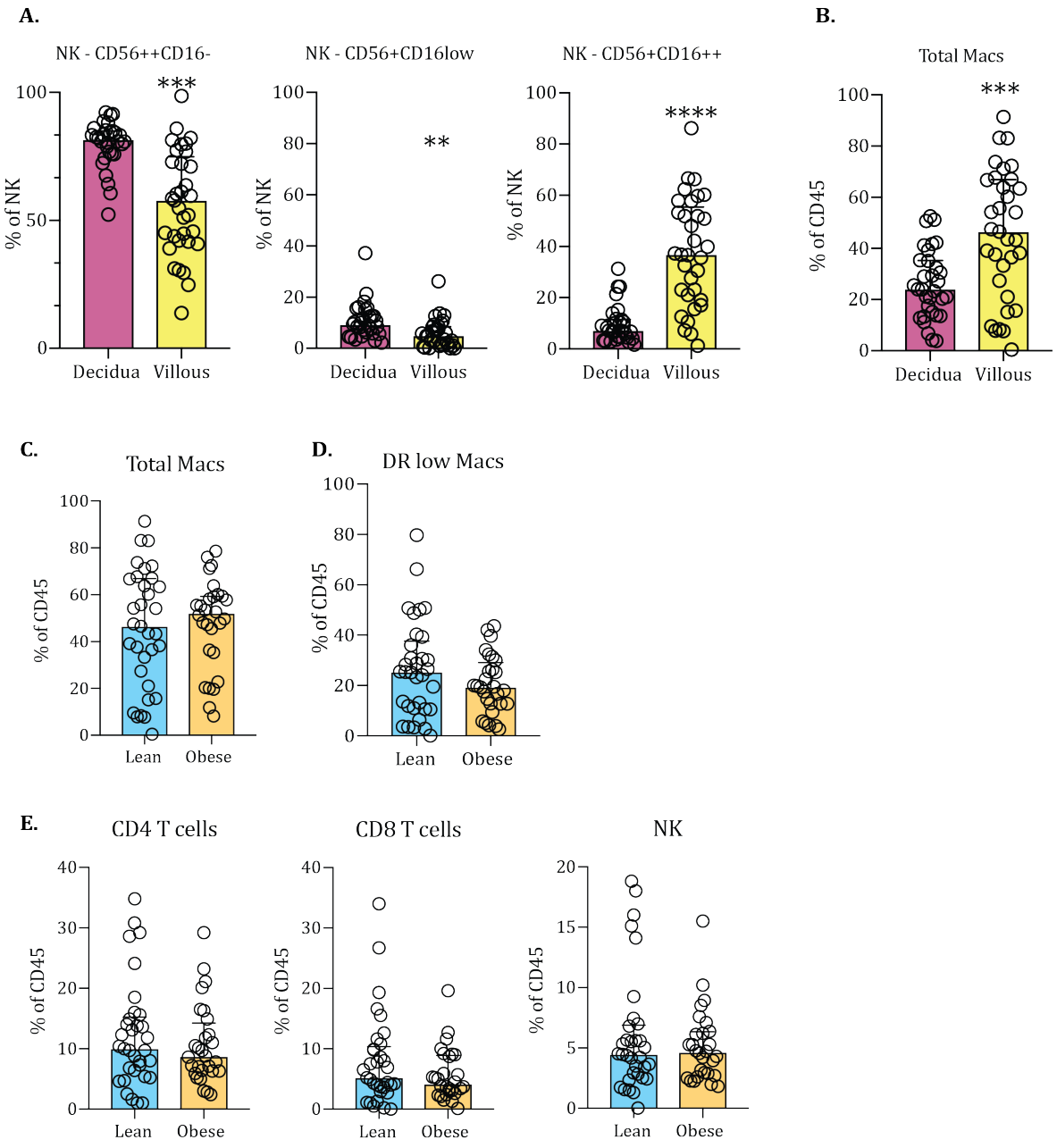

Supplemental Figure 3.8 Comparing decidual and villous immune landscapes at term. (A) Bar graphs comparing NK cell subsets and (B) total macrophages (CD14+) in decidual and villous chorion. Bar graphs comparing changes in (C) total macrophages, (D) HLA-DR low macrophage subset, and (E) CD4 T cells, CD8 T cells, and NK cells with maternal obesity in the villous compartment. Bar graphs represent medians with IQR (p-values: ** - p<0.01; *** - p<0.001; **** - p<0.0001)

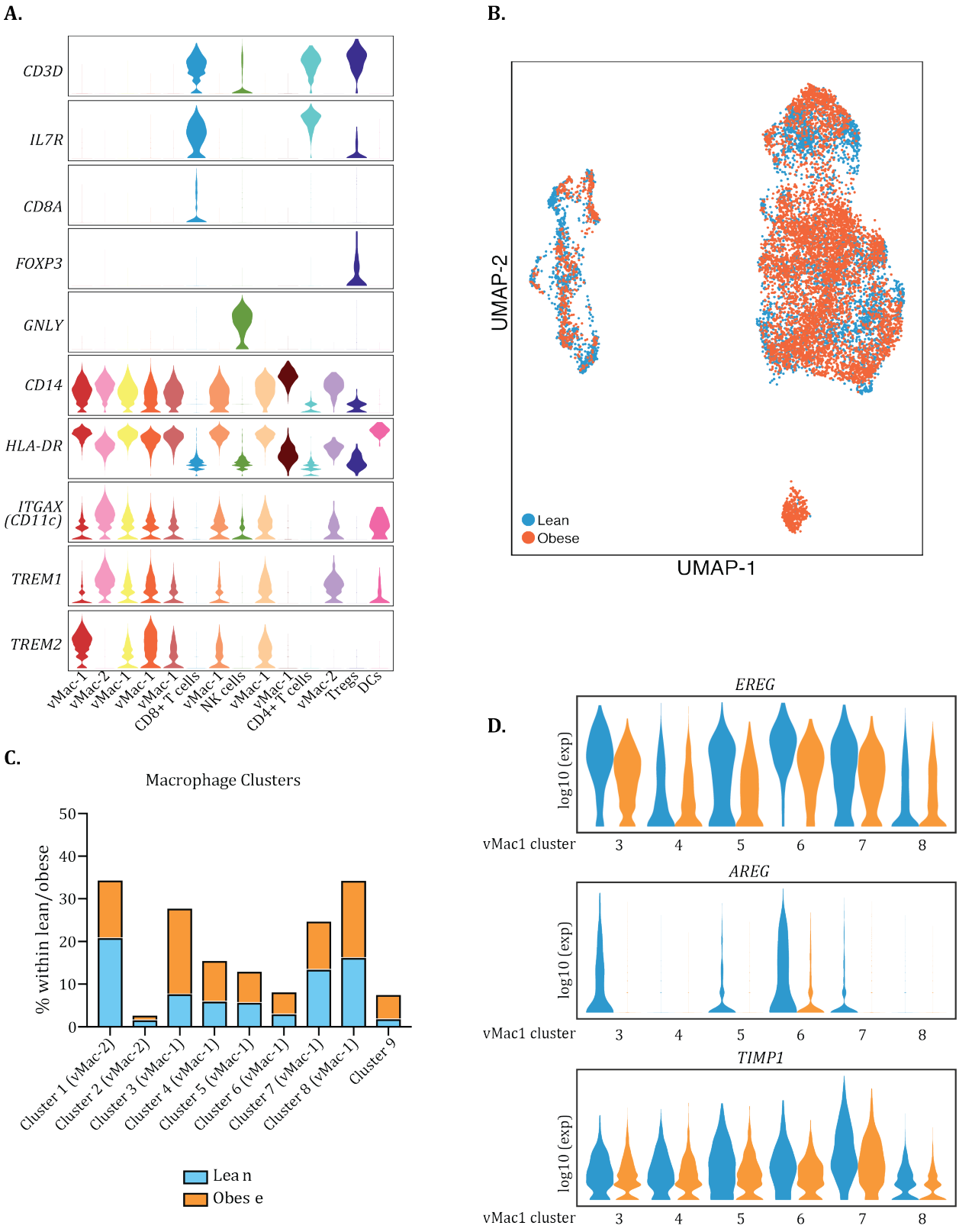
A.
CD3D
IL7R
CD8A
FOXP3
GNLY
CD14
HLA-DR
ITGAX (CD11c)
TREM1
TREM2
vMac-1
vMac-2
vMac-1
vMac-1
vMac-1 CD8+ T cells
vMac-1 NK cells
vMac-1
vMac-1 CD4+ T cells
vMac-2
Tregs
DCs
B.
UMAP-2
UMAP-1
Lean
Obese
C.
Macrophage Clusters
% within lean/obese
50
40
30
20
10
0
Cluster 1 (vMac-2)
Cluster 2 (vMac-2)
Cluster 3 (vMac-1)
Cluster 4 (vMac-1)
Cluster 5 (vMac-1)
Cluster 6 (vMac-1)
Cluster 7 (vMac-1)
Cluster 8 (vMac-1)
Cluster 9
Lean
Obese
D.
EREG
AREG
TIMP1
log10 (exp)
vMac1 cluster
3
4
5
6
7
8

(previous page) **Supplemental Figure 3.9 Villous immune landscape at term.**
(A) Feature plots confirming identity of UMAP clusters of isolated CD45+ villous cells. Y-axis represents log-transformed normalized transcript counts. (B) UMAP projection of villous leukocyte clusters with cells stratified as lean and obese group. (C) Bar graphs comparing varying frequencies of individual macrophage clusters with maternal obesity. (D) Violin plots of select growth factors down-regulated across several vMac-2 clusters with maternal obesity. Y-axis represents normalized log-transformed transcript counts.

CHAPTER 4

Maternal obesity disrupts the inflammatory program of umbilical cord blood monocytes

Suhas Sureshchandra[1, 2], Randall M. Wilson[3], Norma E. Mendoza[1], Maham Rais[3], Allen Jankeel[1], Gouri Ajith[1], Sneha Anand[1], Nicole E. Marshall[4], Jonathan Q. Purnell[5], Kent L. Thornburg[5], Ilhem Messaoudi[1, 2]

[1]Department of Molecular Biology and Biochemistry, University of California- Irvine, Irvine CA, USA
[2]Institute for Immunology, University of California-Irvine, Irvine CA, USA
[3]Division of Biomedical Sciences, University of California-Riverside, Riverside, CA, USA.
[4]Maternal Fetal Medicine, Oregon Health and Science University, Portland OR, USA.
[5]The Knight Cardiovascular Institute, Oregon Health and Science University, Portland OR, USA

Incorporates components from the published article:

Sureshchandra S, Wilson RM, Rais M, Marshall NE, Purnell JQ, Thornburg KL, et al. Maternal Pregravid Obesity Remodels the DNA Methylation Landscape of Cord Blood Monocytes Disrupting Their Inflammatory Program. J Immunol. 2017;199(8):2729-44. doi: 10.4049/jimmunol.1700434. PubMed PMID: 28887432.

ABSTRACT

Pre-pregnancy obesity is associated with adverse outcomes for the offspring, including increased incidence of neonatal bacterial sepsis, necrotizing enterocolitis, and RSV infections. We recently reported that umbilical cord blood (UCB) monocytes from babies born to obese mothers generate a reduced IL6/TNFα response to Toll-like receptors 1/2 and 4 ligands compared to those collected from lean mothers. We, therefore, investigated monocyte responses to pathogen and baseline epigenetic and functional differences in monocytes that could potentially explain this refractory phenotype. We show that UCB monocytes from babies born to obese mothers mount a dampened cytokine response to both TLR agonists and *E. coli* but not RSV. RNA-Seq analysis suggests attenuated inflammatory response to both LPS and *E. coli*. However, with RSV infection, monocytes from obese group exhibit poor transcriptional response to secondary interferon stimulation. Interestingly, DNA methylation status of resting cells was predictive of transcriptional changes post LPS stimulation, particularly of loci regulating monocyte/macrophage development. Furthermore, monocytes from obese group were more phagocytic but less migratory towards a chemokine gradient, confirming their regulatory phenotype. These findings further our understanding of mechanisms that explain the increased risk of infection in neonates born to mothers with high pre-pregnancy BMI.

INTRODUCTION

Almost 37% of women of childbearing age are categorized as obese, making obesity one of the most common co-morbidities during pregnancy (Gaillard et al., 2013). It is well established that a high pre-pregnancy (pregravid) body mass index (BMI) is associated with detrimental health outcomes for both mother and child (Leddy et al., 2008; O'Reilly and Reynolds, 2013; Scott-Pillai et al., 2013). Maternal complications of pregravid obesity include increased rates of preeclampsia, gestational hypertension, gestational diabetes, placental abruption, preterm delivery, and cesarean delivery (Gaillard et al., 2013). For the fetus, complications include increased risk of stillbirth, abnormal growth, and cardiac/neural tube defects (Gaillard et al., 2013; Scott-Pillai et al., 2013). Moreover, neonates born to obese mothers are at increased risk of bacterial sepsis and necrotizing enterocolitis, requiring admission to the neonatal intensive care unit (NICU) (Rastogi et al., 2015; Suk et al., 2016). High maternal BMI has also been shown to increase risk for *B. streptococcus*, *S. aureus*, and *E. coli* infections (Villamor E., 2020). Some adverse health outcomes for the offspring persist into adulthood, including increased susceptibility to respiratory infections such as respiratory syncytial virus (Griffiths et al., 2016; Haberg et al., 2009), asthma (Dumas et al., 2016), wheezing (Guerra et al., 2013), cancer (Eriksson et al., 2014), type-2 diabetes (Morgan et al., 2010), and cardiovascular disease (Gaillard, 2015), culminating in an increased risk for all-cause offspring mortality (Reynolds et al., 2013).

The aforementioned observations strongly suggest that pregravid obesity disrupts the development and maturation of the offspring's immune system *in utero*. This hypothesis is supported by studies in murine models that have shown detrimental effects

on the immune system of pups born to obese compared with lean dams (Myles et al., 2013; Odaka et al., 2010). Specifically, pups born to obese dams generated disparate IgG (smaller) and IgE (larger) antibody responses following vaccination with ovalbumin (Odaka et al., 2010). If these results are true in humans, they could explain the increased incidence of asthma (Dumas et al., 2016) and wheezing (Guerra et al., 2013) in children born to obese mothers. Additional rodent studies reported greater morbidity and mortality following bacterial infection (*Escherichia. coli* sepsis and methicillin resistant *Staphylococcus. aureus* infection) and greater susceptibility to autoimmune encephalitis in pups born to obese dams (Myles et al., 2013). Lastly, *ex-vivo* LPS stimulation of colonic lamina propria lymphocytes resulted in increased secretion of inflammatory cytokines IL6, IL1β and IL17, whereas LPS stimulation of splenocytes resulted in decreased levels of TNFα and IL6 in pups born to obese dams (Myles et al., 2013). Collectively, these data strongly suggest dysregulated immunity in pups born to obese dams where aberrant responses (such as to auto-antigens) are exaggerated while protective anti-microbial responses are reduced. Similarly, a baboon study reported significant changes in the expression of genes involved in antigen presentation, complement and coagulation cascade, leukocyte migration, and B cell receptor signaling, in peripheral blood mononuclear cells (PBMC) collected from infants born to obese compared to lean dams (Farley et al., 2009).

However, only a few studies have explored the impact of maternal pregravid obesity on neonatal immune function in humans. One study reported that children born to obese mothers have a 16-fold higher risk of having detectable levels of C reactive protein (CRP) after adjusting for BMI, Tanner stages, and gender compared to children born to lean mothers, suggesting that high pregravid maternal BMI results in dysregulated

inflammatory responses in the offspring (Leibowitz et al., 2012). More recently, we have demonstrated that pregravid maternal BMI is associated with a reduced number of umbilical cord blood (UCB) CD4+ T-cells, IL-4 secreting CD4+ T-cells, and a diminished ability of monocytes and myeloid dendritic cells to respond to *ex vivo* stimulation with LPS (TLR4 ligand) and HKLM/Pam3CSK4 (TLR1/2 ligands) (Wilson et al., 2015). However, the mechanisms that drive these dysregulated processes are unknown.

Therefore, in this study, we sought to investigate if poor monocyte responses are regulated in a cell intrinsic manner. We stimulated monocytes with LPS, E. coli, and RSV, and measured both cytokine responses using luminex, and transcriptional responses using RNA-Seq. Baseline differences in epigenetic states were measured to verify if cells are poised for poor responses. We carried out a combination of functional and genomics analyses to uncover the impact of pregravid obesity on purified UCB monocytes. Our analyses revealed significant dampening of immune mediator production when stimulated with TLR agonists and *E. coli*. These trends were observed at transcript levels as well. Maternal obesity did not alter interferon secretion following RSV infection, but significantly dampened interferon stimulated gene (ISG) expression. DNA methylation changes with obesity, when correlated with gene expression changes identified hypomethylation of genes driving macrophage M2-like phenotype. Functional assays confirmed this skewing of cells towards a regulatory phenotype. These findings suggest that the maternal obesogenic environment potentially alters monocyte development, reprogramming them towards a regulatory phenotype, perhaps as a mechanism to limit inflammatory exposures to the developing fetus.

MATERIALS AND METHODS

Human Subjects

This research project was approved by the Institutional Ethics Review Boards (IRB) of Oregon Health and Science University, University of California Riverside, and University of California Irvine. All subjects provided signed consent before enrolling in the study. Three cohorts of mothers (Cohorts I, II, III) with uncomplicated, singleton gestation was used. From cohort I, a total 18 umbilical cord blood mononuclear cells (UCBMC) samples collected from mothers at term delivery time point: 8 women with a mean pre-pregnancy BMI of 21.8 ± 1.9 kg/m^2 (lean); and 10 women with a pre-pregnancy BMI of 36.6 ± 4.5 kg/m^2 (obese) (Table 2.1). From cohorts II and III, a total of 50 UCMBC samples were collected from mothers at delivery time point: 27 women from lean group and 23 women from obese group (Table 2.2). Exclusion criteria for both cohorts include active maternal infection, documented fetal anomalies, gestational diabetes, gestational hypertension, chorioamnionitis, significant medical conditions or an abnormal glucose tolerance test.

UCBMC Isolation

Cord Blood was collected at delivery in OHSU and shipped to UCR/UCI. UCBMC were obtained by standard density gradient centrifugation over Ficoll (BD Bioscience, San Jose CA), resuspended in 10% DMSO/FBS, frozen using Mr. Frosty Freezing Containers (Thermo Fisher, Waltham MA), and stored in liquid nitrogen until analysis.

Flow Cytometry

Freshly thawed UCBMC (10^6 cells/sample) (Cohorts II and III) were washed in DPBS and stained using the following cocktail of antibodies to characterize innate immune cells and their subsets: PE-CD3, PE-CD19, PB-CD16, PE-Cy7-CD11c, AF700-CD14, PCP-Cy5.5-CD123,

BV711-CD56, and APC-Cy7-HLA-DR for 30 minutes at 4C. Cell pellets were then washed twice in DPBS and resuspended in cold FACS buffer (PBS with 2% FBS and 1mM EDTA). All samples were acquired with the Attune NxT Flow Cytometer and analyzed using FlowJo 10.5.0.

Intracellular Cytokine Measurements

Freshly thawed UCBMC (10^6 cells/sample) (Cohort II) were stimulated for 16h at 37C in RPMI supplemented with 10% FBS in the presence or absence of 1 ug/mL LPS (TLR4 ligand, *E. coli* 055:B55). Brefeldin A was added after 1 hour incubation to block secreted of proteins. Next morning, cells were stained for AF700-CD14 and PCP-Cy5.5-HLADR, fixed, permeabilized, and stained intracellularly for APC-TNFα and PE-IL-6. Cell pellets were washed thoroughly, resuspended in FACS buffer and analyzed on Attune NxT flow cytometer.

UCB monocyte purification

Frozen UCBMC were thawed and UCB monocytes were purified using CD14 antibodies conjugated to magnetic microbeads per manufacturer's recommendations (Miltenyi Biotech, San Diego CA). Magnetically bound UCB monocytes were washed and eluted for collection. Positive selection of UCB monocytes was chosen to ensure high purity of the population, which was assessed using flow cytometry and was ≥90% for all samples analyzed.

TLR Stimulation

Purified UCB monocytes (Cohort I) were plated at $2x10^5$/well and stimulated with 1ug/mL of LPS (TLR4 ligand, *E. coli* 055:B5; InvivoGen, San Diego CA) or left untreated for 16 hours at 37C and 5% CO2. The above concentration of LPS (1 ug/mL) has been previously

standardized for robust detection of gene expression in primary human monocytes (NE et al., 2014; Suzuki et al., 2000). In a smaller subset of samples, cells were stimulated with additional TLR agonists – Pam3CSK4 (TLR1/2 agonist) at 1ug/mL and FSL-1 (TLR2/6 agonist) at 1ug/mL concentrations. Following 16hr incubation, cells were spun down. Supernatants were collected and stored in -80C for analysis using Luminex.

***E. coli* and RSV infections**:

Approximately $150x10^5$ purified UCB monocytes (Cohort II) were infected with RSV (Human respiratory syncytial virus ATCC® VR-1540) or *E. coli* (Escherichia coli (Migula) Castellani and Chalmers ATCC 11775). RSV was added at a multiplicity of infection (MOI) of 5 and *E.coli* at $6x10^5$ cfu/mL for 16 hours. This MOI and time has been optimized in the lab to show maximal cytokine release without any evidence of cytotoxicity in UCBMC. Cell pellets were frozen in Trizol to generate RNA-Seq libraries. Cell supernatants were frozen to measure the concentrations of chemokines and cytokines using Luminex.

Luminex

Plasma proteins and proteins secreted in supernatants were measured using the human ProcartaPlex multiplex immunoassay (eBioscience/Affymetrix) on the MAGPIX (Luminex, Austin TX), which simultaneously measures the concentration of 45 cytokines (TNFα, TNFβ, IFNγγ, IL-1α, IL-1β, IL-6, IL-13, IL-15, IL-18, IL-22, IL-23, and IL27, IL-1RA, IL4, and IL-10), chemokines (MIP-1α, MIP-1β, MCP-1, IL-8, IP-10, RANTES, and Eotaxin), and growth factors (VEGF, SDF-1α, EGF, PDGF, GMCSF, HGF, and FGF2) (http://www.ebioscience.com/human-cytokine-chemokine-growth-factor-1-45-plex-procartaplex-multiplex-kit.htm). Values below the limit of detection were replaced by half

of the lowest limit. Standard curves were fit on the Xponent software (Luminex Corp) using 5-parameter logistic regression.

Cell Migration Assay

Migratory potential of monocytes to supernatants containing chemokines was measured using CytoSelect 96-well Cell Migration Assay Cell Migration assay (Cell Biolabs, San Diego CA). Briefly, $2x10^5$ adult PBMC were incubated in serum free media in the upper wells of the migration plate, while supernatants collected following LPS stimulation of UCB monocytes were placed in lower wells and incubated at 37C and 5% CO_2 for 5hr. As a reciprocal assay, $2x10^5$ UCB monocytes were incubated in serum free media in the upper wells of the migration plate, while supernatants collected from PMA (phorbol myristate acetate) stimulated peripheral blood mononuclear cells (PBMC) were placed in lower wells and incubated at 37C with 5% CO_2 for 2hr. For both experiments, number of cells that migrated into the lower wells was quantified using CyQuant cell proliferation assay per manufacturer's instructions. Absolute numbers of migrated cells were calculated using a standard curve for CyQuant assay with a linear range of fluorescence limited from 50 to 50,000 cells. Supernatants from LPS stimulated purified adult monocytes (n=2) were used as a positive control, whereas cell free media served as negative control.

Phagocytosis Assay:

To quantify phagocytic ability of UCB monocytes, purified cells were activated with LPS and cultured with *E. coli* particles conjugated with HRP (horseradish peroxidase) in 96-well plates for 3 hours in 37C incubator with 5% CO2. Cells were washed three times, fixed, permeabilized, incubated with substrate and quantified using colorimetry.

RNA-Seq

Total RNA was isolated from cell pellets using mRNeasy kit (Qiagen) and quantified using Agilent 2100 Bioanalyzer. Following rRNA depletion, libraries were generated using NEBNext Ultra RNA library prep kit. Briefly, mRNA was fragmented for 8 min, converted to double stranded cDNA and purified. Size and quality of the library was verified using Qubit and Bioanalyzer. Libraries were multiplexed and sequenced on the HiSeq4000 platform to yield an average 20 million 100bp single end reads.

RNA from stimulated and unstimulated monocyte cell pellets were extracted using Zymo Research Direct-zol RNA mini-prep (Zymo Research, San Diego CA) per manufacturer's instructions. RNA concentration and integrity was determined using Agilent 2100 Bioanalyzer. Following ribosomal RNA depletion using Ribo-Gone rRNA removal kit (Clontech, Mountain View CA), libraries were constructed using SMARTer Stranded RNA-Seq kit (Clontech, Mountain View CA). Briefly, rRNA-depleted RNA was fragmented, converted to ds cDNA and ligated to adapters. The roughly 300 bp long fragments were then amplified by PCR and selected by size exclusion. Each library was prepared with unique index facilitating multiplexing of several samples for sequencing. Following QC for size, quality and concentrations, libraries were multiplexed and sequenced to single-end 100-bp sequencing using the Illumina HiSeq2500 platform.

RNA-Seq analysis

Raw reads assessed for quality using FASTQC (www.bioinformatics.babraham.ac.uk/projects/fastqc) and trimmed using TrimGalore

(www.bioinformatics.babraham.ac.uk/projects/trim_galore/). To conform to Clontech library prep protocol, five bases from leading end and 3 bases at the trailing end were trimmed, with minimum base quality of 30 ensuring reads of a minimum length of 50 bases. Reads were then aligned to the human genome using TopHat2 (https://ccb.jhu.edu/software/tophat/index.shtml). Reads mapping uniquely to exonic regions were counted gene-wise using GenomicRanges package in R. Differentially expressed genes (DEG) were determined using edgeR (https://bioconductor.org/packages/release/bioc/html/edgeR.html) and defined as those with fold-change ≥2 and an FDR corrected p value of ≤0.05. Functional enrichment of DEG and pathway over-representation was performed using DAVID, InnateDB(http://www.innatedb.com/redirect.do?go=batchGo) and Metascape (Zhou et al., 2019). Transcriptional regulation of DEG was performed using cisRed (http://www.cisred.org/). All plots were generated in R using gplots.

Methyl-Seq

DNA cytosine methylation levels in purified resting UCB monocytes was measured at single base resolution using a targeted bisulfite sequencing approach (SureSelectXT Human Methyl-Seq enrichment system, Agilent, Santa Clara CA), focusing on regions where methylation is known to impact gene regulation (cancer tissue-specific differentially methylated regions or DMRs, GENCODE promoters, CpG islands, shores and shelves ±4kb, DNase I hypersensitive sites and RefGenes). Restricting methylation measurements to a relevant portion of the genome increases the statistical power for detecting subtle alterations in gene regulatory regions**.** Briefly, 200 ng genomic DNA was isolated from resting 2-5x10^5 CD14+ monocytes using *Quick-gDNA* MiniPrep (Zymo Research, Irvine CA),

sheared to 100-200 bp using Covaris Ultrasonicator (Covaris, Woburn MA) and verified using Agilent 2100 Bioanalyzer. The ends of sheared DNA were repaired, 3' adenylated, and ligated with methylated adapters. These DNA fragments were then hybridized with 120 nt biotinylated RNA library fragments that recognize methylated DNA regions and isolated using streptavidin beads followed by bisulfite conversion using Zymo EZ DNA Methylation-Gold Kit (Zymo, Irvine CA), which converts unmethylated cytosines to uracils. Libraries were then PCR amplified, ligated with unique indices, and sequenced on Illumina NextSeq500 platform to generate 60 million 50 bp paired-end reads per sample. Efficiency of bisulfite conversion was measured using 20 pg of unmethylated phage lambda DNA spiked in with each sample before DNA fragmentation. The bisulfite non-conversion rate was calculated as the percentage of cytosines sequenced at cytosine reference positions in lambda genome. Only subsets of samples were included in this experiment (lean n=6, obese n=3), and among them 3 lean and 3 obese samples were included in the stimulation studies allowing us to carry out a pair wise correlation analysis between gene expression and DNA methylation patterns.

Methyl-Seq analysis

Raw reads were assessed for quality and trimmed to ensure bases with quality scores less than 30 and reads shorter than 50 bases were eliminated. QC passed reads were aligned to the human genome hg19 using Bismark (http://www.bioinformatics.babraham.ac.uk/projects/bismark/). To measure bisulfite conversion rates, reads were mapped to phage lambda genome that was spiked into each library. PCR duplicates in the alignment files were filtered using picard tools (https://broadinstitute.github.io/picard/) and file conversions were performed using

samtools (http://samtools.sourceforge.net/). Single base resolution methylation calls were made using the R package methylKit (https://github.com/al2na/methylKit). Differences in methylation between lean and obese groups was measured using a logistic regression model built in methylKit, allowing us to identify differentially methylated cytosines (DMCs) with at least 25% difference in methylation levels and an FDR corrected p-value of at least 0.05. DMCs overlapping chromosomes X, Y and mitochondrial genome were eliminated from subsequent analyses. We performed optimized region analysis of methylation using eDMR (https://github.com/ShengLi/edmr), which uses a bimodal distribution to identify accurate boundaries of regions/loci harboring significant epigenetic changes without *a priori* assignment of DMR length. DMC and DMR locations were annotated using HOMER (http://homer.salk.edu). DMRs overlapping genic and intergenic regions were enriched using InnateDB, DAVID, and GREAT (http://bejerano.stanford.edu/great/public/html/).

Correlation between DNA methylation and gene expression

For context-specific association between DNA methylation changes and gene expression, we first compared DMR annotations with gene expression changes between stimulated cells from both groups after correcting basal transcription levels in resting cells. For each DMR, the methylation difference scores were considered. For the expression of genes associated with the genomic context, the fold change in obese group relative to leans following stimulation was considered after correcting the transcriptional levels in corresponding unstimulated cells. Only DEG with FDR ≤ 10% were considered.

We then used a second approach for genome-wide correlations between methylation and gene expression. Using an extension of the established statistical framework, sample specific correlations were evaluated (Smallwood et al., 2014). Briefly, for each gene,

association regions were extended 5KB upstream of transcription start site (TSS) and 5KB downstream of transcription termination site (TTS) with the RPKM of the gene assigned as the expression value for the sample (Supplement Figure 4). For methylation scores, we considered only cytosines with measured values across all samples. Median beta levels within each region for a sample were assigned as the methylation level for the particular sample. Beta values were measured taking into consideration differing coverage at different genomic locations allowing us to perform a weighted correlation analysis. Next, for each gene, sample wise weighted correlation between beta values and RPKM was performed using rcorr function from Hmisc package (http://biostat.mc.vanderbilt.edu/wiki/Main/Hmisc) in R, and corrected for multiple hypothesis testing generating false discovery rates for each association.

Statistics

Principal component analysis of cytokine, chemokine, and growth factors was performed using prcomp function and visualized using ggbiplot package in R. Differences between protein levels between the two groups before and after stimulation were statistically assessed using two-way ANOVA and corrected for multiple comparisons using Sidak's multiple comparison test. Differences in protein levels following stimulation after corrections for resting levels was statistically assessed using unpaired t-test (GraphPad, San Diego, CA).

RESULTS

UCB monocytes from babies born to obese mothers respond poorly to LPS.

Our previous studies in Cohort I (Table 2.1) showed a reduced ability of monocytes from babies born to obese mothers to respond to LPS (TLR4 agonist) as well as HKLM/Pam3CSK (TLR1/2 ligands) (Wilson et al., 2015). However, these experiments were carried out using total umbilical cord blood mononuclear cells (UCBMC) and only measured intracellular levels of TNFα and IL-6. To specifically assess the impact of pregravid (pre-pregnancy) BMI on the functional ability of UCB monocytes to respond to the TLR4 ligand LPS, CD14+ monocytes were purified from UCBMC collected from babies born to lean (lean group) and obese (obese group) mothers, then cultured overnight in the presence or absence of LPS (Figure 4.1A). Production of cytokines, chemokines and growth factors was determined in supernatants using Luminex. Principal component analysis (PCA) clearly indicates that while unstimulated and stimulated UCB monocytes isolated from the lean group formed distinct immune mediator production profiles, those from the obese group had overlapping profiles indicative of the lack of response to LPS (Figure 4.1B).

In particular, we observed dampened responses across several mediators secreted following LPS stimulation including pro-inflammatory mediators IL-1α and IL-1β (Figure 4.1C), regulatory cytokines IL-1RA and IL-10 (Figure 4.1D), and chemokines CXCL1, CCL4, CCL5, and CXCL10 (Figure 4.1E). These differences in the levels of secreted immune mediators was observed in the absence of any variations in the frequencies of either total or CD16+ UCB monocytes from the lean or obese group (Wilson et al., 2015). Moreover, expression of cell surface receptors CD14, CD16, and TLR4 was comparable between lean and obese groups (Supplemental Figure 4.1A). However, defects in response to stimulation

extended to other TLRs such as TLR1/2 and TLR2/6 stimulation, potentially suggesting that the cells are refractory to external pathogen sensing (Figure 4.1F).

In order to determine whether the reduced production of soluble mediators by UCB monocytes from the obese group was functionally relevant, we measured the ability of adult peripheral blood mononuclear cells (PBMC) to migrate in response to the supernatant collected from LPS stimulated UCB monocytes from lean and obese groups. In line with the reduced concentration of several chemokines, we detected a significant reduction in the ability of adult PBMC to migrate in response to the LPS-supernatant from the obese group compared to the lean group (Supplemental Figure 4.1B).

UCB monocytes from lean and obese groups are transcriptionally distinct following LPS stimulation.

We next investigated if the dampened response of neonatal monocytes from the obese group stems from reduced transcriptional activation following LPS stimulation using RNA-Seq (Figure 4.1A). Interestingly, no differentially expressed genes (DEG) were identified at baseline. However, despite comparable surface and gene expression of TLR4 (Supplemental Figures 4.1B and 4.1C), large gene expression changes in response to LPS were only observed in the lean (Figure 4.2A) but not the obese group (Figure 4.2B). More specifically, while 825 upregulated and 890 downregulated genes were identified in UCB monocytes from lean group following LPS stimulation (FDR ≤ 5%, |Fold Change| ≥ 2) (Figure 4.2A), monocytes from the obese group show very limited gene expression changes following stimulation (93 up- and 3 downregulated) (Figure 4.2B). This attenuated response in obese group included several genes regulated by all classes of transcription factors that mount an inflammatory response to TLR activation (Figure 4.2C)

Only 48 genes were up regulated in both lean and obese groups in response to LPS, with 777 and 45 genes up regulated exclusively in the lean and obese groups respectively (Supplemental Figure 4.1D). The 48 shared DEG enriched to pathways associated with LPS response (Figure 4.2D) and comprised genes important for the inflammatory response including cytokines and chemokines (*IL1B*, *IL6*, *IL2RA, IL10*, and *CXCL1*), regulators of T-cell activation (*CD80*, *CD274*, and *SLAMF1*), and cell adhesion (*MUCL1*, *LIMK2*, and *ITGB8*) (Figure 4.2D and Supplemental Figure 4.1E). However, the magnitudes of fold change of these shared up-regulated genes was lower in the obese group compared to the lean group (Supplemental Figure 4.1E). These observations suggest an overall suppression of the LPS-induced transcriptional program in UCB monocytes from the obese group.

UCB monocytes from the obese group fail to transcriptionally activate and suppress key regulatory processes involved in cellular response to LPS

Functional enrichment of the 777 genes up-regulated exclusively in UCB monocytes from the lean group following LPS stimulation revealed significant over representation of inflammatory innate immune processes, such as "JUN kinase activity" and "MyD88-dependent TLR signaling pathway" (Figure 4.2E). Some of the notable DEG within these processes include genes involved in toll-like receptor engagement (*TLR1*, *TLR2*, *TLR8*, *PTX3*, *TNIP1*, and *ACOD1*), pro-inflammatory responses (*TNF*, *IL1A*, *IL15*, *TNFAIP*, and *IRGM*), cell migration (*CCR7*, *CCL20*, *CCL19*, *CXCL3*, and *CXCL8*), and pathogen pattern recognition (*FPR2*, *NOD1*, *TLRs 1*, *2*, and *8*) (Figure 4.2F).

Some of the 45 genes up regulated exclusively in UCB monocytes from the obese group played a role in signaling (*CACNA1F*, *MECOM*, *PPP2R2C*, and *CSF2*) and metabolism (*EPHX2*, *NUBP2*, and *CHRM3*) (Table 4.1). A large number of genes were down regulated

exclusively in UCB monocytes from the lean group. These DEG enriched to regulatory processes such as mRNA catabolic processes (e.g. L ribosomal proteins), translation initiation, and termination (Supplemental Figure 4.1F). We also observed down-regulation of genes involved in antigen presentation (*HLADMA*, *HLADPA1*, *HLADPB1*, *HLADQA1*, *HLADQB1*, and *HLADRA*), T-cell co-stimulation (*CD4*, *CD86*, *PAK1*, *SPN*, *ICOSLG*, and *MAP3K14*) (innate immune response, and response to wounding (Figure 4.2G).

Maternal obesity is associated with global hypomethylation in UCB monocytes.

Given previous reports of maternal obesity-associated DNA methylation changes in select loci in offspring PBMC, and its role in predicting cellular responses to biological stimuli like LPS (Lam et al., 2012), we investigated pregravid obesity-induced changes in methylome of UCB monocytes (Figure 4.1A). We measured global changes in methylation levels of 2,278,000 – 3,392,222 cytosines at single nucleotide resolution, using a targeted approach. After filtering methylation changes that weren't measured across all samples and those located on X and Y-chromosomes, a total of 1,769,148 differentially methylated cytosines (DMCs) were included in our analysis. Overall, maternal obesity was associated with more hypomethylation (8,887 cytosines, $\Delta\beta \geq 25\%$, $q \leq 0.05$) than hypermethylation (4,838 cytosines, $\Delta\beta \leq 25\%$, $q \leq 0.05$) in UCB monocytes (Figure 4.3A). Methylation changes were more pronounced in 5' regulatory and promoter regions (Figure 4.3B).

Functional enrichment of genes differentially methylated in 5' regulatory and promoter regions using DAVID revealed over-representation of gene ontology (GO) terms such as immune response (*HLAG*, *CCR3*, *CCR6*, *CCR9*, *NCR2*, *ITK*, and *LSP1*) and inflammatory response (*NFKB1*, *NFKBIZ*, *NLRC4*, *S100A12*, *IL37*, *IL23A*, *IL36G*, *CLEC7A*, *CXCR6*, and *CXCL10*) (Figure 4.3C). Moreover, differential methylation of cytosines within

CpG islands was associated with genes involved in regulating IL4 synthesis (*ICOSLG*, *IRF4*, and *ZFPM1*), myeloid cell differentiation (*CBFA2T3*, *FAM20C*, *NFATC1*, and *ZFPM1*), and transcriptional repression (*HDAC4*, *NCOR2, PRDM16*, *CTBP2*, and *ZFPM1*) as determined using GREAT (Figure 4.3D).

Maternal obesity induces DNA methylation changes in key inflammatory genes in UCB monocytes

Having established the general pattern of methylation changes in promoter regions, we next asked if resolution of these DMCs into differentially methylated regions (DMRs) would allow us to identify changes in specific genes with higher confidence and biological relevance. Without *a priori* assignment of region lengths, eDMR (https://github.com/ShengLi/edmr) identified 1506 DMRs with 1020 DMRs containing at least 2 DMCs: 375 hypermethylated ($\Delta\beta \geq 20\%$, $q \leq 0.05$) and 645 hypomethylated ($\Delta\beta \leq 20\%$, $q \leq 0.05$) DMRs (Figure 4.3E). Importantly, our analysis revealed hypomethylation in promoters and 5' regulatory regions of genes involved in metabolism (*CAMK1*, *PPARG*, *PAQR8*, *FOLR2*, *LDLRAD4*, *ENO1*, and *ICA1*) (Figure 4.3F). Additionally, some DMRs overlapped genes important in cell migration and adhesion in myeloid cells (*FGR*, *ITGAX*, *CDH5*, and *LAMB3*), and defense response (*DOK3*, *TRIM40*, *TREM1*, *CD59*, *IRF5*, and *DEFB1*) (Figure 4.3F). We observed very limited hypermethylation overlapping metabolic genes (*RHOH*, *MGAT4A)*, but large hypermethylated changes occurring at 3' and promoter regions of immune genes (*CD101*, *ETV3*, *S100B*, *HLAE*, *HLAC*, *ITK*, *RHOH*, *ZFP36L1*, and *TNFRSF25*), and stress response genes (*TXNIP* and *DDIT4*) (Figure 4.3F).

Intergenic DNA methylation changes overlap cis elements regulating defense response and immune development

Since a large number of DMRs overlapped intergenic regions (Supplement Figure 3D), we asked if these changes overlap cis regulatory regions with possible associations with coding regions. We addressed this question using GREAT, with a proximal regulatory assignment of 5 kb upstream and 1 kb downstream of transcriptional start sites (TSS), and a distal regulatory assignment of 100 kb on either side of TSS. This analysis revealed significant methylation changes in intergenic regions regulating defense response (*HLA-DRA*, *HLA-DRB5*, *IFNAR1*, *IFNGR2*, *IRF2, CD180,* and *CXCL1*), hematopoietic development (*KLF4*, *CD28*, *CEBPA*, *VEGFA*, and *EPHA2*) and apoptosis (*BCL6*, *KDM2B*, *PSMA6*, *FLT4*, *DAD1*, and *ERCC3*) (Figure 4.3G).

High pregravid maternal BMI-associated DNA methylation patterns correlate with altered gene expression in UCB monocytes

Next, we integrated the expression and methylation datasets to identify correlations between maternal pregravid obesity-induced DNA methylation changes in resting UCB monocytes and corresponding gene expression changes following LPS stimulation. We used a robust and sensitive method to measure sample-wise association between DNA methylation levels and gene expression levels, allowing us to measure association before and after stimulation separately (Supplemental Figure 4.2). This approach not only accounts for contributions of intergenic DNA methylation changes, but also captures heterogeneity in methylation and expression changes among individual samples before and after LPS stimulation. This approach revealed no statistically significant associations in unstimulated cells, but 54 positive and negative associations were detected in post LPS

stimulation expression profiles (Figure 4.4A). This finding suggests that maternal obesity associated DNA methylation changes are more predictive of gene expression changes following *ex vivo* stimulation, as previously reported in adult PBMC (Lam et al., 2012) (Figure 7A).

Significant associations between gene expression and DNA methylation were detected in several genes that regulate monocyte activation and response to LPS (Figure 4.4B and Table 4.1). This list includes positive associations of obesity associated changes with expression of several M1 macrophage (*TREM1* and *IRF5*) and M2 macrophage associated molecules (*PPARG*). The most striking example of a robust association was the correlation between expression and methylation of *PPARG* (Figure 4.4C), a critical metabolically sensitive TF that regulates LPS inducible gene expression. In particular, PPARG promotes monocyte/macrophage differentiation and regulates uptake of oxidized LDL (Nagy et al., 1998; Tontonoz et al., 1998). Negative associations were also significant for *NFATC1*, a transcription factor that mediates cell differentiation events in response to TNF (Yarilina et al., 2011) and *IL1R1*. These observations suggest that DNA methylation changes observed with maternal obesity in UCB monocytes potentially regulate their phenotype following differentiation.

Maternal obesity alters the effector function of cord blood monocytes.

We next asked if maternal obesity alters the function of cord blood monocytes. We leveraged a new cohort of UCBMC (cohorts II and III) (Table 2.2) and tested functional attributes of UCB monocytes (Figure 4.5A). As described for cohort I (Wilson et al., 2015), we confirmed hypo-responsiveness in UCB monocytes in these new cohorts, with fewer IL6+TNF+ monocytes in the obese group following LPS stimulation (Figure 4.5B).

Furthermore, as described before (Wilson et al., 2015) we report no differences in plasma CRP (Supplemental Figure 4.3A) or insulin levels (Supplemental Figure 4.3B) with maternal obesity. Interestingly, circulating leptin levels in the obese group was significantly higher relative to the leans (Supplemental Figure 4.3C). More importantly, with obesity we observed significantly higher numbers of non-classical monocytes (Supplemental Figure 4.3D) and lower levels of plasmacytoid dendritic cells (pDCs) (Supplemental Figure 4.3E). These observations are unique findings of this cohort reflecting both statistical strength of a larger sample size and heterogeneity in human subject studies.

Given these significant differences in cytokine responses to TLR agonists, we asked if pregravid obesity rewired effector function of cord blood monocytes (Figure 4.5A). Using a transwell assay, we first tested the ability of purified monocytes to migrate towards a chemokine gradient generated by stimulated PBMC (n=10/group). Our analyses revealed that fewer cells from the obese group migrated towards the gradient (Figure 4.5C). However, ex vivo phagocytosis assay using *E. coli* conjugated to HRP revealed enhanced engulfment of bacteria in the obese group (n=13/group) (Figure 4.5D). Taken together, these findings suggest that in addition to poor responses to TLR agonists, cord blood monocytes of babies born to obese mothers exhibit functional differences relative to their lean counterparts.

Cord blood monocytes from babies born to obese mothers exhibit dampened cytokine responses to *E. coli*

Given the poor cytokine responses to bacteria derived products in UCB monocytes from the lean group, we next infected purified UCB monocytes from either group

(n=4/group) with E. coli for 16 hours. Protein analysis of the supernatants suggest strong pro-inflammatory responses (TNFα, IL-12) in both groups, but a more attenuated signal in the obese group (Figures 4.6A and 4.6B). Furthermore, we report dampened secretion of regulatory IL-10 (Figure 4.6C) and chemokine CCL4/MIP-1β (Figure 4.6D) in response to *E. coli* in the obese group. We extracted RNA from cell pellets in this experiment, and compared the transcriptional program to infection using RNA sequencing. Bioinformatics analysis identified only a small percentage of common DEG (13-upregulated; 71 down-regulated) compared to 220 DEG (84-upregulated; 136 downregulated) unique in lean group and 494 DEG (173 up regulated; 321 down regulated) unique in the obese group. Two-way functional enrichment of DEG using Metascape identified unique and common gene ontology terms, identifying relative contributions of genes from either group towards enrichment (Figure 4.6E). Interestingly, only the pathogen responsive genes from lean group enriched to terms associated with cytokine responses (Regulation of TNF, cytokine production), immune activation, and cell migration. Comparison of normalized transcript levels (TPM) before and after infection corroborates these observations, with dampened expression of key cytokine genes (*IL1B*, *IL10*, *CXCL8*) (Figure 4.6F). Interestingly, several genes involved in chromatin remodeling (*CITED2*, *JARID2*, *DNMT1*) were exclusively down regulated in the lean group, suggesting potentially dampened induction of epigenetic modification required for anti-microbial responses (Figure 4.6G).

Maternal obesity does not alter interferon responses to RSV but disrupts its interferon stimulated gene expression program

In addition to susceptibility to bacterial infections and sepsis, babies born to mothers with obesity are also at high risks for severe outcomes following respiratory

syncytial virus (RSV) infections. We therefore infected purified UCB monocytes from lean and obese group (n=4/group) with RSV and measured cytokine responses using Luminex (Figure 4.5A). Surprisingly, maternal BMI is not a significant determinant of RSV induced IFNβ release from cord blood monocytes. (Figure 4.7A). In addition to IFNβ, we report comparable levels of growth factor VEGF (Figure 4.7B) between the two groups following RSV infection.

Interestingly, analysis of RNA-Seq data suggests unique sets of genes differentially expressed in lean group (Figure 4.7C), enriching to GO terms such as "defense response to virus", "cytokine mediated signaling pathway", "leukocyte activation" (Figure 4.7D). Importantly, genes mapping to the term "response to type-I interferon" were more significantly enriched in the lean group (Figure 4.7D), which included several interferon-stimulated genes (ISGs) such as *IRF1*, *IFITM1*, *IFITM2*, *OASL*, *IFIT3*, *TRIM4*, *TRIM6*, and *IFNK* (Figure 4.7E). Collectively, these observations suggest that while the RSV induced secretion of type-I interferons in UCB monocytes is not impacted with maternal obesity, the cells themselves respond poorly to secondary interferon stimulation.

DISCUSSION

In utero exposure to environmental factors can influence cellular developmental processes and long-term health outcomes in the offspring (Barker, 1995). Of particular importance, maternal nutrition serves as a critical early environmental signal that can perturb the gestational milieu to influence metabolic plasticity during fetal development (Gluckman et al., 2007; Godfrey et al., 2007). This phenomenon has been demonstrated in animal models of nutritional constraint (Burdge et al., 2007; Gluckman et al., 2007; Lillycrop et al., 2007), intrauterine growth restriction (Fu et al., 2006; Fu et al., 2004; MacLennan et al., 2004), and epidemiological studies (Eriksson, 2001; Klebanoff et al., 1989). Findings from these studies demonstrate that reprogramming of gene expression and rewiring of epigenetic circuitry mediate early alteration of offspring cellular and developmental function. However, although pregravid obesity is widespread and has been linked to several adverse outcomes for both mother and child, the mechanisms remain under-studied. Therefore, in this study, we investigated how the maternal obese environment reprograms the neonatal immune system.

Initial studies from our laboratory demonstrated that UCB monocytes collected form babies born to obese mothers fail to respond vigorously to TLR1/2 and TLR4 ligands (Wilson et al., 2015). TLRs play a critical role in the recognition of pathogens that are relevant to neonates, including ones recognized by TLR2 (group B *Streptococcus* (Henneke and Berner, 2006), *Listeria monocytogenes*, *Mycoplasma hominis*, (Peltier et al., 2005) *C. albicans* hyphae, and cytomegalovirus (van der Graaf et al., 2005)) and TLR4 (*Enterobacteriaceae, C. albicans* blastoconidia) (van der Graaf et al., 2005), and respiratory

syncytial virus (Kurt-Jones et al., 2000)). Dysregulated TLR signaling has been attributed to development of several early diseases in neonates such as necrotizing enterocolitis (Jilling et al., 2006). Given that babies born to obese mothers are at increased risk of neonatal infections such as necrotizing enterocolitis, bacterial sepsis (Blomberg, 2013; Rastogi et al., 2015; Suk et al., 2016; Villamor E., 2020), we investigated the impact of pregravid obesity on functional, transcriptional and epigenetic profiles of UCB monocytes in response to LPS stimulation.

In agreement with our previous study (Wilson et al., 2015), we report dampened UCB monocyte cytokine and chemokine responses in the obese group following LPS. Furthermore, our data agree with a previous study that documented reduced IL6 and TNFα production in response to LPS by splenocytes isolated from pups born to obese dams fed a high fat WD during gestation (Myles et al., 2013). Interestingly, we observed reduced IL4 levels in resting cells from obese group. IL4 suppresses LPS-induced production of IL-12 and IL-10 in human peripheral blood monocytes (Bonder et al., 1999) and inhibits adipogenesis by down-regulating expression of *PPARG* and *CEBPA* in adipocytes (Tsao et al., 2014). All four of these genes were downregulated in UCB monocytes from the obese group relative to the lean group. Transcriptional analysis using RNA-Seq confirmed the failure of UCB monocytes from the obese group to fully activate LPS-inducible inflammatory gene expression program. Even genes activated by LPS stimulation in both groups showed relatively lower magnitudes of up-regulation in the obese group compared to the lean group. These transcriptional differences were seen despite comparable levels of CD14 and TLR4 expression as well as frequencies of non-classical monocytes (CD14+CD16+) in unstimulated UCB monocytes.

Interestingly, monocytes responded poorly to other TLR agonists as well (TLR1/2, TLR2/6), suggesting that these defects are not TLR4 specific. We infected cells with bacteria and virus to test if pathogen responses are impacted. Following infection with *E. coli*, we observed dampened secretion of proinflammatory cytokines TNFα and IL-12, regulatory IL-10, and chemokine CCL4/MIP-1β in obese group. The overrepresentation of GO terms associated with cytokine responses, immune activation, and cell migration in lean group monocytes is consistent with the dampened expression of key cytokine genes in monocytes from obese group. These differences in cytokine gene expression correlate with the observed suppression of TLR signaling. Surprisingly, maternal BMI is not a significant determinant of RSV induced IFNβ release from cord blood monocytes. RSV is sensed via TLR4 and TLR8 signaling pathways, and therefore this observation suggests the likelihood of TLR8 signaling compensating for potential TLR4 signaling defects. RNA-Seq data, however, suggests poor induction of interferon-stimulated genes (ISGs), which are induced by interferon stimulation. We therefore conclude that while primary interferon secretion is unaffected, there exist defects in ISG expression necessary for effector response to combat the virus. Evidence of downregulated genes associated with histone modification in the lean group alone hints at the possible role of epigenetic mechanisms in regulating this defect. These findings are consistent with animal models, where pups born to dams on HFD are more likely to sustain severe respiratory infections such as RSV (Griffiths et al., 2016).

Several mechanisms have been shown to alter inflammatory gene expression program. Previous studies have shown that maternal pregravid obesity-associated high concentrations of glucose, insulin, and fatty acids, as well as hormones (e.g. insulin and leptin), and inflammatory mediators (e.g. IL-6 and TNFα) cross the placenta and influence

neuroendocrine and brain development (Rivera et al., 2015). These changes are mediated, in part, by epigenetic mechanisms, including DNA methylation, that affect pathways including lipid peroxidation and corticosteroid-receptor expression (Kang et al., 2014). Similarly, previous clinical studies have demonstrated that maternal BMI is associated with hypomethylation of offspring's peripheral blood cells at genes involved in inflammatory and metabolic pathways that can persist for years (Herbstman et al., 2013; Liu et al., 2014). However, no studies to date have investigated the relationship between pregravid maternal obesity-induced methylation changes and immune function in the offspring. Moreover, DNA methylation is highly cell specific, and measurements made in heterogeneous populations of cells such as PBMC do not necessarily allow us to infer contributions of cell subsets. Therefore, we interrogated methylation changes at a single cytosine resolution in UCB monocytes and its association with LPS-induced gene expression changes.

As previously shown in total blood leukocytes (Herbstman et al., 2013; Liu et al., 2014), our analysis revealed global hypomethylation in UCB monocytes from babies born to mothers with obesity relative to their lean counterparts. Profiling these changes in intergenic and gene regulatory regions revealed significant over-representation of critical innate immune genes with potential functional relevance to both the metabolic status of neonatal monocytes and its ability to participate in host defense and inflammation. Additional analysis of intergenic regions and regulatory regions showed statistically significant methylation changes in genomic regions critical for monocyte ability to respond to LPS (AP1, CEPBP) and differentiation (PU.1). These transcription factors dictate both early and late transcriptional responses to LPS and mediate cytokine responses and cell differentiation events in monocytes, suggesting that maternal obesity associated changes in

DNA methylation levels in UCB monocytes predispose the cells to respond differently following secondary stimulation such as with LPS.

Recent studies in human immune cells have shown that although DNA methylation is stable, when cells are presented with acute biological stimulus like LPS (Furukawa et al., 2016), it is predictive of that response to stimulus (Lam et al., 2012). We therefore used this rationale to determine if maternal obesity associated methylation changes in resting UCB monocytes was predictive of its transcriptional response to an *ex vivo* stimulation. As recently described for adult PBMC (Lam et al., 2012), sample-wise association between transcriptional and methylation levels, suggest that methylation levels of genes in resting cells are more predictive of gene expression patterns following LPS stimulation than in resting UCB monocytes. The association between methylation and post-LPS gene expression profiles also suggests differences in polarization potential of UCB monocytes. Particularly, transcription factors such as *PPARG* (Nagy et al., 1998; Tontonoz et al., 1998), *IRF5*(Krausgruber et al., 2011), and *FOXP1*(Shi et al., 2008) have established critical roles in regulating the differentiation of monocytes into pro-inflammatory (M1) or regulatory (M2) macrophages. Indeed, transcriptional analysis of resting UCB monocytes indicate higher levels of M1 genes in lean and M2 genes in obese groups suggesting that UCB monocytes from the obese group may be poised towards a regulatory phenotype. Furthermore, a recent study revealed that cord monocyte derived macrophages from mothers with obesity show a basal anti-inflammatory state and shown unbalanced response to M1 and M2 skewing conditions (Cifuentes-Zuniga et al., 2017). In our study, this poised M2-like phenotype was supported by functional assays, where fewer cells from obese group migrated towards a chemokine gradient, relative to the lean group. Poor ability to migrate

to a chemokine gradient suggests the lack of inflammatory sensing necessary for circulating monocytes to eventually migrate to tissue to fight infections. Furthermore, monocytes from obese group were more phagocytic, a functional attribute associated with regulatory cells.

The small number of associations detected suggests that in the context of maternal obesity, DNA methylation is not the sole regulatory mechanism for gene expression. Alternative regulatory mechanisms include histone posttranslational modifications that could result in active chromatin remodeling. Indeed, maternal high-fat diet induced epigenetic changes in inhibitory histone marks in offspring monocytes such as H3K9 trimethylation have been reported in rodent models (Strakovsky et al., 2011; Yang et al., 2012). While lack of extracellular sensing of pathogens/TLR agonists is highly unlikely, dysregulated signaling cannot be ruled out. These include either signaling pathways downstream of TLRs or nuclear translocation of transcription factors essential to mount inflammatory responses. Future studies should address the role of cellular, metabolic, and chromatin associated epigenetic mechanisms that could contribute to this immune defect.

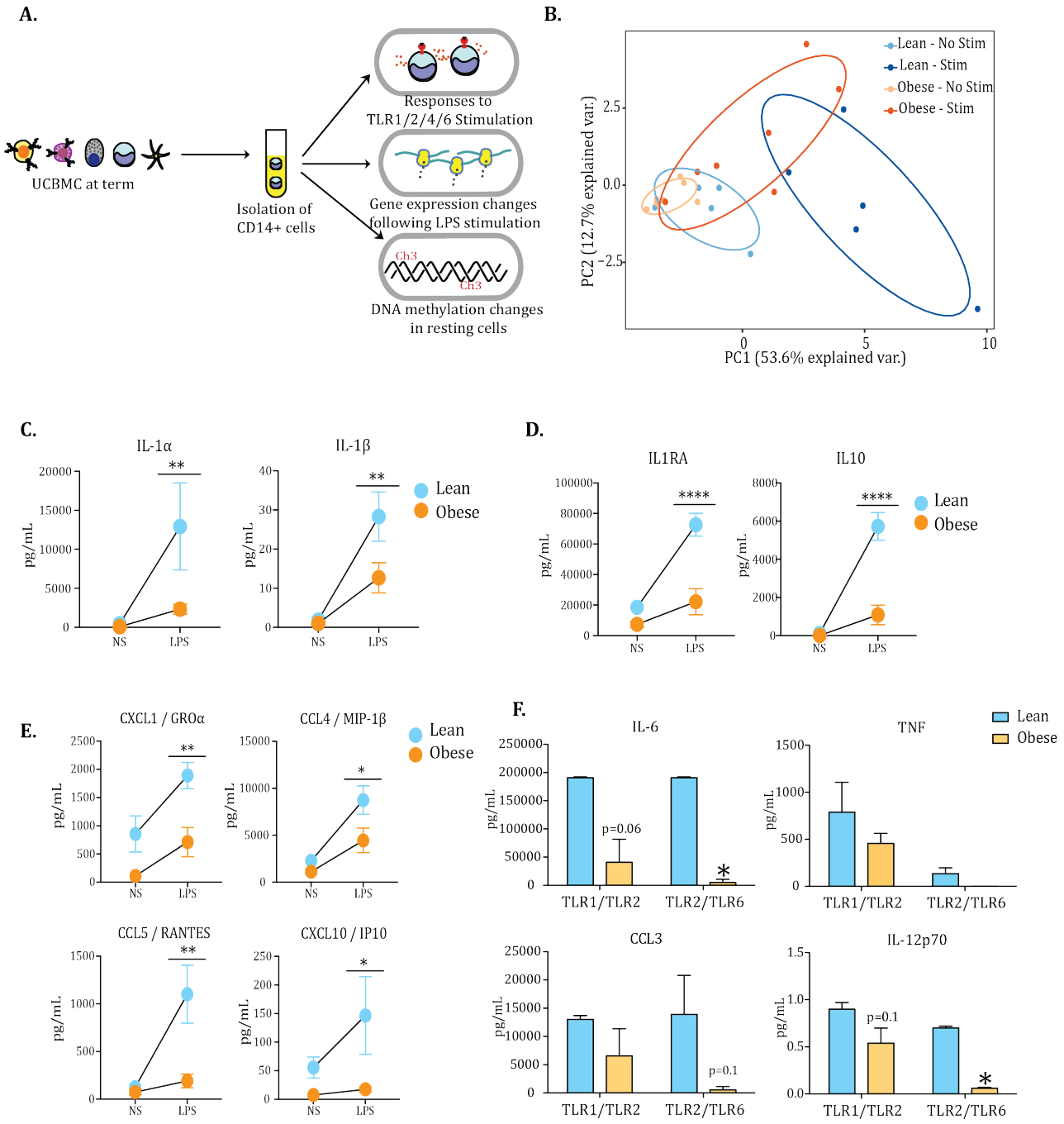

Figure 4.1 UCB monocytes from babies born to obese mothers generate dampened responses following ex vivo LPS stimulation.

(A) Experimental design interrogating the influence of maternal pregravid obesity on transcriptional, epigenetic, and functional responses of cord blood monocytes (B) Principal Component Analysis of immune mediators released by monocytes from lean and obese

groups in the presence and absence of LPS as measured by luminex (C) Secreted levels of proinflammatory mediators, (D) regulatory cytokines, and (E) chemokines following LPS stimulation. Secreted TNFα and IL-12 levels following LPS and IFNγ stimulation on day 7 using luminex. (F) Corrected levels of select secreted cytokines and chemokines following TLR1/2 and TLR2/6 stimulation. Secreted IL-10 levels following IL-4 stimulation on day 7. P-values: * - $p<0.05$; ** - $p<0.01$; **** - $p<0.0001$.

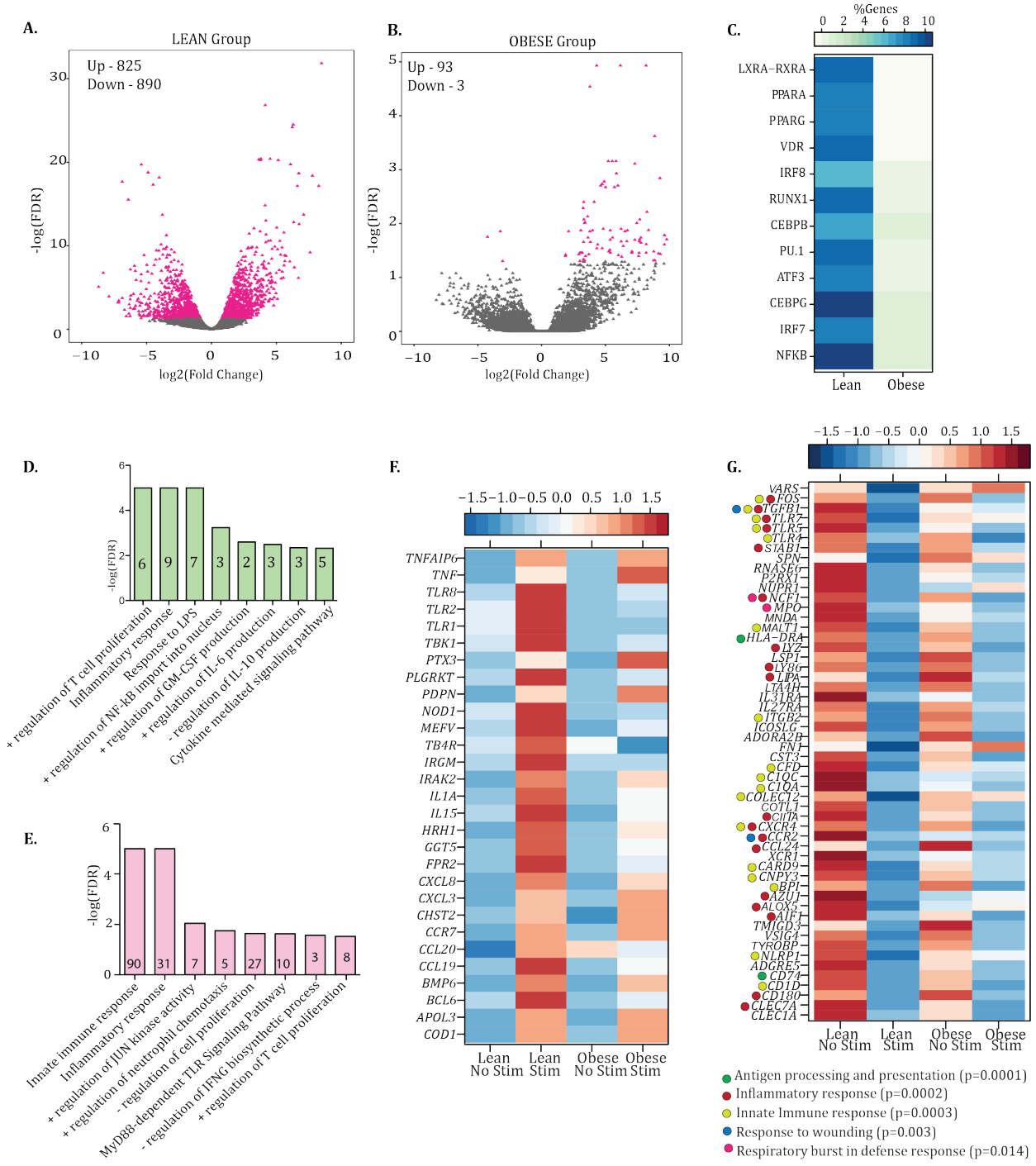

Figure 4.2 Blunted transcriptional responses to LPS in UCB monocytes from babies born to obese mothers.

Volcano plots representing overall gene expression changes observed in (A) lean and (B) obese group following LPS stimulation. Genes displaying statistically significant differences in expression following LPS stimulation compared with resting state are marked in pink.

The numbers of DEG that are either upregulated (Up) or downregulated (Down) are indicated. (C) Heatmap of the percentages of genes regulated by LPS inducible and metabolically sensitive TFs in lean and obese groups. The percentages were calculated based on total number of predicted genes regulated by each TF as determined by cisRed. (D) Functional enrichment (biological processes) of the 48 DEG upregulated in both obese and lean groups carried out using InnateDB. Numbers within the bars indicate the number of genes that mapped to the GO term. (E) Functional enrichment of the 777 genes upregulated exclusively in the lean group carried out using InnateDB. Numbers within the bars indicate the number of genes that mapped to each of the GO terms. (F) Heatmap displaying expression levels (RPKM) of the 31 genes that mapped to the GO term "inflammatory response." (G) Heatmap of immune-related genes downregulated exclusively in the lean group.

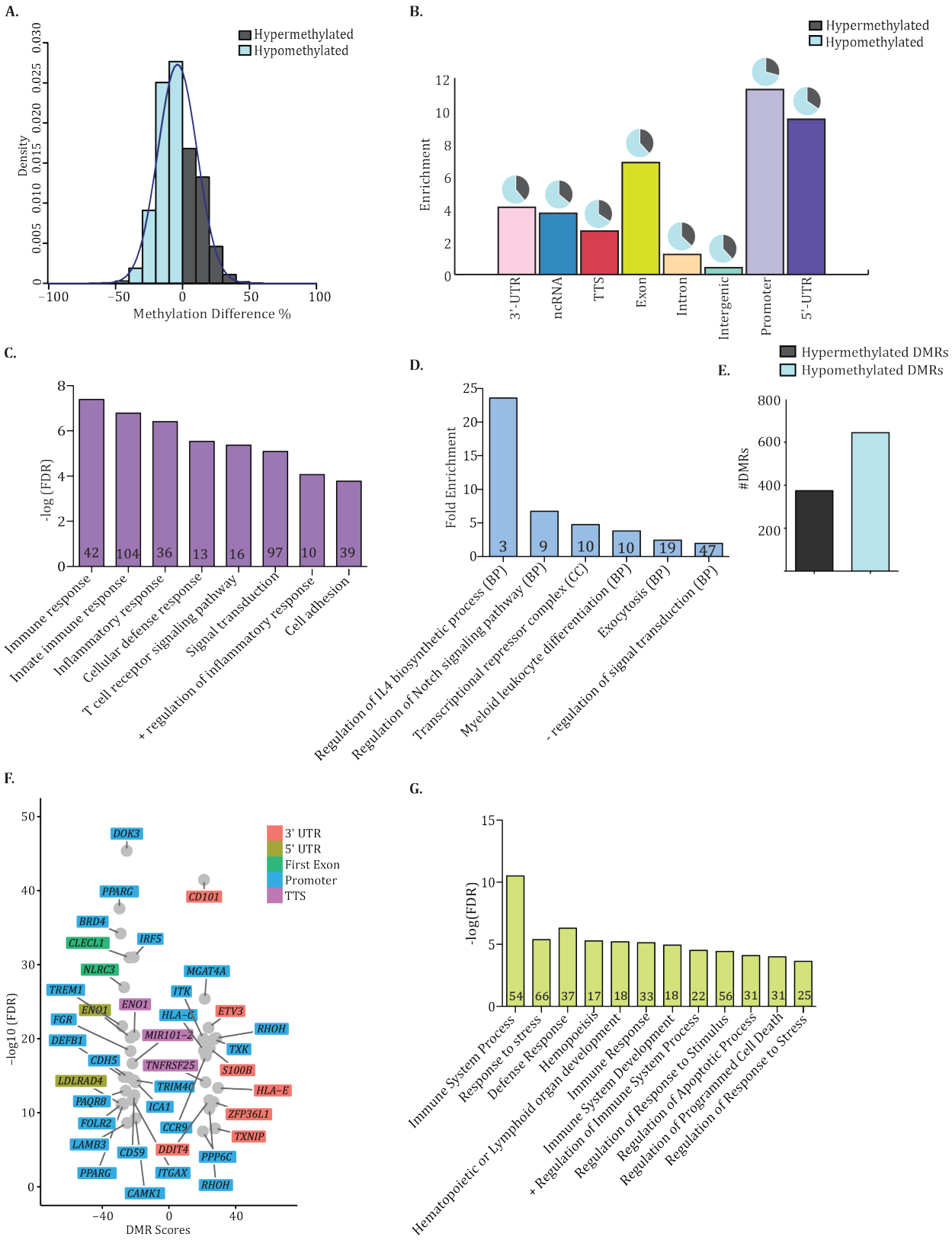
A.
Hypermethylated
Hypomethylated
Density
Methylation Difference %
B.
Hypermethylated
Hypomethylated
Enrichment
3'-UTR
ncRNA
TTS
Exon
Intron
Intergenic
Promoter
5'-UTR
C.
-log (FDR)
Immune response
Innate immune response
Inflammatory response
Cellular defense response
T cell receptor signaling pathway
Signal transduction
+ regulation of inflammatory response
Cell adhesion
D.
Fold Enrichment
Regulation of IL4 biosynthetic process (BP)
Regulation of Notch signaling pathway (BP)
Transcriptional repressor complex (CC)
Myeloid leukocyte differentiation (BP)
Exocytosis (BP)
- regulation of signal transduction (BP)
E.
Hypermethylated DMRs
Hypomethylated DMRs
#DMRs
F.
3' UTR
5' UTR
First Exon
Promoter
TTS
-log10 (FDR)
DMR Scores
DOK3
PPARG
CD101
BRD4
CLECL1
IRF5
NLRC3
MGAT4A
TREM1
ITK
ENO1
ETV3
FGR
HLA-G
RHOH
DEFB1
MIR101-2
TXK
CDH5
TNFRSF25
S100B
LDLRAD4
TRIM40
HLA-E
PAQR8
ICA1
ZFP36L1
FOLR2
CCR9
TXNIP
LAMB3
CD59
DDIT4
PPP6C
PPARG
ITGAX
RHOH
CAMK1
G.
-log(FDR)
Immune System Process
Response to stress
Defense Response
Hemopoeisis
Hematopoietic or Lymphoid organ development
Immune Response
Immune System Development
+ Regulation of Immune System Process
Regulation of Response to Stimulus
Regulation of Apoptotic Process
Regulation of Programmed Cell Death
Regulation of Response to Stress

Figure 4.3 Maternal pregravid obesity is associated with global hypomethylation in UCB monocytes.

(A) Distribution of overall single base resolution methylation changes in UCB monocytes from obese group relative to lean group. (B) Bar graph representing context-specific changes in methylation following correction for lengths of genomic regions indicates particular enrichment at the 59 regulatory and promoter regions. The pie charts above each bar represent the proportion of raw number of hypo- and hypermethylated cytosines in each context after including corrections for genomic lengths. (C) Genes with DMCs in 5' regulatory regions preferentially enrich to immune system processes. Numbers within the bars indicate the number of genes that mapped to the GO term. (D) Functional enrichment of genes regulated by DMCs in CpG islands using cis-regulatory model described by GREAT shows overrepresentation of inflammatory processes. Numbers within the bars indicate the number of genes that mapped to the GO term. (E) Bar graph representing the number of hyper- and hypomethylated DMRs. (F) Volcano plot of immune genes with DMRs overlapping 3' and 5' regulatory regions. (G) Functional enrichment of cis-regulatory associations of intergenic DMRs as predicted by GREAT indicates impact on immune system response, development, and apoptosis.

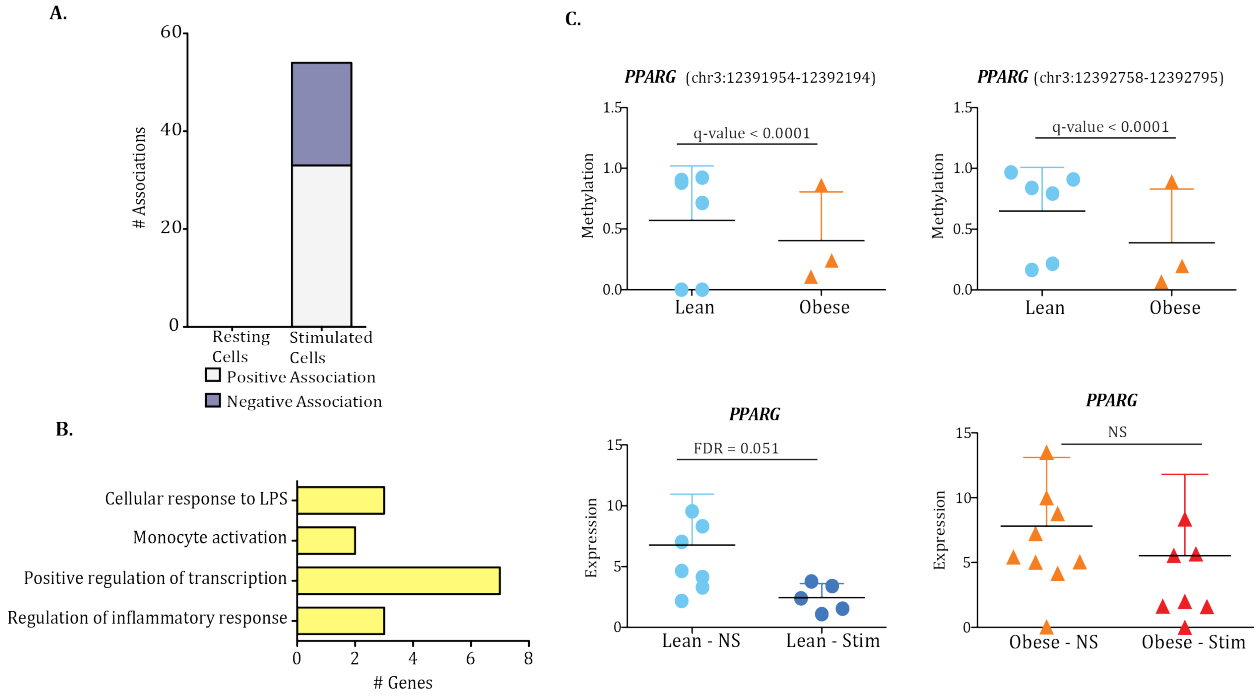

Figure 4.4 Pregravid obesity associated alterations in cytosine methylation within resting UCB monocytes are predictive of LPS-inducible transcriptional responses. (A) Bar graph representing number of significant associations reported by pair wise weighted integration of DNA methylation and gene expression profiles following corrections for multiple testing. (B) Assignment of biological functions to 54 genes with significant associations between expression profile and methylation status 5KB surrounding gene body. (C) DNA methylation changes within two DMRs overlapping *PPARG* gene (top). Gene expression changes in lean (left bottom) and obese (right bottom) groups following stimulation.

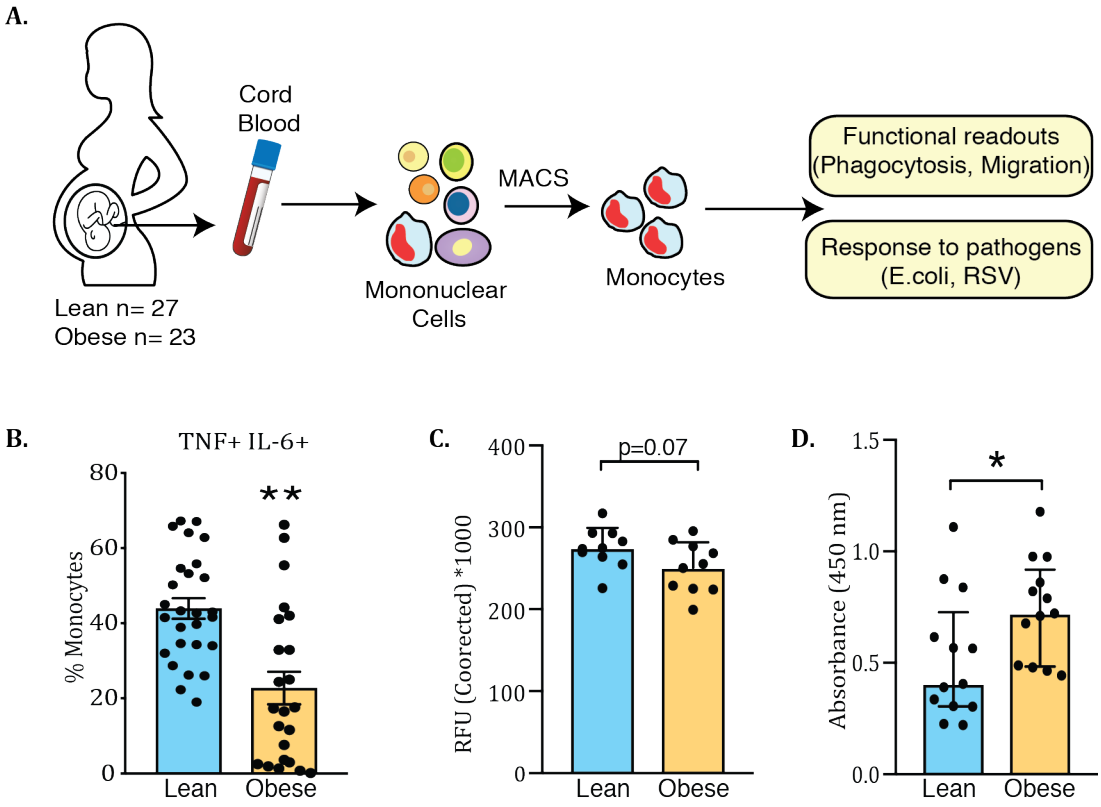

Figure 4.5 Functional rewiring of UCB monocytes with maternal obesity.
(A) Sample collection and experimental design. Purified monocytes were purified from UCBMC and functional defects testing using phagocytosis and migration assays. Monocytes were also infected with *E. coli* and RSV, and inflammatory responses measured using luminex and RNA-Seq (B) Frequency of TNF and IL6 producing cells in LPS stimulated UCBMC from cohort II measured using flow cytometry. (C) Comparison of relative fluorescence intensities proportional to monocytes migrating towards a chemokine gradient in a transwell assay. (D) Bar graphs comparing phagocytosis of E. coli by UCB monocytes using colorimetry. P-values: * - $p<0.05$; ** - $p<0.01$. Bars represent median values with interquartile ranges.

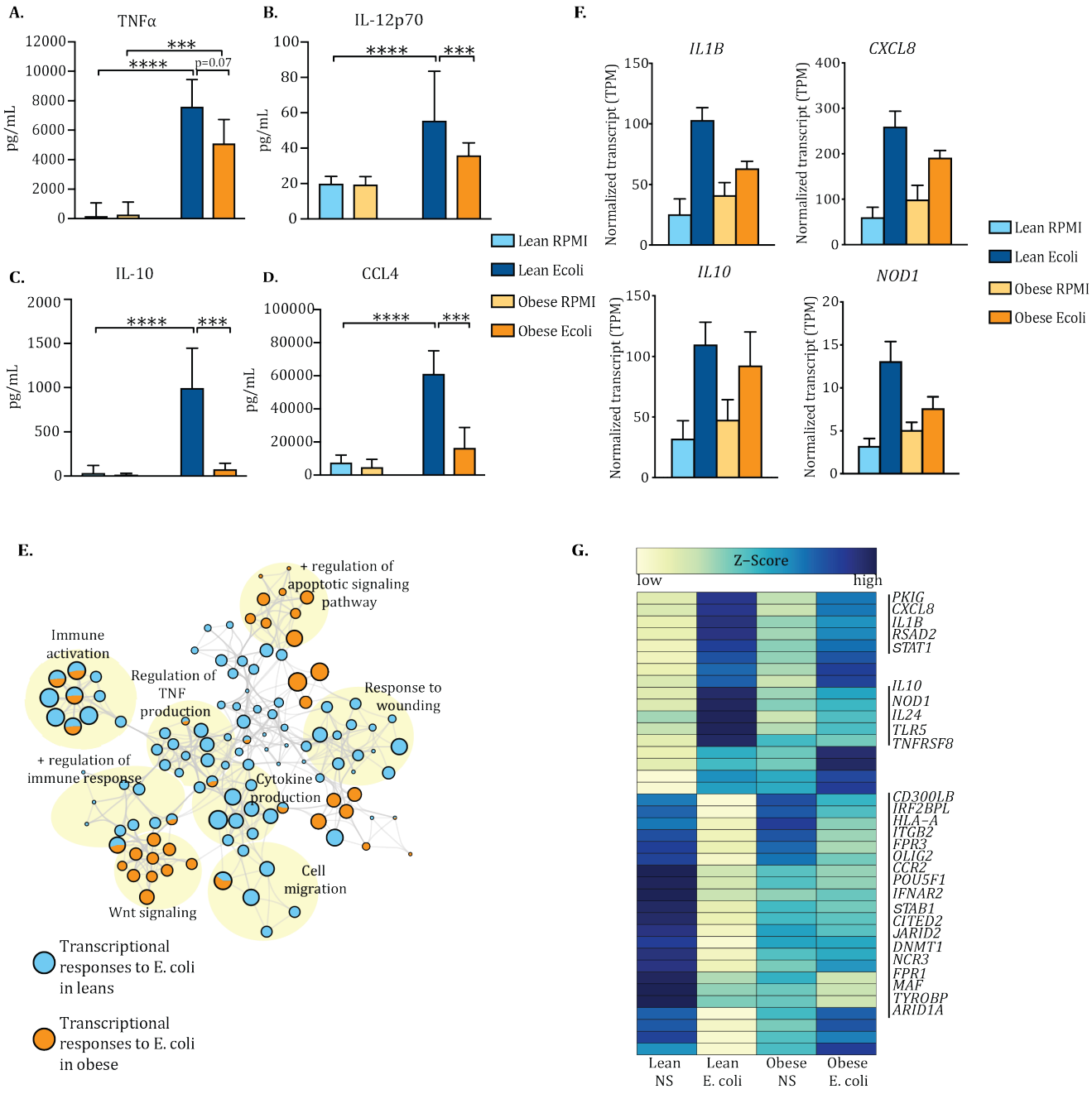

Figure 4.6 UCB monocyte responses to ex vivo *E. coli* infection.
(A-D) Secreted protein levels of key inflammatory mediators following ex vivo *E. coli* infection. Bars represent median values with interquartile range. P-values: *** - p<0.001; ****-p<0.0001 (E) Two-way functional enrichment of gene expression changes following infection generated using Metascape. Each bubble is a pie chart representing a gene ontology term. Relative contributions of genes from lean (blue) and obese (orange) groups are documented in the pie. Clusters of enrichment are colored in yellow and annotated. (F)

Bar graphs comparing transcripts per million (TPM) of select genes differentially responsive in lean group alone. (G) Heatmap of normalized transcript expression of genes responsive to E. coli infection only in lean group. Genes belonging to inflammatory and interferon signaling pathways were selected. Colors ranging from yellow (low expression) to blue (high expression) are indicative of z-scores generated from TPM.

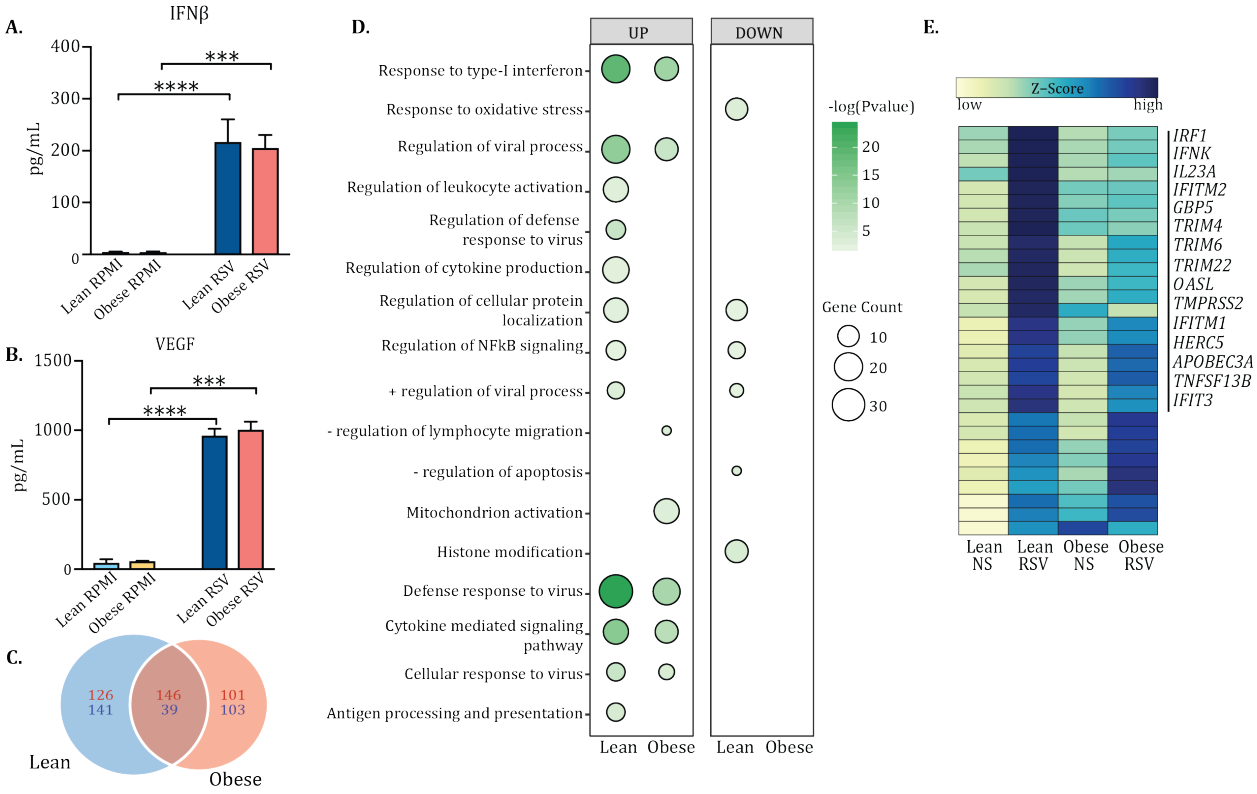

Figure 4.7 UCB monocyte responses to ex vivo RSV infection.
(A-B) Secreted protein levels of key inflammatory mediators following ex vivo Respiratory Syncytial Virus (RSV) infection. Bars represent median values with interquartile range (p-value: *** - p<0.001; ****-p<0.0001 (C) Venn diagram comparing differentially expressed genes following infection. Up-regulated (red) and down-regulated (blue) genes are annotated. (D) Four-way functional enrichment of gene expression changes following infection generated using Metascape. Size of the bubble is representative of numbers of genes contributing to the ontology term. Color represents the statistical significance. Up- and down-regulated genes were independently enriched (E) Heatmap comparing median TPM values of genes involved in Response to type-I interferons. Colors ranging from yellow (low expression) to blue (high expression) are indicative of z-scores generated from TPM.

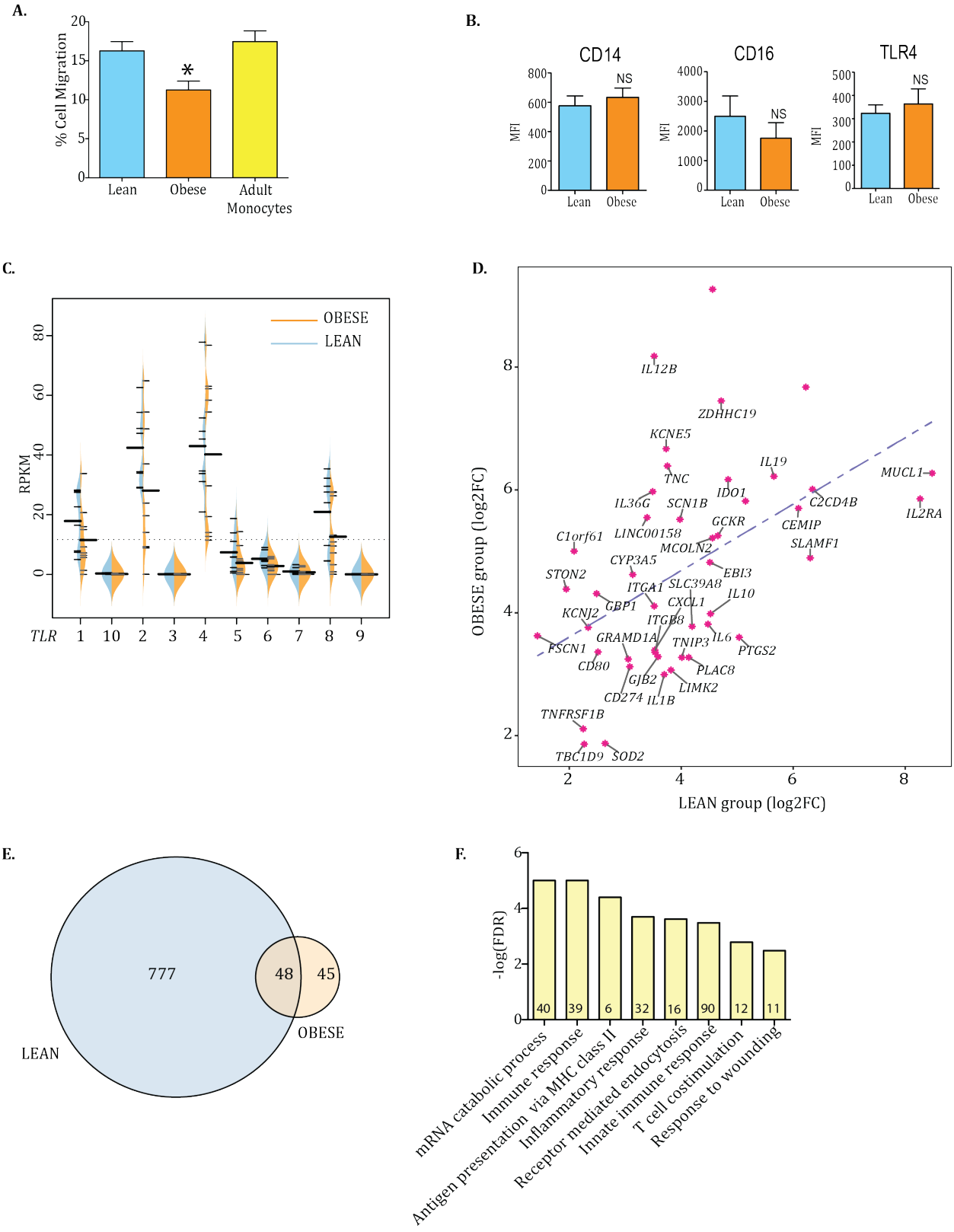
A.
% Cell Migration
Lean
Obese
Adult Monocytes
B.
CD14
CD16
TLR4
MFI
NS
Lean
Obese
C.
OBESE
LEAN
RPKM
TLR
D.
OBESE group (log2FC)
LEAN group (log2FC)
IL12B
ZDHHC19
KCNE5
TNC
IL19
MUCL1
IL36G
SCN1B
IDO1
C2CD4B
IL2RA
GCKR
CEMIP
C1orf61
LINC00158
MCOLN2
SLAMF1
CYP3A5
STON2
EBI3
ITGA1
SLC39A8
IL10
KCNJ2
GBP1
CXCL1
ITGB8
GRAMD1A
TNIP3
IL6
PTGS2
FSCN1
CD80
PLAC8
GJB2
LIMK2
CD274
IL1B
TNFRSF1B
TBC1D9
SOD2
E.
777
48
45
LEAN
OBESE
F.
-log(FDR)
40
39
6
32
16
90
12
11
mRNA catabolic process
Immune response
Antigen presentation via MHC class II
Inflammatory response
Receptor mediated endocytosis
Innate immune response
T cell costimulation
Response to wounding

(previous page) **Supplemental Figure 4.1 Transcriptional responses to LPS stimulation.** (A) Bar graphs representing migration of adult PBMC toward the media of LPS-stimulated UCB monocytes from lean and obese groups. (B) Surface expression of CD14, CD16, and TLR4 markers in UCB monocytes measured using flow cytometry (C) Bean plot representing expression of TLRs in resting UCB monocytes in lean and obese groups. (D) Scatter plot of FCs and regression line based on best fit of the 48 DEG upregulated in both groups revealed lower magnitudes of upregulation in the obese group. (E) Venn diagram identifying overlap of upregulated DEG in lean and obese groups following LPS stimulation (F) Functional enrichment of 890 genes upregulated only in the lean group following LPS stimulation as reported by InnateDB. Numbers within the bars indicate the number of DEG that mapped to each of the GO terms. P-values: * - $p<0.05$

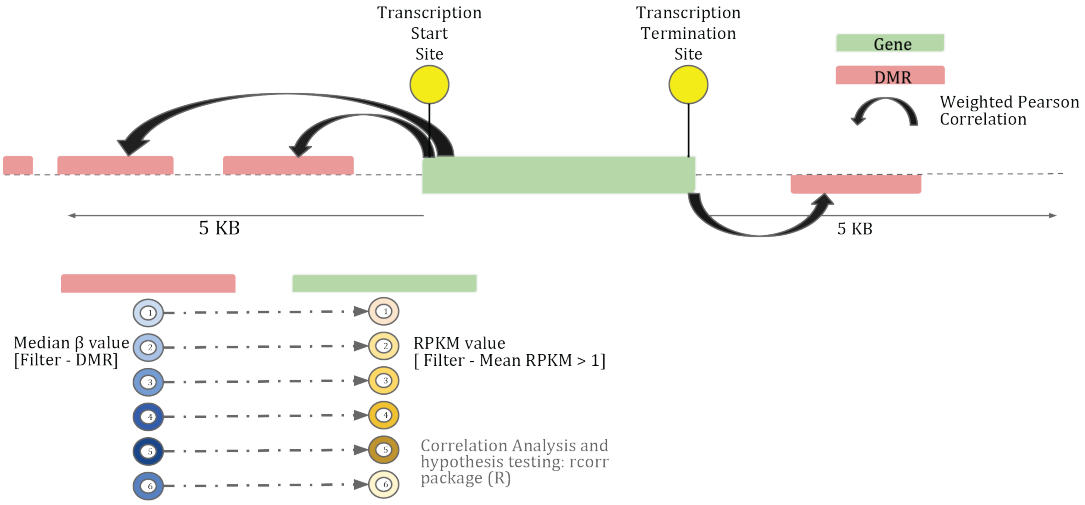

Supplemental Figure 4.2 Weighted pair-wise correlation analysis provides a robust method for comparing gene expression and methylation levels.
5 KB upstream of transcription start site (TSS) and 5 KB downstream of transcription termination site (TTS) of every gene with mean RPKM > 1 is scanned for presence of DMRs. For every gene-DMR pair, correlation analysis and hypothesis testing is performed in a sample-wise manner, allowing us to account for changes in intergenic regions as well. For correlation measures, median beta values for methylation are correlated with RPKM and tested using rcorr package.

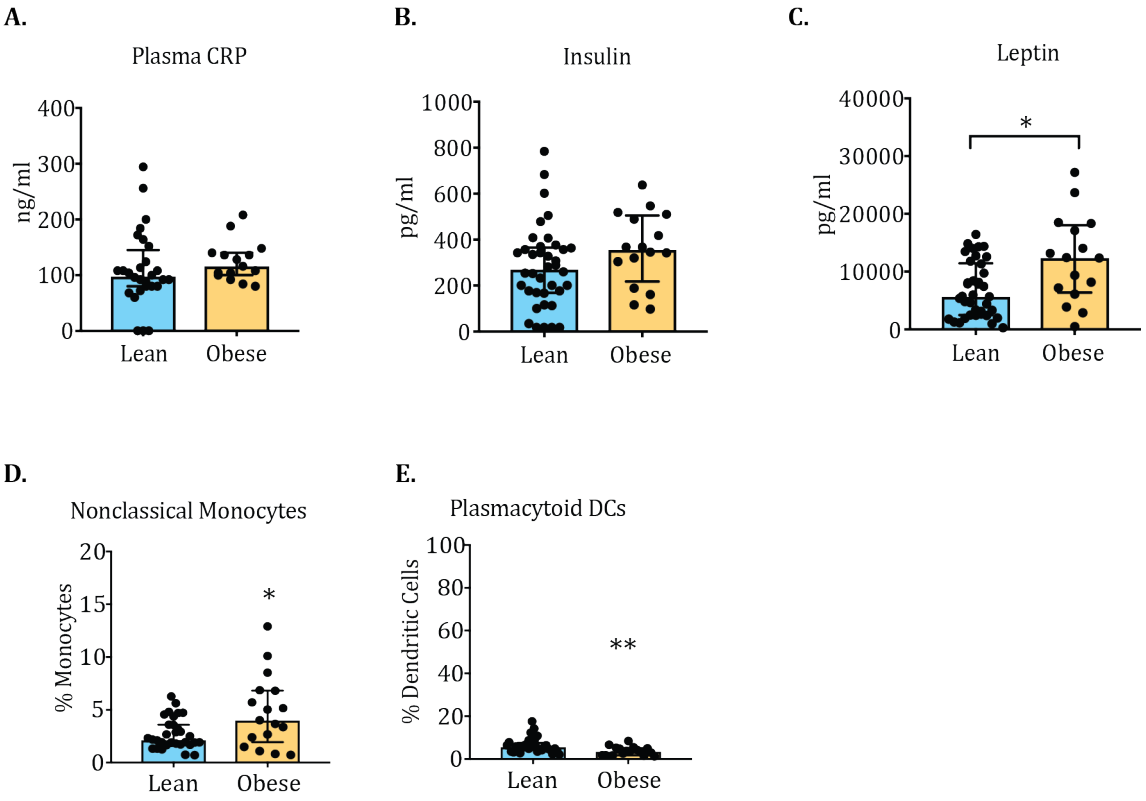

Supplemental Figure 4.3 Changes in circulating fetal immune environment with maternal obesity.

(A-C) Plasma levels of (A) CRP measured using ELISA and (B) insulin and (C) leptin measured using ELISA (C) CD86 expression following LPS and IFNγ stimulation on day 7. (D) Percentages of non-classical monocytes within monocyte population, and (E) plasmacytoid dendritic cells within HLA-DR+ DC population. P-values: * - $p<0.05$; ** - $p<0.01$. Bars represent medians with interquartile ranges.

CHAPTER 5

Summary and Conclusions

Summary

During pregnancy, the maternal immune system undergoes several coordinated adaptations in both innate and adaptive immune systems to enable both fetal tolerance and defense against pathogens. For example, the innate immune system in mothers during late stages of pregnancy seem to respond more vigorously to viral infections compared to early stages of pregnancy, or even compared to a non-gravid state (Le Gars et al., 2016). Another example is the amelioration of autoimmune conditions such as rheumatoid arthritis (RA) during by rebalancing both pro-inflammatory and anti-inflammatory factors (Forger and Villiger, 2020). These adaptations have been recently coined as an "immunological clock of healthy pregnancy" (Aghaeepour et al., 2017). Obesity is a condition of chronic low-grade inflammation that has the potential to disrupt this immunological clock. However, the precise burden of obesity on the maternal immune system is still unclear. This work was aimed at characterizing the impact of pre-pregnancy (pregravid) obesity both during early and late stages of pregnancy (**Chapter 2**). Our studies revealed that super-imposition of maternal obesity and pregnancy associated inflammation at term (37 weeks of pregnancy) attenuated monocyte activation trajectory normally observed in lean pregnancy (Le Gars et al., 2016).

This "rebalancing" of maternal systemic factors at term was characterized by skewing of cytokine and chemokine profiles towards a regulatory state. In addition to these systemic changes, we argue that this long-term exposure to a maternal obesogenic

environment rewires circulating monocytes towards a state of immunotolerance. This hypothesis was supported by metabolic, epigenetic, and functional assays suggesting the notion that the monocytes were poised towards a state that promoted weakened responses when challenged (**Chapter 2**). In addition to systemic inflammatory changes, it is likely that a combination of factors such as metabolic hormones (leptin, insulin), placenta derived factors and lipids can play a significant role in rewiring circulating monocytes towards this tolerant state. Furthermore, monocyte derived macrophages from mothers with obesity were less plastic under M1 skewing conditions, but secreted reduced levels of cytokines under both M1 and M2 skewing conditions. Collectively, these observations provide a potential explanation for increased susceptibility to viral infection observed in mothers with obesity, both during pregnancy and postpartum. However, these findings could potentially have broad implications on immune cells at the maternal fetal interface, given that a majority of decidual macrophages are repopulated by monocytes in circulation.

Pregravid Obesity and placental macrophages

Abnormal maternal immunological adaptations have been proposed as a critical factor in the etiology and progression of pathologies such as preeclampsia and fetal growth restriction (Aplin et al., 2020). To verify if obesity results in any placental immune adaptations, we profiled CD45+ cells in placental decidua and villous chorion from lean mothers and mothers with obesity (**Chapter 3**). Single cell RNA sequencing allowed us to profile tissue resident macrophages in an unbiased manner, and remove any infiltrating blood monocytes computationally via integration. In both the decidua and villous, we identified a population of tissue resident macrophages, and a population of macrophages that shared features with blood. We argue that this population of monocyte-derived

macrophages is of maternal origin, and has been shown to populate both maternal and fetal membranes of the placenta (Pique-Regi et al., 2019; Vento-Tormo et al., 2018). Nevertheless, obesity was associated with increased frequencies of tissue resident macrophages (HLA-DR^{high}) in both the decidua and villous. However, to our surprise, these cells had a basal anti-inflammatory phenotype and secreted lower levels of pro-inflammatory cytokines at baseline. In the decidua, which is composed of mostly lymphoid cells at term, we observed significant reduction in both CD4 and CD8 T cells. Single cell profiles demonstrated a reduction in decidual regulatory T cells with maternal obesity. While the precise placenta derived factors or cells that recruit monocytes into the decidua is still unclear, this rebalancing of decidual immune space with obesity could potentially alter the yin and yang of fetal tolerance and host defense. However, the regulatory phenotype of these macrophages and diminished levels of inflammatory factors detected in decidual tissue of mothers with obesity collectively suggest that the placental microenvironment is limiting inflammation at the interface. This approach of restraining inflammation is clearer on the fetal front of the placenta. Maternal obesity also resulted in increased frequency of macrophages in the villous, which is mostly comprised of fetal macrophages, called the Hofbauer cells. As described in the decidua, fetal macrophages from obese mothers had a regulatory phenotype, diminished ROS levels, and responded poorly to LPS. These adaptations may limit fetal exposure to inflammation. An interesting finding from single cell experiments was enrichment of macrophage fractions in the villi that had signatures associated with macrophage-stromal cell crosstalk (fat, muscle, epithelial cell). Future work should focus on understanding non-immune factors that

recruit macrophages into the placenta and assess the role of accessory cells such as trophoblasts and their interactions with macrophages in limiting fetal inflammation.

Pregravid Obesity and fetal monocytes

The relevance of Developmental Origins of Health and Disease (DOHaD) has piqued our interest in identifying the impact of an environmental factors such as maternal obesity on fetal immune development. Defects in developmental trajectories *in utero* can impact immune fitness or exacerbate autoimmune responses through epigenetic mechanisms. Our studies in three independent cohorts now have shown umbilical cord blood monocytes obtained from babies born to obese mothers have intrinsic defects that result in poor cytokine responses to TLR4 agonist LPS. As a part of this thesis, we demonstrate that these defects extend to other TLRs, and alter cord blood monocyte responses to pathogens such as *E. coli* and RSV. Functional assays support the hypothesis that these cells follow similar patterns of tolerance as seen in maternal monocytes. DNA methylation studies support this hypothesis and partially explain cellular defects seen in cord blood monocytes. However, potential maternal factors that rewire fetal monocyte are still unknown. It could be argued that maternal hormones, lipids, cytokines could directly or indirectly expose the fetal immune system to aberrant activation/inflammation over the course of gestation, and what we observe at birth is just the end result of this prolonged activation.

A major limitation of our clinical studies is that they only provide a snapshot of immune system at birth. While it can be argued that cord blood monocytes might not be the best surrogate for fetal immune system of the developing offspring/adolescent, these cells are derived from the same precursors that populate the blood into adulthood. Studies in animal models have demonstrated that high fat diet induced maternal obesity alters the

balance of myeloid-lymphoid fate in bone marrow precursors and dysregulates inflammatory responses of macrophages from tissue compartments such as lung, gut, liver, adipose tissue, spleen, and the central nervous system. These findings suggest that the impact of obesity on monocyte/macrophage is long lasting and could provide useful insight into explaining the high prevalence of cardiometabolic disorders, allergies, cognitive impairment, infectious morbidities and cancer in offspring of mothers with obesity.

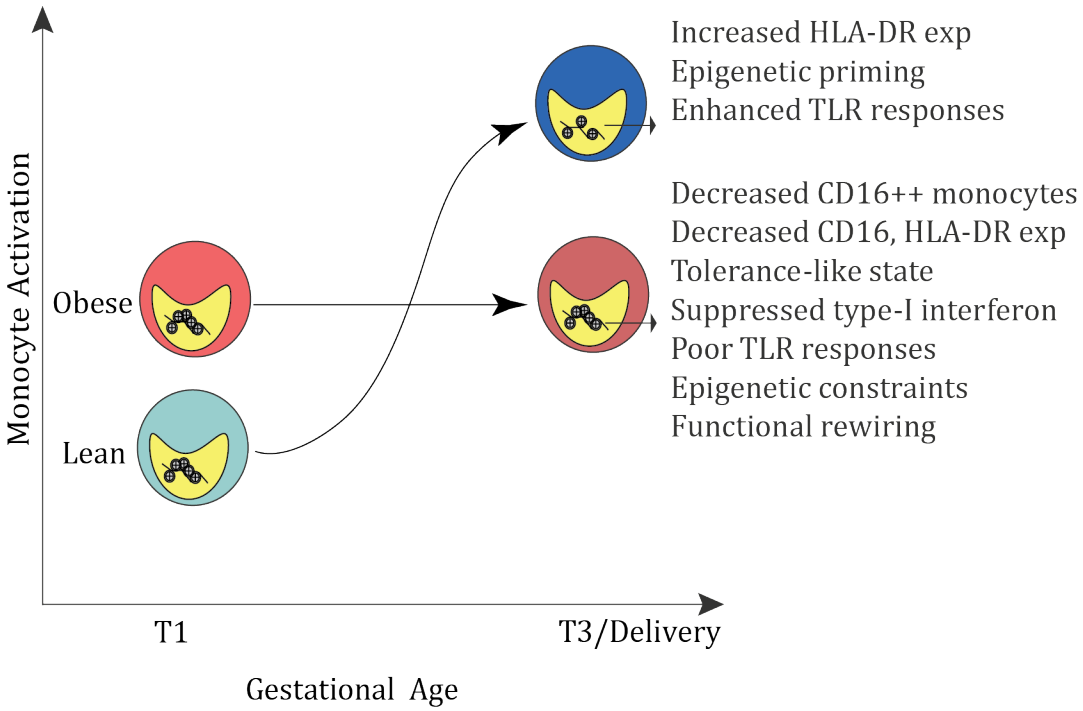

Figure 5.1 Evolving model describing the trajectory of monocyte activation with gestation and pregravid obesity

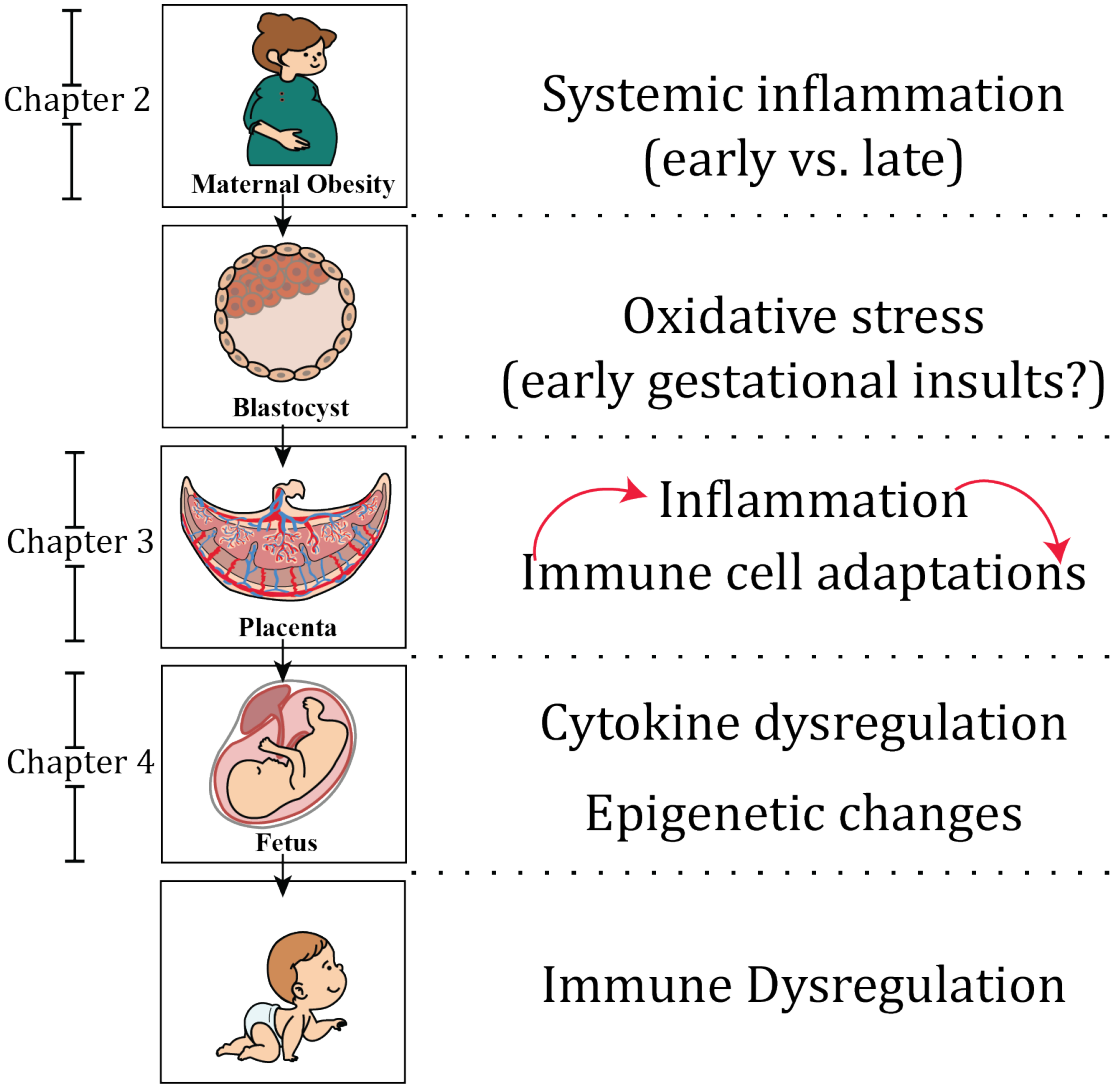

Figure 5.2 Mechanisms linking obesity associated changes with fetal immune reprogramming.

REFERENCES

Aagaard, K., Ma, J., Antony, K.M., Ganu, R., Petrosino, J., and Versalovic, J. (2014). The placenta harbors a unique microbiome. Sci Transl Med *6*, 237ra265.

Aagaard-Tillery, K.M., Grove, K., Bishop, J., Ke, X., Fu, Q., McKnight, R., and Lane, R.H. (2008). Developmental origins of disease and determinants of chromatin structure: maternal diet modifies the primate fetal epigenome. J Mol Endocrinol *41*, 91-102.

Aaltonen, R., Heikkinen, T., Hakala, K., Laine, K., and Alanen, A. (2005). Transfer of proinflammatory cytokines across term placenta. Obstet Gynecol *106*, 802-807.

Abrahams, V.M., Kim, Y.M., Straszewski, S.L., Romero, R., and Mor, G. (2004). Macrophages and apoptotic cell clearance during pregnancy. Am J Reprod Immunol *51*, 275-282.

Acosta, C.D., Bhattacharya, S., Tuffnell, D., Kurinczuk, J.J., and Knight, M. (2012). Maternal sepsis: a Scottish population-based case-control study. BJOG *119*, 474-483.

Acosta, O., Ramirez, V.I., Lager, S., Gaccioli, F., Dudley, D.J., Powell, T.L., and Jansson, T. (2015). Increased glucose and placental GLUT-1 in large infants of obese nondiabetic mothers. Am J Obstet Gynecol *212*, 227 e221-227.

Aghaeepour, N., Ganio, E.A., McIlwain, D., Tsai, A.S., Tingle, M., Van Gassen, S., Gaudilliere, D.K., Baca, Q., McNeil, L., Okada, R.*, et al.* (2017). An immune clock of human pregnancy. Sci Immunol *2*.

Aghaeepour, N., Lehallier, B., Baca, Q., Ganio, E.A., Wong, R.J., Ghaemi, M.S., Culos, A., El-Sayed, Y.Y., Blumenfeld, Y.J., Druzin, M.L.*, et al.* (2018). A proteomic clock of human pregnancy. Am J Obstet Gynecol *218*, 347 e341-347 e314.

Airas, L., Saraste, M., Rinta, S., Elovaara, I., Huang, Y.H., Wiendl, H., Finnish Multiple, S., and Pregnancy Study, G. (2008). Immunoregulatory factors in multiple sclerosis patients during and after pregnancy: relevance of natural killer cells. Clin Exp Immunol *151*, 235-243.

Alfaradhi, M.Z., and Ozanne, S.E. (2011). Developmental programming in response to maternal overnutrition. Front Genet *2*, 27.

Altmae, S., Segura, M.T., Esteban, F.J., Bartel, S., Brandi, P., Irmler, M., Beckers, J., Demmelmair, H., Lopez-Sabater, C., Koletzko, B.*, et al.* (2017). Maternal Pre-Pregnancy Obesity Is Associated with Altered Placental Transcriptome. PLoS One *12*, e0169223.

Amarasekara, R., Jayasekara, R.W., Senanayake, H., and Dissanayake, V.H. (2015). Microbiome of the placenta in pre-eclampsia supports the role of bacteria in the multifactorial cause of pre-eclampsia. J Obstet Gynaecol Res *41*, 662-669.

Ander, S.E., Diamond, M.S., and Coyne, C.B. (2019). Immune responses at the maternal-fetal interface. Sci Immunol *4*.

Anderson, V., Chaboyer, W., and Gillespie, B. (2013). The relationship between obesity and surgical site infections in women undergoing caesarean sections: an integrative review. Midwifery *29*, 1331-1338.

Antony, K.M., Ma, J., Mitchell, K.B., Racusin, D.A., Versalovic, J., and Aagaard, K. (2015). The preterm placental microbiome varies in association with excess maternal gestational weight gain. Am J Obstet Gynecol *212*, 653 e651-616.

Aplin, J.D., Myers, J.E., Timms, K., and Westwood, M. (2020). Tracking placental development in health and disease. Nat Rev Endocrinol.

Aune, D., Saugstad, O.D., Henriksen, T., and Tonstad, S. (2014). Maternal body mass index and the risk of fetal death, stillbirth, and infant death: a systematic review and meta-analysis. JAMA *311*, 1536-1546.
Aye, I.L., Lager, S., Ramirez, V.I., Gaccioli, F., Dudley, D.J., Jansson, T., and Powell, T.L. (2014). Increasing maternal body mass index is associated with systemic inflammation in the mother and the activation of distinct placental inflammatory pathways. Biol Reprod *90*, 129.
Aye, I.L., Rosario, F.J., Powell, T.L., and Jansson, T. (2015). Adiponectin supplementation in pregnant mice prevents the adverse effects of maternal obesity on placental function and fetal growth. Proc Natl Acad Sci U S A *112*, 12858-12863.
Baban, R.S., Ali, N.M., and Al-Moayed, H.A. (2010). Serum leptin and insulin hormone level in recurrent pregnancy loss. Oman Med J *25*, 203-207.
Bardou, M., Hadi, T., Mace, G., Pesant, M., Debermont, J., Barrichon, M., Wendremaire, M., Laurent, N., Sagot, P., and Lirussi, F. (2014). Systemic increase in human maternal circulating CD14+CD16- MCP-1+ monocytes as a marker of labor. Am J Obstet Gynecol *210*, 70 e71-79.
Barker, D.J. (1995). Fetal origins of coronary heart disease. BMJ *311*, 171-174.
Bartsch, E., Medcalf, K.E., Park, A.L., Ray, J.G., and High Risk of Pre-eclampsia Identification, G. (2016). Clinical risk factors for pre-eclampsia determined in early pregnancy: systematic review and meta-analysis of large cohort studies. BMJ *353*, i1753.
Basu, S., Haghiac, M., Surace, P., Challier, J.C., Guerre-Millo, M., Singh, K., Waters, T., Minium, J., Presley, L., Catalano, P.M., and Hauguel-de Mouzon, S. (2011a). Pregravid obesity associates with increased maternal endotoxemia and metabolic inflammation. Obesity (Silver Spring) *19*, 476-482.
Basu, S., Leahy, P., Challier, J.C., Minium, J., Catalano, P., and Hauguel-de Mouzon, S. (2011b). Molecular phenotype of monocytes at the maternal-fetal interface. Am J Obstet Gynecol *205*, 265 e261-268.
Bauche, D., and Marie, J.C. (2017). Transforming growth factor beta: a master regulator of the gut microbiota and immune cell interactions. Clin Transl Immunology *6*, e136.
Ben Amara, A., Gorvel, L., Baulan, K., Derain-Court, J., Buffat, C., Verollet, C., Textoris, J., Ghigo, E., Bretelle, F., Maridonneau-Parini, I., and Mege, J.L. (2013). Placental macrophages are impaired in chorioamnionitis, an infectious pathology of the placenta. J Immunol *191*, 5501-5514.
Bianchi, D.W., Zickwolf, G.K., Weil, G.J., Sylvester, S., and DeMaria, M.A. (1996). Male fetal progenitor cells persist in maternal blood for as long as 27 years postpartum. Proc Natl Acad Sci U S A *93*, 705-708.
Bibi, S., Kang, Y., Du, M., and Zhu, M.J. (2017). Maternal high-fat diet consumption enhances offspring susceptibility to DSS-induced colitis in mice. Obesity (Silver Spring) *25*, 901-908.
Blomberg, M. (2013). Maternal obesity, mode of delivery, and neonatal outcome. Obstet Gynecol *122*, 50-55.
Bonder, C.S., Finlay-Jones, J.J., and Hart, P.H. (1999). Interleukin-4 regulation of human monocyte and macrophage interleukin-10 and interleukin-12 production. Role of a functional interleukin-2 receptor gamma-chain. Immunology *96*, 529-536.
Borengasser, S.J., Lau, F., Kang, P., Blackburn, M.L., Ronis, M.J., Badger, T.M., and Shankar, K. (2011). Maternal obesity during gestation impairs fatty acid oxidation and mitochondrial SIRT3 expression in rat offspring at weaning. PLoS One *6*, e24068.

Bouanane, S., Merzouk, H., Benkalfat, N.B., Soulimane, N., Merzouk, S.A., Gresti, J., Tessier, C., and Narce, M. (2010). Hepatic and very low-density lipoprotein fatty acids in obese offspring of overfed dams. Metabolism *59*, 1701-1709.
Boucas, A.P., de Souza, B.M., Bauer, A.C., and Crispim, D. (2017). Role of Innate Immunity in Preeclampsia: A Systematic Review. Reprod Sci *24*, 1362-1370.
Briana, D.D., and Malamitsi-Puchner, A. (2009). Reviews: adipocytokines in normal and complicated pregnancies. Reprod Sci *16*, 921-937.
Bronson, S.L., and Bale, T.L. (2014). Prenatal stress-induced increases in placental inflammation and offspring hyperactivity are male-specific and ameliorated by maternal antiinflammatory treatment. Endocrinology *155*, 2635-2646.
Burdge, G.C., Slater-Jefferies, J., Torrens, C., Phillips, E.S., Hanson, M.A., and Lillycrop, K.A. (2007). Dietary protein restriction of pregnant rats in the F0 generation induces altered methylation of hepatic gene promoters in the adult male offspring in the F1 and F2 generations. Br J Nutr *97*, 435-439.
Calkins, K., Roy, D., Molchan, L., Bradley, L., Grogan, T., Elashoff, D., and Walker, V. (2015). Predictive value of cord blood bilirubin for hyperbilirubinemia in neonates at risk for maternal-fetal blood group incompatibility and hemolytic disease of the newborn. J Neonatal Perinatal Med *8*, 243-250.
Cane, S., Ugel, S., Trovato, R., Marigo, I., De Sanctis, F., Sartoris, S., and Bronte, V. (2019). The Endless Saga of Monocyte Diversity. Front Immunol *10*, 1786.
Cappelletti, M., Della Bella, S., Ferrazzi, E., Mavilio, D., and Divanovic, S. (2016). Inflammation and preterm birth. J Leukoc Biol *99*, 67-78.
Castellana, B., Perdu, S., Kim, Y., Chan, K., Atif, J., Marziali, M., and Beristain, A.G. (2018). Maternal obesity alters uterine NK activity through a functional KIR2DL1/S1 imbalance. Immunol Cell Biol *96*, 805-819.
Catalano, P.M., and Ehrenberg, H.M. (2006). The short- and long-term implications of maternal obesity on the mother and her offspring. BJOG *113*, 1126-1133.
Catalano, P.M., Farrell, K., Thomas, A., Huston-Presley, L., Mencin, P., de Mouzon, S.H., and Amini, S.B. (2009a). Perinatal risk factors for childhood obesity and metabolic dysregulation. Am J Clin Nutr *90*, 1303-1313.
Catalano, P.M., Presley, L., Minium, J., and Hauguel-de Mouzon, S. (2009b). Fetuses of obese mothers develop insulin resistance in utero. Diabetes Care *32*, 1076-1080.
Challier, J.C., Basu, S., Bintein, T., Minium, J., Hotmire, K., Catalano, P.M., and Hauguel-de Mouzon, S. (2008). Obesity in pregnancy stimulates macrophage accumulation and inflammation in the placenta. Placenta *29*, 274-281.
Chandra, S., Tripathi, A.K., Mishra, S., Amzarul, M., and Vaish, A.K. (2012). Physiological changes in hematological parameters during pregnancy. Indian J Hematol Blood Transfus *28*, 144-146.
Christian, L.M., and Porter, K. (2014). Longitudinal changes in serum proinflammatory markers across pregnancy and postpartum: effects of maternal body mass index. Cytokine *70*, 134-140.
Chu, S.Y., Callaghan, W.M., Kim, S.Y., Schmid, C.H., Lau, J., England, L.J., and Dietz, P.M. (2007a). Maternal obesity and risk of gestational diabetes mellitus. Diabetes Care *30*, 2070-2076.

Chu, S.Y., Kim, S.Y., Lau, J., Schmid, C.H., Dietz, P.M., Callaghan, W.M., and Curtis, K.M. (2007b). Maternal obesity and risk of stillbirth: a metaanalysis. Am J Obstet Gynecol *197*, 223-228.
Chu, S.Y., Kim, S.Y., Schmid, C.H., Dietz, P.M., Callaghan, W.M., Lau, J., and Curtis, K.M. (2007c). Maternal obesity and risk of cesarean delivery: a meta-analysis. Obes Rev *8*, 385-394.
Cifuentes-Zuniga, F., Arroyo-Jousse, V., Soto-Carrasco, G., Casanello, P., Uauy, R., Krause, B.J., and Castro-Rodriguez, J.A. (2017). IL-10 expression in macrophages from neonates born from obese mothers is suppressed by IL-4 and LPS/INFgamma. J Cell Physiol *232*, 3693-3701.
Cnattingius, S., Villamor, E., Johansson, S., Edstedt Bonamy, A.K., Persson, M., Wikstrom, A.K., and Granath, F. (2013). Maternal obesity and risk of preterm delivery. JAMA *309*, 2362-2370.
Collado, M.C., Isolauri, E., Laitinen, K., and Salminen, S. (2010). Effect of mother's weight on infant's microbiota acquisition, composition, and activity during early infancy: a prospective follow-up study initiated in early pregnancy. Am J Clin Nutr *92*, 1023-1030.
Comuzzie, A.G., Cole, S.A., Martin, L., Carey, K.D., Mahaney, M.C., Blangero, J., and VandeBerg, J.L. (2003). The baboon as a nonhuman primate model for the study of the genetics of obesity. Obes Res *11*, 75-80.
Conner, S.N., Verticchio, J.C., Tuuli, M.G., Odibo, A.O., Macones, G.A., and Cahill, A.G. (2014). Maternal obesity and risk of postcesarean wound complications. Am J Perinatol *31*, 299-304.
Corces, M.R., Trevino, A.E., Hamilton, E.G., Greenside, P.G., Sinnott-Armstrong, N.A., Vesuna, S., Satpathy, A.T., Rubin, A.J., Montine, K.S., Wu, B.*, et al.* (2017). An improved ATAC-seq protocol reduces background and enables interrogation of frozen tissues. Nat Methods *14*, 959-962.
Costa, S.M., Isganaitis, E., Matthews, T.J., Hughes, K., Daher, G., Dreyfuss, J.M., da Silva, G.A., and Patti, M.E. (2016). Maternal obesity programs mitochondrial and lipid metabolism gene expression in infant umbilical vein endothelial cells. Int J Obes (Lond) *40*, 1627-1634.
Curry, A.E., Vogel, I., Skogstrand, K., Drews, C., Schendel, D.E., Flanders, W.D., Hougaard, D.M., and Thorsen, P. (2008). Maternal plasma cytokines in early- and mid-gestation of normal human pregnancy and their association with maternal factors. J Reprod Immunol *77*, 152-160.
De Kleer, I., Willems, F., Lambrecht, B., and Goriely, S. (2014). Ontogeny of myeloid cells. Front Immunol *5*, 423.
Denney, J.M., Nelson, E.L., Wadhwa, P.D., Waters, T.P., Mathew, L., Chung, E.K., Goldenberg, R.L., and Culhane, J.F. (2011). Longitudinal modulation of immune system cytokine profile during pregnancy. Cytokine *53*, 170-177.
Devevre, E.F., Renovato-Martins, M., Clement, K., Sautes-Fridman, C., Cremer, I., and Poitou, C. (2015). Profiling of the three circulating monocyte subpopulations in human obesity. J Immunol *194*, 3917-3923.
Doi, L., Williams, A.J., Marryat, L., and Frank, J. (2020). Cohort study of high maternal body mass index and the risk of adverse pregnancy and delivery outcomes in Scotland. BMJ Open *10*, e026168.
Dos Santos, C.O., Dolzhenko, E., Hodges, E., Smith, A.D., and Hannon, G.J. (2015). An epigenetic memory of pregnancy in the mouse mammary gland. Cell Rep *11*, 1102-1109.

Dosch, N.C., Guslits, E.F., Weber, M.B., Murray, S.E., Ha, B., Coe, C.L., Auger, A.P., and Kling, P.J. (2016). Maternal Obesity Affects Inflammatory and Iron Indices in Umbilical Cord Blood. J Pediatr *172*, 20-28.
Dowling, D.J., and Levy, O. (2014). Ontogeny of early life immunity. Trends Immunol *35*, 299-310.
Du, M.R., Wang, S.C., and Li, D.J. (2014). The integrative roles of chemokines at the maternal-fetal interface in early pregnancy. Cell Mol Immunol *11*, 438-448.
Dubova, E.A., Pavlov, K.A., Borovkova, E.I., Bayramova, M.A., Makarov, I.O., and Shchegolev, A.I. (2011). Vascular endothelial growth factor and its receptors in the placenta of pregnant women with obesity. Bull Exp Biol Med *151*, 253-258.
Dulloo, A.G., Jacquet, J., Solinas, G., Montani, J.P., and Schutz, Y. (2010). Body composition phenotypes in pathways to obesity and the metabolic syndrome. Int J Obes (Lond) *34 Suppl 2*, S4-17.
Dumas, O., Varraso, R., Gillman, M.W., Field, A.E., and Camargo, C.A., Jr. (2016). Longitudinal study of maternal body mass index, gestational weight gain, and offspring asthma. Allergy *71*, 1295-1304.
Dunn, G.A., and Bale, T.L. (2009). Maternal high-fat diet promotes body length increases and insulin insensitivity in second-generation mice. Endocrinology *150*, 4999-5009.
Edlow, A.G., Glass, R.M., Smith, C.J., Tran, P.K., James, K., and Bilbo, S. (2018). Placental Macrophages: A Window Into Fetal Microglial Function in Maternal Obesity. Int J Dev Neurosci.
Edlow, A.G., Hui, L., Wick, H.C., Fried, I., and Bianchi, D.W. (2016). Assessing the fetal effects of maternal obesity via transcriptomic analysis of cord blood: a prospective case-control study. BJOG *123*, 180-189.
Elahi, M.M., Cagampang, F.R., Mukhtar, D., Anthony, F.W., Ohri, S.K., and Hanson, M.A. (2009). Long-term maternal high-fat feeding from weaning through pregnancy and lactation predisposes offspring to hypertension, raised plasma lipids and fatty liver in mice. Br J Nutr *102*, 514-519.
Eriksson, J.G. (2001). [Proved association between low birth weight and coronary disease in adulthood. Too quick weight gain can disturb the muscle-fat balance]. Lakartidningen *98*, 5306-5307, 5310.
Eriksson, J.G., Sandboge, S., Salonen, M.K., Kajantie, E., and Osmond, C. (2014). Long-term consequences of maternal overweight in pregnancy on offspring later health: findings from the Helsinki Birth Cohort Study. Ann Med *46*, 434-438.
Faas, M.M., and de Vos, P. (2017). Uterine NK cells and macrophages in pregnancy. Placenta *56*, 44-52.
Faas, M.M., and De Vos, P. (2018). Innate immune cells in the placental bed in healthy pregnancy and preeclampsia. Placenta *69*, 125-133.
Faas, M.M., Schuiling, G.A., Linton, E.A., Sargent, I.L., and Redman, C.W. (2000). Activation of peripheral leukocytes in rat pregnancy and experimental preeclampsia. Am J Obstet Gynecol *182*, 351-357.
Faas, M.M., Spaans, F., and De Vos, P. (2014). Monocytes and macrophages in pregnancy and pre-eclampsia. Front Immunol *5*, 298.
Fan, L., Lindsley, S.R., Comstock, S.M., Takahashi, D.L., Evans, A.E., He, G.W., Thornburg, K.L., and Grove, K.L. (2013). Maternal high-fat diet impacts endothelial function in nonhuman primate offspring. Int J Obes (Lond) *37*, 254-262.

Farah, N., Hogan, A.E., O'Connor, N., Kennelly, M.M., O'Shea, D., and Turner, M.J. (2012). Correlation between maternal inflammatory markers and fetomaternal adiposity. Cytokine *60*, 96-99.
Farley, D., Tejero, M.E., Comuzzie, A.G., Higgins, P.B., Cox, L., Werner, S.L., Jenkins, S.L., Li, C., Choi, J., Dick, E.J., Jr.*, et al.* (2009). Feto-placental adaptations to maternal obesity in the baboon. Placenta *30*, 752-760.
Farlik, M., Halbritter, F., Muller, F., Choudry, F.A., Ebert, P., Klughammer, J., Farrow, S., Santoro, A., Ciaurro, V., Mathur, A.*, et al.* (2016). DNA Methylation Dynamics of Human Hematopoietic Stem Cell Differentiation. Cell Stem Cell *19*, 808-822.
Ferolla, F.M., Hijano, D.R., Acosta, P.L., Rodriguez, A., Duenas, K., Sancilio, A., Barboza, E., Caria, A., Gago, G.F., Almeida, R.E.*, et al.* (2013). Macronutrients during pregnancy and life-threatening respiratory syncytial virus infections in children. Am J Respir Crit Care Med *187*, 983-990.
Ferraro, Z.M., Qiu, Q., Gruslin, A., and Adamo, K.B. (2012). Characterization of the insulin-like growth factor axis in term pregnancies complicated by maternal obesity. Hum Reprod *27*, 2467-2475.
Flegal, K.M., Kruszon-Moran, D., Carroll, M.D., Fryar, C.D., and Ogden, C.L. (2016). Trends in Obesity Among Adults in the United States, 2005 to 2014. JAMA *315*, 2284-2291.
Forger, F., and Villiger, P.M. (2020). Immunological adaptations in pregnancy that modulate rheumatoid arthritis disease activity. Nat Rev Rheumatol *16*, 113-122.
Founds, S.A., Powers, R.W., Patrick, T.E., Ren, D., Harger, G.F., Markovic, N., and Roberts, J.M. (2008). A comparison of circulating TNF-alpha in obese and lean women with and without preeclampsia. Hypertens Pregnancy *27*, 39-48.
Franco-Sena, A.B., Rebelo, F., Pinto, T., Farias, D.R., Silveira, G.E., Mendes, R.H., Henriques, V.T., and Kac, G. (2016). The effect of leptin concentrations and other maternal characteristics on gestational weight gain is different according to pre-gestational BMI: results from a prospective cohort. BJOG *123*, 1804-1813.
Frias, A.E., Morgan, T.K., Evans, A.E., Rasanen, J., Oh, K.Y., Thornburg, K.L., and Grove, K.L. (2011). Maternal high-fat diet disturbs uteroplacental hemodynamics and increases the frequency of stillbirth in a nonhuman primate model of excess nutrition. Endocrinology *152*, 2456-2464.
Friedman, J.E., Dobrinskikh, E., Alfonso-Garcia, A., Fast, A., Janssen, R.C., Soderborg, T.K., Anderson, A.L., Reisz, J.A., D'Alessandro, A., Frank, D.N.*, et al.* (2018). Pyrroloquinoline quinone prevents developmental programming of microbial dysbiosis and macrophage polarization to attenuate liver fibrosis in offspring of obese mice. Hepatol Commun *2*, 313-328.
Friis, C.M., Paasche Roland, M.C., Godang, K., Ueland, T., Tanbo, T., Bollerslev, J., and Henriksen, T. (2013). Adiposity-related inflammation: effects of pregnancy. Obesity (Silver Spring) *21*, E124-130.
Fu, Q., McKnight, R.A., Yu, X., Callaway, C.W., and Lane, R.H. (2006). Growth retardation alters the epigenetic characteristics of hepatic dual specificity phosphatase 5. FASEB J *20*, 2127-2129.
Fu, Q., McKnight, R.A., Yu, X., Wang, L., Callaway, C.W., and Lane, R.H. (2004). Uteroplacental insufficiency induces site-specific changes in histone H3 covalent modifications and affects DNA-histone H3 positioning in day 0 IUGR rat liver. Physiol Genomics *20*, 108-116.

Fukuda, T. (1973). Fetal hemopoiesis. I. Electron microscopic studies on human yolk sac hemopoiesis. Virchows Arch B Cell Pathol *14*, 197-213.
Furukawa, R., Hachiya, T., Ohmomo, H., Shiwa, Y., Ono, K., Suzuki, S., Satoh, M., Hitomi, J., Sobue, K., and Shimizu, A. (2016). Intraindividual dynamics of transcriptome and genome-wide stability of DNA methylation. Sci Rep *6*, 26424.
Gaillard, R. (2015). Maternal obesity during pregnancy and cardiovascular development and disease in the offspring. Eur J Epidemiol *30*, 1141-1152.
Gaillard, R., Durmus, B., Hofman, A., Mackenbach, J.P., Steegers, E.A., and Jaddoe, V.W. (2013). Risk factors and outcomes of maternal obesity and excessive weight gain during pregnancy. Obesity (Silver Spring) *21*, 1046-1055.
Gaillard, R., Felix, J.F., Duijts, L., and Jaddoe, V.W. (2014a). Childhood consequences of maternal obesity and excessive weight gain during pregnancy. Acta Obstet Gynecol Scand *93*, 1085-1089.
Gaillard, R., Steegers, E.A., Duijts, L., Felix, J.F., Hofman, A., Franco, O.H., and Jaddoe, V.W. (2014b). Childhood cardiometabolic outcomes of maternal obesity during pregnancy: the Generation R Study. Hypertension *63*, 683-691.
Gaillard, R., Steegers, E.A., Franco, O.H., Hofman, A., and Jaddoe, V.W. (2015). Maternal weight gain in different periods of pregnancy and childhood cardio-metabolic outcomes. The Generation R Study. Int J Obes (Lond) *39*, 677-685.
Gallardo, J.M., Gomez-Lopez, J., Medina-Bravo, P., Juarez-Sanchez, F., Contreras-Ramos, A., Galicia-Esquivel, M., Sanchez-Urbina, R., and Klunder-Klunder, M. (2015). Maternal obesity increases oxidative stress in the newborn. Obesity (Silver Spring) *23*, 1650-1654.
Galley, J.D., Bailey, M., Kamp Dush, C., Schoppe-Sullivan, S., and Christian, L.M. (2014). Maternal obesity is associated with alterations in the gut microbiome in toddlers. PLoS One *9*, e113026.
Gamliel, M., Goldman-Wohl, D., Isaacson, B., Gur, C., Stein, N., Yamin, R., Berger, M., Grunewald, M., Keshet, E., Rais, Y.*, et al.* (2018). Trained Memory of Human Uterine NK Cells Enhances Their Function in Subsequent Pregnancies. Immunity *48*, 951-962 e955.
Gardner, R.M., Lee, B.K., Magnusson, C., Rai, D., Frisell, T., Karlsson, H., Idring, S., and Dalman, C. (2015). Maternal body mass index during early pregnancy, gestational weight gain, and risk of autism spectrum disorders: Results from a Swedish total population and discordant sibling study. Int J Epidemiol *44*, 870-883.
Gavrila, A., Chan, J.L., Yiannakouris, N., Kontogianni, M., Miller, L.C., Orlova, C., and Mantzoros, C.S. (2003). Serum adiponectin levels are inversely associated with overall and central fat distribution but are not directly regulated by acute fasting or leptin administration in humans: cross-sectional and interventional studies. J Clin Endocrinol Metab *88*, 4823-4831.
Geldenhuys, J., Rossouw, T.M., Lombaard, H.A., Ehlers, M.M., and Kock, M.M. (2018). Disruption in the Regulation of Immune Responses in the Placental Subtype of Preeclampsia. Front Immunol *9*, 1659.
George, L.A., Uthlaut, A.B., Long, N.M., Zhang, L., Ma, Y., Smith, D.T., Nathanielsz, P.W., and Ford, S.P. (2010). Different levels of overnutrition and weight gain during pregnancy have differential effects on fetal growth and organ development. Reprod Biol Endocrinol *8*, 75.
Gluckman, P.D., Lillycrop, K.A., Vickers, M.H., Pleasants, A.B., Phillips, E.S., Beedle, A.S., Burdge, G.C., and Hanson, M.A. (2007). Metabolic plasticity during mammalian

development is directionally dependent on early nutritional status. Proc Natl Acad Sci U S A *104*, 12796-12800.
Godfrey, K.M., Lillycrop, K.A., Burdge, G.C., Gluckman, P.D., and Hanson, M.A. (2007). Epigenetic mechanisms and the mismatch concept of the developmental origins of health and disease. Pediatr Res *61*, 5R-10R.
Godfrey, K.M., Reynolds, R.M., Prescott, S.L., Nyirenda, M., Jaddoe, V.W., Eriksson, J.G., and Broekman, B.F. (2017). Influence of maternal obesity on the long-term health of offspring. Lancet Diabetes Endocrinol *5*, 53-64.
Gomez-Lopez, N., StLouis, D., Lehr, M.A., Sanchez-Rodriguez, E.N., and Arenas-Hernandez, M. (2014). Immune cells in term and preterm labor. Cell Mol Immunol *11*, 571-581.
Gomez-Lopez, N., Vega-Sanchez, R., Castillo-Castrejon, M., Romero, R., Cubeiro-Arreola, K., and Vadillo-Ortega, F. (2013). Evidence for a role for the adaptive immune response in human term parturition. Am J Reprod Immunol *69*, 212-230.
Gonzalez-Espinosa, L.O., Montiel-Cervantes, L.A., Guerra-Marquez, A., Penaflor-Juarez, K., Reyes-Maldonado, E., and Vela-Ojeda, J. (2016). Maternal obesity associated with increase in natural killer T cells and CD8+ regulatory T cells in cord blood units. Transfusion *56*, 1075-1081.
Griffiths, P.S., Walton, C., Samsell, L., Perez, M.K., and Piedimonte, G. (2016). Maternal high-fat hypercaloric diet during pregnancy results in persistent metabolic and respiratory abnormalities in offspring. Pediatr Res *79*, 278-286.
Grigsby, P.L. (2016). Animal Models to Study Placental Development and Function throughout Normal and Dysfunctional Human Pregnancy. Semin Reprod Med *34*, 11-16.
Grondman, I., Arts, R.J.W., Koch, R.M., Leijte, G.P., Gerretsen, J., Bruse, N., Kempkes, R.W.M., Ter Horst, R., Kox, M., Pickkers, P.*, et al.* (2019). Frontline Science: Endotoxin-induced immunotolerance is associated with loss of monocyte metabolic plasticity and reduction of oxidative burst. J Leukoc Biol *106*, 11-25.
Guerra, S., Sartini, C., Mendez, M., Morales, E., Guxens, M., Basterrechea, M., Arranz, L., and Sunyer, J. (2013). Maternal prepregnancy obesity is an independent risk factor for frequent wheezing in infants by age 14 months. Paediatr Perinat Epidemiol *27*, 100-108.
Gustafsson, C., Mjosberg, J., Matussek, A., Geffers, R., Matthiesen, L., Berg, G., Sharma, S., Buer, J., and Ernerudh, J. (2008). Gene expression profiling of human decidual macrophages: evidence for immunosuppressive phenotype. PLoS One *3*, e2078.
Gutvirtz, G., Wainstock, T., Landau, D., and Sheiner, E. (2019). Maternal Obesity and Offspring Long-Term Infectious Morbidity. J Clin Med *8*.
Haberg, S.E., Stigum, H., London, S.J., Nystad, W., and Nafstad, P. (2009). Maternal obesity in pregnancy and respiratory health in early childhood. Paediatr Perinat Epidemiol *23*, 352-362.
Hadley, E.E., Discacciati, A., Costantine, M.M., Munn, M.B., Pacheco, L.D., Saade, G.R., and Chiossi, G. (2019). Maternal obesity is associated with chorioamnionitis and earlier indicated preterm delivery among expectantly managed women with preterm premature rupture of membranes. J Matern Fetal Neonatal Med *32*, 271-278.
Hafemeister, C., and Satija, R. (2019). Normalization and variance stabilization of single-cell RNA-seq data using regularized negative binomial regression. Genome Biol *20*, 296.
Hanna, J., Goldman-Wohl, D., Hamani, Y., Avraham, I., Greenfield, C., Natanson-Yaron, S., Prus, D., Cohen-Daniel, L., Arnon, T.I., Manaster, I.*, et al.* (2006). Decidual NK cells regulate

key developmental processes at the human fetal-maternal interface. Nat Med *12*, 1065-1074.
Hayes, E.K., Tessier, D.R., Percival, M.E., Holloway, A.C., Petrik, J.J., Gruslin, A., and Raha, S. (2014). Trophoblast invasion and blood vessel remodeling are altered in a rat model of lifelong maternal obesity. Reprod Sci *21*, 648-657.
Heerwagen, M.J., Miller, M.R., Barbour, L.A., and Friedman, J.E. (2010). Maternal obesity and fetal metabolic programming: a fertile epigenetic soil. Am J Physiol Regul Integr Comp Physiol *299*, R711-722.
Henneke, P., and Berner, R. (2006). Interaction of neonatal phagocytes with group B streptococcus: recognition and response. Infect Immun *74*, 3085-3095.
Herbstman, J.B., Wang, S., Perera, F.P., Lederman, S.A., Vishnevetsky, J., Rundle, A.G., Hoepner, L.A., Qu, L., and Tang, D. (2013). Predictors and consequences of global DNA methylation in cord blood and at three years. PLoS One *8*, e72824.
Herrera, E., Amusquivar, E., Lopez-Soldado, I., and Ortega, H. (2006). Maternal lipid metabolism and placental lipid transfer. Horm Res *65 Suppl 3*, 59-64.
Hirschmugl, B., Desoye, G., Catalano, P., Klymiuk, I., Scharnagl, H., Payr, S., Kitzinger, E., Schliefsteiner, C., Lang, U., Wadsack, C., and Hauguel-de Mouzon, S. (2017). Maternal obesity modulates intracellular lipid turnover in the human term placenta. Int J Obes (Lond) *41*, 317-323.
Holladay, S.D., and Smialowicz, R.J. (2000). Development of the murine and human immune system: differential effects of immunotoxicants depend on time of exposure. Environ Health Perspect *108 Suppl 3*, 463-473.
Holtan, S.G., Chen, Y., Kaimal, R., Creedon, D.J., Enninga, E.A., Nevala, W.K., and Markovic, S.N. (2015). Growth modeling of the maternal cytokine milieu throughout normal pregnancy: macrophage-derived chemokine decreases as inflammation/counterregulation increases. J Immunol Res *2015*, 952571.
Houser, B.L. (2012). Decidual macrophages and their roles at the maternal-fetal interface. Yale J Biol Med *85*, 105-118.
Houser, B.L., Tilburgs, T., Hill, J., Nicotra, M.L., and Strominger, J.L. (2011). Two unique human decidual macrophage populations. J Immunol *186*, 2633-2642.
Huang, Y., Yan, X., Zhao, J.X., Zhu, M.J., McCormick, R.J., Ford, S.P., Nathanielsz, P.W., Ren, J., and Du, M. (2010). Maternal obesity induces fibrosis in fetal myocardium of sheep. Am J Physiol Endocrinol Metab *299*, E968-975.
Huda, S.S., Forrest, R., Paterson, N., Jordan, F., Sattar, N., and Freeman, D.J. (2014). In preeclampsia, maternal third trimester subcutaneous adipocyte lipolysis is more resistant to suppression by insulin than in healthy pregnancy. Hypertension *63*, 1094-1101.
Iaffaldano, L., Nardelli, C., D'Alessio, F., D'Argenio, V., Nunziato, M., Mauriello, L., Procaccini, C., Maruotti, G.M., Martinelli, P., Matarese, G.*, et al.* (2018). Altered Bioenergetic Profile in Umbilical Cord and Amniotic Mesenchymal Stem Cells from Newborns of Obese Women. Stem Cells Dev *27*, 199-206.
Ibrahim, M.H., Moustafa, A.N., Saedii, A.A.F., and Hassan, E.E. (2017). Cord blood erythropoietin and cord blood nucleated red blood cells for prediction of adverse neonatal outcome associated with maternal obesity in term pregnancy: prospective cohort study. J Matern Fetal Neonatal Med *30*, 2237-2242.

Jansson, N., Rosario, F.J., Gaccioli, F., Lager, S., Jones, H.N., Roos, S., Jansson, T., and Powell, T.L. (2013). Activation of placental mTOR signaling and amino acid transporters in obese women giving birth to large babies. J Clin Endocrinol Metab *98*, 105-113.
Jiang, X., and Wang, H. (2020). Macrophage subsets at the maternal-fetal interface. Cell Mol Immunol.
Jilling, T., Simon, D., Lu, J., Meng, F.J., Li, D., Schy, R., Thomson, R.B., Soliman, A., Arditi, M., and Caplan, M.S. (2006). The roles of bacteria and TLR4 in rat and murine models of necrotizing enterocolitis. J Immunol *177*, 3273-3282.
Jo, H., Schieve, L.A., Sharma, A.J., Hinkle, S.N., Li, R., and Lind, J.N. (2015). Maternal prepregnancy body mass index and child psychosocial development at 6 years of age. Pediatrics *135*, e1198-1209.
Jones, H.N., Woollett, L.A., Barbour, N., Prasad, P.D., Powell, T.L., and Jansson, T. (2009). High-fat diet before and during pregnancy causes marked up-regulation of placental nutrient transport and fetal overgrowth in C57/BL6 mice. FASEB J *23*, 271-278.
Kac, G., Vaz, J.S., Schlussel, M.M., and Moura, A.S. (2011). C-reactive protein and hormones but not IL-6 are associated to body mass index in first trimester of pregnancy. Arch Gynecol Obstet *284*, 567-573.
Kadakia, R., Zheng, Y., Zhang, Z., Zhang, W., Hou, L., and Josefson, J.L. (2017). Maternal pre-pregnancy BMI downregulates neonatal cord blood LEP methylation. Pediatr Obes *12 Suppl 1*, 57-64.
Kalliolias, G.D., and Ivashkiv, L.B. (2008). IL-27 activates human monocytes via STAT1 and suppresses IL-10 production but the inflammatory functions of IL-27 are abrogated by TLRs and p38. J Immunol *180*, 6325-6333.
Kamada, R., Yang, W., Zhang, Y., Patel, M.C., Yang, Y., Ouda, R., Dey, A., Wakabayashi, Y., Sakaguchi, K., Fujita, T.*, et al.* (2018). Interferon stimulation creates chromatin marks and establishes transcriptional memory. Proc Natl Acad Sci U S A *115*, E9162-E9171.
Kamimae-Lanning, A.N., Krasnow, S.M., Goloviznina, N.A., Zhu, X., Roth-Carter, Q.R., Levasseur, P.R., Jeng, S., McWeeney, S.K., Kurre, P., and Marks, D.L. (2015). Maternal high-fat diet and obesity compromise fetal hematopoiesis. Mol Metab *4*, 25-38.
Kang, S.S., Kurti, A., Fair, D.A., and Fryer, J.D. (2014). Dietary intervention rescues maternal obesity induced behavior deficits and neuroinflammation in offspring. J Neuroinflammation *11*, 156.
Karlsson, E.A., Marcelin, G., Webby, R.J., and Schultz-Cherry, S. (2012). Review on the impact of pregnancy and obesity on influenza virus infection. Influenza Other Respir Viruses *6*, 449-460.
Kay, A.W., Fukuyama, J., Aziz, N., Dekker, C.L., Mackey, S., Swan, G.E., Davis, M.M., Holmes, S., and Blish, C.A. (2014). Enhanced natural killer-cell and T-cell responses to influenza A virus during pregnancy. Proc Natl Acad Sci U S A *111*, 14506-14511.
Kim, S.S., Zhu, Y., Grantz, K.L., Hinkle, S.N., Chen, Z., Wallace, M.E., Smarr, M.M., Epps, N.M., and Mendola, P. (2016). Obstetric and Neonatal Risks Among Obese Women Without Chronic Disease. Obstet Gynecol *128*, 104-112.
Kirk, S.L., Samuelsson, A.M., Argenton, M., Dhonye, H., Kalamatianos, T., Poston, L., Taylor, P.D., and Coen, C.W. (2009). Maternal obesity induced by diet in rats permanently influences central processes regulating food intake in offspring. PLoS One *4*, e5870.
Klebanoff, M.A., Meirik, O., and Berendes, H.W. (1989). Second-generation consequences of small-for-dates birth. Pediatrics *84*, 343-347.

Kleweis, S.M., Cahill, A.G., Odibo, A.O., and Tuuli, M.G. (2015). Maternal Obesity and Rectovaginal Group B Streptococcus Colonization at Term. Infect Dis Obstet Gynecol *2015*, 586767.
Kollmann, T.R., Kampmann, B., Mazmanian, S.K., Marchant, A., and Levy, O. (2017). Protecting the Newborn and Young Infant from Infectious Diseases: Lessons from Immune Ontogeny. Immunity *46*, 350-363.
Kollmann, T.R., Levy, O., Montgomery, R.R., and Goriely, S. (2012). Innate immune function by Toll-like receptors: distinct responses in newborns and the elderly. Immunity *37*, 771-783.
Korkmaz, L., Bastug, O., and Kurtoglu, S. (2016). Maternal Obesity and its Short- and Long-Term Maternal and Infantile Effects. J Clin Res Pediatr Endocrinol *8*, 114-124.
Krausgruber, T., Blazek, K., Smallie, T., Alzabin, S., Lockstone, H., Sahgal, N., Hussell, T., Feldmann, M., and Udalova, I.A. (2011). IRF5 promotes inflammatory macrophage polarization and TH1-TH17 responses. Nat Immunol *12*, 231-238.
Kumar, R., Story, R.E., Pongracic, J.A., Hong, X., Arguelles, L., Wang, G., Kuptsova-Clarkson, N., Pearson, C., Ortiz, K., Bonzagni, A.*, et al.* (2010). Maternal Pre-Pregnancy Obesity and Recurrent Wheezing in Early Childhood. Pediatr Allergy Immunol Pulmonol *23*, 183-190.
Kurt-Jones, E.A., Popova, L., Kwinn, L., Haynes, L.M., Jones, L.P., Tripp, R.A., Walsh, E.E., Freeman, M.W., Golenbock, D.T., Anderson, L.J., and Finberg, R.W. (2000). Pattern recognition receptors TLR4 and CD14 mediate response to respiratory syncytial virus. Nat Immunol *1*, 398-401.
Kusminski, C.M., McTernan, P.G., and Kumar, S. (2005). Role of resistin in obesity, insulin resistance and Type II diabetes. Clin Sci (Lond) *109*, 243-256.
Ladics, G.S., Smith, C., Bunn, T.L., Dietert, R.R., Anderson, P.K., Wiescinski, C.M., and Holsapple, M.P. (2000). CHARACTERIZATION OF AN APPROACH TO DEVELOPMENTAL IMMUNOTOXICOLOGY ASSESSMENT IN THE RAT USING SRBC AS THE ANTIGEN. Toxicology Methods *10*, 283-311.
Lager, S., Ramirez, V.I., Gaccioli, F., Jang, B., Jansson, T., and Powell, T.L. (2016). Protein expression of fatty acid transporter 2 is polarized to the trophoblast basal plasma membrane and increased in placentas from overweight/obese women. Placenta *40*, 60-66.
Laird, S.M., Quinton, N.D., Anstie, B., Li, T.C., and Blakemore, A.I. (2001). Leptin and leptin-binding activity in women with recurrent miscarriage: correlation with pregnancy outcome. Hum Reprod *16*, 2008-2013.
Laivuori, H., Kaaja, R., Koistinen, H., Karonen, S.L., Andersson, S., Koivisto, V., and Ylikorkala, O. (2000). Leptin during and after preeclamptic or normal pregnancy: its relation to serum insulin and insulin sensitivity. Metabolism *49*, 259-263.
Lam, L.L., Emberly, E., Fraser, H.B., Neumann, S.M., Chen, E., Miller, G.E., and Kobor, M.S. (2012). Factors underlying variable DNA methylation in a human community cohort. Proc Natl Acad Sci U S A *109 Suppl 2*, 17253-17260.
Lampe, R., Kover, A., Szucs, S., Pal, L., Arnyas, E., Adany, R., and Poka, R. (2015). Phagocytic index of neutrophil granulocytes and monocytes in healthy and preeclamptic pregnancy. J Reprod Immunol *107*, 26-30.
Lane, M., Robker, R.L., and Robertson, S.A. (2014). Parenting from before conception. Science *345*, 756-760.

Lane, M., Zander-Fox, D.L., Robker, R.L., and McPherson, N.O. (2015). Peri-conception parental obesity, reproductive health, and transgenerational impacts. Trends Endocrinol Metab *26*, 84-90.
Laskewitz, A., van Benthem, K.L., Kieffer, T.E.C., Faas, M.M., Verkaik-Schakel, R.N., Plosch, T., Scherjon, S.A., and Prins, J.R. (2019). The influence of maternal obesity on macrophage subsets in the human decidua. Cell Immunol *336*, 75-82.
Le Bouteiller, P. (2013). Human decidual NK cells: unique and tightly regulated effector functions in healthy and pathogen-infected pregnancies. Front Immunol *4*, 404.
Le Gars, M., Kay, A.W., Bayless, N.L., Aziz, N., Dekker, C.L., Swan, G.E., Davis, M.M., and Blish, C.A. (2016). Increased Proinflammatory Responses of Monocytes and Plasmacytoid Dendritic Cells to Influenza A Virus Infection During Pregnancy. J Infect Dis *214*, 1666-1671.
Leddy, M.A., Power, M.L., and Schulkin, J. (2008). The impact of maternal obesity on maternal and fetal health. Rev Obstet Gynecol *1*, 170-178.
Leibowitz, K.L., Moore, R.H., Ahima, R.S., Stunkard, A.J., Stallings, V.A., Berkowitz, R.I., Chittams, J.L., Faith, M.S., and Stettler, N. (2012). Maternal obesity associated with inflammation in their children. World J Pediatr *8*, 76-79.
Lenartowicz, M., Kennedy, C., Hayes, H., and McArdle, H.J. (2015). Transcriptional regulation of copper metabolism genes in the liver of fetal and neonatal control and iron-deficient rats. Biometals *28*, 51-59.
Levy, O. (2005). Innate immunity of the human newborn: distinct cytokine responses to LPS and other Toll-like receptor agonists. J Endotoxin Res *11*, 113-116.
Lewis, E.L., Sierra, L.J., Barila, G.O., Brown, A.G., Porrett, P.M., and Elovitz, M.A. (2018). Placental immune state shifts with gestational age. Am J Reprod Immunol *79*, e12848.
Li, M., Sloboda, D.M., and Vickers, M.H. (2011). Maternal obesity and developmental programming of metabolic disorders in offspring: evidence from animal models. Exp Diabetes Res *2011*, 592408.
Li, Y.M., Ou, J.J., Liu, L., Zhang, D., Zhao, J.P., and Tang, S.Y. (2016). Association Between Maternal Obesity and Autism Spectrum Disorder in Offspring: A Meta-analysis. J Autism Dev Disord *46*, 95-102.
Lillycrop, K.A., Slater-Jefferies, J.L., Hanson, M.A., Godfrey, K.M., Jackson, A.A., and Burdge, G.C. (2007). Induction of altered epigenetic regulation of the hepatic glucocorticoid receptor in the offspring of rats fed a protein-restricted diet during pregnancy suggests that reduced DNA methyltransferase-1 expression is involved in impaired DNA methylation and changes in histone modifications. Br J Nutr *97*, 1064-1073.
Liu, A., Chen, M., Kumar, R., Stefanovic-Racic, M., O'Doherty, R.M., Ding, Y., Jahnen-Dechent, W., and Borghesi, L. (2018). Bone marrow lympho-myeloid malfunction in obesity requires precursor cell-autonomous TLR4. Nat Commun *9*, 708.
Liu, S., Diao, L., Huang, C., Li, Y., Zeng, Y., and Kwak-Kim, J.Y.H. (2017). The role of decidual immune cells on human pregnancy. J Reprod Immunol *124*, 44-53.
Liu, X., Chen, Q., Tsai, H.J., Wang, G., Hong, X., Zhou, Y., Zhang, C., Liu, C., Liu, R., Wang, H., *et al.* (2014). Maternal preconception body mass index and offspring cord blood DNA methylation: exploration of early life origins of disease. Environ Mol Mutagen *55*, 223-230.
Long, N.M., Rule, D.C., Tuersunjiang, N., Nathanielsz, P.W., and Ford, S.P. (2015). Maternal obesity in sheep increases fatty acid synthesis, upregulates nutrient transporters, and

increases adiposity in adult male offspring after a feeding challenge. PLoS One *10*, e0122152.
Lowe, A., Braback, L., Ekeus, C., Hjern, A., and Forsberg, B. (2011). Maternal obesity during pregnancy as a risk for early-life asthma. J Allergy Clin Immunol *128*, 1107-1109 e1101-1102.
Luppi, P., Haluszczak, C., Betters, D., Richard, C.A., Trucco, M., and DeLoia, J.A. (2002a). Monocytes are progressively activated in the circulation of pregnant women. J Leukoc Biol *72*, 874-884.
Luppi, P., Haluszczak, C., Trucco, M., and Deloia, J.A. (2002b). Normal pregnancy is associated with peripheral leukocyte activation. Am J Reprod Immunol *47*, 72-81.
MacLennan, N.K., James, S.J., Melnyk, S., Piroozi, A., Jernigan, S., Hsu, J.L., Janke, S.M., Pham, T.D., and Lane, R.H. (2004). Uteroplacental insufficiency alters DNA methylation, one-carbon metabolism, and histone acetylation in IUGR rats. Physiol Genomics *18*, 43-50.
Madan, J.C., Davis, J.M., Craig, W.Y., Collins, M., Allan, W., Quinn, R., and Dammann, O. (2009). Maternal obesity and markers of inflammation in pregnancy. Cytokine *47*, 61-64.
Magann, E.F., Doherty, D.A., Sandlin, A.T., Chauhan, S.P., and Morrison, J.C. (2013). The effects of an increasing gradient of maternal obesity on pregnancy outcomes. Aust N Z J Obstet Gynaecol *53*, 250-257.
Maltepe, E., and Fisher, S.J. (2015). Placenta: the forgotten organ. Annu Rev Cell Dev Biol *31*, 523-552.
Malti, N., Merzouk, H., Merzouk, S.A., Loukidi, B., Karaouzene, N., Malti, A., and Narce, M. (2014). Oxidative stress and maternal obesity: feto-placental unit interaction. Placenta *35*, 411-416.
Manaster, I., and Mandelboim, O. (2010). The unique properties of uterine NK cells. Am J Reprod Immunol *63*, 434-444.
Marchi, J., Berg, M., Dencker, A., Olander, E.K., and Begley, C. (2015). Risks associated with obesity in pregnancy, for the mother and baby: a systematic review of reviews. Obes Rev *16*, 621-638.
McCloskey, K., Ponsonby, A.L., Collier, F., Allen, K., Tang, M.L.K., Carlin, J.B., Saffery, R., Skilton, M.R., Cheung, M., Ranganathan, S*., et al.* (2018). The association between higher maternal pre-pregnancy body mass index and increased birth weight, adiposity and inflammation in the newborn. Pediatr Obes *13*, 46-53.
McCurdy, C.E., Bishop, J.M., Williams, S.M., Grayson, B.E., Smith, M.S., Friedman, J.E., and Grove, K.L. (2009). Maternal high-fat diet triggers lipotoxicity in the fetal livers of nonhuman primates. J Clin Invest *119*, 323-335.
McLean, M., Hines, R., Polinkovsky, M., Stuebe, A., Thorp, J., and Strauss, R. (2012). Type of skin incision and wound complications in the obese parturient. Am J Perinatol *29*, 301-306.
Meenakshi, Srivastava, R., Sharma, N.R., Kushwaha, K.P., and Aditya, V. (2012). Obstetric behavior and pregnancy outcome in overweight and obese women: maternal and fetal complications and risks in relation to maternal overweight and obesity. J Obstet Gynaecol India *62*, 276-280.
Melczer, Z., Banhidy, F., Csomor, S., Kovacs, M., Siklos, P., Winkler, G., and Cseh, K. (2002). Role of tumour necrosis factor-alpha in insulin resistance during normal pregnancy. Eur J Obstet Gynecol Reprod Biol *105*, 7-10.

Mellembakken, J.R., Aukrust, P., Olafsen, M.K., Ueland, T., Hestdal, K., and Videm, V. (2002). Activation of leukocytes during the uteroplacental passage in preeclampsia. Hypertension *39*, 155-160.
Mikkola, H.K., and Orkin, S.H. (2006). The journey of developing hematopoietic stem cells. Development *133*, 3733-3744.
Miller, A., Riehle-Colarusso, T., Siffel, C., Frias, J.L., and Correa, A. (2011). Maternal age and prevalence of isolated congenital heart defects in an urban area of the United States. Am J Med Genet A *155A*, 2137-2145.
Mor, G., and Abrahams, V.M. (2003). Potential role of macrophages as immunoregulators of pregnancy. Reprod Biol Endocrinol *1*, 119.
Mor, G., Aldo, P., and Alvero, A.B. (2017). The unique immunological and microbial aspects of pregnancy. Nat Rev Immunol *17*, 469-482.
Mor, G., and Cardenas, I. (2010). The immune system in pregnancy: a unique complexity. Am J Reprod Immunol *63*, 425-433.
Mor, G., Cardenas, I., Abrahams, V., and Guller, S. (2011). Inflammation and pregnancy: the role of the immune system at the implantation site. Ann N Y Acad Sci *1221*, 80-87.
Morgan, A.R., Thompson, J.M., Murphy, R., Black, P.N., Lam, W.J., Ferguson, L.R., and Mitchell, E.A. (2010). Obesity and diabetes genes are associated with being born small for gestational age: results from the Auckland Birthweight Collaborative study. BMC Med Genet *11*, 125.
Mouralidarane, A., Soeda, J., Visconti-Pugmire, C., Samuelsson, A.M., Pombo, J., Maragkoudaki, X., Butt, A., Saraswati, R., Novelli, M., Fusai, G.*, et al.* (2013). Maternal obesity programs offspring nonalcoholic fatty liver disease by innate immune dysfunction in mice. Hepatology *58*, 128-138.
Mueller, N.T., Shin, H., Pizoni, A., Werlang, I.C., Matte, U., Goldani, M.Z., Goldani, H.A., and Dominguez-Bello, M.G. (2016). Birth mode-dependent association between pre-pregnancy maternal weight status and the neonatal intestinal microbiome. Sci Rep *6*, 23133.
Murabayashi, N., Sugiyama, T., Zhang, L., Kamimoto, Y., Umekawa, T., Ma, N., and Sagawa, N. (2013). Maternal high-fat diets cause insulin resistance through inflammatory changes in fetal adipose tissue. Eur J Obstet Gynecol Reprod Biol *169*, 39-44.
Myatt, L., and Maloyan, A. (2016). Obesity and Placental Function. Semin Reprod Med *34*, 42-49.
Myles, I.A., Fontecilla, N.M., Janelsins, B.M., Vithayathil, P.J., Segre, J.A., and Datta, S.K. (2013). Parental dietary fat intake alters offspring microbiome and immunity. J Immunol *191*, 3200-3209.
Naccasha, N., Gervasi, M.T., Chaiworapongsa, T., Berman, S., Yoon, B.H., Maymon, E., and Romero, R. (2001). Phenotypic and metabolic characteristics of monocytes and granulocytes in normal pregnancy and maternal infection. Am J Obstet Gynecol *185*, 1118-1123.
Nagamatsu, T., and Schust, D.J. (2010). The immunomodulatory roles of macrophages at the maternal-fetal interface. Reprod Sci *17*, 209-218.
Nagy, L., Tontonoz, P., Alvarez, J.G., Chen, H., and Evans, R.M. (1998). Oxidized LDL regulates macrophage gene expression through ligand activation of PPARgamma. Cell *93*, 229-240.
Nathanielsz, P.W., Poston, L., and Taylor, P.D. (2007). In utero exposure to maternal obesity and diabetes: animal models that identify and characterize implications for future health. Obstet Gynecol Clin North Am *34*, 201-212, vii-viii.

NE, I.I., Heward, J.A., Roux, B., Tsitsiou, E., Fenwick, P.S., Lenzi, L., Goodhead, I., Hertz-Fowler, C., Heger, A., Hall, N.*, et al.* (2014). Long non-coding RNAs and enhancer RNAs regulate the lipopolysaccharide-induced inflammatory response in human monocytes. Nat Commun *5*, 3979.
Nicholas, L.M., Rattanatray, L., MacLaughlin, S.M., Ozanne, S.E., Kleemann, D.O., Walker, S.K., Morrison, J.L., Zhang, S., Muhlhausler, B.S., Martin-Gronert, M.S., and McMillen, I.C. (2013). Differential effects of maternal obesity and weight loss in the periconceptional period on the epigenetic regulation of hepatic insulin-signaling pathways in the offspring. FASEB J *27*, 3786-3796.
Nogues, P., Dos Santos, E., Jammes, H., Berveiller, P., Arnould, L., Vialard, F., and Dieudonne, M.N. (2019). Maternal obesity influences expression and DNA methylation of the adiponectin and leptin systems in human third-trimester placenta. Clin Epigenetics *11*, 20.
Norman, J.E., and Reynolds, R.M. (2011). The consequences of obesity and excess weight gain in pregnancy. Proc Nutr Soc *70*, 450-456.
O'Carroll, C., Fagan, A., Shanahan, F., and Carmody, R.J. (2014). Identification of a unique hybrid macrophage-polarization state following recovery from lipopolysaccharide tolerance. J Immunol *192*, 427-436.
O'Reilly, J.R., and Reynolds, R.M. (2013). The risk of maternal obesity to the long-term health of the offspring. Clin Endocrinol (Oxf) *78*, 9-16.
Odaka, Y., Nakano, M., Tanaka, T., Kaburagi, T., Yoshino, H., Sato-Mito, N., and Sato, K. (2010). The influence of a high-fat dietary environment in the fetal period on postnatal metabolic and immune function. Obesity (Silver Spring) *18*, 1688-1694.
Ogden, C.L., Carroll, M.D., Kit, B.K., and Flegal, K.M. (2013). Prevalence of obesity among adults: United States, 2011-2012. NCHS Data Brief, 1-8.
Orlova, E.G., and Shirshev, S.V. (2009). Leptin as an immunocorrecting agent during normal pregnancy. Bull Exp Biol Med *148*, 75-78.
Ou, J., Liu, H., Yu, J., Kelliher, M.A., Castilla, L.H., Lawson, N.D., and Zhu, L.J. (2018). ATACseqQC: a Bioconductor package for post-alignment quality assessment of ATAC-seq data. BMC Genomics *19*, 169.
Ozias, M.K., Li, S., Hull, H.R., Brooks, W.M., and Carlson, S.E. (2015). Relationship of circulating adipokines to body composition in pregnant women. Adipocyte *4*, 44-49.
Paiva, L.V., Nomura, R.M., Dias, M.C., and Zugaib, M. (2012). Maternal obesity in high-risk pregnancies and postpartum infectious complications. Rev Assoc Med Bras (1992) *58*, 453-458.
Palik, E., Baranyi, E., Melczer, Z., Audikovszky, M., Szocs, A., Winkler, G., and Cseh, K. (2007). Elevated serum acylated (biologically active) ghrelin and resistin levels associate with pregnancy-induced weight gain and insulin resistance. Diabetes Res Clin Pract *76*, 351-357.
Park, S.H., Kang, K., Giannopoulou, E., Qiao, Y., Kang, K., Kim, G., Park-Min, K.H., and Ivashkiv, L.B. (2017). Type I interferons and the cytokine TNF cooperatively reprogram the macrophage epigenome to promote inflammatory activation. Nat Immunol *18*, 1104-1116.
Parnell, L.A., Briggs, C.M., Cao, B., Delannoy-Bruno, O., Schrieffer, A.E., and Mysorekar, I.U. (2017). Microbial communities in placentas from term normal pregnancy exhibit spatially variable profiles. Sci Rep *7*, 11200.
Parsons, T.J., Power, C., and Manor, O. (2001). Fetal and early life growth and body mass index from birth to early adulthood in 1958 British cohort: longitudinal study. BMJ *323*, 1331-1335.

Patel, S.P., Rodriguez, A., Little, M.P., Elliott, P., Pekkanen, J., Hartikainen, A.L., Pouta, A., Laitinen, J., Harju, T., Canoy, D., and Jarvelin, M.R. (2012). Associations between pre-pregnancy obesity and asthma symptoms in adolescents. J Epidemiol Community Health *66*, 809-814.
Peltier, M.R., Freeman, A.J., Mu, H.H., and Cole, B.C. (2005). Characterization and partial purification of a macrophage-stimulating factor from Mycoplasma hominis. Am J Reprod Immunol *54*, 342-351.
Pendeloski, K.P.T., Ono, E., Torloni, M.R., Mattar, R., and Daher, S. (2017). Maternal obesity and inflammatory mediators: A controversial association. Am J Reprod Immunol *77*.
Perdu, S., Castellana, B., Kim, Y., Chan, K., DeLuca, L., and Beristain, A.G. (2016). Maternal obesity drives functional alterations in uterine NK cells. JCI Insight *1*, e85560.
Pike, K.C., Inskip, H.M., Robinson, S.M., Cooper, C., Godfrey, K.M., Roberts, G., Lucas, J.S., and Southampton Women's Survey Study, G. (2013). The relationship between maternal adiposity and infant weight gain, and childhood wheeze and atopy. Thorax *68*, 372-379.
Pique-Regi, R., Romero, R., Tarca, A.L., Sendler, E.D., Xu, Y., Garcia-Flores, V., Leng, Y., Luca, F., Hassan, S.S., and Gomez-Lopez, N. (2019). Single cell transcriptional signatures of the human placenta in term and preterm parturition. Elife *8*.
Polese, B., Gridelet, V., Araklioti, E., Martens, H., Perrier d'Hauterive, S., and Geenen, V. (2014). The Endocrine Milieu and CD4 T-Lymphocyte Polarization during Pregnancy. Front Endocrinol (Lausanne) *5*, 106.
Polnaszek, B.E., Raghuraman, N., Lopez, J.D., Frolova, A.L., Wesevich, V., Tuuli, M.G., and Cahill, A.G. (2018). Neonatal Morbidity in the Offspring of Obese Women Without Hypertension or Diabetes. Obstet Gynecol *132*, 835-841.
Poobalan, A.S., Aucott, L.S., Gurung, T., Smith, W.C., and Bhattacharya, S. (2009). Obesity as an independent risk factor for elective and emergency caesarean delivery in nulliparous women--systematic review and meta-analysis of cohort studies. Obes Rev *10*, 28-35.
Prince, A.L., Ma, J., Kannan, P.S., Alvarez, M., Gisslen, T., Harris, R.A., Sweeney, E.L., Knox, C.L., Lambers, D.S., Jobe, A.H.*, et al.* (2016). The placental membrane microbiome is altered among subjects with spontaneous preterm birth with and without chorioamnionitis. Am J Obstet Gynecol *214*, 627 e621-627 e616.
Przybyl, L., Haase, N., Golic, M., Rugor, J., Solano, M.E., Arck, P.C., Gauster, M., Huppertz, B., Emontzpohl, C., Stoppe, C.*, et al.* (2016). CD74-Downregulation of Placental Macrophage-Trophoblastic Interactions in Preeclampsia. Circ Res *119*, 55-68.
Rajappan, A., Pearce, A., Inskip, H.M., Baird, J., Crozier, S.R., Cooper, C., Godfrey, K.M., Roberts, G., Lucas, J.S.A., Pike, K.C., and Southampton Women's Survey Study, G. (2017). Maternal body mass index: Relation with infant respiratory symptoms and infections. Pediatr Pulmonol *52*, 1291-1299.
Ramsay, J.E., Ferrell, W.R., Crawford, L., Wallace, A.M., Greer, I.A., and Sattar, N. (2002). Maternal obesity is associated with dysregulation of metabolic, vascular, and inflammatory pathways. J Clin Endocrinol Metab *87*, 4231-4237.
Rastogi, S., Rojas, M., Rastogi, D., and Haberman, S. (2015). Neonatal morbidities among full-term infants born to obese mothers. J Matern Fetal Neonatal Med *28*, 829-835.
Rea, R., and Donnelly, R. (2004). Resistin: an adipocyte-derived hormone. Has it a role in diabetes and obesity? Diabetes Obes Metab *6*, 163-170.

Redman, C.W., Tannetta, D.S., Dragovic, R.A., Gardiner, C., Southcombe, J.H., Collett, G.P., and Sargent, I.L. (2012). Review: Does size matter? Placental debris and the pathophysiology of pre-eclampsia. Placenta *33 Suppl*, S48-54.
Reynolds, R.M., Allan, K.M., Raja, E.A., Bhattacharya, S., McNeill, G., Hannaford, P.C., Sarwar, N., Lee, A.J., Bhattacharya, S., and Norman, J.E. (2013). Maternal obesity during pregnancy and premature mortality from cardiovascular event in adult offspring: follow-up of 1 323 275 person years. BMJ *347*, f4539.
Rivera, H.M., Kievit, P., Kirigiti, M.A., Bauman, L.A., Baquero, K., Blundell, P., Dean, T.A., Valleau, J.C., Takahashi, D.L., Frazee, T.*, et al.* (2015). Maternal high-fat diet and obesity impact palatable food intake and dopamine signaling in nonhuman primate offspring. Obesity (Silver Spring) *23*, 2157-2164.
Roberts, K.A., Riley, S.C., Reynolds, R.M., Barr, S., Evans, M., Statham, A., Hor, K., Jabbour, H.N., Norman, J.E., and Denison, F.C. (2011). Placental structure and inflammation in pregnancies associated with obesity. Placenta *32*, 247-254.
Robinson, H.E., O'Connell, C.M., Joseph, K.S., and McLeod, N.L. (2005). Maternal outcomes in pregnancies complicated by obesity. Obstet Gynecol *106*, 1357-1364.
Rodriguez, A. (2010). Maternal pre-pregnancy obesity and risk for inattention and negative emotionality in children. J Child Psychol Psychiatry *51*, 134-143.
Romero, R., Espinoza, J., Goncalves, L.F., Kusanovic, J.P., Friel, L.A., and Nien, J.K. (2006). Inflammation in preterm and term labour and delivery. Semin Fetal Neonatal Med *11*, 317-326.
Rosales, C. (2018). Neutrophil: A Cell with Many Roles in Inflammation or Several Cell Types? Front Physiol *9*, 113.
Rosario, F.J., Kanai, Y., Powell, T.L., and Jansson, T. (2015). Increased placental nutrient transport in a novel mouse model of maternal obesity with fetal overgrowth. Obesity (Silver Spring) *23*, 1663-1670.
Saben, J., Lindsey, F., Zhong, Y., Thakali, K., Badger, T.M., Andres, A., Gomez-Acevedo, H., and Shankar, K. (2014). Maternal obesity is associated with a lipotoxic placental environment. Placenta *35*, 171-177.
Sacks, G.P., Clover, L.M., Bainbridge, D.R., Redman, C.W., and Sargent, I.L. (2001). Flow cytometric measurement of intracellular Th1 and Th2 cytokine production by human villous and extravillous cytotrophoblast. Placenta *22*, 550-559.
Sacks, G.P., Redman, C.W., and Sargent, I.L. (2003). Monocytes are primed to produce the Th1 type cytokine IL-12 in normal human pregnancy: an intracellular flow cytometric analysis of peripheral blood mononuclear cells. Clin Exp Immunol *131*, 490-497.
Sacks, G.P., Studena, K., Sargent, K., and Redman, C.W. (1998). Normal pregnancy and preeclampsia both produce inflammatory changes in peripheral blood leukocytes akin to those of sepsis. Am J Obstet Gynecol *179*, 80-86.
Salihu, H.M., De La Cruz, C., Rahman, S., and August, E.M. (2012). Does maternal obesity cause preeclampsia? A systematic review of the evidence. Minerva Ginecol *64*, 259-280.
Salim, R., Braverman, M., Teitler, N., Berkovic, I., Suliman, A., and Shalev, E. (2012). Risk factors for infection following cesarean delivery: an interventional study. J Matern Fetal Neonatal Med *25*, 2708-2712.
Samuelsson, A.M., Matthews, P.A., Argenton, M., Christie, M.R., McConnell, J.M., Jansen, E.H., Piersma, A.H., Ozanne, S.E., Twinn, D.F., Remacle, C.*, et al.* (2008). Diet-induced obesity in

female mice leads to offspring hyperphagia, adiposity, hypertension, and insulin resistance: a novel murine model of developmental programming. Hypertension *51*, 383-392.
Satija, R., Farrell, J.A., Gennert, D., Schier, A.F., and Regev, A. (2015). Spatial reconstruction of single-cell gene expression data. Nat Biotechnol *33*, 495-502.
Schmatz, M., Madan, J., Marino, T., and Davis, J. (2010). Maternal obesity: the interplay between inflammation, mother and fetus. J Perinatol *30*, 441-446.
Scholtens, S., Wijga, A.H., Brunekreef, B., Kerkhof, M., Postma, D.S., Oldenwening, M., de Jongste, J.C., and Smit, H.A. (2010). Maternal overweight before pregnancy and asthma in offspring followed for 8 years. Int J Obes (Lond) *34*, 606-613.
Schubring, C., Englaro, P., Siebler, T., Blum, W.F., Demirakca, T., Kratzsch, J., and Kiess, W. (1998). Longitudinal analysis of maternal serum leptin levels during pregnancy, at birth and up to six weeks after birth: relation to body mass index, skinfolds, sex steroids and umbilical cord blood leptin levels. Horm Res *50*, 276-283.
Scott-Pillai, R., Spence, D., Cardwell, C.R., Hunter, A., and Holmes, V.A. (2013). The impact of body mass index on maternal and neonatal outcomes: a retrospective study in a UK obstetric population, 2004-2011. BJOG *120*, 932-939.
Sebire, N.J., Jolly, M., Harris, J.P., Wadsworth, J., Joffe, M., Beard, R.W., Regan, L., and Robinson, S. (2001). Maternal obesity and pregnancy outcome: a study of 287,213 pregnancies in London. Int J Obes Relat Metab Disord *25*, 1175-1182.
Segerer, S., Kammerer, U., Kapp, M., Dietl, J., and Rieger, L. (2009). Upregulation of chemokine and cytokine production during pregnancy. Gynecol Obstet Invest *67*, 145-150.
Sen, S., Iyer, C., Klebenov, D., Histed, A., Aviles, J.A., and Meydani, S.N. (2013). Obesity impairs cell-mediated immunity during the second trimester of pregnancy. Am J Obstet Gynecol *208*, 139 e131-138.
Sen, S., Iyer, C., and Meydani, S.N. (2014). Obesity during pregnancy alters maternal oxidant balance and micronutrient status. J Perinatol *34*, 105-111.
Shankar, K., Harrell, A., Liu, X., Gilchrist, J.M., Ronis, M.J., and Badger, T.M. (2008). Maternal obesity at conception programs obesity in the offspring. Am J Physiol Regul Integr Comp Physiol *294*, R528-538.
Sharp, G.C., Lawlor, D.A., Richmond, R.C., Fraser, A., Simpkin, A., Suderman, M., Shihab, H.A., Lyttleton, O., McArdle, W., Ring, S.M.*, et al.* (2015). Maternal pre-pregnancy BMI and gestational weight gain, offspring DNA methylation and later offspring adiposity: findings from the Avon Longitudinal Study of Parents and Children. Int J Epidemiol *44*, 1288-1304.
Sharp, G.C., Salas, L.A., Monnereau, C., Allard, C., Yousefi, P., Everson, T.M., Bohlin, J., Xu, Z., Huang, R.C., Reese, S.E.*, et al.* (2017). Maternal BMI at the start of pregnancy and offspring epigenome-wide DNA methylation: findings from the pregnancy and childhood epigenetics (PACE) consortium. Hum Mol Genet *26*, 4067-4085.
Shetty, G.K., Economides, P.A., Horton, E.S., Mantzoros, C.S., and Veves, A. (2004). Circulating adiponectin and resistin levels in relation to metabolic factors, inflammatory markers, and vascular reactivity in diabetic patients and subjects at risk for diabetes. Diabetes Care *27*, 2450-2457.
Shi, C., Sakuma, M., Mooroka, T., Liscoe, A., Gao, H., Croce, K.J., Sharma, A., Kaplan, D., Greaves, D.R., Wang, Y., and Simon, D.I. (2008). Down-regulation of the forkhead transcription factor Foxp1 is required for monocyte differentiation and macrophage function. Blood *112*, 4699-4711.

Singh, U., Nicholson, G., Urban, B.C., Sargent, I.L., Kishore, U., and Bernal, A.L. (2005). Immunological properties of human decidual macrophages--a possible role in intrauterine immunity. Reproduction *129*, 631-637.
Smallwood, S.A., Lee, H.J., Angermueller, C., Krueger, F., Saadeh, H., Peat, J., Andrews, S.R., Stegle, O., Reik, W., and Kelsey, G. (2014). Single-cell genome-wide bisulfite sequencing for assessing epigenetic heterogeneity. Nat Methods *11*, 817-820.
Soderborg, T.K., Clark, S.E., Mulligan, C.E., Janssen, R.C., Babcock, L., Ir, D., Lemas, D.J., Johnson, L.K., Weir, T., Lenz, L.L.*, et al.* (2018). The gut microbiota in infants of obese mothers increases inflammation and susceptibility to NAFLD. Nat Commun *9*, 4462.
Stapleton, R.D., Kahn, J.M., Evans, L.E., Critchlow, C.W., and Gardella, C.M. (2005). Risk factors for group B streptococcal genitourinary tract colonization in pregnant women. Obstet Gynecol *106*, 1246-1252.
Stewart, F.M., Freeman, D.J., Ramsay, J.E., Greer, I.A., Caslake, M., and Ferrell, W.R. (2007). Longitudinal assessment of maternal endothelial function and markers of inflammation and placental function throughout pregnancy in lean and obese mothers. J Clin Endocrinol Metab *92*, 969-975.
Strakovsky, R.S., Zhang, X., Zhou, D., and Pan, Y.X. (2011). Gestational high fat diet programs hepatic phosphoenolpyruvate carboxykinase gene expression and histone modification in neonatal offspring rats. J Physiol *589*, 2707-2717.
Stuart, T., Butler, A., Hoffman, P., Hafemeister, C., Papalexi, E., Mauck, W.M., 3rd, Hao, Y., Stoeckius, M., Smibert, P., and Satija, R. (2019). Comprehensive Integration of Single-Cell Data. Cell *177*, 1888-1902 e1821.
Stuart, T.J., O'Neill, K., Condon, D., Sasson, I., Sen, P., Xia, Y., and Simmons, R.A. (2018). Diet-induced obesity alters the maternal metabolome and early placenta transcriptome and decreases placenta vascularity in the mouse. Biol Reprod *98*, 795-809.
Suk, D., Kwak, T., Khawar, N., Vanhorn, S., Salafia, C.M., Gudavalli, M.B., and Narula, P. (2016). Increasing maternal body mass index during pregnancy increases neonatal intensive care unit admission in near and full-term infants. J Matern Fetal Neonatal Med *29*, 3249-3253.
Sullivan, E.L., Grayson, B., Takahashi, D., Robertson, N., Maier, A., Bethea, C.L., Smith, M.S., Coleman, K., and Grove, K.L. (2010). Chronic consumption of a high-fat diet during pregnancy causes perturbations in the serotonergic system and increased anxiety-like behavior in nonhuman primate offspring. J Neurosci *30*, 3826-3830.
Sureshchandra, S., Marshall, N.E., and Messaoudi, I. (2019). Impact of pregravid obesity on maternal and fetal immunity: Fertile grounds for reprogramming. J Leukoc Biol *106*, 1035-1050.
Sureshchandra, S., Marshall, N.E., Wilson, R.M., Barr, T., Rais, M., Purnell, J.Q., Thornburg, K.L., and Messaoudi, I. (2018). Inflammatory Determinants of Pregravid Obesity in Placenta and Peripheral Blood. Front Physiol *9*, 1089.
Sureshchandra, S., Wilson, R.M., Rais, M., Marshall, N.E., Purnell, J.Q., Thornburg, K.L., and Messaoudi, I. (2017). Maternal Pregravid Obesity Remodels the DNA Methylation Landscape of Cord Blood Monocytes Disrupting Their Inflammatory Program. J Immunol *199*, 2729-2744.
Suryawanshi, H., Morozov, P., Straus, A., Sahasrabudhe, N., Max, K.E.A., Garzia, A., Kustagi, M., Tuschl, T., and Williams, Z. (2018). A single-cell survey of the human first-trimester placenta and decidua. Sci Adv *4*, eaau4788.

Suter, M.A., Chen, A., Burdine, M.S., Choudhury, M., Harris, R.A., Lane, R.H., Friedman, J.E., Grove, K.L., Tackett, A.J., and Aagaard, K.M. (2012). A maternal high-fat diet modulates fetal SIRT1 histone and protein deacetylase activity in nonhuman primates. FASEB J *26*, 5106-5114.
Suzuki, T., Hashimoto, S., Toyoda, N., Nagai, S., Yamazaki, N., Dong, H.Y., Sakai, J., Yamashita, T., Nukiwa, T., and Matsushima, K. (2000). Comprehensive gene expression profile of LPS-stimulated human monocytes by SAGE. Blood *96*, 2584-2591.
Szabo, P.A., Levitin, H.M., Miron, M., Snyder, M.E., Senda, T., Yuan, J., Cheng, Y.L., Bush, E.C., Dogra, P., Thapa, P.*, et al.* (2019). Single-cell transcriptomics of human T cells reveals tissue and activation signatures in health and disease. Nat Commun *10*, 4706.
Tang, M.X., Hu, X.H., Liu, Z.Z., Kwak-Kim, J., and Liao, A.H. (2015). What are the roles of macrophages and monocytes in human pregnancy? J Reprod Immunol *112*, 73-80.
Thilaganathan, B., Nicolaides, K.H., Mansur, C.A., Levinsky, R.J., and Morgan, G. (1993). Fetal B lymphocyte subpopulations in normal pregnancies. Fetal Diagn Ther *8*, 15-21.
Thornburg, K.L., and Marshall, N. (2015). The placenta is the center of the chronic disease universe. Am J Obstet Gynecol *213*, S14-20.
Tie, H.T., Xia, Y.Y., Zeng, Y.S., Zhang, Y., Dai, C.L., Guo, J.J., and Zhao, Y. (2014). Risk of childhood overweight or obesity associated with excessive weight gain during pregnancy: a meta-analysis. Arch Gynecol Obstet *289*, 247-257.
Tontonoz, P., Nagy, L., Alvarez, J.G., Thomazy, V.A., and Evans, R.M. (1998). PPARgamma promotes monocyte/macrophage differentiation and uptake of oxidized LDL. Cell *93*, 241-252.
Torloni, M.R., Betran, A.P., Horta, B.L., Nakamura, M.U., Atallah, A.N., Moron, A.F., and Valente, O. (2009). Prepregnancy BMI and the risk of gestational diabetes: a systematic review of the literature with meta-analysis. Obes Rev *10*, 194-203.
Tsao, C.H., Shiau, M.Y., Chuang, P.H., Chang, Y.H., and Hwang, J. (2014). Interleukin-4 regulates lipid metabolism by inhibiting adipogenesis and promoting lipolysis. J Lipid Res *55*, 385-397.
van der Graaf, C.A., Netea, M.G., Verschueren, I., van der Meer, J.W., and Kullberg, B.J. (2005). Differential cytokine production and Toll-like receptor signaling pathways by Candida albicans blastoconidia and hyphae. Infect Immun *73*, 7458-7464.
van der Wijden, C.L., Delemarre-van der Waal, H.A., van Mechelen, W., and van Poppel, M.N. (2013). The concurrent validity between leptin, BMI and skin folds during pregnancy and the year after. Nutr Diabetes *3*, e86.
Vento-Tormo, R., Efremova, M., Botting, R.A., Turco, M.Y., Vento-Tormo, M., Meyer, K.B., Park, J.E., Stephenson, E., Polanski, K., Goncalves, A.*, et al.* (2018). Single-cell reconstruction of the early maternal-fetal interface in humans. Nature *563*, 347-353.
Villamor E., N.M., Johansson S., Cnattingius S. (2020). Maternal obesity and risk of early-onset neonatal bacterial sepsis: Nationwide cohort and sibling-controlled studies. Clinical Infectious Diseases.
Wallace, J.G., Bellissimo, C.J., Yeo, E., Fei Xia, Y., Petrik, J.J., Surette, M.G., Bowdish, D.M.E., and Sloboda, D.M. (2019). Obesity during pregnancy results in maternal intestinal inflammation, placental hypoxia, and alters fetal glucose metabolism at mid-gestation. Sci Rep *9*, 17621.
Walsh, J.M., McGowan, C.A., Byrne, J.A., Rath, A., and McAuliffe, F.M. (2013). The association between TNF-alpha and insulin resistance in euglycemic women. Cytokine *64*, 208-212.

Wang, Z., Wang, P., Liu, H., He, X., Zhang, J., Yan, H., Xu, D., and Wang, B. (2013). Maternal adiposity as an independent risk factor for pre-eclampsia: a meta-analysis of prospective cohort studies. Obes Rev *14*, 508-521.
Watson, P.E., and McDonald, B.W. (2013). Subcutaneous body fat in pregnant New Zealand women: association with wheeze in their infants at 18 months. Matern Child Health J *17*, 959-967.
Williams, L., Seki, Y., Vuguin, P.M., and Charron, M.J. (2014). Animal models of in utero exposure to a high fat diet: a review. Biochim Biophys Acta *1842*, 507-519.
Williams, P.J., Searle, R.F., Robson, S.C., Innes, B.A., and Bulmer, J.N. (2009). Decidual leucocyte populations in early to late gestation normal human pregnancy. J Reprod Immunol *82*, 24-31.
Wilson, R.M., Marshall, N.E., Jeske, D.R., Purnell, J.Q., Thornburg, K., and Messaoudi, I. (2015). Maternal obesity alters immune cell frequencies and responses in umbilical cord blood samples. Pediatr Allergy Immunol *26*, 344-351.
Wolk, K., Kunz, S., Crompton, N.E., Volk, H.D., and Sabat, R. (2003). Multiple mechanisms of reduced major histocompatibility complex class II expression in endotoxin tolerance. J Biol Chem *278*, 18030-18036.
Wu, L.L., Russell, D.L., Wong, S.L., Chen, M., Tsai, T.S., St John, J.C., Norman, R.J., Febbraio, M.A., Carroll, J., and Robker, R.L. (2015). Mitochondrial dysfunction in oocytes of obese mothers: transmission to offspring and reversal by pharmacological endoplasmic reticulum stress inhibitors. Development *142*, 681-691.
Yan, X., Huang, Y., Wang, H., Du, M., Hess, B.W., Ford, S.P., Nathanielsz, P.W., and Zhu, M.J. (2011). Maternal obesity induces sustained inflammation in both fetal and offspring large intestine of sheep. Inflamm Bowel Dis *17*, 1513-1522.
Yan, X., Sun, M., and Gibb, W. (2002). Localization of nuclear factor-kappa B (NF kappa B) and inhibitory factor-kappa B (I kappa B) in human fetal membranes and decidua at term and preterm delivery. Placenta *23*, 288-293.
Yang, K.F., Cai, W., Xu, J.L., and Shi, W. (2012). Maternal high-fat diet programs Wnt genes through histone modification in the liver of neonatal rats. J Mol Endocrinol *49*, 107-114.
Yang, Q.Y., Liang, J.F., Rogers, C.J., Zhao, J.X., Zhu, M.J., and Du, M. (2013). Maternal obesity induces epigenetic modifications to facilitate Zfp423 expression and enhance adipogenic differentiation in fetal mice. Diabetes *62*, 3727-3735.
Yang, X., Li, M., Haghiac, M., Catalano, P.M., O'Tierney-Ginn, P., and Hauguel-de Mouzon, S. (2016). Causal relationship between obesity-related traits and TLR4-driven responses at the maternal-fetal interface. Diabetologia *59*, 2459-2466.
Yarilina, A., Xu, K., Chen, J., and Ivashkiv, L.B. (2011). TNF activates calcium-nuclear factor of activated T cells (NFAT)c1 signaling pathways in human macrophages. Proc Natl Acad Sci U S A *108*, 1573-1578.
Young, O.M., Twedt, R., and Catov, J.M. (2016). Pre-pregnancy maternal obesity and the risk of preterm preeclampsia in the American primigravida. Obesity (Silver Spring) *24*, 1226-1229.
Yu, Z., Han, S., Zhu, J., Sun, X., Ji, C., and Guo, X. (2013). Pre-pregnancy body mass index in relation to infant birth weight and offspring overweight/obesity: a systematic review and meta-analysis. PLoS One *8*, e61627.
Zaretsky, M.V., Alexander, J.M., Byrd, W., and Bawdon, R.E. (2004). Transfer of inflammatory cytokines across the placenta. Obstet Gynecol *103*, 546-550.

Zhao, P., Wong, K.I., Sun, X., Reilly, S.M., Uhm, M., Liao, Z., Skorobogatko, Y., and Saltiel, A.R. (2018). TBK1 at the Crossroads of Inflammation and Energy Homeostasis in Adipose Tissue. Cell *172*, 731-743 e712.
Zheng, G.X., Terry, J.M., Belgrader, P., Ryvkin, P., Bent, Z.W., Wilson, R., Ziraldo, S.B., Wheeler, T.D., McDermott, G.P., Zhu, J.*, et al.* (2017). Massively parallel digital transcriptional profiling of single cells. Nat Commun *8*, 14049.
Zhou, Y., Zhou, B., Pache, L., Chang, M., Khodabakhshi, A.H., Tanaseichuk, O., Benner, C., and Chanda, S.K. (2019). Metascape provides a biologist-oriented resource for the analysis of systems-level datasets. Nat Commun *10*, 1523.